1-1-2012

Anticancer and antibiotic leads from marine organis

Bin Wang
University of Mississippi

ANTICANCER AND ANTIBIOTIC LEADS FROM MARINE ORGANISMS

A Dissertation
presented in partial fulfillment of requirements
for the degree of Doctor of Philosophy
in Pharmaceutical Sciences (with Emphasis in Pharmacognosy)
The University of Mississippi

by

BIN WANG

August 2012

ABSTRACT

During the past three decades, the development of marine natural products as drug leads has become a promising avenue for research. As our efforts towards the discovery of anticancer and antibiotic drug leads from marine organisms, modifications of anticancer drug candidate kahalalide F, isolations of new peptides from the mollusk, *Elysia rufescens* and anticancer drug leads from the NCI repository, as well as chemical regulation of antibiotic production from marine *Pseudomonas aeruginosa* were investigated.

Kahalalide F (KF) is a potent anticancer lead isolated from the herbivorous marine mollusk *E. rufescens* and its algal diet *Bryopsis pennata*. Our semisynthesis approach was aimed to improve the efficacy or prolong the half-life resulted in 15 KF analogues. These analogues included eight elongation products with nonpolar amino acid residues, four analogues with modified amino group at the Orn residue, one dehydration product of KF, and two new cyclization products of kahalalide G. All the analogues are being evaluated by Wayne State University for solid tumor cytotoxicity.

In the course of the isolation of KF as starting material for its analogues, nine new and 10 known peptides were isolated from *E. rufescens.* However, only five structures were determined and the remaining four structures could not be assigned due to limited sample amounts (less than 1 mg). Future work will focus on the structure assignment using FTMS amino acid sequence analysis or 700 MHz NMR.

During the screening of anticancer drug leads from the NCI repository, 27 extracts from marine organisms were tested, and 12 known compounds including tetracyclic aromatic alkaloids, diterpenoids and pyrroloaminopropylimidazole alkaloids were purified.

Bioassay-guided isolation from marine *P. aeruginosa* collected in the Gulf of Mexico afforded 15 known antibiotics including two phenazines, six 2-alkyl-4-quinolones, and seven rhamnolipids. 2-Nonyl-4(1*H*)-quinolone and 2-(1-nonenyl)-4(1*H*)-quinolone displayed potent antimalarial activity, which was first reported here. Based on the metabolic profile of antibiotics from *P. aeruginosa*, chemical regulation and its impact on the yield of these metabolites were investigated. Treatment of *P. aeruginosa* with sceptrin and co-culturing with another *Pseudomonas* sp. increased antibiotic production significantly. This could be attributed to the activation of antibiotic biosynthetic gene expression under stress conditions.

DEDICATION

The work is dedicated to my family

LIST OF ABBREVIATION AND SYMBOLS

BAST: bis(2-methoxyethyl)aminosulfur trifluoride

BCS: bovine calf serum

Boc: *tert*-butyloxycarbonyl

BLAST: basic local alignment search tool

CDC: Centers for Disease Control

CLSI: Clinical and Laboratory Standards Institute

DAST: diethylaminosulfur trifluoride

DCM: dichloromethane

DMAP: 4-dimethylaminopyridine

DMEM: Dulbecco's modified eagle medium

DMF: dimethylformamide

DMSO: dimethyl sulfoxide

EIC: extracted ion chromatogram

ESI: electrospray ionization

EtOH: ethanol

EtOAc: ethyl acetate

EDCI: 1-ethyl-3-(3-dimethylaminopropyl)carbodiimide

FDA: U.S. Food and Drug Administration

FDAA: *Nα*-(2,4-dinitro-5-fluorophenyl)-L-alaninamide

FTMS: Fourier transform mass spectrometry

Fmoc-Cl: 9-fluorenylmethyl chloroformate

Fmoc-OSu: *N*-(9-fluorenylmethoxycarbonyloxy)succinimide

GSK: glycogen synthase kinase

HMBC: heteronuclear multiple bond correlation

HOBt: hydroxybenzotrazole

HOSu: *N*-hydroxysuccinimide

HP-20: high porous styrenic adsorbent resin

HPLC: high performance liquid chromatography

HRMS: high resolution mass spectrometry

HSQC: heteronuclear single quantum coherence

IC_{50}: the half maximal inhibitory concentration

LDH: lactate dehydrogenase

MALDI: matrix-assisted laser desorption/ionization

MDR: multidrug resistance

MeCN: acetonitrile

MeOH: methanol

MRS: methicillin-resistant *Staphylococcus aureus*

NAD(P): nicotinamide adenine dinucleotide (phosphate)

NBS: *N*-bromosuccinimide

NCI: National Cancer Institute

NMR: nuclear magnetic resonance

NOESY: nuclear overhauser effect spectroscopy

NSCLC: non-small cell lung cancer

PCR: polymerase chain reaction

R*t*: retention time

SAR: structure-activity relationship

SPPS: solid-phase peptide synthesis

TFA: trifluoroacetic acid

THF: tetrahydrofuran

TIC: total ion chromatogram

TOF: time-of-flight

VLC: vacuum-liquid chromatography

WHO: World Health Organization

ACKNOWLEDGEMENTS

First of all, I would like to extend my sincere gratitude to my advisor, Professor Mark T. Hamann, for his guidance, encouragement, and continuous support of the research towards earning my doctoral degree.

I would like to thank my committee members, Drs. Daneel Ferreira, Jordan K. Zjawiony, Russell T. Hill, John S. Williamson and Mitchell A. Avery for their advice and valuable scientific discussions.

I would like to thank Drs. Marc Slattery, Dale G. Nagle and Yu-Dong Zhou for their outstanding teaching, patience, and encouragement. I would like to thank Ms. Casey Stauber for all her help during the five years.

I would especially like to thank Dr. David J. Newman at the NCI for providing us extracts for the screening of anticancer drug leads. I would like to acknowledge Dr. Fred Valeriote at Wayne State University for performing anticancer bioassay, Dr. Pieter C. Dorrestein at University of California at San Diego for performing MALDI imaging mass spectrometry, Drs. Melissa Jacob and Shabana Khan at the National Center for Natural Product Research for performing antibacterial, antifungal, and antimalarial assays.

I also would like to acknowledge Dr. Robert J. Doerksen and his group members at the Department of Medicinal Chemistry, Dr. Angela I. Calderon at Auburn University for their contribution to Mtb kinase review; Dr. Seongbong Jo at the Department of Pharmaceutics for providing us the benzoquinone derivative; Mr. John Bowling for his help in acquiring NMR data; Dr. James W. Sims, Dr. Xia Yan, Ms. Amanda L. Waters, Ms. Alexis Fullmer, and Ms. Serena

Ellison for their efforts towards the collection, isolation, and identification of microbes from the Gulf of Mexico, screening of microbial extracts, as well as the large scale fermentation; Mr. Mohamed Albadry for providing kahalalide G.

I am grateful to all the previous and present members in our laboratory, students of the Department of Pharmacognosy, as well as my friends in Oxford for all their help and encouragement.

I sincerely appreciate Triton Biopharma, Kraft Food Global Inc., and the Graduate School of the University of Mississippi for financial support.

Last but not least, I would give my special thanks to all my family: my father, my mother, my brother, and my fiancé, for their selfless love. I could not finish my five years of study and research without their steady support.

TABLE OF CONTENTS

LIST OF TABLES

LIST OF FIGURES

LIST OF SCHEMES

PART I

EXPLORATION OF ANTICANCER LEADS FROM MARINE ORGANISMS

Cancer is the second leading cause of death worldwide. In 2008, around 12.7 million new cancer cases had been diagnosed worldwide, and 7.6 million people died of cancer. This accounted for 12.5% of all deaths.[1] According to the statistics published by the American Cancer Society from 2006 to 2012, the number of people being diagnosed with cancer each year is increasing in the U.S. **(Figure 1)**. However, deaths caused by cancer each year are stabilizing **(Figure 2)**. The 5-year relative rate of survival of cancer in the U.S. has increased from 49% in the 1980s to 67% in the 2000s,[1g] which can be directly attributed to the improvement of early diagnosis and treatments.

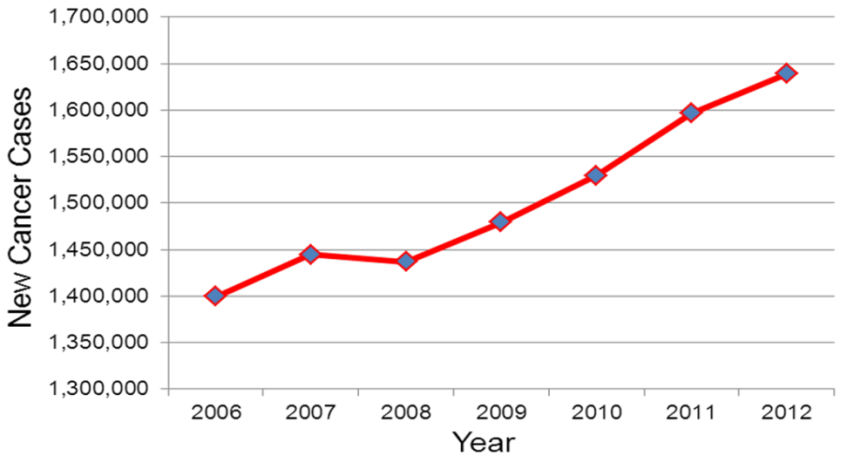

Figure 1 Estimated new cancer cases in the U.S from 2006-2012

Treatments for cancer include surgery, radiation therapy, chemotherapy, hormone therapy, and others such as targeted, biological and gene therapies. Major strategies of cancer treatment are surgery or radiation therapy followed by chemotherapy, or chemotherapy itself,[2] which reveals the reliance on chemotherapy for the treatment of cancer. However, chemotherapy has significant limitations. Chemotherapeutic drugs can also kill normal cells thus lacking selectivity. They might cause MDR as well. These problems result in serious side effects, immunity suppression, and poor treatment outcomes. Scientists are making great efforts to overcome these problems caused by chemotherapy. One approach is to use targeted therapies which target

kinases involved in the regulation of the cell cycle. In 2001, with the launch of a tyrosine kinase inhibitor imatinib (Gleevec/Glivec) registered by Novartis, cancer treatment was brought into a new era of targeted therapies. However, these types of inhibitors have been reported to acquire drug resistance in many clinical cases.[3] Efforts are now focusing on the exploration of a new generation of kinase inhibitors based on known mechanisms of acquired resistance. Other approaches include development of new molecules targeting hormone, MDR proteins which can be given in the combination with chemotherapy.

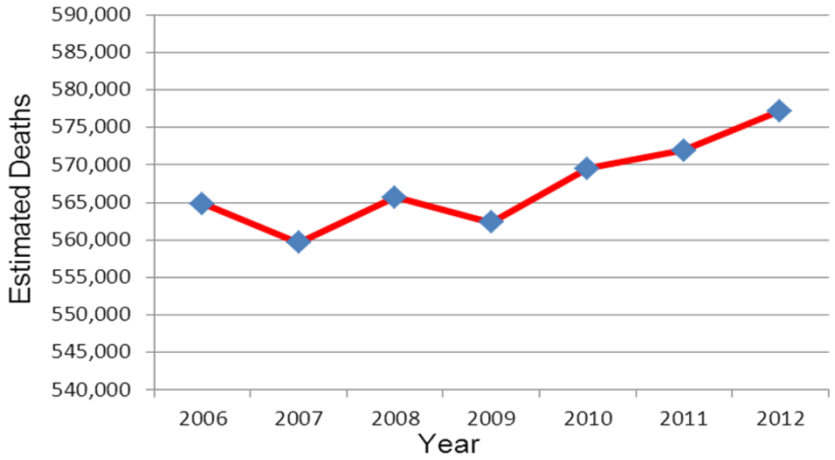

Figure 2 Estimated deaths in the U.S. from 2006-2012

After analyzing the current approaches for treating cancer, it is apparent that new molecules are needed to continue the fight. Major tools used in new drug development include the screening of drug leads from natural products and drug design based on combinatorial and rational strategies. Natural products provide a major source of new drug candidates. It is estimated that there are at least 250,000 species of higher plants around the world, while marine organisms are widely distributed over 70% of the earth's surface. All of these species are able to produce secondary metabolites with different activities due to defense, competition, or a number of other environmental reasons. In addition, combinatorial and rational methods need model compounds. These compounds are often chemically complex and would take humans years to

synthesize if they were ever considered as possibilities in the first place. As such natural products are becoming more and more important as lead compounds. From the 1940s to 2006, 175 anticancer drugs were discovered, among which 14% are natural products and 43% are derived from natural products by semisynthesis or using them as pharmacophore.[4] During the past two decades, the development of marine natural products as anticancer drugs has become a promising avenue for research. The first commercially available anticancer drug from a marine source was ecteinascidin-743 (Yondelis®) isolated from the Caribbean tunicate *Ecteinascidia turbinata*.[5] Four compounds isolated from marine sources including aplidine, bryostatin 1, spisulosine, and salinosporamide A, as well as eight synthetic compounds derived from marine products are under phase I or phase II clinical trials.[6] Other compounds such as didemnin B, dolastatin 10, kahalalide F, discodermolide, and girolline were discontinued due to toxicity or efficacy deficiencies. Considering the potency of the dropped compounds, however, modifications were conducted. One of the successful cases is soblidotin (TZT-1027) which was derived from dolastatin 10. Dolastatin 10 was isolated from the mollusk *Dolabella auricularia* with promising activity against several tumor cell lines.[7] It was dropped from the phase II clinical trial due to the lack of efficacy and its toxicity.[8,9] Its analogue soblidotin which is modified by removing the thiazole residue displayed higher potency.[10] Currently, soblidotin is under phase III clinical trials **(Figure 3)**. Another example is isoKF, an isomer of KF, of which the potency increased 10 times by switching the methyl group from C-5 to C-4 at the terminal fatty acid moiety. Kahalalide F will be discussed in detail in the first chapter.

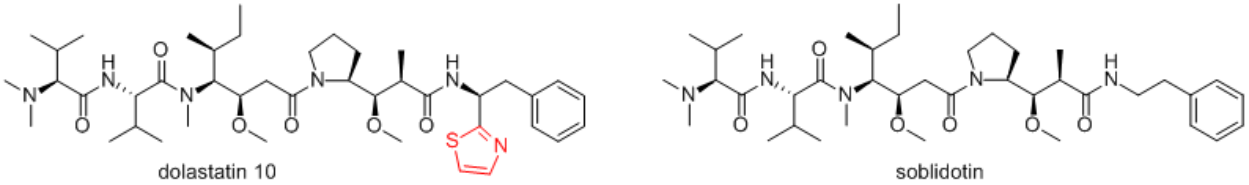

Figure 3 Structures of dolastatin 10 and soblidotin

Based on the examples of these marine-derived anticancer drugs, the general procedures of drug development from natural sources are summarized as in **Figure 4**. In the first part, three projects are involved in several steps in drug development from marine sources aimed to explore anticancer drug leads from marine organisms. They consist of the modification of anticancer drug candidate kahalalide F, isolation of new peptides from the mollusk *Elysia rufescens*, and anticancer drug leads from the NCI repository.

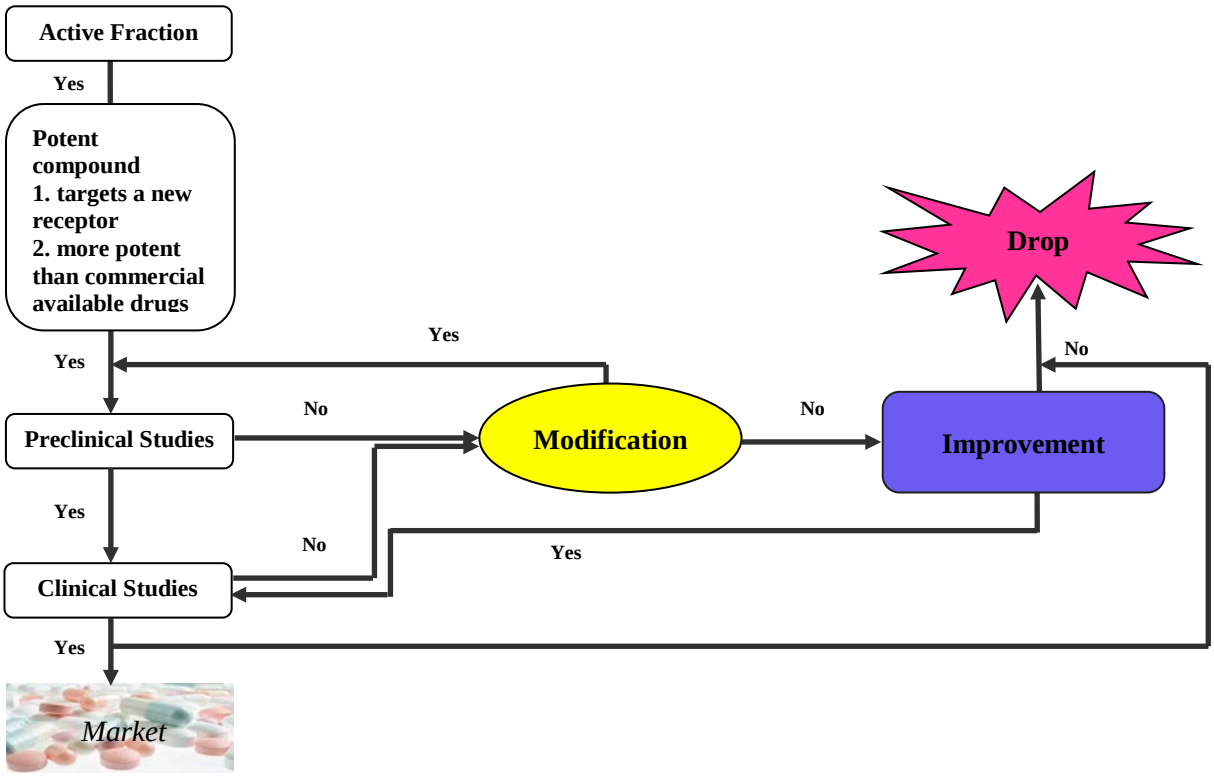

Figure 4 Procedures of drug development from natural sources

CHAPTER *1*

SEMISYNTHESIS OF KAHALALIDE F ANALOGUES AS POTENTIAL ANTICANCER AGENTS

1. Introduction

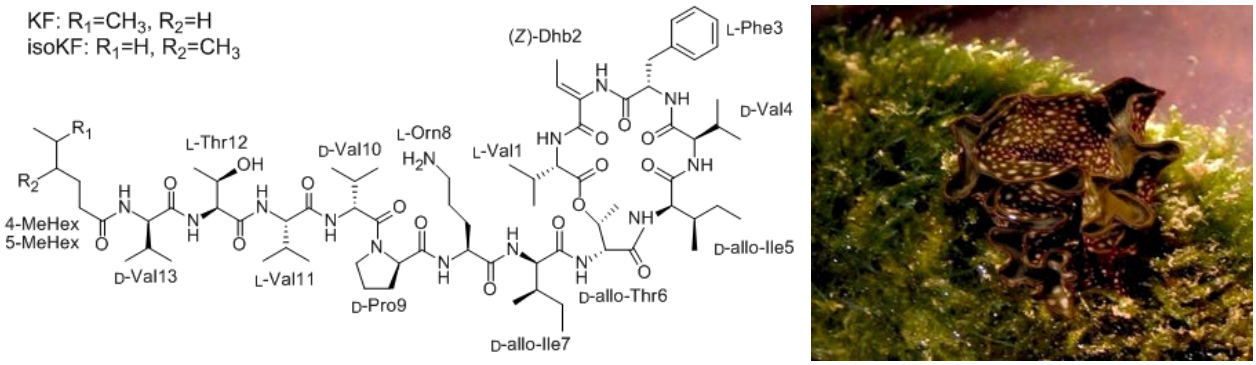

Figure 5 KF and isoKF from *Elysia rufescens* and *Bryopsis pennata*

Kahalalide F (KF), naturally occurring as a mixture with its isomer isoKF, is a depsipeptide isolated from the herbivorous marine mollusk *Elysia rufescens* and its algal diet *Bryopsis pennata* **(Figure 5)**.[11,12] The distribution of compounds in the snail and its *B. pennata* food source implied that they were accumulated from either the food source or probably a microbial association. Later studies suggested that the peptides are produced by a *Vibrio* sp. that associated with both *E. rufescens* and *B. pennata.*[13] The ^{13}C NMR spectra display an unequal ratio of these two isomers in algal, mollusk, and bacterium by comparing the presence of 4-/5-methyl group on the hexanoic lipid chain **(Figures 6-8)**. This also can explain the variance of KF production under different environments.

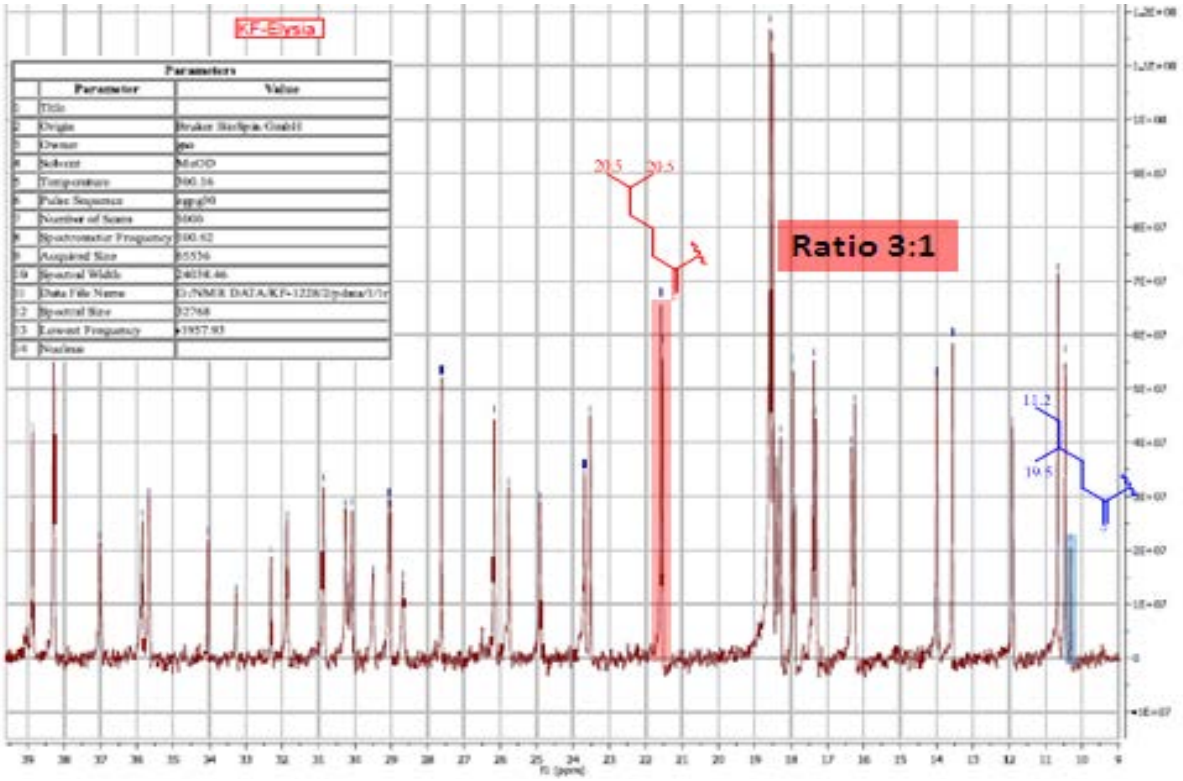

Figure 6 ^{13}C NMR spectrum of a mixture of KF and isoKF in *E. rufescens* at the ratio of 3:1

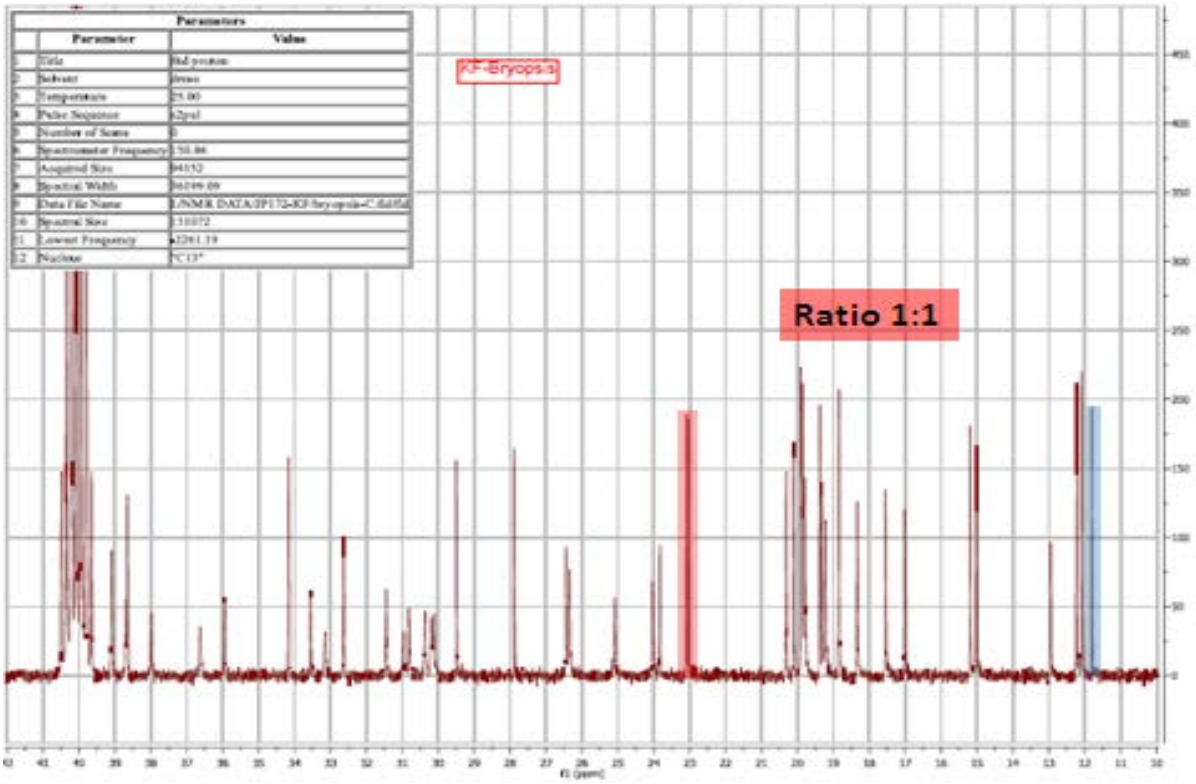

Figure 7 ^{13}C NMR spectrum of a mixture of KF and isoKF in *B. pennata* at the ratio of 1:1

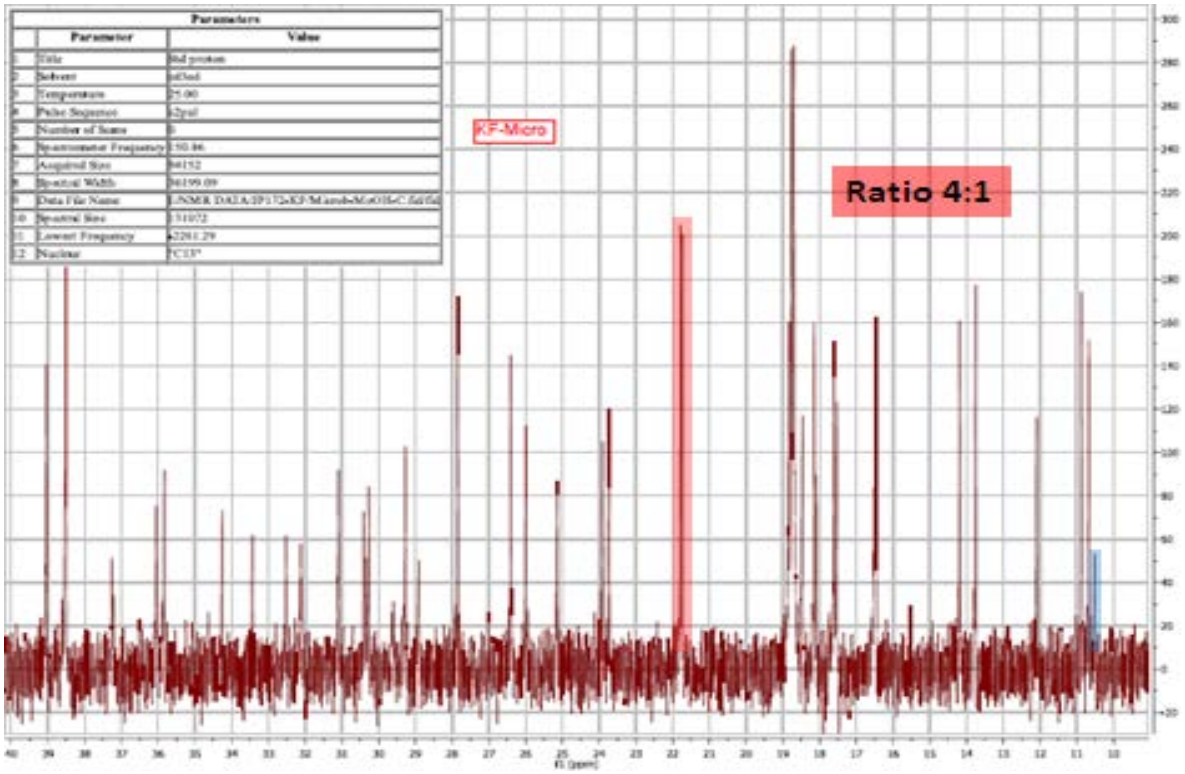

Figure 8 ^{13}C NMR spectrum of a mixture of KF and isoKF in a *Vibrio* sp. at the ratio of 4:1

Both KF and isoKF exhibit significant activity in vitro against human prostate, breast, non-small cell lung, and colon solid tumors.[11,12,14] They also showed activity against human prostate cancer xenografts.[14] The cytotoxicity of KF and isoKF did not correlate with the expression level of MDR1 in prostate and breast cancer, indicating their potential in the treatment of multiple drug resistant cancers.[15] The mechanism of them is not completely elucidated. In the NCI-COMPARE analysis which is used to compare the patterns of drug sensitivity in 60 human cancer cell lines between target molecule and compounds in the library, KF and isoKF appeared negative suggesting that they have a unique mode of action.[16] They interfere with cell lysosome organization.[17] Subsequently, they were shown to down-regulate ErbB3 and inhibit Akt signaling.[18] The ErbB family comprises epidermal growth factor receptor (EGFR) tyrosine kinases that function to mediate cell interactions. In humans, it contains four subfamilies, Her1/EGFR/ErbB1, Her2/ErbB2, Her3/ErbB3, and Her4/ErbB4. In cancer cells,

with an increasing release of EGF ligands that can bind to ErbB receptors, phosphorylation on specific tyrosine residues of ErbB receptors are induced, thus activating intracellular signaling pathways to promote cancer cell growth.[19] Inhibitors targeting the ErbB family displayed potency in cancer prevention.[20,21] Several ErbB1 and ErbB2 inhibitors have been approved for cancer treatment **(Table 1)**. An ErbB4 inhibitor, dacomitinib, developed by Pfizer has entered phase III clinical trials.[22] However, there is no ErbB3 inhibitor available thus far. KF and isoKF, therefore, could be promising candidates to target the ErbB3 receptor.

Table 1 ErbB inhibitors approved for cancer treatment

Year of approval	Name	Structure	Target
1998	Trastuzumab	Antibody	ErbB2
2003	Gefitinib	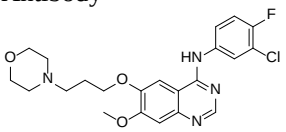	ErbB1
2004	Erlotinib	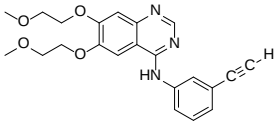	ErbB1
2004	Cetuximab	Antibody	ErbB1
2005	Panitumumab	Antibody	ErbB1
2007	Lapatinib	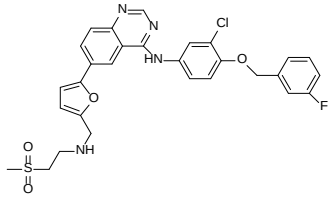	ErbB1, ErbB2
2011	Vandetanib	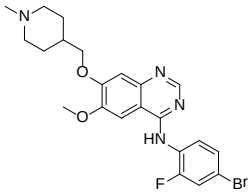	ErbB1
2012	Pertuzumab	Antibody	ErbB2

KF has completed phase I and phase II clinical trials to treat various solid tumors, such as melanoma, colorectal, no-small cell lung, pancreas, prostate cancers,[23,24,25] and psoriasis.[26] IsoKF was in a late phase I study with preliminary evidence of antitumor activity. However, both KF and isoKF were discontinued for treatment of cancers recently, in part due to a short half-life (35

minutes) and limited efficacy. One goal of this project was to modify KF to produce analogues with a higher potency, better delivery, or longer half-life. An SAR of over 130 KF analogues has been studied based on an SPPS approach by replacing different amino acid residues.[27,28] However, this total synthesis approach has several drawbacks. Although the SPPS technique is well developed, more than 29 steps were involved in the synthesis of KF and its analogues.[27] Challenges such as the peptide cyclization by coupling L-Phe3 with D-Val4 and the formation of *Z*-didehydroaminobutyric acid2 [(*Z*)-Dhb2] residue decreased the overall yield. Additionally, it is estimated to cost over one million dollars to synthesize 1 kg of KF partly due to the high cost of Fmoc-D-allo-Ile and Fmoc-D-allo-Thr. A semisynthetic approach based on natural KF isolated from *B. pennata* could provide a less expensive method to produce KF analogues. *B. pennata* is a potentially invasive green alga native in Hawaii.[29] When conditions are favorable, *B. pennata* grows quickly and becomes toxic to most herbivorous organisms due to its secondary metabolites, thus damaging the ecosystem.[29] During the algal bloom season, considerable quantities *B. pennata* is washed onto the seashore. Tons of algae producing kgs of the KF (0.003% yield[11]) can be collected easily. This approach can not only provide a sustainable resource of KF, but also benefit environmental improvement. Additionally, the discovery of a culturable bacterium provides another opportunity for the sustainable supply of KF.[13] Our group has synthesized several Orn- derivatives using the semisynthetic approach. Two analogues showed a similar or higher potency in selected cancer cell lines.[30,31] In this study, an addition of amino acid residue on the side chain, the modifications of L-Orn8 and L-Thr12, as well as the formation of a new cyclic peptide system were performed to produce KF analogues **1-15 (Figure 9)**.

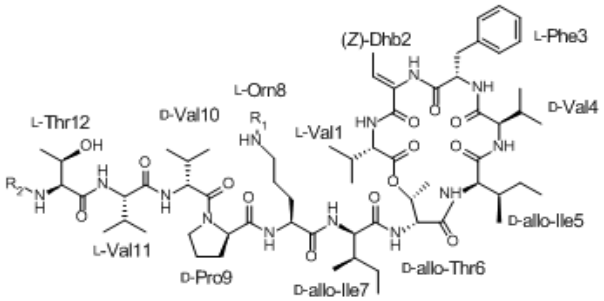

Compound	R_1	R_2	Compound	R_1	R_2
isoKF **(1)**	H	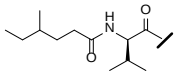	D-Phe14-isoKF **(7)**	H	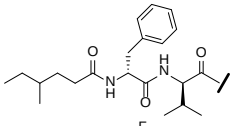
de-D-Val13-isoKF **(2)**	H	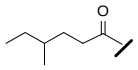	3,4-2F-D-Phe14-isoKF **(8)**	H	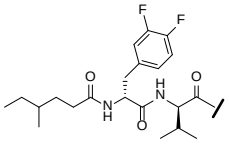
D-Val14-isoKF **(3)**	H	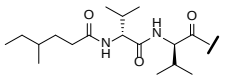	carbamyl-KF **(9)**		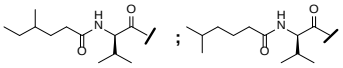
Val13-Val14-isoKF **(4)**	H	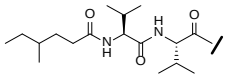	carbamyl-de-D-Val13-isoKF **(10)**		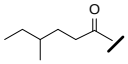
D-Leu14-isoKF **(5)**	H	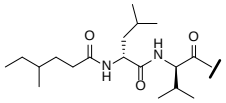	4Mecaproyl-de-D-Val13-isoKF **(11)**	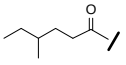	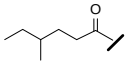
D-Pro14-isoKF **(6)**	H	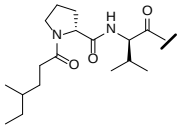	benzoquinone-KF **(15)**	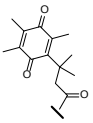	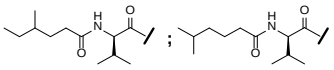

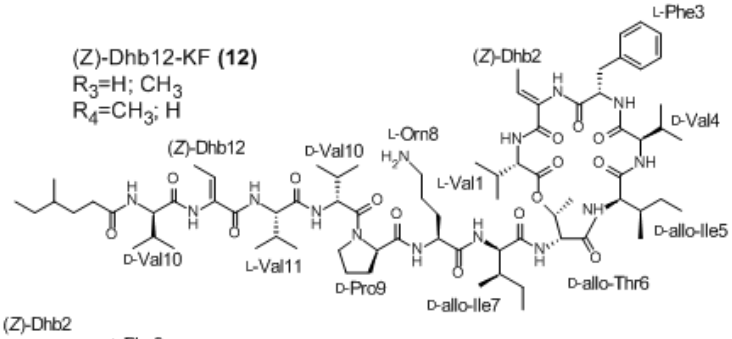

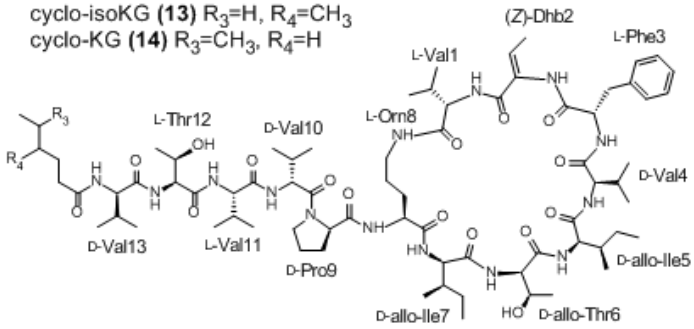

Figure 9 Structures of KF analogues

2. Results and Discussion

2.1 Amino Acid Chain Elongation of KF. According to the SAR study, KF analogues with focusing on halogenations of L-Phe3, modifications of L-Orn8, as well as replacements of L-Thr12 and MeHex with lower polar residues displayed an increase of activity or selectivity.[30,32] Moreover, the 4*S*-configured MeHex of the *N*-terminal aliphatic chain can improve the efficacy in the xenograft murine model.[33] The elongation of the *N*-terminal aliphatic chain caused increased activity,[32] which could be attributed to improvement of membrane permeability. However, no modification focused on elongation of the side chain of amino acid residues has been completed thus far. There was evidence that the substitution of D-configured amino acid residue with L-configured might lead to a loss or decrease of activity.[34] This is likely attributed to the preference of the D-amino acid on the target protein binding site over its L-amino acid counterpart.[35] In addition, introduction of the D-amino acids may prevent the degradation of peptides and consequently enhance the metabolic stability.[36] Therefore, elongation with nonploar amino acids, mostly D-configured, was explored. Considering that isoKF showed a better efficacy than KF in vivo, 4-MeHex was used as the side chain in all the analogues. An analogue with the deletion of D-Val13 **(2)** was prepared to compare the biological activity **(Table 2)**.

The amino group of L-Orn8 was protected using Fmoc-OSu. *N*-protected KF was hydrolyzed at the amide linkage between L-Thr12 and D-Val13 using MeOH – 6 M HCl (2:1) at 70 ℃ for 12 hours. The synthesis of *C*-terminal fragment was started with the formation of hexanoic succinimide ester by reacting 4-methylhexanoic acid with HOSu using anhydrous DCM in the presence of 2 eq. of EDCI for 2 days, followed by reaction with mono- or di-peptides. Final coupling reactions were performed between the Fmoc-KF hydrolysis product and the *C*-terminal fragment in anhydrous DMF using 5 eq. EDCI and HOBt for 2 days, followed by

the deprotection of the Fmoc group using 10% piperidine in DMF for 2 hours **(Scheme 1)**. The products were purified by HPLC. The overall yield (synthesis and purification) was 45.3%.

Table 2 Structures of KF analogues **1-8**

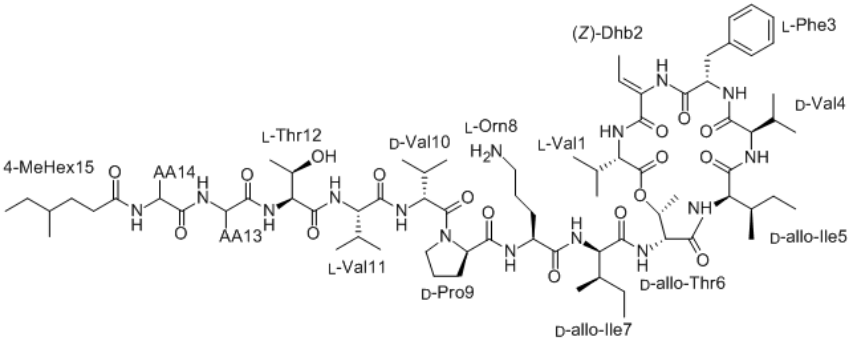

		isoKF (1)	**de-D-Val13-isoKF (2)**	**D-Val14-isoKF (3)**	**Val13-Val14-isoKF (4)**	**D-Leu14-isoKF (5)**	**D-Pro14-isoKF (6)**	**D-Phe14-isoKF (7)**	**3,4-2F-D-Phe14-isoKF (8)**
Structure	AA13	D-Val	-	D-Val	L-Val	D-Val	D-Val	D-Val	D-Val
	AA14	-	-	D-Val	L-Val	D-Leu	*trans*-D-Pro	D-Phe	3,4-2F-D-Phe

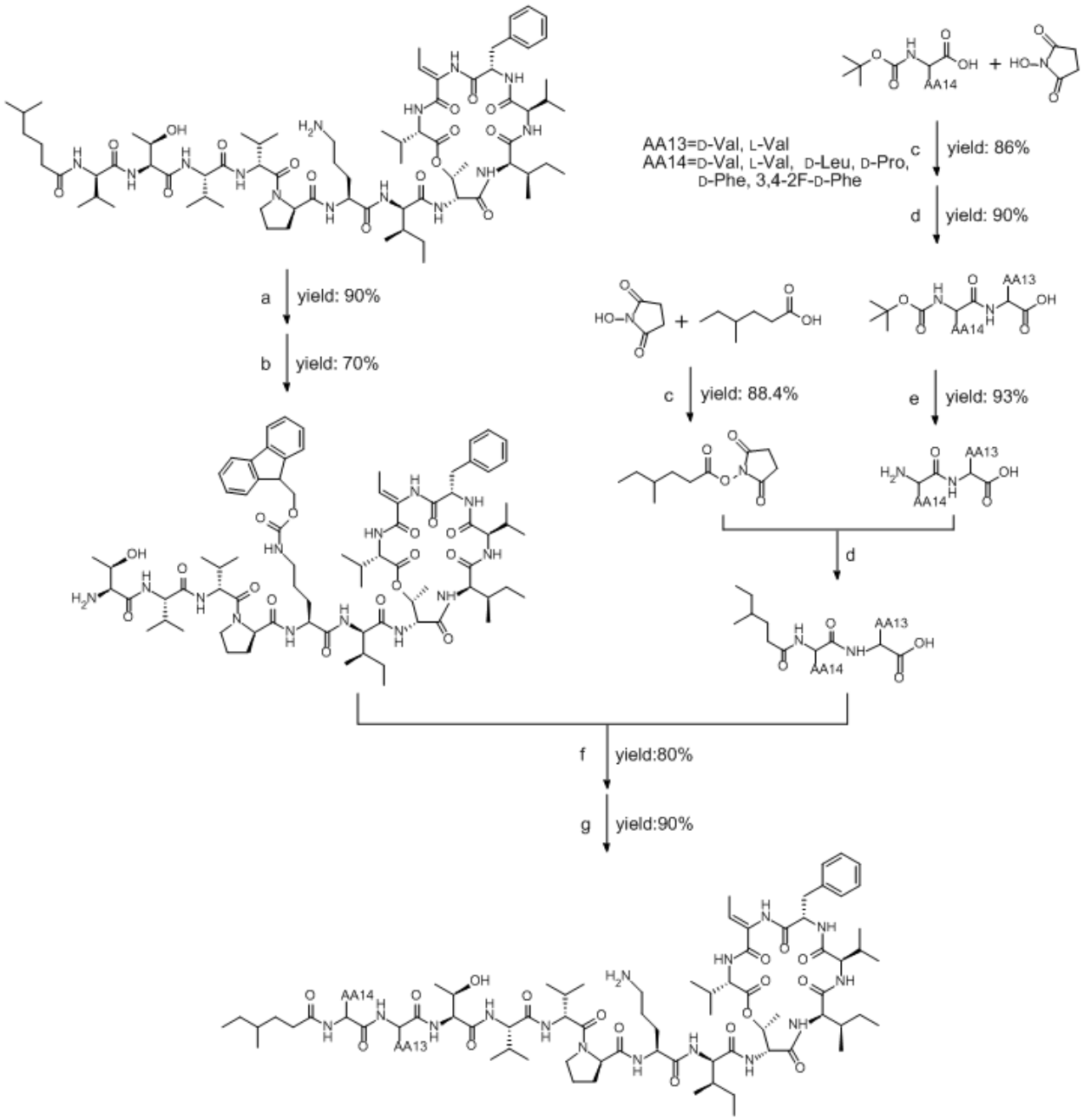

Scheme 1 Elongation of the amino acid chain of KF

When performing the partial hydrolysis of Fmoc-KF at 70-80 ℃, a cleavage of the amide bond between L-Thr12 and D-Val13 was predominant (70% yield). It is hypothesized that the release of the MeHex-D-Val13 fragment is kinetically faster than any other residue, which could

result from the presence of the hydroxy group of L-Thr12. The proposed mechanism of the partial hydrolysis is based on N→O acyl rearrangement.[37] The oxygens on the amide carbonyl groups would be protonated under acidic conditions. Only when the nucleophilic β-hydroxy group interacts with the carbonyl of D-Val13, a hydroxyoxazolidine could be formed as an intermediate, followed by acyl rearrangement to produce an ester which is more easily hydrolyzed than the amide linkage **(Scheme 2)**.

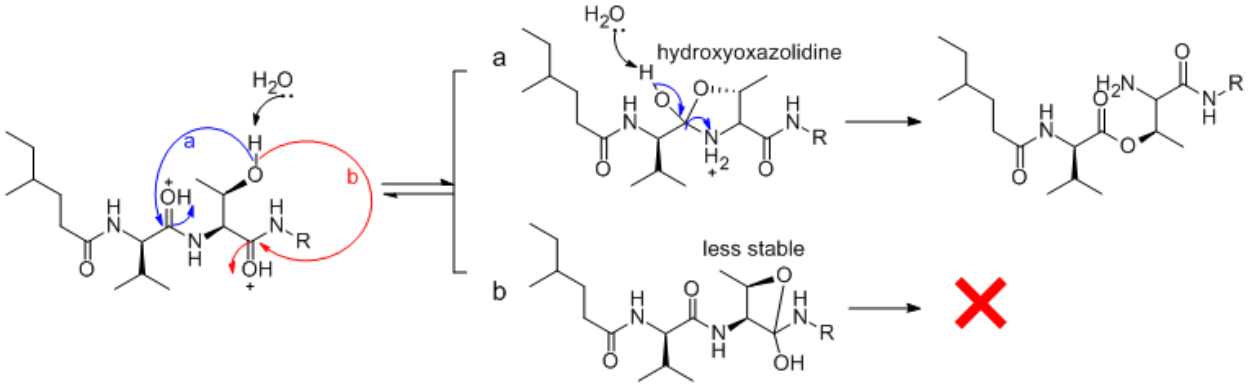

Scheme 2 Proposed mechanism of the partial hydrolysis of Fmoc-KF

In the amidation reaction, EDCI was used as a coupling reagent and HOBt as an activator to improve the yield of the reactions **(Scheme 3)**. The amino group may be deprotonated in the presence of a base, thus facilitating the reaction. However, even a weak base has the potential to cause the racemization of amino acid residues by attacking the α-proton on the amino acid residues **(Scheme 4)**. Hence, the presence of base was avoided in the reactions. Another key factor in the amidation is to keep the reaction in an anhydrous condition, especially in a small-scale coupling reaction. Even a small amount of water could cause a low yield of the amide product. The challenge was that most of the synthetic *C*-terminal fragments were obtained as sticky solid, from which the water is difficult to remove. Therefore, an excess, mostly 5 eq. of EDCI was applied. An excess of EDCI is capable of absorbing water in the reagent or solvent to form a urea, thus facilitating the coupling reaction **(Scheme 5)**.

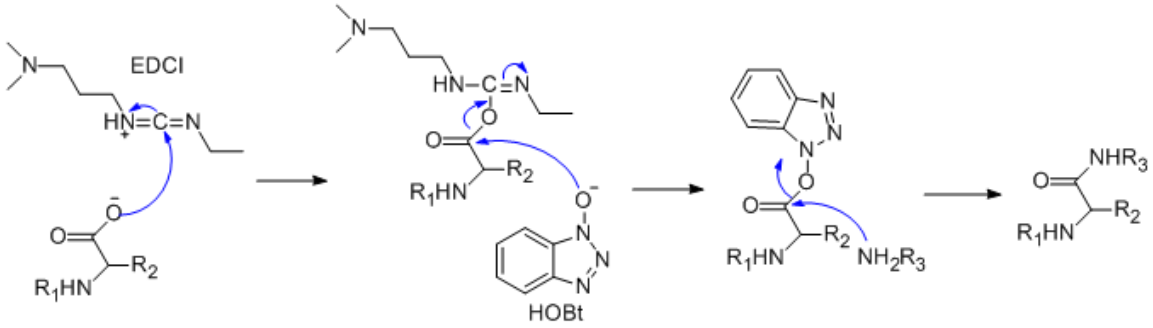

Scheme 3 Mechanism of EDCI coupling

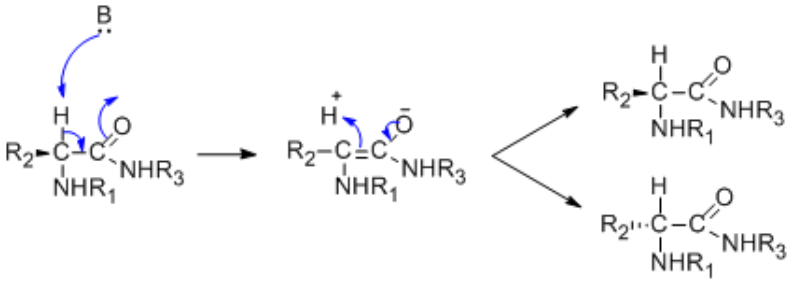

Scheme 4 Mechanism of racemization of peptide

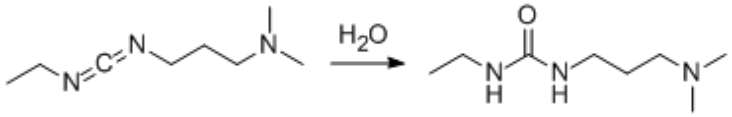

Scheme 5 Formation of a urea when EDCI reacting with water

The structures of amino acid elongation analogues are confirmed with HRMS, ^{1}H, ^{13}C, and/or HSQC NMR overlay experiments. Product **1** is the semisynthetic isoKF. It provided the same quasi-molecular ion signals as KF of $[M+2H]^{2+}$ at *m/z* 739.4842, $[M+H+Na]^{2+}$ at *m/z* 750.4757, $[M+H]^{+}$ at *m/z* 1477.9453 for a molecular formula of $C_{75}H_{125}N_{14}O_{16}$ (calc. 1477.9393, Δ +4.1 ppm) **(Figure 10)**. The only difference between **1** and natural KF is that the aliphatic chain of natural KF is a mixture of 4-MeHex and 5-MeHex, while that of **1** is 4-MeHex. The ^{1}H NMR spectrum of **1** did not show significant difference with KF **(Figure 11)**. However, comparison of the ^{13}C NMR spectra between **1** and KF suggested that signals at δ_C 22.84, 22.89, 23.61, 27.66, 35.74, 39.13, and 172.98, which are corresponding to 5-MeHex, were missing from **1 (Figures 12, 13)**. Therefore, the structure of **1** was confirmed.

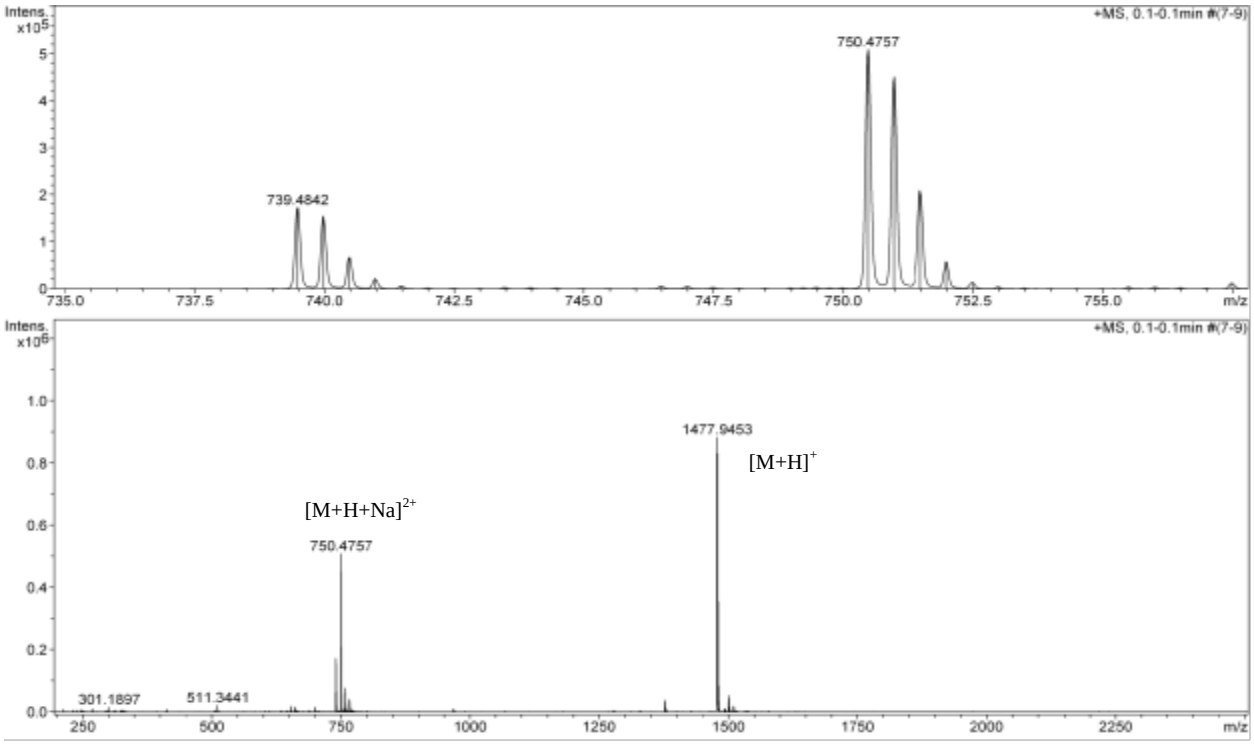

Figure 10 HRMS spectrum of isoKF **(1)**

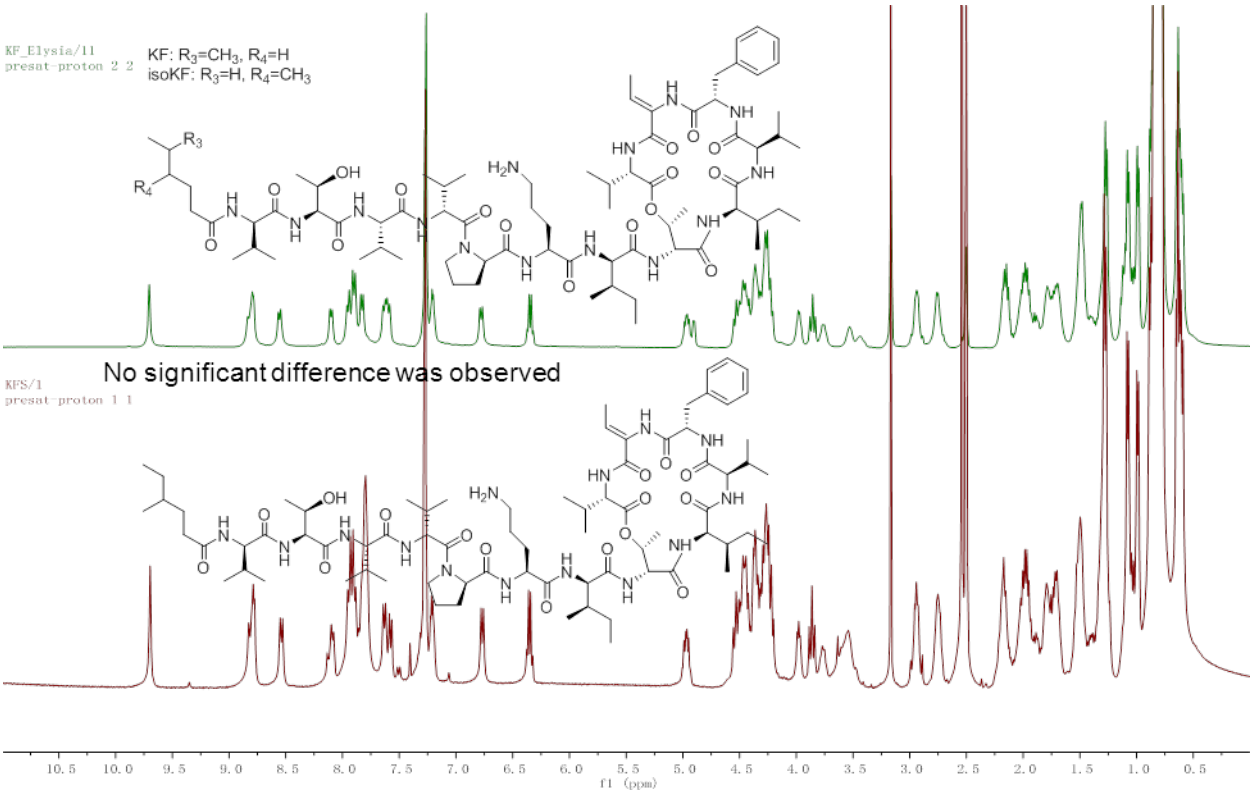

Figure 11 ^{1}H NMR spectra of KF (top) and isoKF **(1)** (bottom) in DMSO-d_6

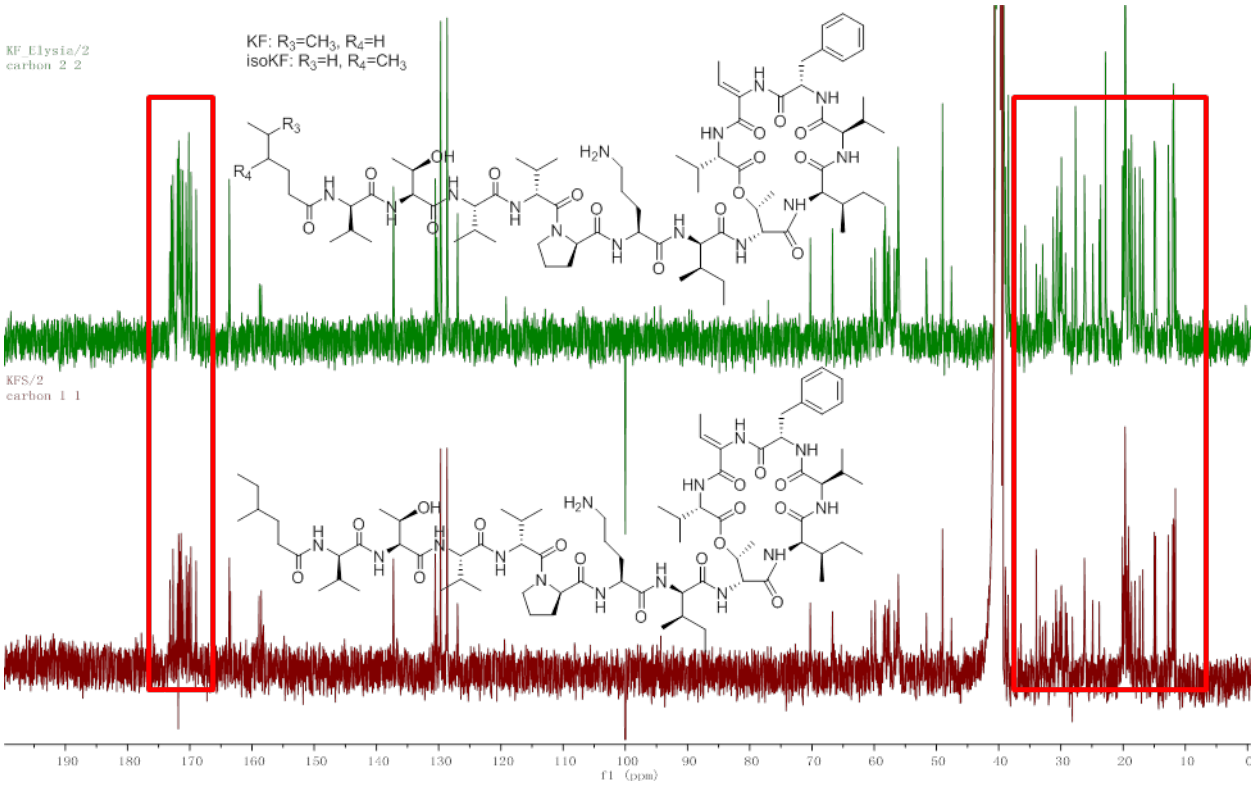

Figure 12 ^{13}C NMR spectra of KF (top) and isoKF **(1)** (bottom) in DMSO-d_6

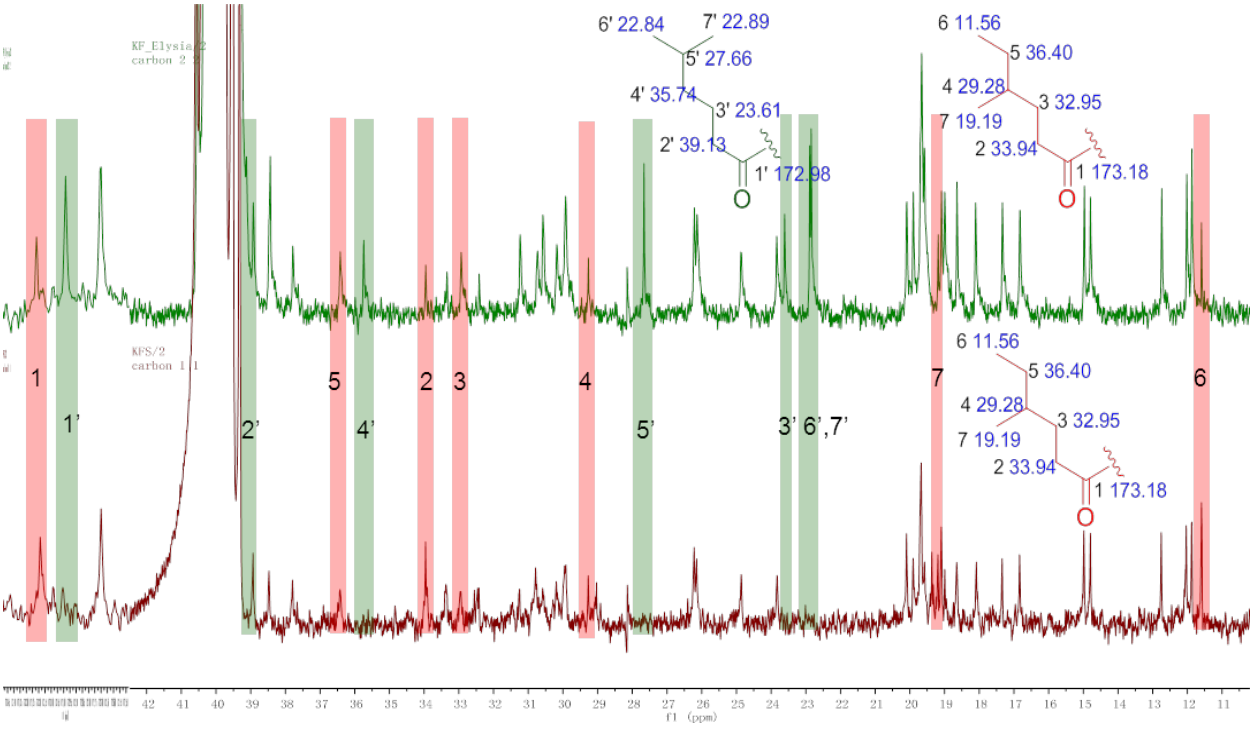

Figure 13 ^{13}C NMR spectra (δ_C 10-40, 165-175) of KF (top) and isoKF **(1)** (bottom)

De-D-Val13-isoKF **(2)** is a molecule with the deletion of D-Val13 compared to isoKF. The analogue provided quasi-molecular ion signals of $[M+H+Na]^{2+}$ at *m/z* 711.8873, $[M+Na]^{+}$ at *m/z* 1400.8471 for a molecular formula of $C_{70}H_{115}N_{13}NaO_{15}$ (calc. 1400.8533, Δ -4.4 ppm) **(Figure 14)**. Comparison of the ^{13}C NMR spectra between isoKF and **2** suggested that **2** lost the signals at δ_C 18.60, 19.86, 28.16, 58.20, and 171.97 representing the residue D-Val13 **(Figures 15-17)**. Carbonyl groups at δ_C 173.19, 171.39, 170.24, and 170.15 corresponding to 4-MeHex, L-Thr12, L-Val11, and D-Val10 shifted downfield due to the deletion of D-Val13.

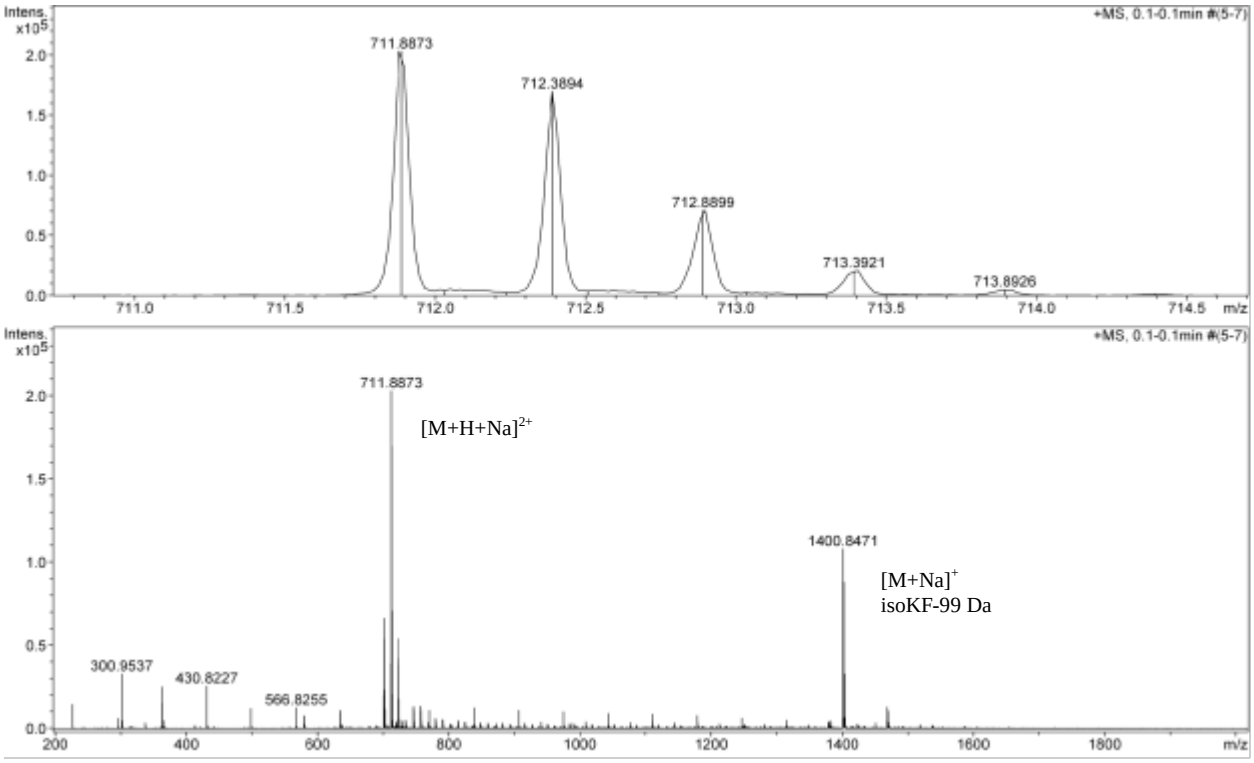

Figure 14 HRMS spectrum of de-D-Val13-isoKF **(2)**

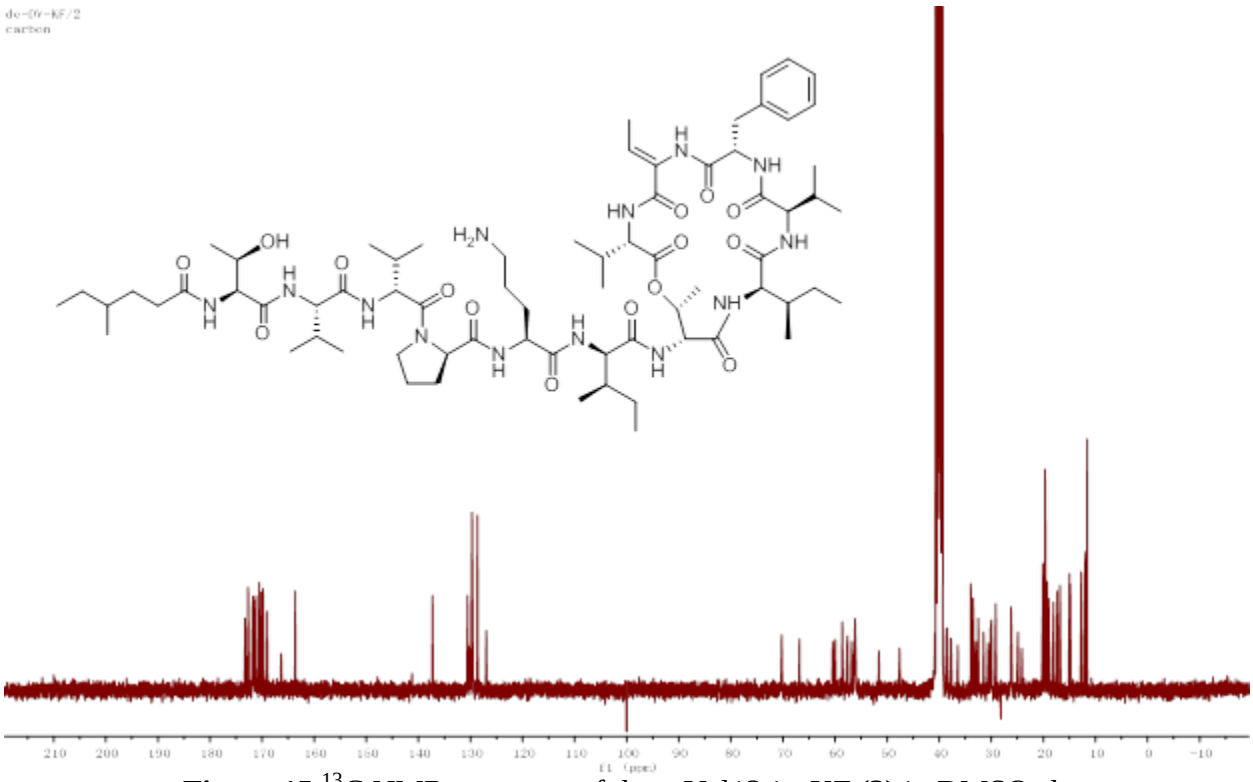

Figure 15 ^{13}C NMR spectrum of de-D-Val13-isoKF **(2)** in DMSO-d_6

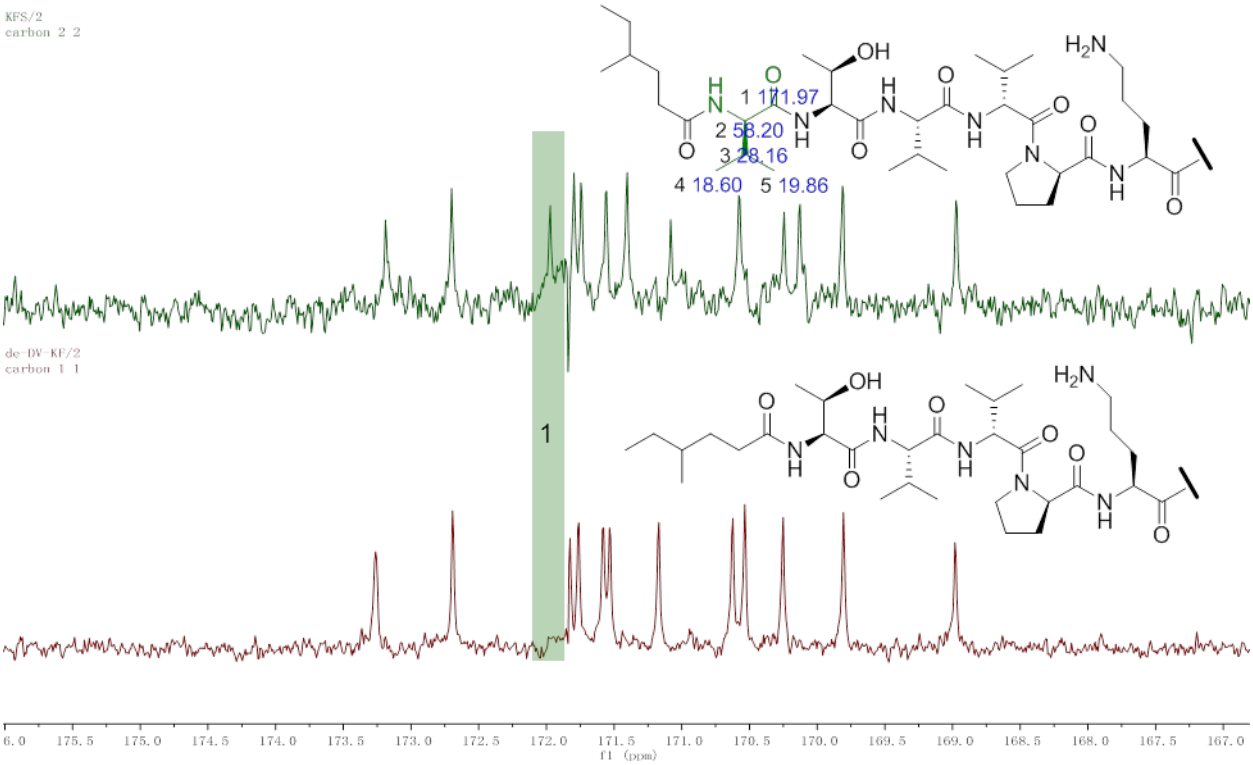

Figure 16 ^{13}C NMR spectra (δ_C 166-176) of isoKF (top) and de-D-Val13-isoKF **(2)** (bottom)

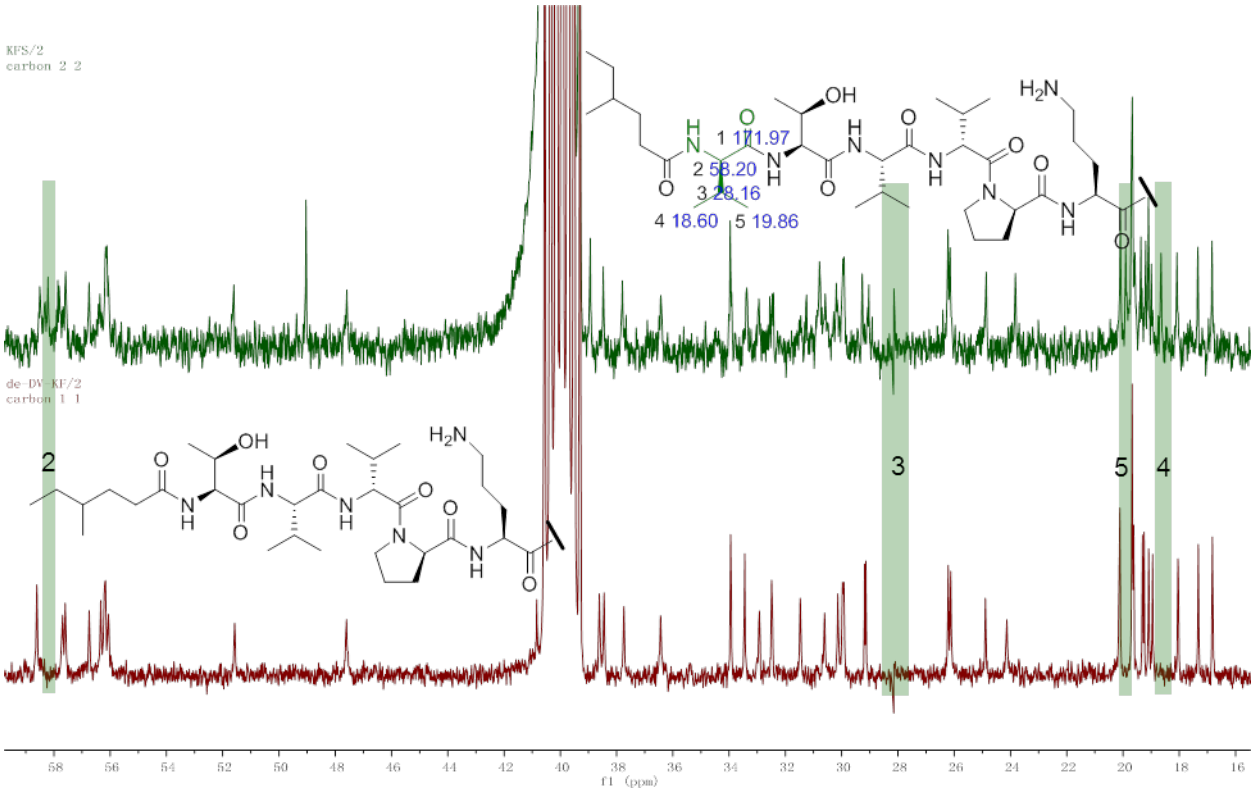

Figure 17 ^{13}C NMR spectra (δ_C 16-60) of isoKF (top) and de-D-Val13-isoKF **(2)** (bottom)

D-Val14-isoKF **(3)** is the molecule with an addition of D-Val14 compared to isoKF, and Val13-Val14-isoKF **(4)** is the molecule replacing D-Val13 and D-Val14 of D-Val14-isoKF **(3)** with L-Val13 and L-Val14. They provided quasi-molecular ion signals $[M+H]^+$ at *m/z* 1577.0082, 1577.0137, respectively, for the same molecular formula of $C_{80}H_{134}N_{15}O_{17}$ (calc. 1577.0077, Δ +0.3 ppm, +3.8 ppm, respectively) **(Figures 18, 21)**. An HSQC overlay experiment as well as comparison of the ^{13}C NMR chemical shift in amide carbonyl and α-carbon regions between isoKF and **3, 4** did not show significant differences **(Figure 19)**. This could result from similar chemical shifts of added Val residue with D-Val13. However, additional methyl groups at δ_C 18.29 and 19.75 in **3**, δ_C 18.31 and 19.74 in **4** suggested the presence of one more Val residue **(Figures 20, 22)**.

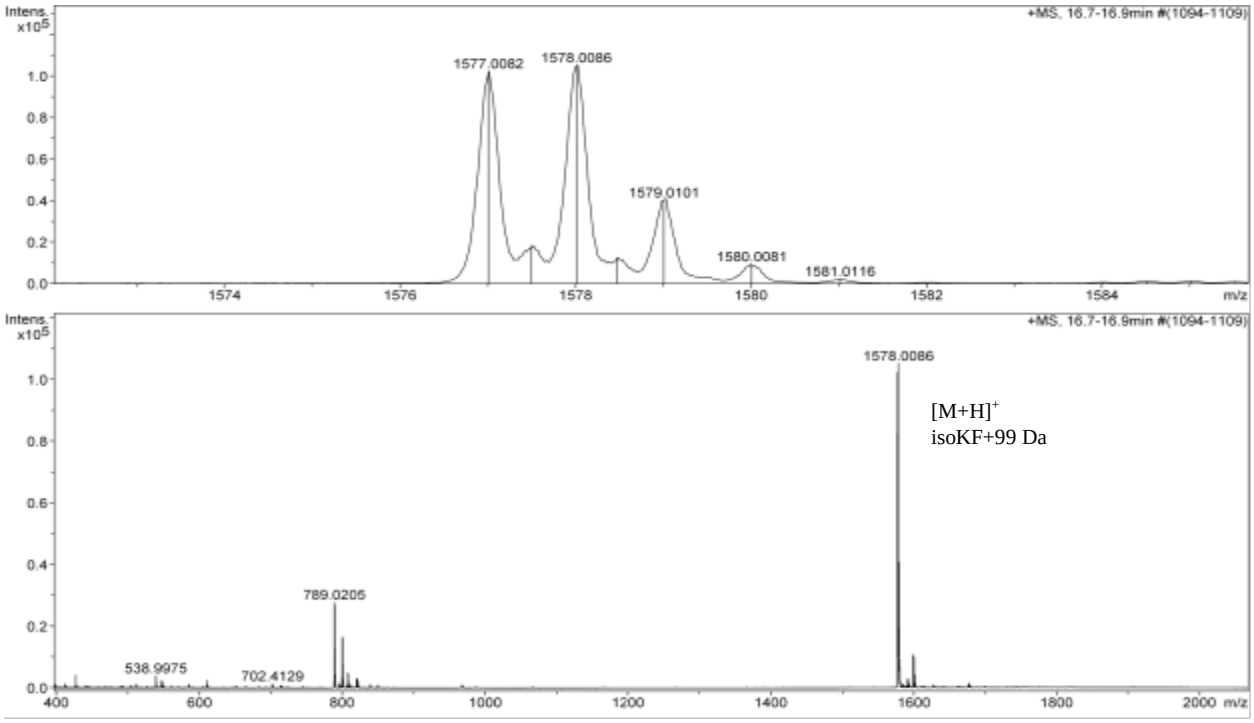

Figure 18 HRMS spectrum of D-Val14-isoKF **(3)**

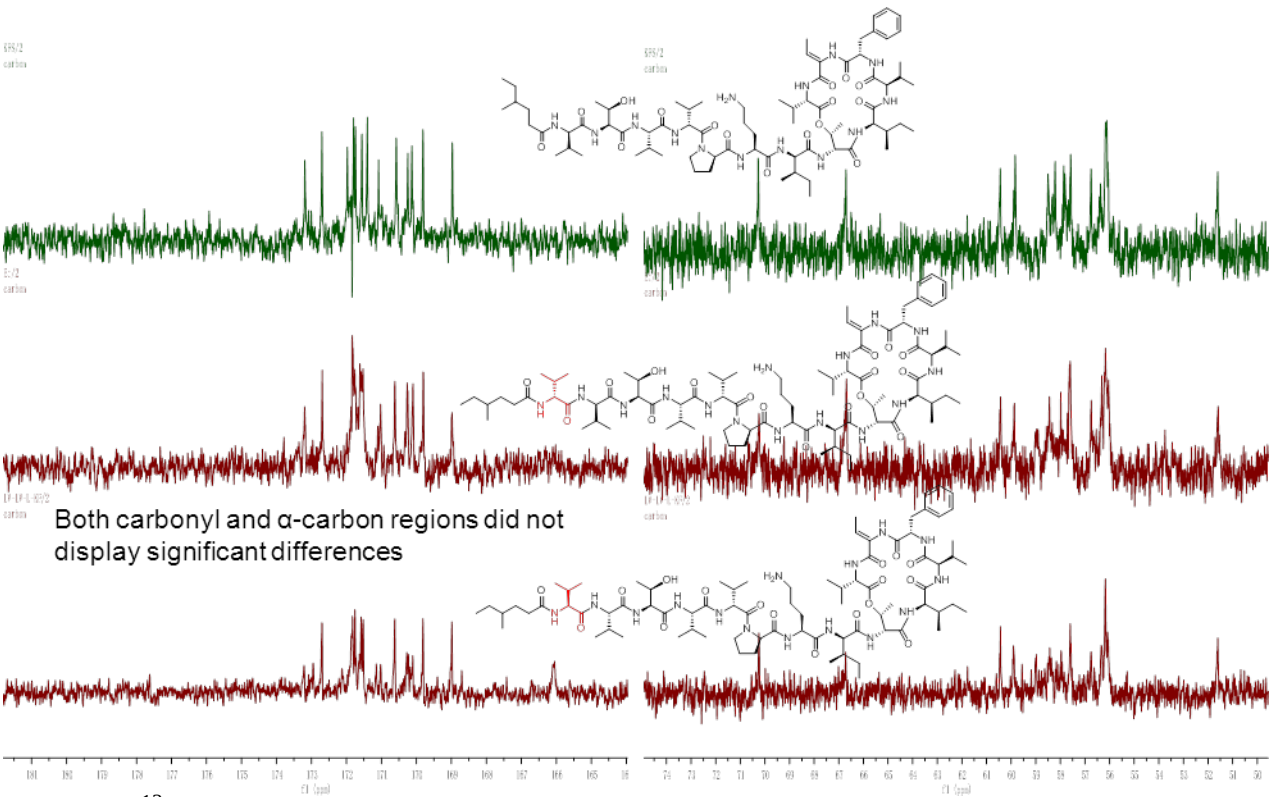

Figure 19 ^{13}C NMR spectra in carbonyl and α-carbon regions of isoKF (top), D-Val14-isoKF **(3)** (middle), and Val13-Val14-isoKF **(4)** (bottom)

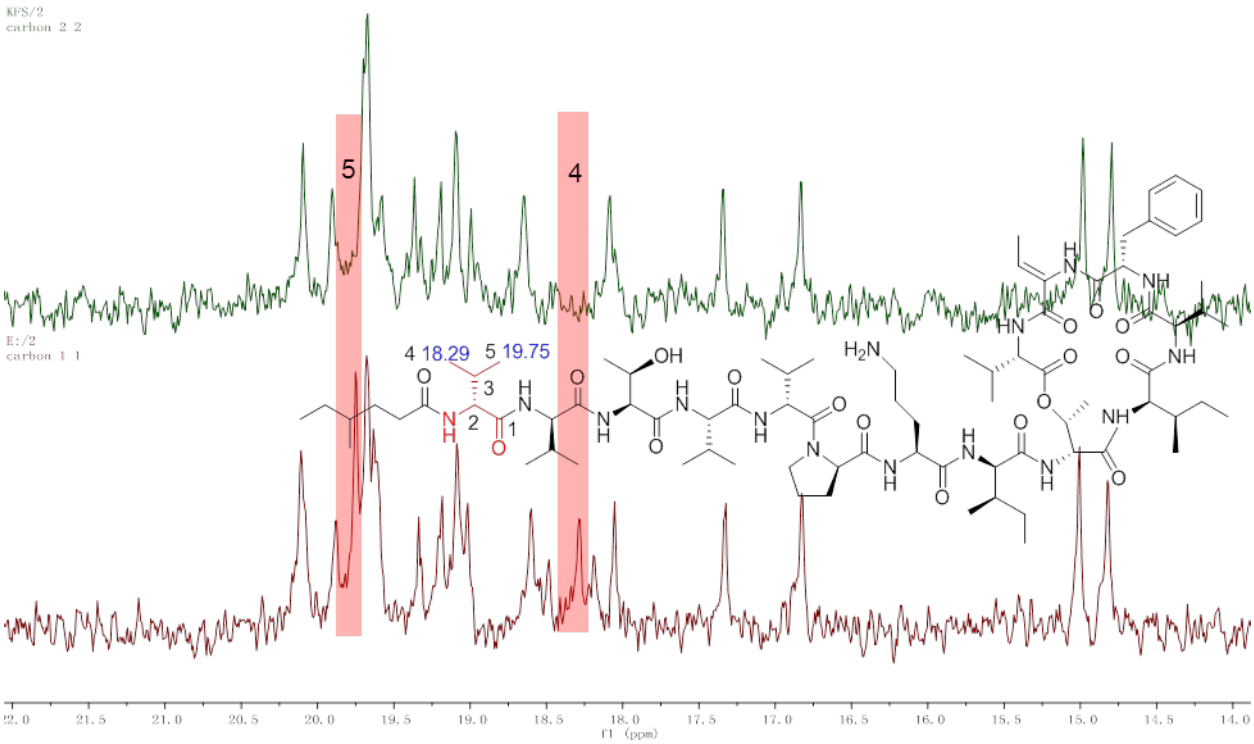

Figure 20 ^{13}C NMR spectra (δ_C 14-22) of isoKF (top) and D-Val14-isoKF **(3)** (bottom)

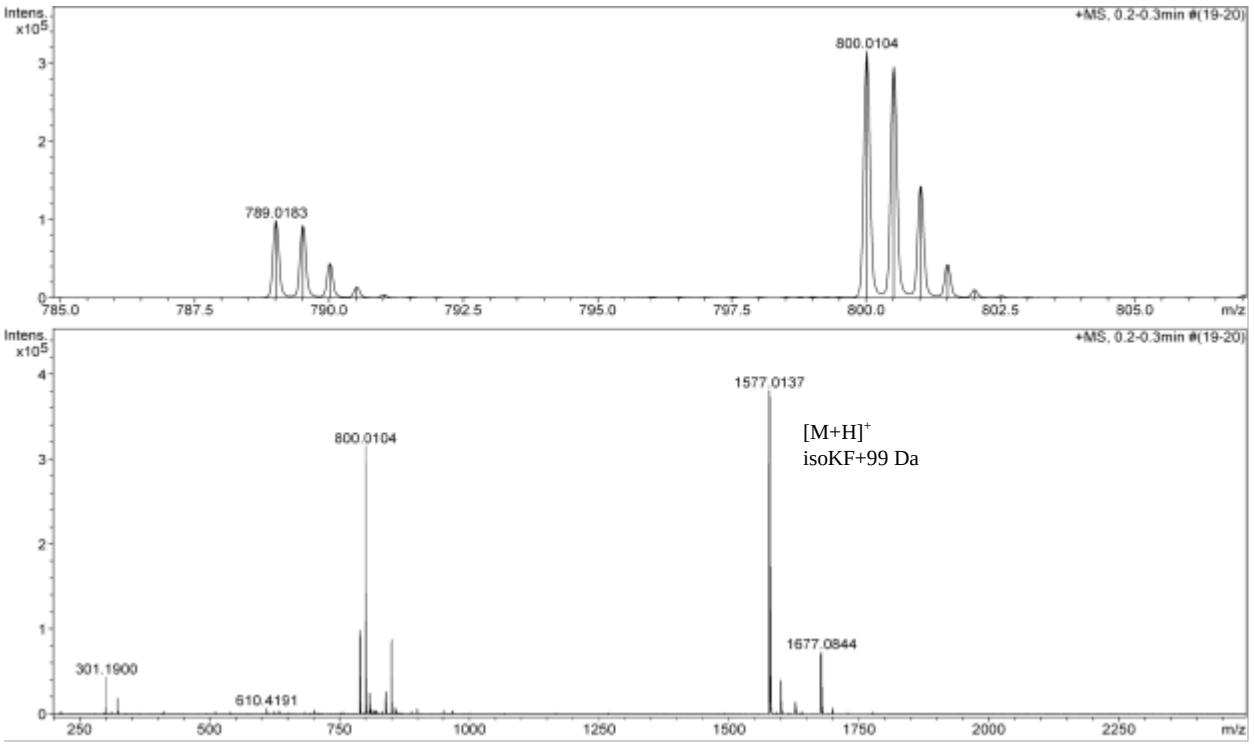

Figure 21 HRMS spectrum of Val13-Val14-isoKF **(4)**

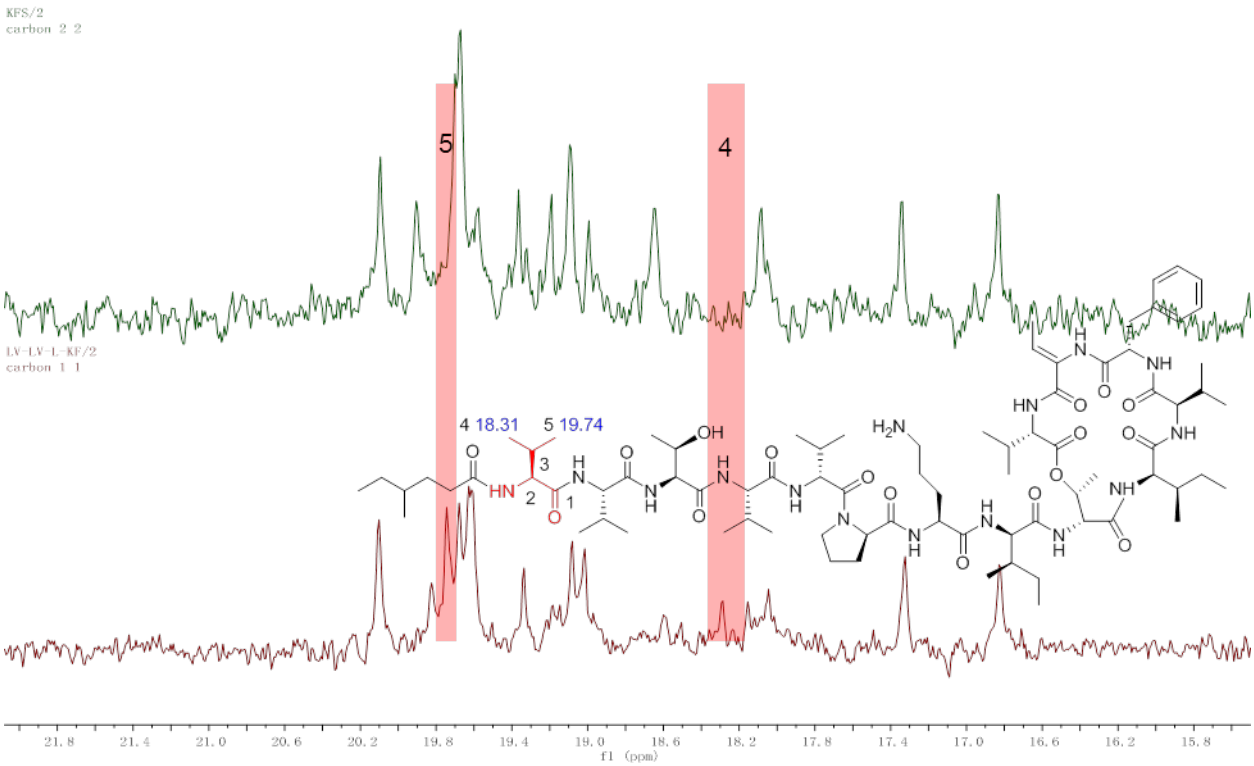

Figure 22 ^{13}C NMR spectra (δ_C 16-22) of isoKF (top) and Val13-Val14-isoKF **(4)** (bottom)

D-Leu14-isoKF **(5)**, D-Pro14-isoKF **(6)**, D-Phe14-isoKF **(7)**, and 3,4-2F-D-Phe14-isoKF **(8)** provided a quasi-molecular ion $[M+H]^+$ or $[M+Na]^+$ signal corresponding to their molecular formula, respectively **(Table 3; Figures 23, 25, 27, 30)**. Their HSQC overlay experiments with isoKF suggested an addition of one amino acid residue **(Figures 24, 26, 29, 32)**. It was observed that in D-Phe14-isoKF **(7)** and 3,4-2F-D-Phe14-isoKF **(8)**, carbon signals at δ_C 29.08, 29.17, 32.42, 32.47, 33.34, 33.98 corresponding to C-2, C-3 and C-4 at both 4*S*- and 4*R*- MeHex shifted upfield **(Figures 28, 31)**. This shielding effect due to the adjacent aromatic ring system confirmed the structures of **7** and **8**.

Table 3 ^{1}H and ^{13}C NMR data of additional amino acid residues of **5-8** [a] (δ in ppm, DMSO-d_6)

Compound	HRMS	Formula	Amino acid	Carbon	δ_C, mult	δ_C, mult
D-Leu14-isoKF (5)	1591.0335 $[M+H]^+$	$C_{81}H_{136}N_{15}O_{17}$	D-Leu 14	1	172.85, qC	
				2	51.45, CH	4.36, m
				3	41.26, CH_2	1.41, 1.48, m
				4	24.96, CH	1.58, m
				5	23.20, CH_3	0.86, m
				6	22.17, CH_3	0.83, m
D-Pro14-isoKF (6)	1596.9690 $[M+Na]^+$	$C_{80}H_{131}N_{15}NaO_{17}$	D-Pro 14	1	172.18, qC	
				2	59.65, CH	4.49, m
				3	31.85, CH_2	2.00, 2.26, m
				4	26.49, CH_2	1.36, 1.51, m
				5	46.48, CH_2	3.38, 3.52, m
D-Phe14-isoKF (7)	1625.0131 $[M+H]^+$	$C_{84}H_{134}N_{15}O_{17}$	D-Phe 14	1	171.41, qC	
				2	54.10, CH	4.60, m
				3	37.48, CH_2	2.75, 3.05, m
				4	138.67, qC	
				5,5'	129.56, CH	7.15, m
				6,6'	128.29, CH	7.17, m
				7	126.53, CH	7.20, m
3,4-2F-D-Phe14-isoKF (8)	1660.9999 $[M+H]^+$	$C_{81}H_{132}F_2N_{15}O_{17}$	3,4-2F-D-Phe 14	1	171.48, qC	
				2	54.09, CH	4.62, m
				3	37.14, CH_2	2.72, 2.98, m
				4	136.24, qC	
				5	117.3, CH	7.26, m
				6	149.46, qC	
				7	148.45, qC	
				8	118.58, CH	7.30, m
				9	126.48, CH	7.07, m

[a] Assignments based on ^{1}H, ^{13}C, and HSQC NMR (100/400 MHz) experiments at room temperature.

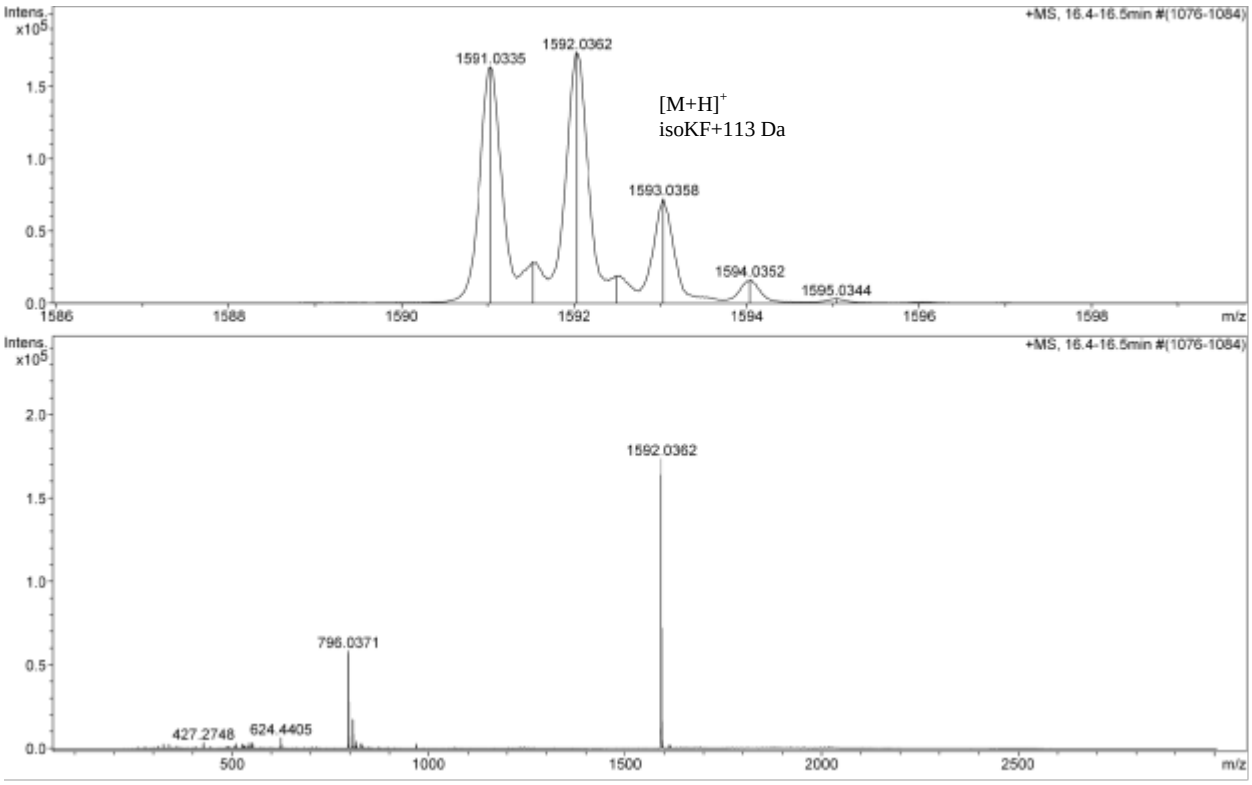

Figure 23 HRMS spectrum of D-Leu14-isoKF **(5)**

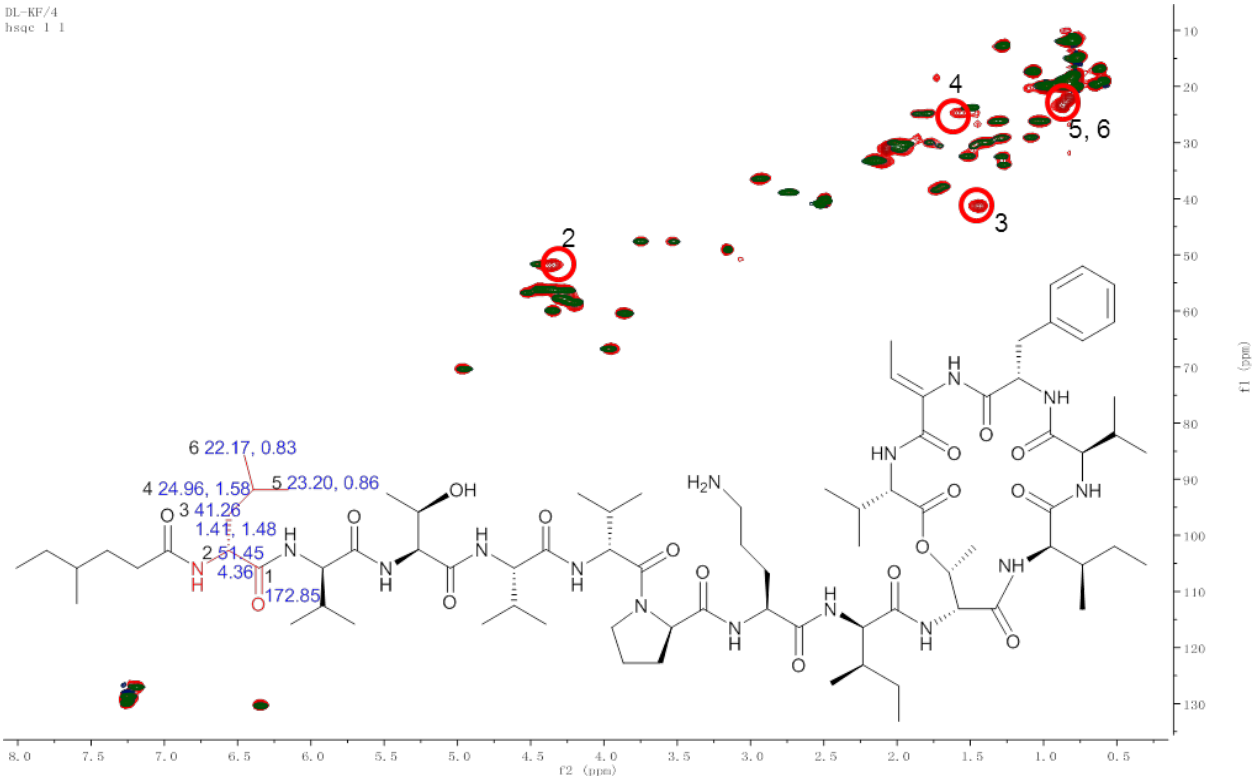

Figure 24 HSQC spectra overlay of isoKF (green) and D-Leu14-isoKF **(5)** (red) in DMSO-d_6

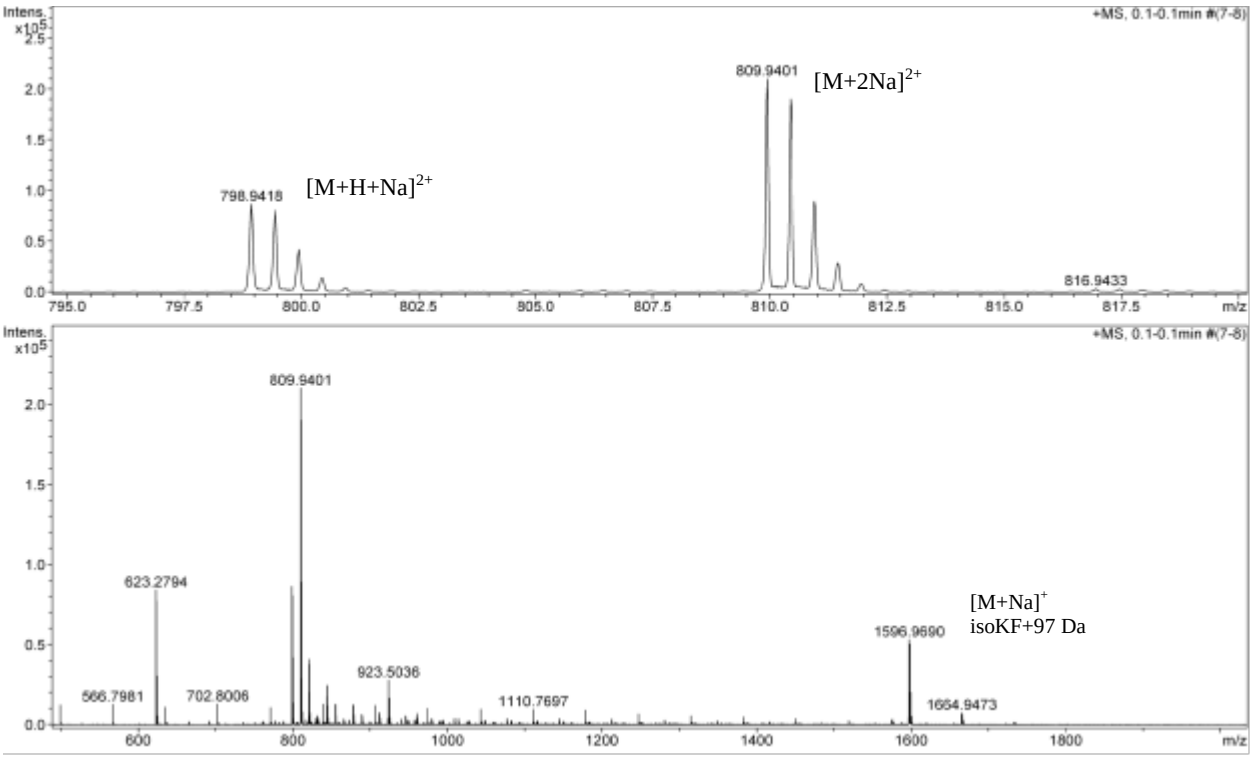

Figure 25 HRMS spectrum of D-Pro14-isoKF **(6)**

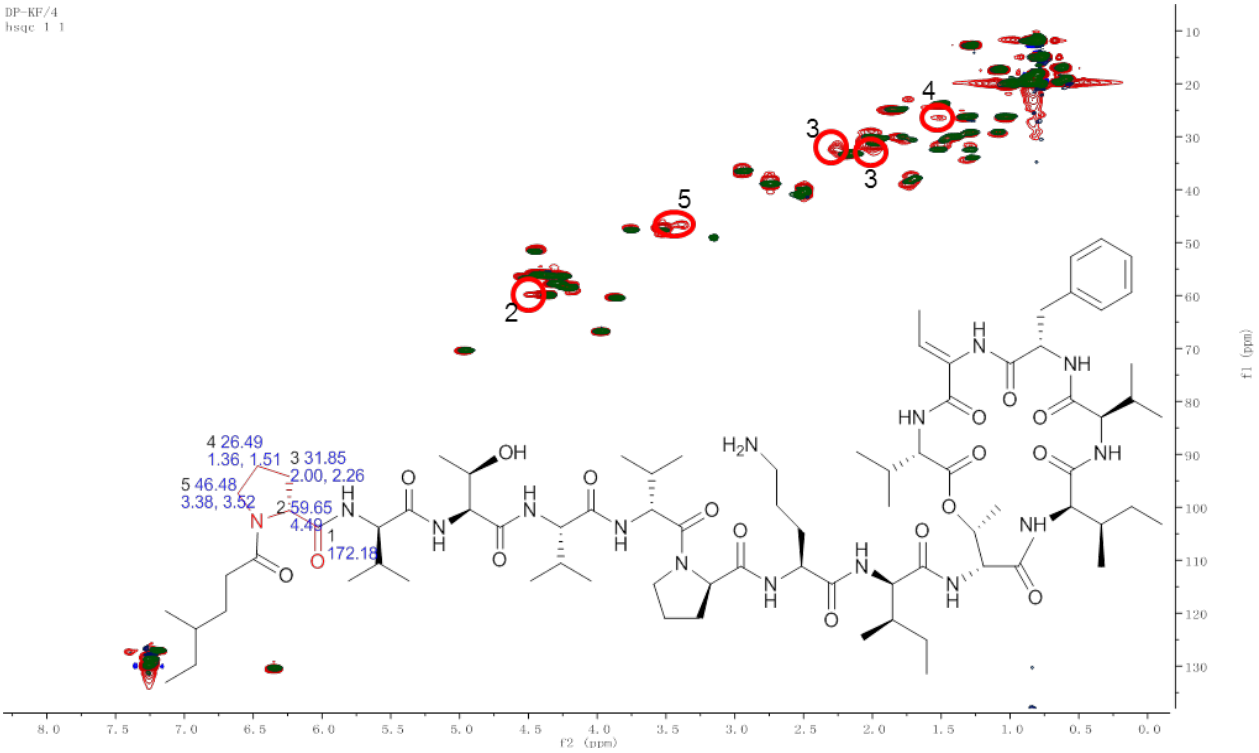

Figure 26 HSQC spectra overlay of isoKF (green) and D-Pro14-isoKF **6** (red) in DMSO-d_6

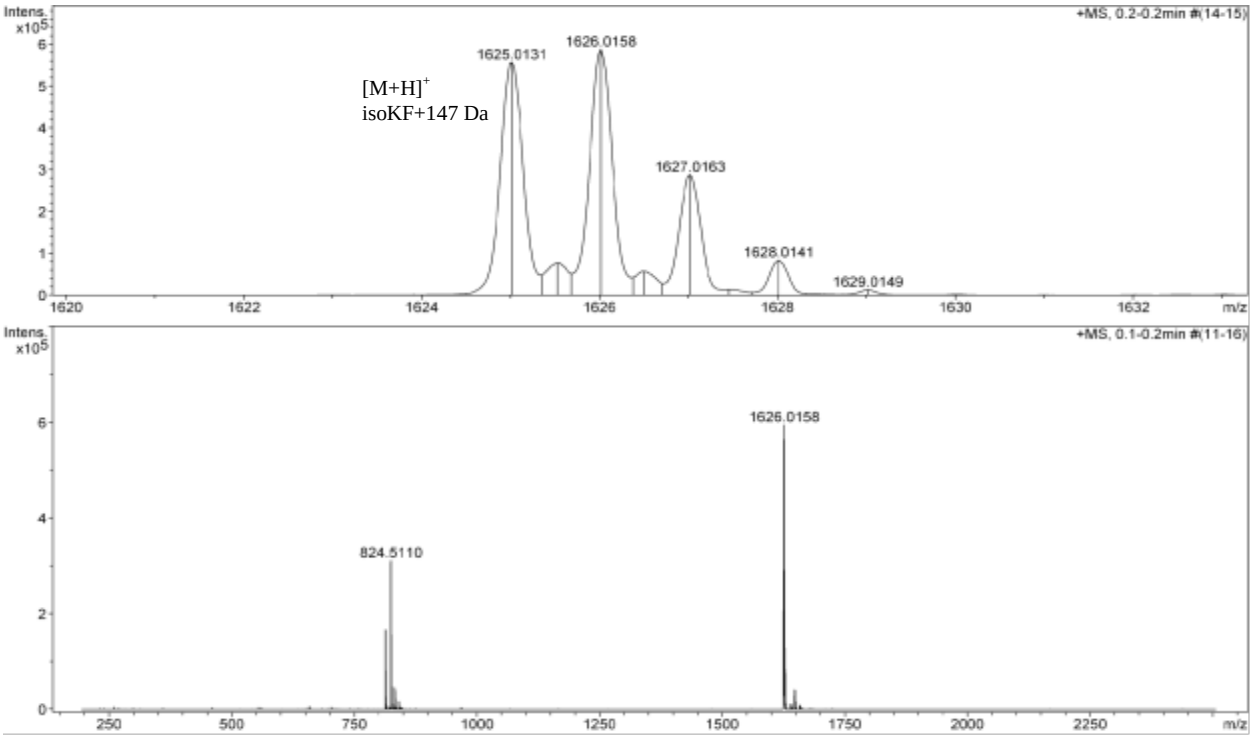

Figure 27 HRMS spectrum of D-Phe14-isoKF **(7)**

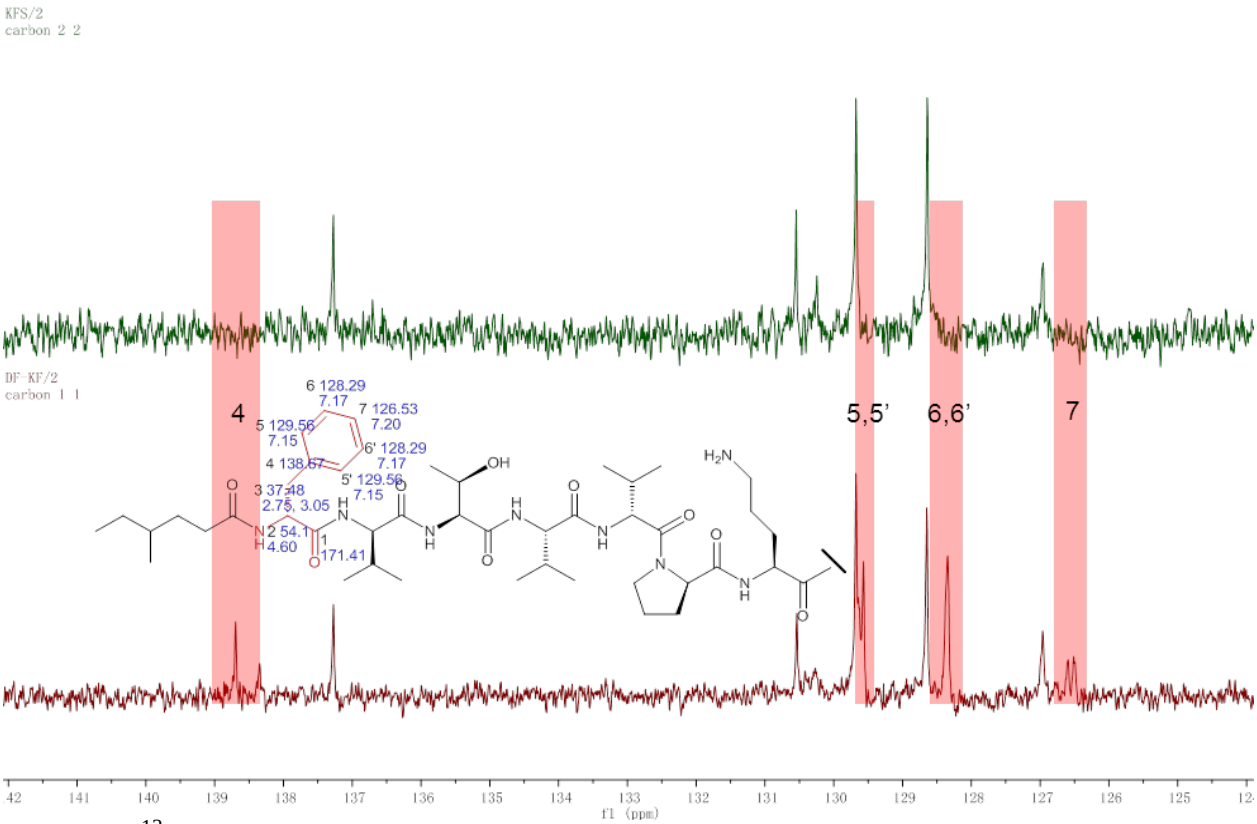

Figure 28 ^{13}C NMR spectra (δ_C 120-142) of isoKF (top) and D-Phe14-isoKF **(7)** (bottom) in DMSO-d_6

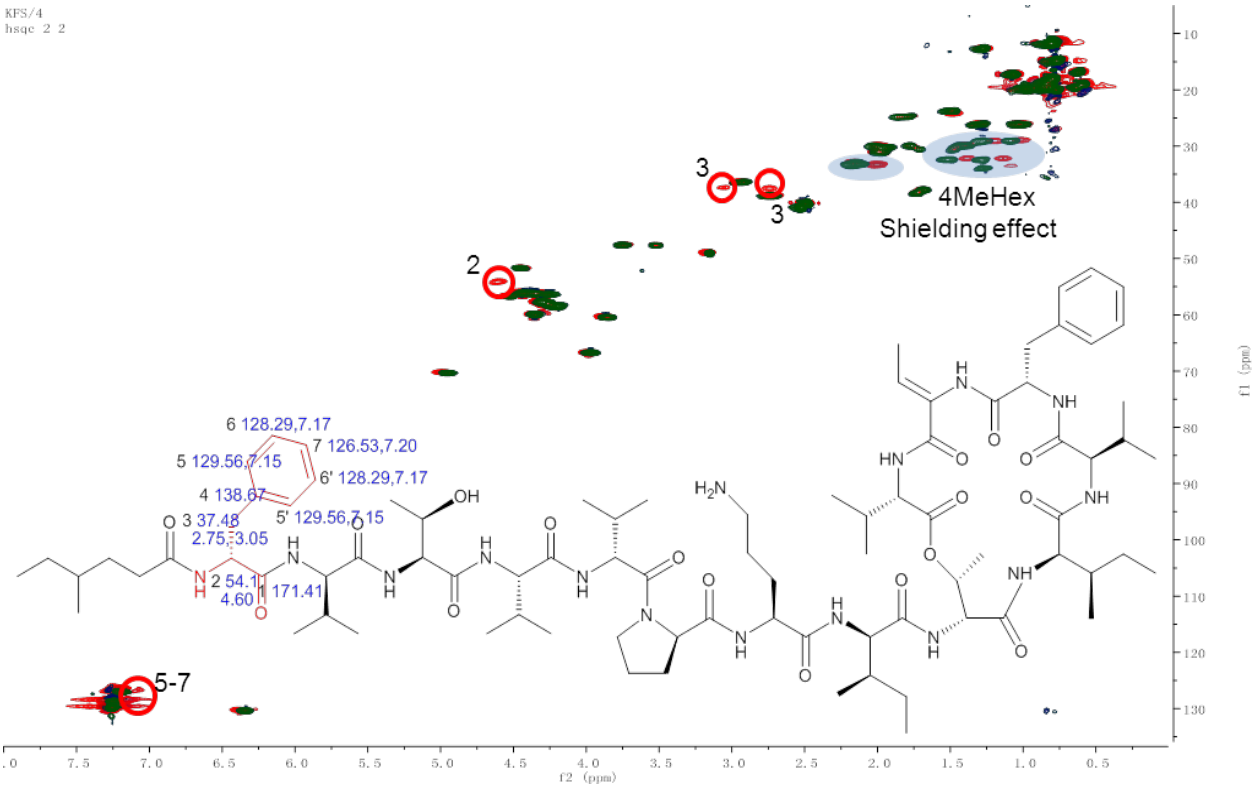

Figure 29 HSQC spectra overlay of isoKF (green) and D-Phe14-isoKF **(7)** (red) in DMSO-d_6

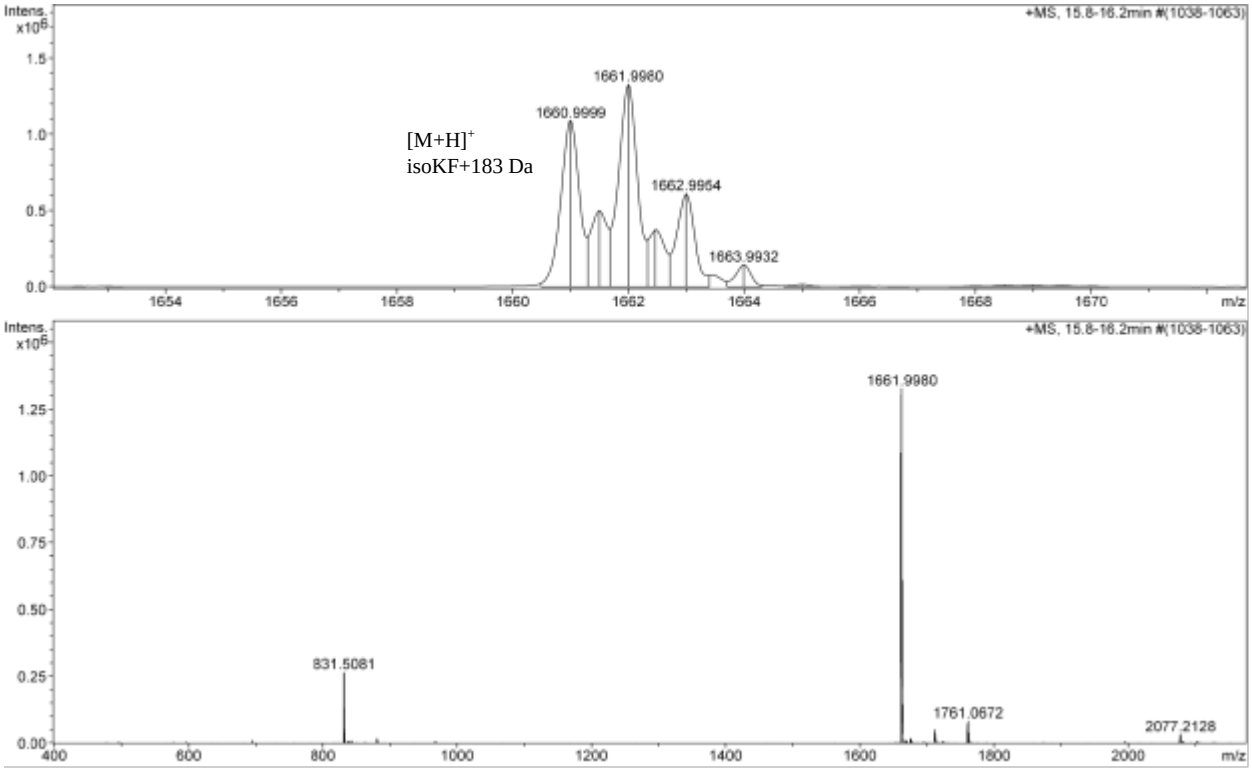

Figure 30 HRMS spectrum of 3,4-2F-D-Phe14-isoKF **(8)**

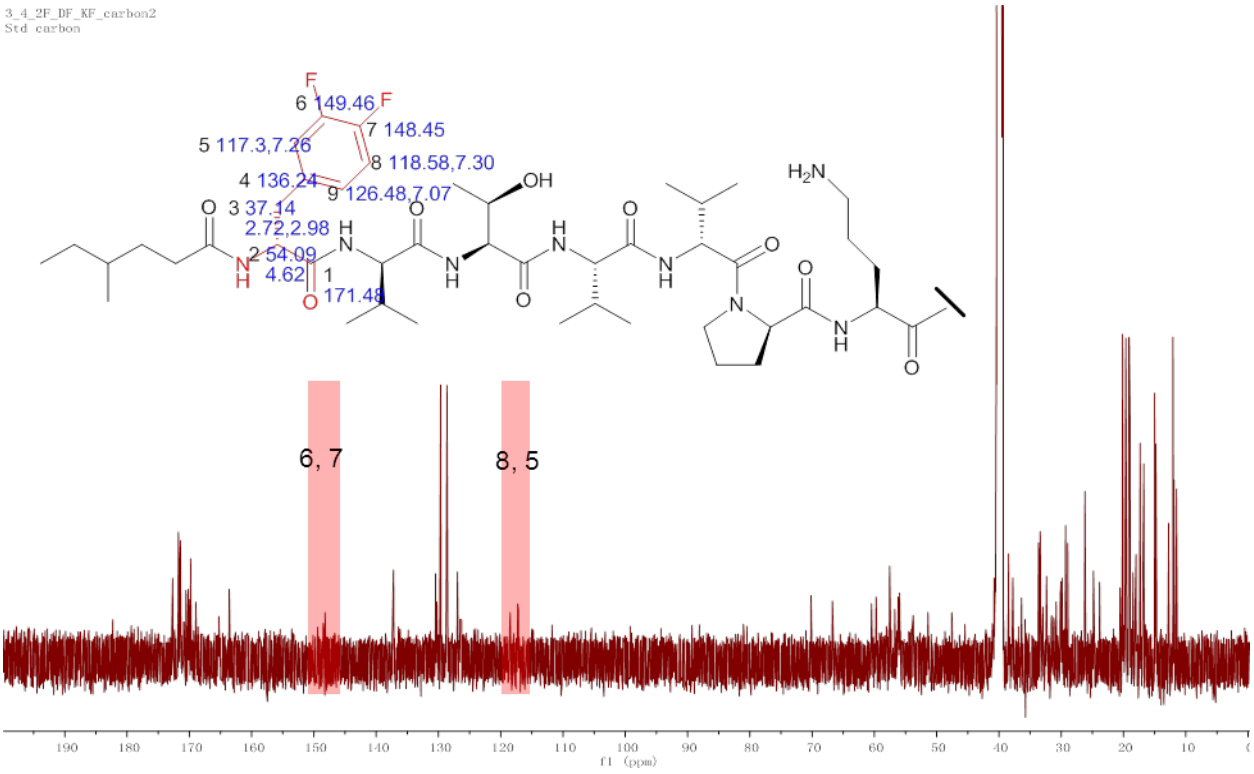

Figure 31 ^{13}C NMR spectrum of 3,4-2F-D-Phe14-isoKF **(8)** in DMSO-d_6

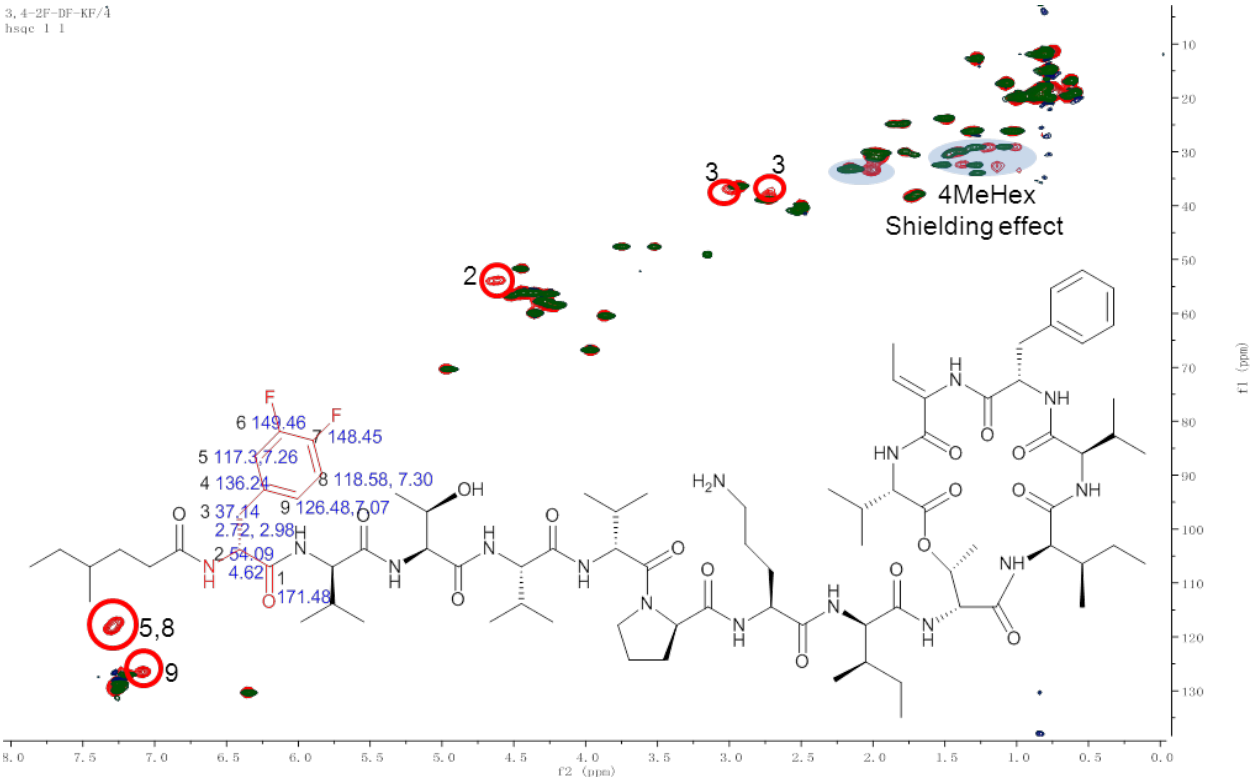

Figure 32 HSQC spectra overlay of isoKF (green) and 3,4-2F-D-Phe14-isoKF **(8)** (red) in DMSO-d_6

For the first attempt of *N*-protection of KF, Fmoc-Cl in the presence of 0.25 eq. DMAP in DMF was used. However, carbamyl-KF **(9)** was the major product. **9** provided a quasi-molecular ion signal $[M+Na]^+$ at *m/z* 1527.9134 for the molecular formula of $C_{76}H_{124}N_{14}NaO_{17}$ (calc. 1527.9167, Δ -2.2 ppm), which was 28 Da more than KF **(Figure 33)**. Comparison of **9** with KF in the amide carbonyl region implied that **9** has one more amide or ester carbonyl signal at δ_C 161.38. Carbonyl groups of L-Orn8 and D-Pro9 in **9** had minor shifts demonstrating that the addition had occurred at the L-Orn8 residue **(Figure 34)**. The HMBC spectrum of **9** displayed a correlation between the new carbonyl and methylene on L-Orn8 at δ_C 37.21. The ^{13}C satellites of δ_H 7.95 in the HMBC spectrum suggested its HSQC correlation with the new carbonyl signal, thus confirming the formamide linkage at L-Orn8 **(Figure 35)**. Partial hydrolysis of both KF and **9** followed by the coupling reactions using the same approach as listed in **Scheme 1** produced carbamyl-de-DV13-isoKF **(10)** and 4MeCap-de-D-Val13-isoKF **(11)**. Compound **10** provided a quasi-molecular ion signal $[M+Na]^+$ at *m/z* 1428.8409 for the molecular formula of $C_{71}H_{115}N_{13}NaO_{16}$ (calc. 1428.8482, Δ -5.1 ppm) **(Figure 36)**. It also displayed a formamide carbonyl signal at δ_C 161.74 **(Figure 37)**. Compound **11** provided a quasi-molecular ion signal $[M+Na]^+$ at *m/z* 1512.9361 for the molecular formula of $C_{77}H_{127}N_{13}NaO_{16}$ (calc. 1512.9421, Δ -3.9 ppm) **(Figure 38)**. Its ^{13}C NMR spectrum displayed that the formamide carbonyl was missing. Instead, an amide carbonyl at δ_C 172.66, one methine at δ_C 33.94, three methylenes at δ_C 33.93, 33.45, and 29.12, two methyls at δ_C 19.29 and 11.60 were observed, indicating the presence of an additional 4-MeHex group at L-Orn8 **(Figures 39-41)**.

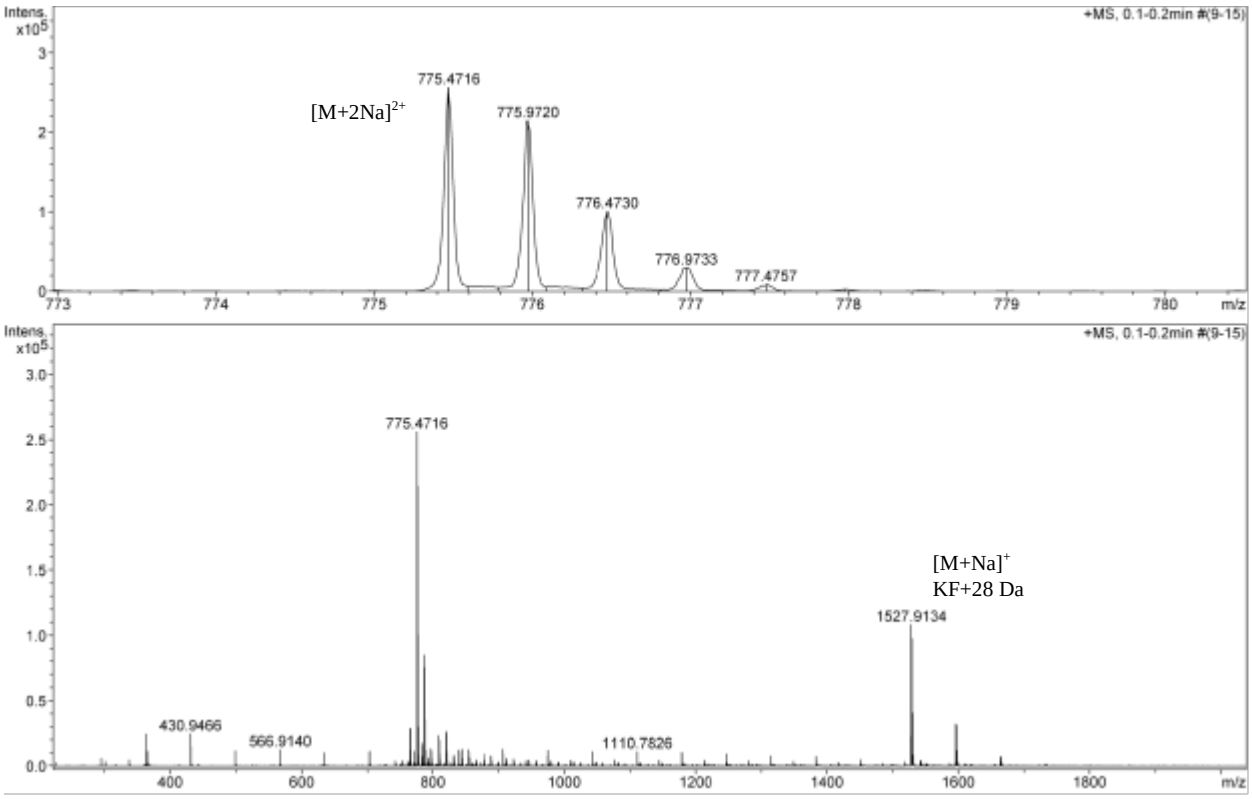

Figure 33 HRMS spectrum of carbamyl-KF **(9)**

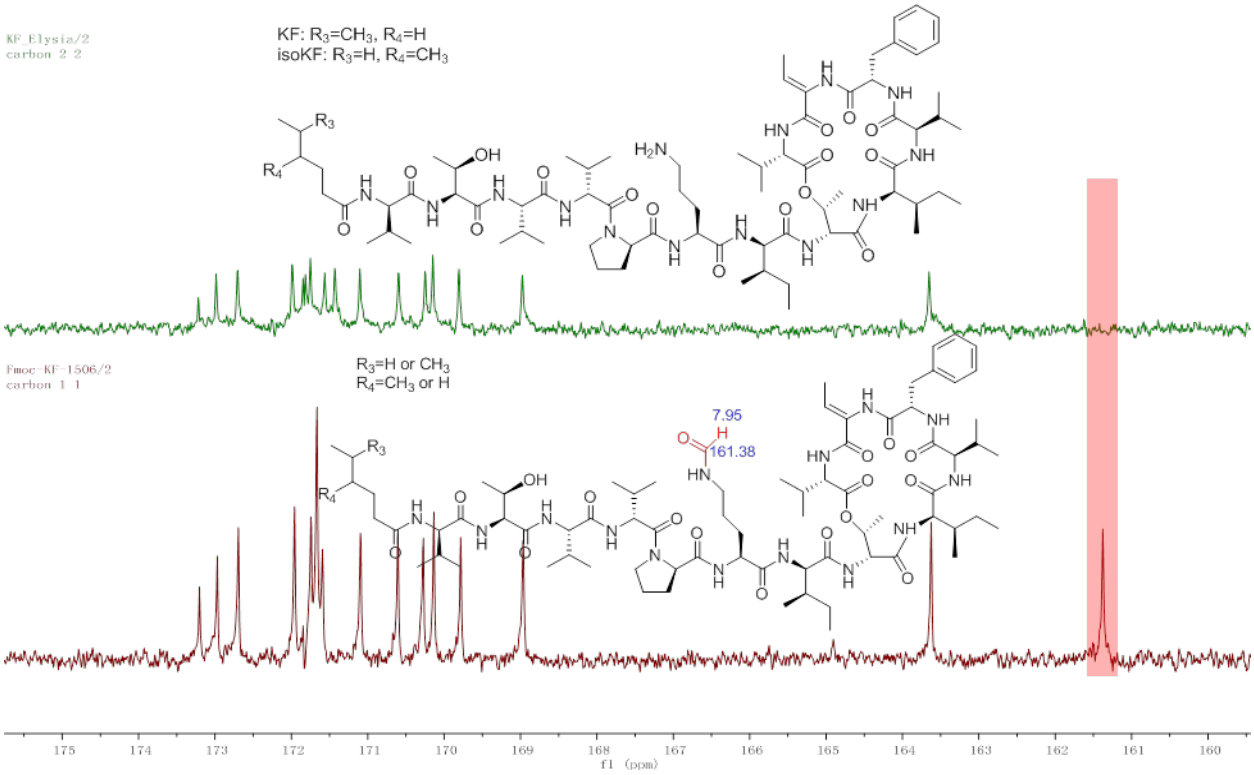

Figure 34 ^{13}C NMR spectra (δ_C 158-176) of isoKF (green) and carbamyl-KF **(9)** (red)

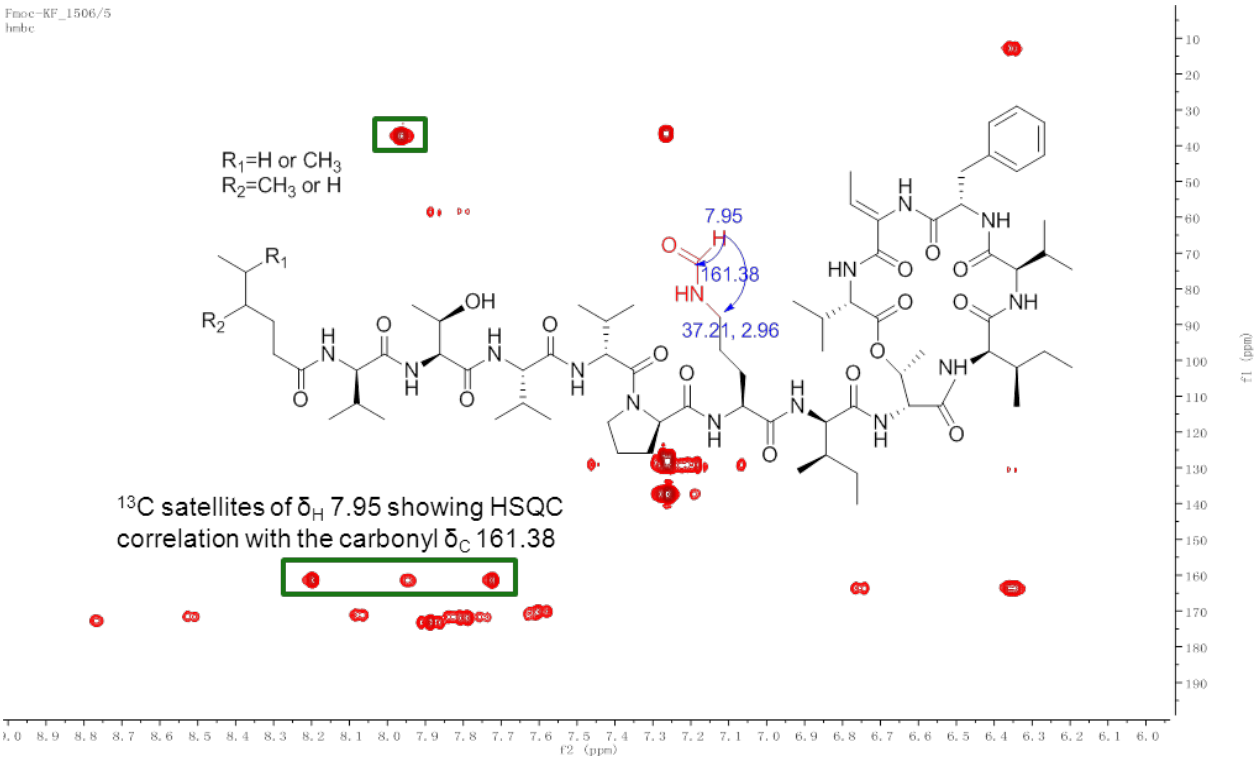

Figure 35 HMBC spectrum of carbamyl-KF **(9)** in DMSO-d_6

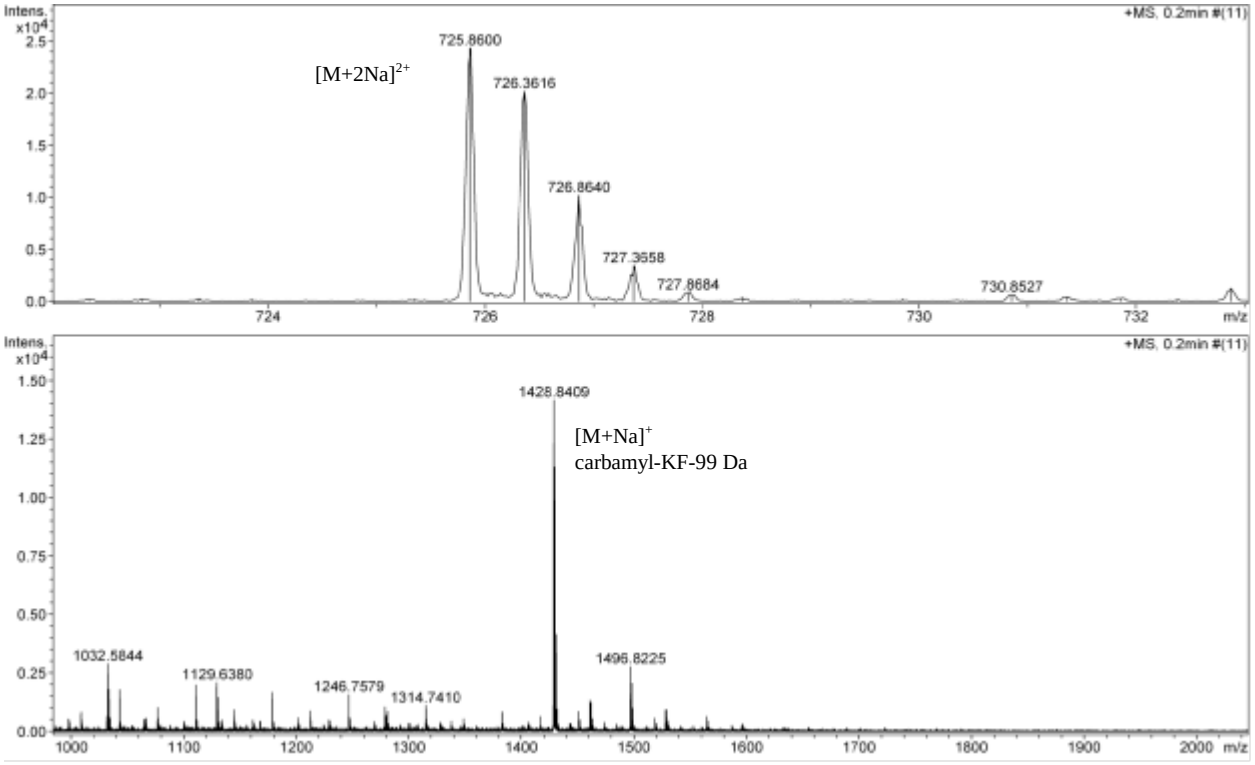

Figure 36 HRMS spectrum of carbamyl-de-D-Val13-isoKF **(10)**

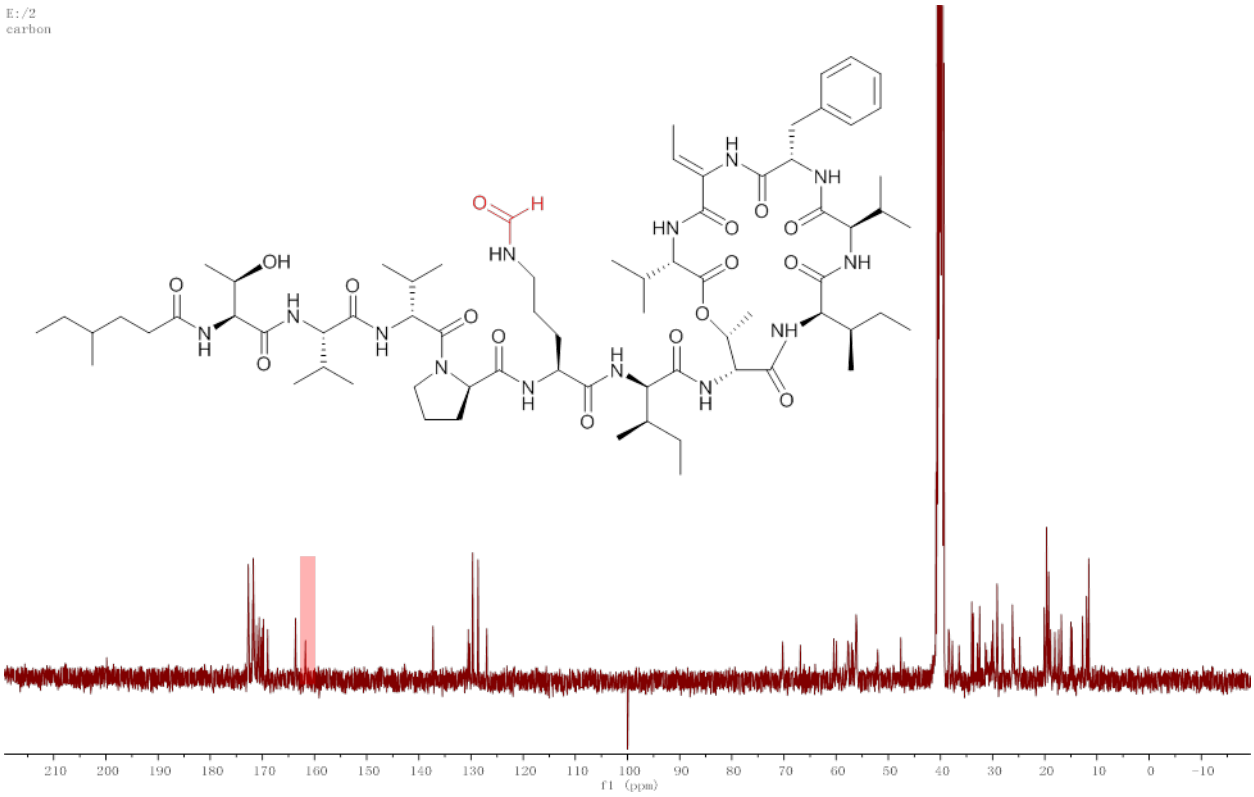

Figure 37 ^{13}C NMR spectrum of carbamyl-de-D-Val13-isoKF **(10)** in DMSO-d_6

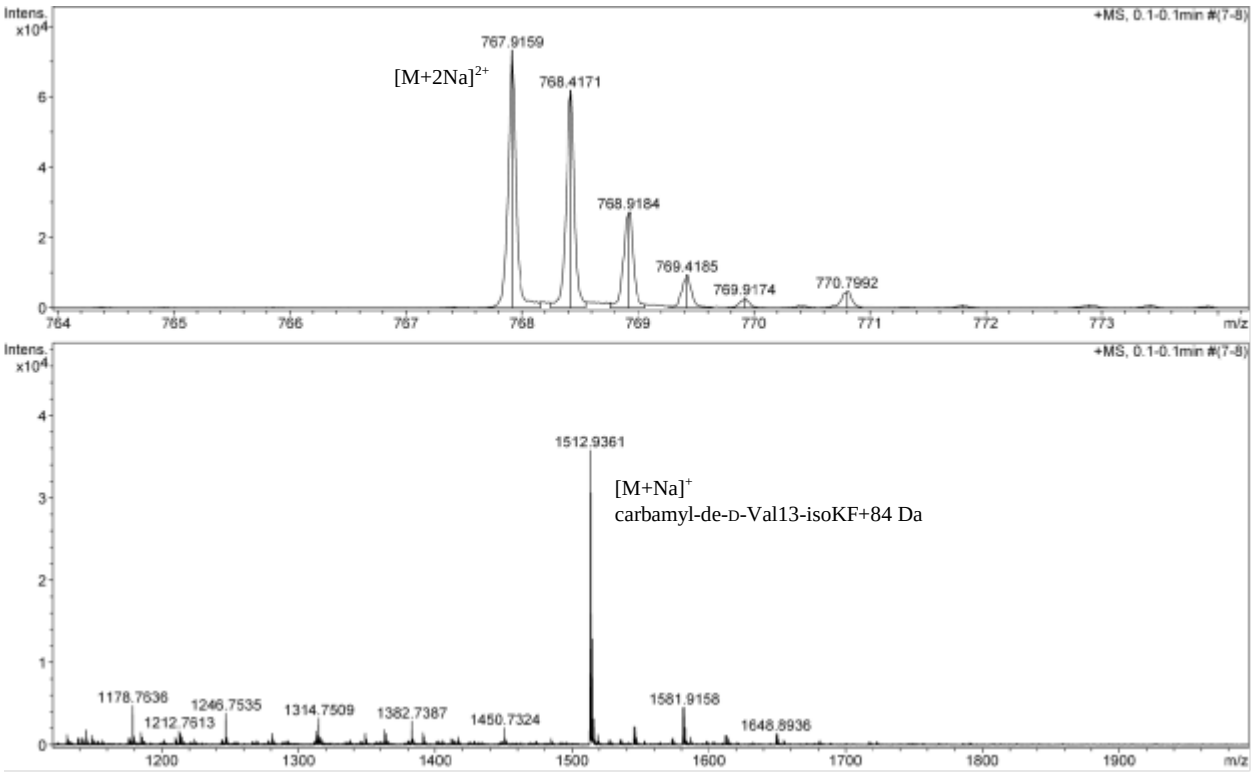

Figure 38 HRMS spectrum of 4MeCap-de-D-Val13-isoKF **(11)**

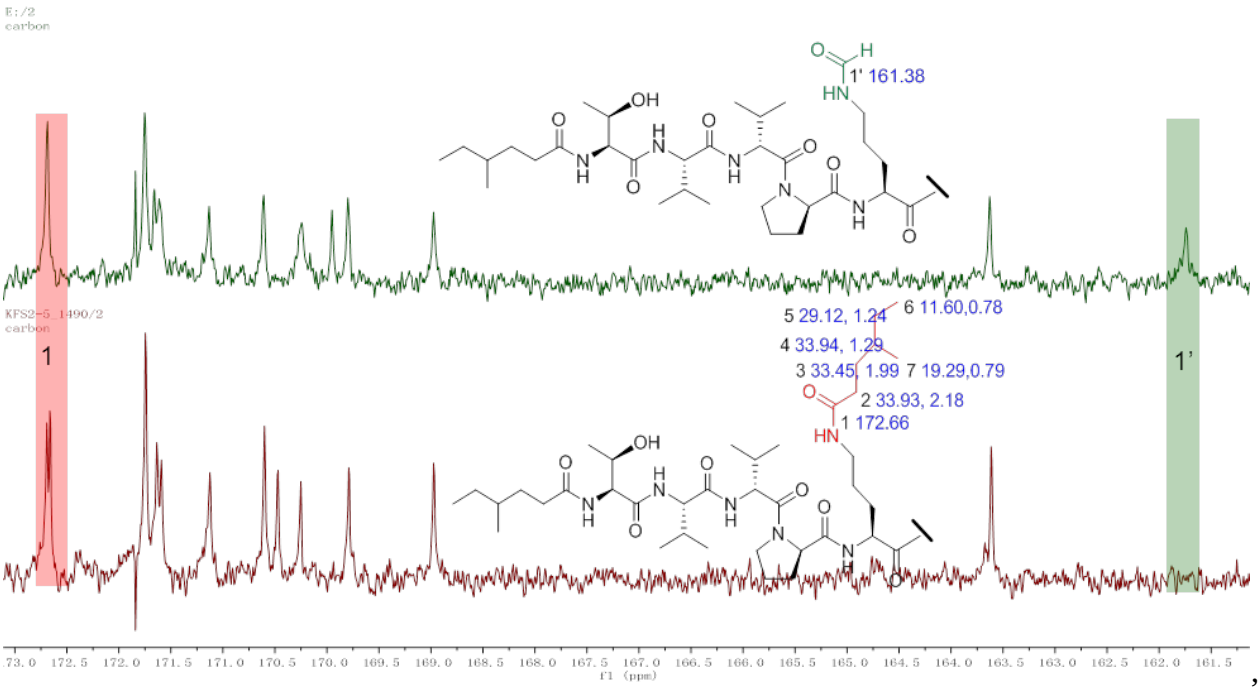

Figure 39 ^{13}C NMR spectra (δ_C 160-176) of carbamyl-de-D-Val13-isoKF **(10)** (top) and 4MeCap-de-D-Val13-isoKF **(11)** (bottom) in DMSO-d_6

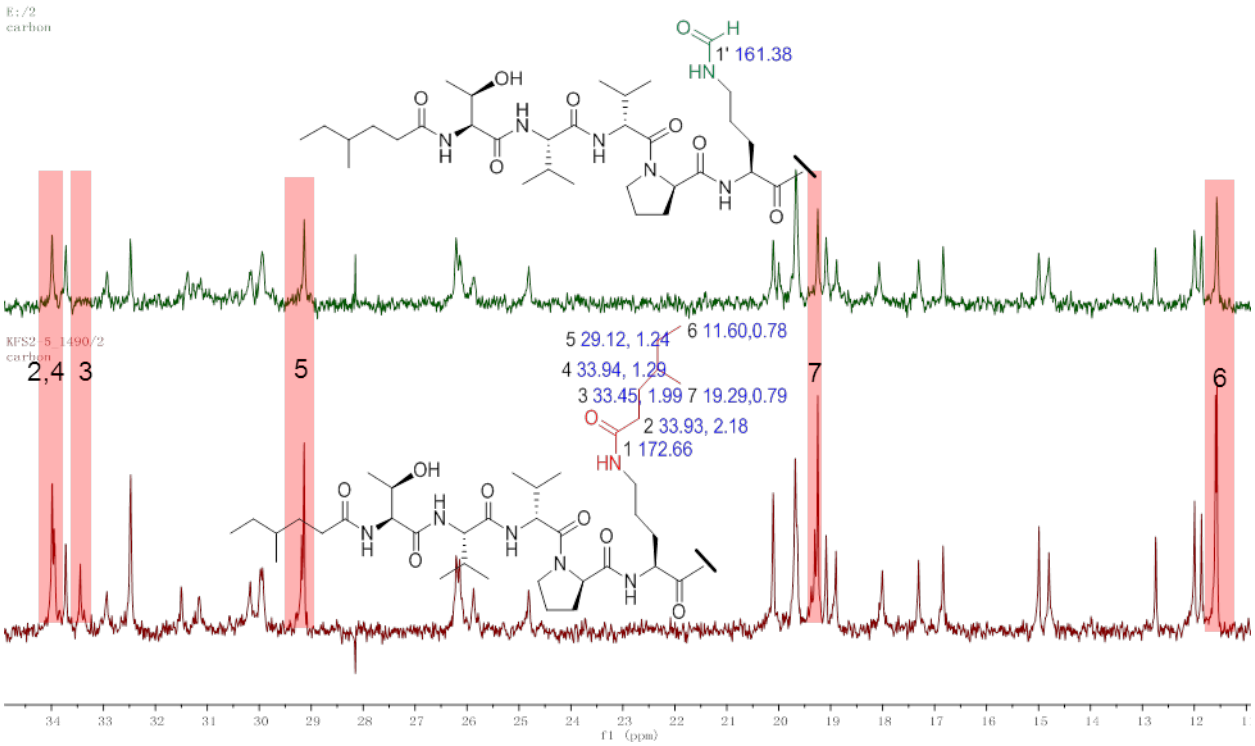

Figure 40 ^{13}C NMR spectra (δ_C 11-35) of carbamyl-de-D-Val13-isoKF **(10)** (top) and 4MeCap-de-D-Val13-isoKF **(11)** (bottom) in DMSO-d_6

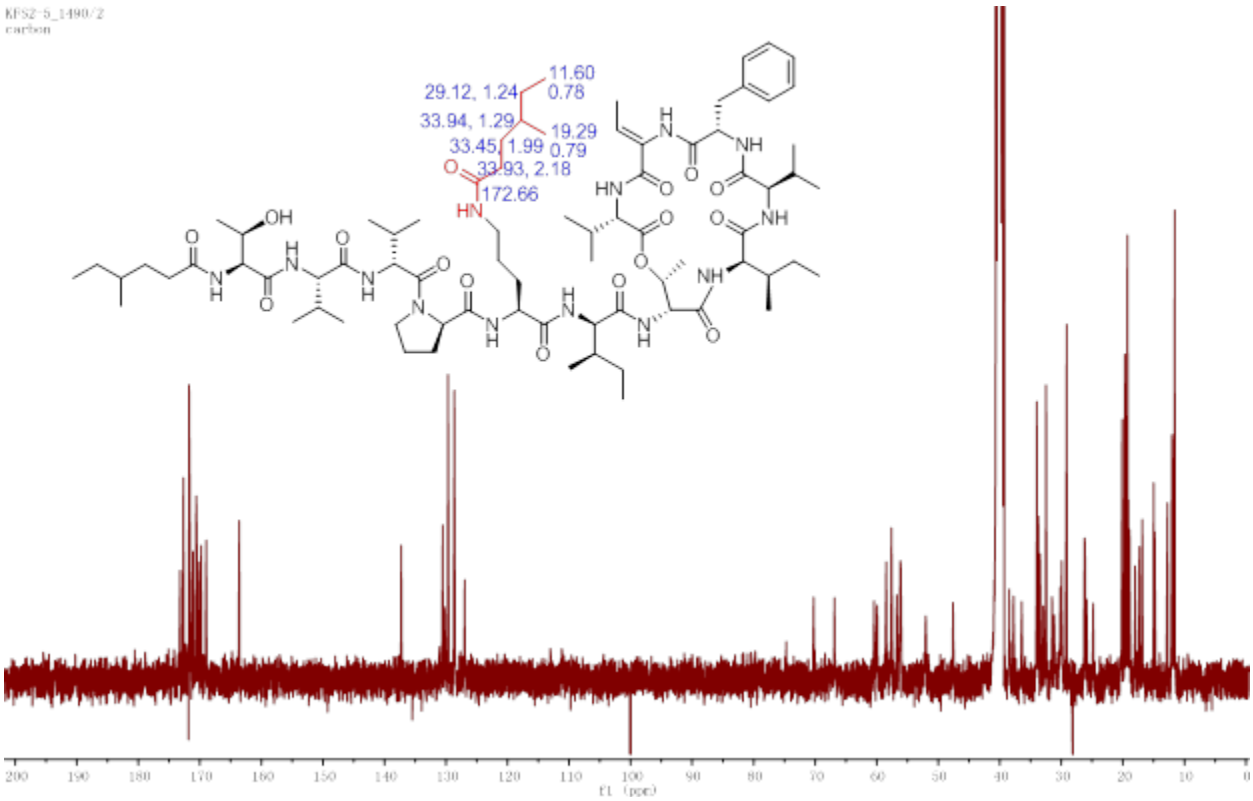

Figure 41 ^{13}C NMR spectrum of 4MeCap-de-D-Val13-isoKF **(11)** in DMSO-d_6

2.2 Modification of L-Thr12. Published SAR results showed that the hydroxy group of L-Thr12 was not necessary for the activity. Additionally, the replacement of L-Thr12 into a nonpolar amino acid residue may increase the activity.[27] Therefore, modifications by either fluorination or dehydration of L-Thr12 were performed using BAST. BAST and its older generation agent DAST are commonly used in fluorination and dehydration reactions of hydroxy group.[38,39] BAST is thermally stable and more capable to perform the reactions in a high yield.[40] In the presence of fluorinating agents, the hydroxy group could attack the reagent at sulfur, thus eliminating hydrogen fluoride to form an alkoxyaminosulfur difluoride as an intermediate. Nucleophilic attack on different positions could generate possible products such as fluorinated and oxazoline through either S_N1 or S_N2 reactions. In some cases, the elimination could occur to produce an olefin under the anhydrous condition **(Scheme 6)**. In the reaction attempted, only the olefin (*Z*)-Dhb12-KF **(12)** was detected (20% yield). It was reported that a trace amount of water

could help the release of HF, thus stabilizing the intermediate and promoting the fluorination.[41] However, no fluorinated product was observed even in the presence of traces of water. This could result from the steric hindrance of KF.

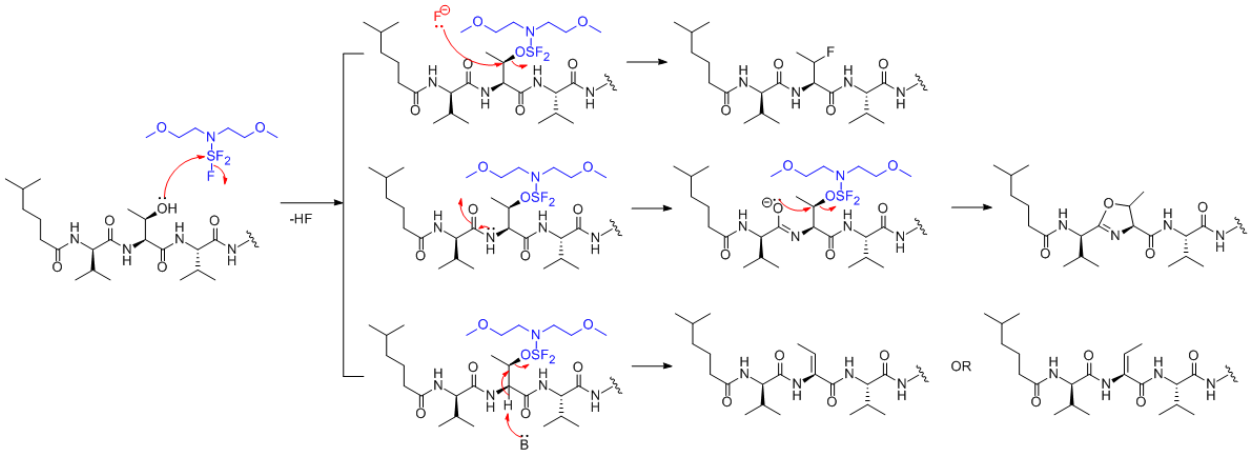

Scheme 6 Possible reactions on L-Thr12 catalyzed by BAST

(*Z*)-Dhb12-KF **(12)** provided quasi-molecular ion signals $[M+H+Na]^{2+}$ at *m/z* 741.4714, $[M+H]^{+}$ at *m/z* 1459.9350 for the molecular formula of $C_{75}H_{123}N_{14}O_{15}$ (calc. 1459.9287, Δ +4.3 ppm) **(Figure 42)**. Comparison of its ^{1}H NMR spectrum with that of KF demonstrated the presence of an olefinic proton at δ_H 6.42 (q, *J*=6.9) **(Figure 43)**. The HSQC overlay experiment showed that **12** lost a hydroxy group at L-Thr12, and the methyl group moved up filed to δ_C 13.66, thus confirming the formation of a double bond between the α- and β- carbons at L-Thr12 **(Figure 44)**. The coupling constant of new olefinic proton determined the double bond is *Z*-configured.

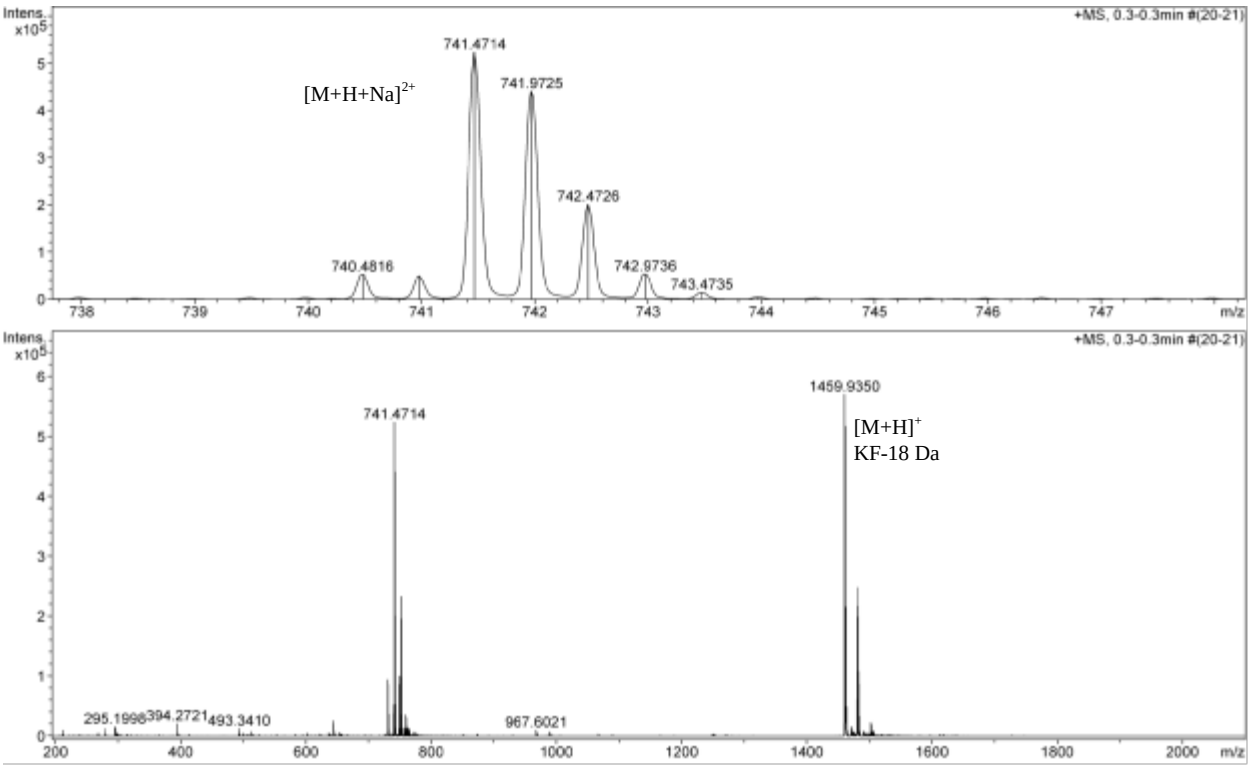

Figure 42 HRMS spectrum of (*Z*)-Dhb12-KF **(12)**

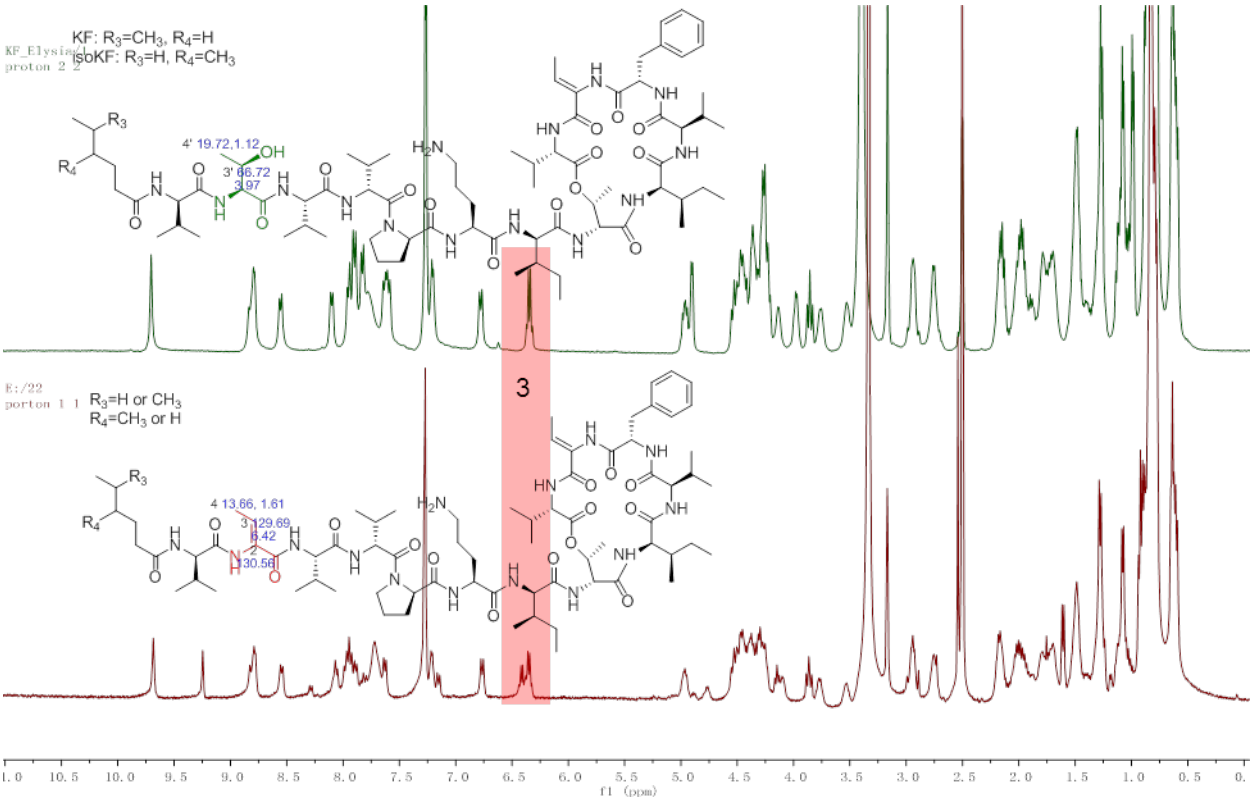

Figure 43 ^{1}H NMR spectra of KFs (top) and (*Z*)-Dhb12-KF **(12)** (bottom) in DMSO-d_6

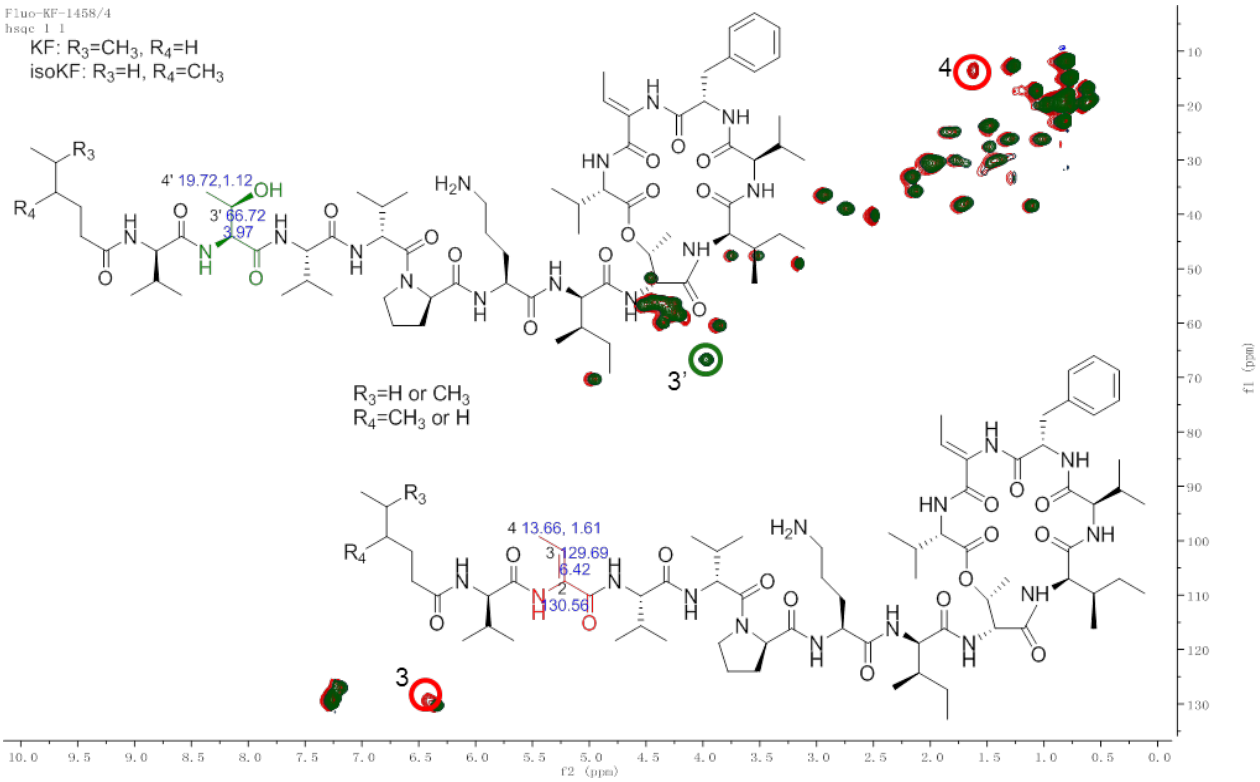

Figure 44 HSQC spectra overlay of KFs (green) and (*Z*)-Dhb12-KF **(12)** (red) in DMSO-d_6

2.3 Cyclization of Kahalalide G. An enzymatic stability study of KF demonstrated that the transformation of KF into kahalalide G (KG) by esterase could be one option for the inactivation of KF.[42] It was hypothesized that an amide bond could be more stable than the ester bond in KF. Therefore, a coupling reaction of KG was performed to generate a new cyclic peptide as cyclo-isoKG **(13)** and its isomer cyclo-KG **(14) (Scheme 7)**.

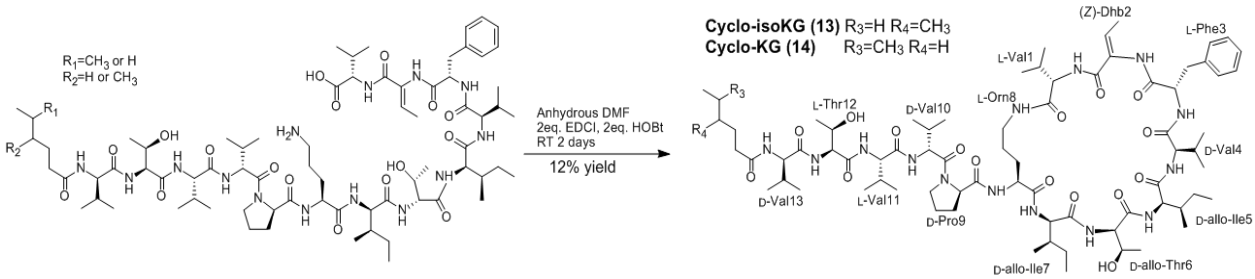

Scheme 7 Cyclization of kahalalide G

Cyclo-isoKG **(13)** and cyclo-KG **(14)** provided a quasi-molecular ion $[M+Na]^+$ at *m/z* 1499.9186 or 1499.9141, respectively, for the same molecular formula as KF of

$C_{75}H_{124}N_{14}NaO_{16}$ (calc. 1499.9217, Δ -2.1 ppm or -5.1 ppm, respectively) **(Figures 45, 49)**. ^{1}H NMR spectra of **13** and **14** did not show difference. However, they shifted significantly in both amide-proton and α-proton regions when compared to KF **(Figure 46)**. The HSQC overlay between KF and **13/14 (Figures 47, 50)** showed that the β-proton of D-allo-Thr6 shifted upfield from δ_H 4.96 to δ_H 3.76 suggesting the presence of a free hydroxy group. The α-carbon of L-Orn 8 shifted downfield from δ_C 51.65 to δ_C 53.34 suggesting the change of chemical environment. Additionally, the α-proton of L-Val1 and δ-protons of L-Orn8 shifted downfield from δ_H 3.85 to δ_H 4.26, δ_H 2.74 to δ_H 3.01 and 3.15, respectively. This deshielding effect indicated the formation of a new amide linkage between L-Val1 and L-Orn8. There were correlations between α-proton of L-Val1 and δ-protons of L-Orn8 observed in the NOESY spectrum, which confirmed the formation of a new cyclic peptide **(Figure 48)**. Both carbon and proton chemical shifts of (*Z*)-Dhb2, L-Phe3, D-allo-Ile7, and D-Pro9 in **13/14** varied compared to KF **(Table 4)**. The variance was attributed to the intramolecular interactions between amino acid residues in the new ring system. The difference between **13** and **14** was the signals in the methylene and methyl regions corresponding to the MeHex lipid chain. The HSQC overlay between KF, **13**, and **14** showed that geminal methyl groups at δ_C 22.5 were missing from **13**, which suggested that **13** is the analogue with 4-MeHex residue. Carbon signals at δ_C 33.7, 33.1, 32.3, and 29.4 corresponding to 4-MeHex residue were missing from **14**, which confirmed that **14** is the molecule with 5-MeHex residue **(Figure 50)**.

Table 4 Selected ^{1}H and ^{13}C NMR data of KF, **13** and **14**[a] (δ in ppm, DMSO-d_6)

		KF		13 & 14	
Amino acid	**Carbon**	**δ_C, mult.**	**δ_H, mult.**	**δ_C, mult.**	**δ_H, mult.**
L-Val1	1	169.82, qC	(NH) 7.59		(NH) 7.33
	2	60.46, CH	3.85, t	58.48, CH	4.17, m
	3	29.92, CH	1.97, m	30.78, CH	1.78, m
	4	19.19, CH_3	0.81, m	19.65, CH_3	0.83, m
	5	18.63, CH_3	0.83, m	18.69, CH_3	0.85, m
(*Z*)-Dhb2	1	163.66, qC	(NH) 9.70		(NH) 9.31
	2	130.54, CH	6.35, q	130.63, CH	6.43, q
	3	130.27, qC			
	4	12.74, CH_3	1.27, d	13.14, CH_3	1.49, d
L-Phe3	1	171.76, qC	(NH) 8.55		(NH) 8.28
	2	56.13, CH	4.42, bs	55.19, CH	4.55, bs
	3	36.59, CH_2	2.97, bs	38.41, CH_2	2.83, 3.15, dd
	4	137.26, qC		138.06, qC	
	5,5'	128.64, CH	7.25, m	128.58, CH	7.25, d
	6,6'	129.67, CH	7.26, m	129.68, CH	7.26, t
	7	126.96	7.20, m	126.85, CH	7.18, m
L-Thr6	1	170.15, qC	(NH) 7.64		(NH) 7.43
	2	56.75, CH	4.52, m	57.97, CH	4.40, t
	3	70.24, CH	4.96, m	68.98, CH	3.76, m
	4	17.25, CH_3	1.09, d	20.58, CH_3	1.05, d
D-allo-Ile7	1	171.45	(NH) 7.82		(NH) 7.32
	2	56.15, CH	4.36, m	56.36, CH	4.24, m
	3	38.50, CH	1.71, m	35.89, CH	1.92, m
	4	14.93, CH_3	0.76, m	14.79, CH_3	0.74, m
	5	26.19, CH_2	1.01, 1.32, m	26.01, CH_2	1.02, 1.29, m
	6	11.87, CH_3	0.81, m	11.74, CH_3	0.80, m
L-Orn8	1	172.70, qC	(NH) 7.92		(NH) 7.29
	2	51.65, CH	4.46, m	53.34, CH	4.11, m
	3	30.55, CH_2	1.96, m	30.04, CH_2	1.76, m
	4	23.84, CH_2	1.49, m	23.58, CH_2	1.47, m
	5	38.95, CH_2	2.74, bs	38.50, CH_2	3.01, 3.15, bs
D-Pro9	1	172.01, qC			
	2	59.86, CH	4.39, m	60.32, CH	4.26, m
	3	29.96, CH_2	1.78, 1.97, m	29.79, CH_2	1.55, 1.72, m
	4	25.14, CH_2	1.79, 1.85, m	24.97, CH_2	1.77, 1.93, m
	5	47.67, CH_2	3.54, 3.79, m	47.81, CH_2	3.55, 3.80, m

[a]Assignments based on ^{1}H, ^{13}C, HSQC, and NOESY NMR (100/400 MHz) experiments at room temperature.

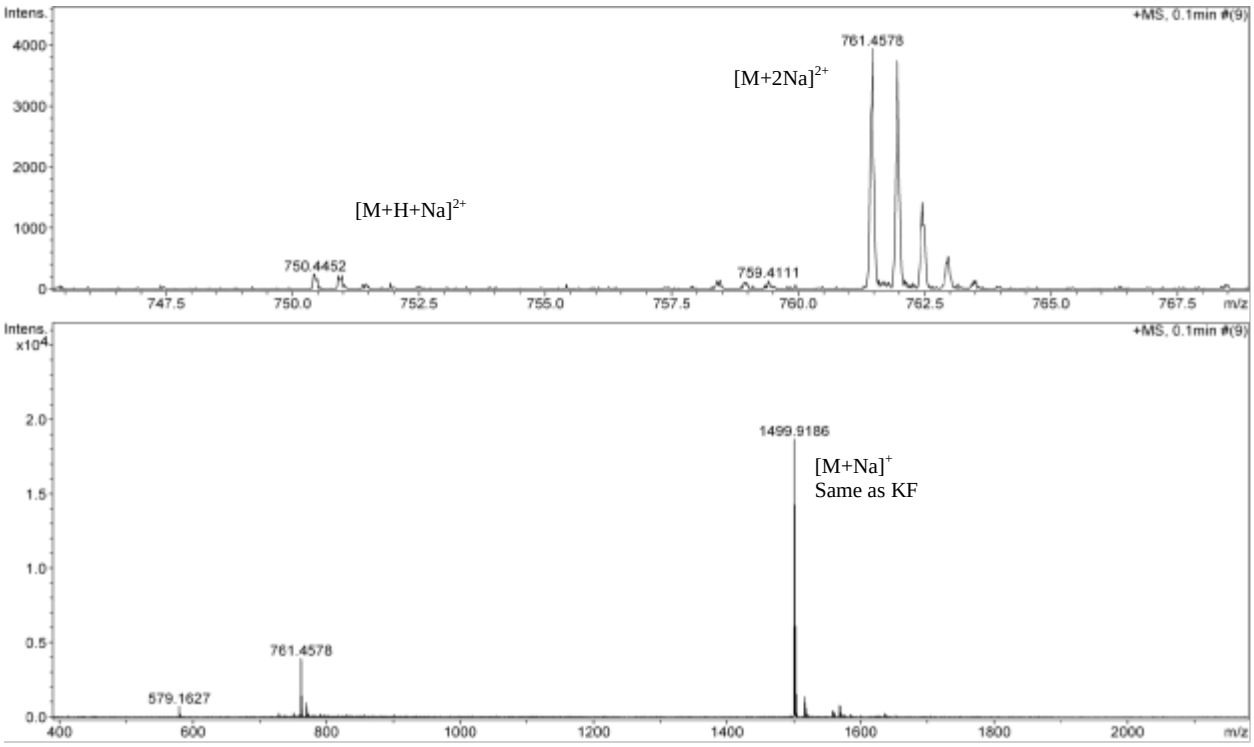

Figure 45 HRMS spectrum of cyclo-isoKG **(13)**

Figure 46 ^{1}H NMR spectra of KF (top), cyclo-isoKG **(13)** (middle) and cyclo-KG **(14)** (bottom) in DMSO-d_6

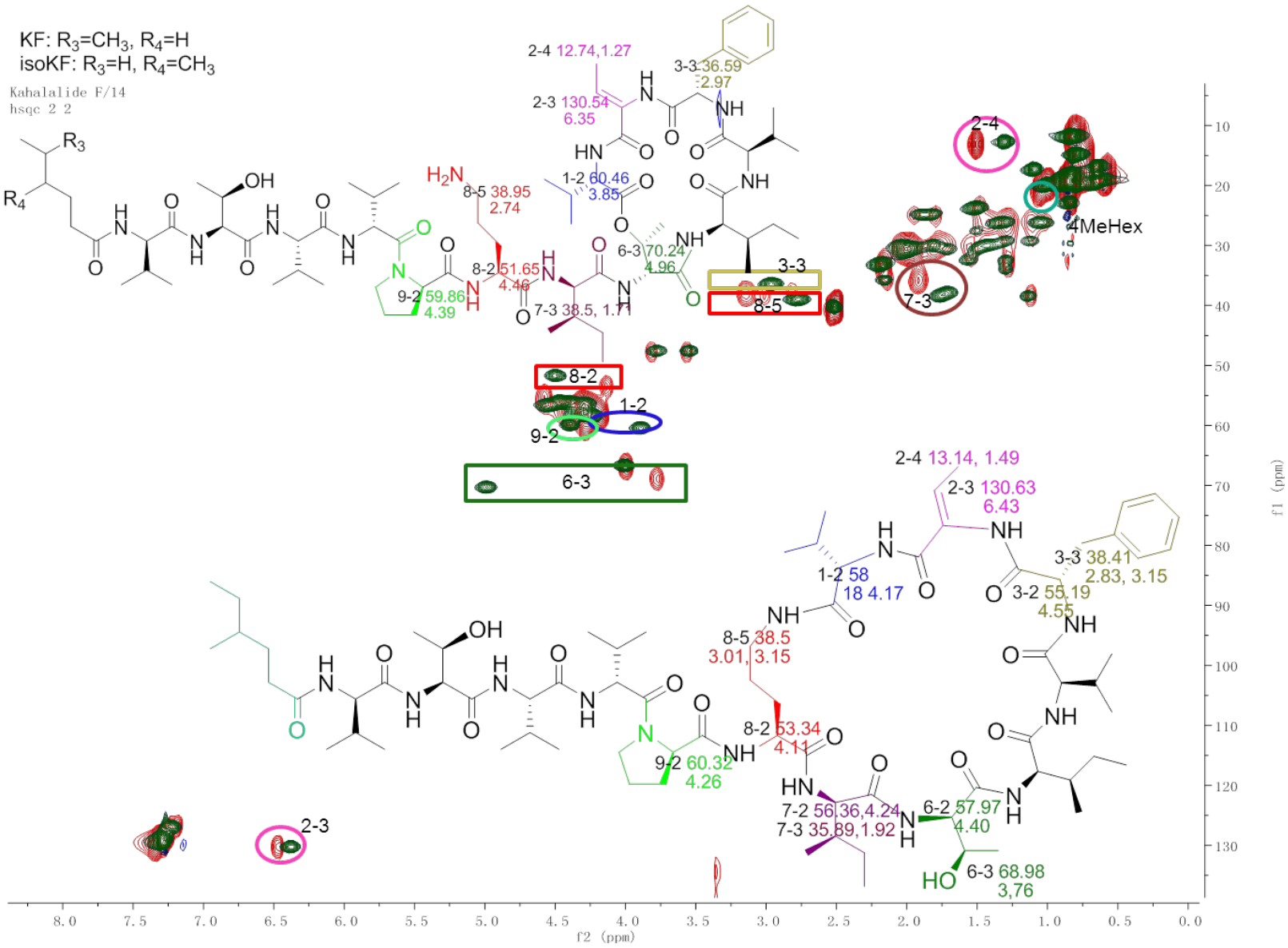

Figure 47 HSQC spectra overlay of KF (green) and cyclo-isoKG **(13)** (red) in DMSO-d_6

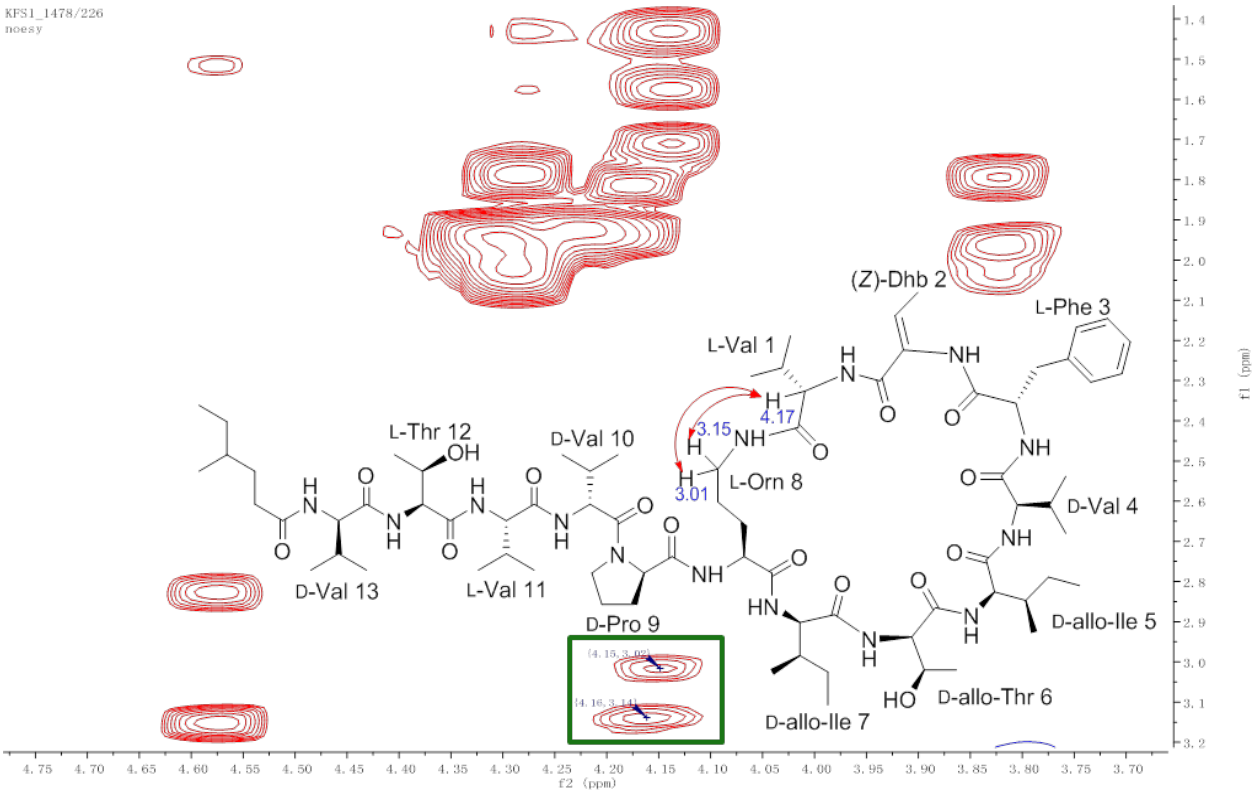

Figure 48 NOESY spectrum of cyclo-isoKG **(13)** in DMSO-d_6

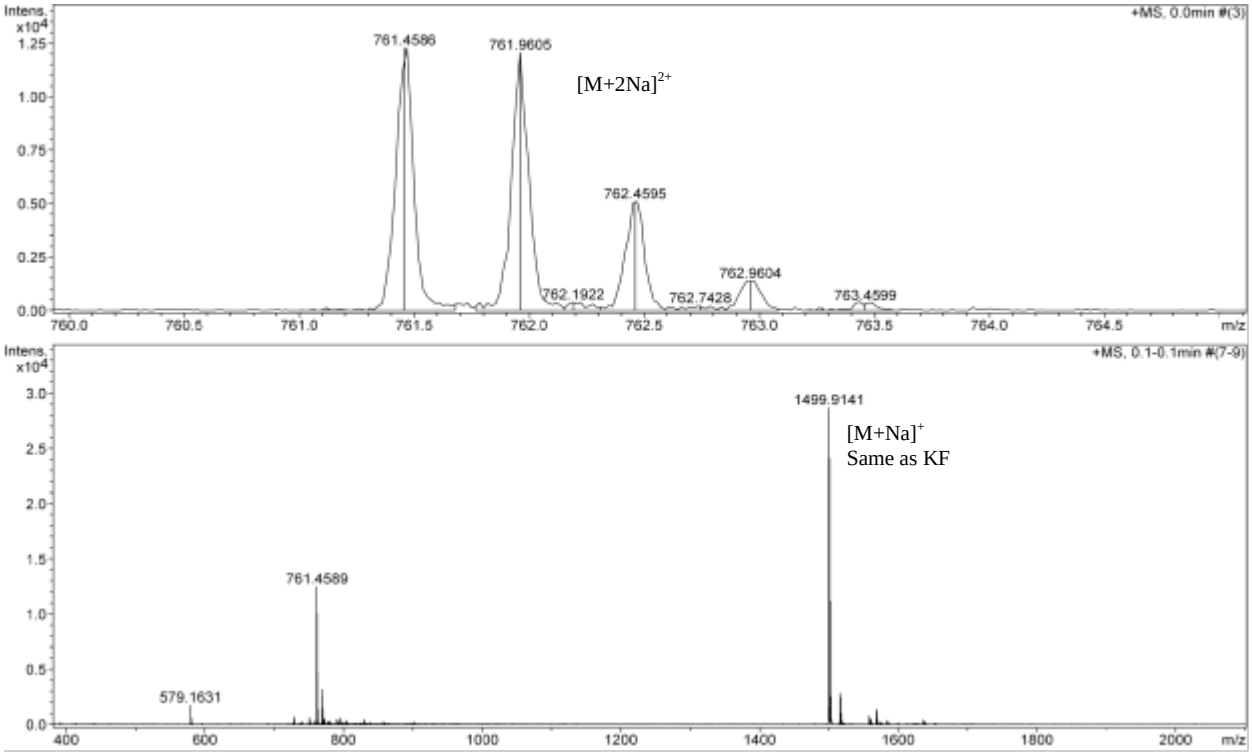

Figure 49 HRMS spectrum of cyclo-KG **(14)**

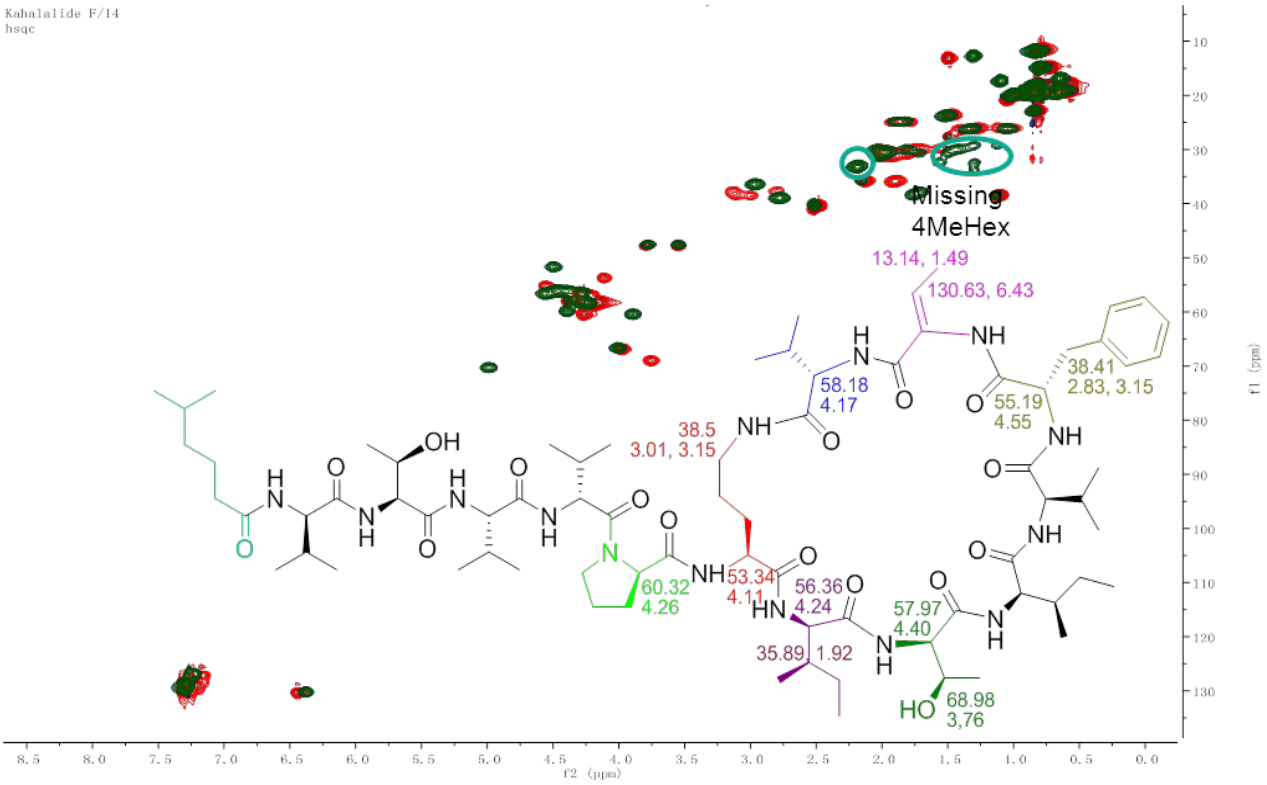

Figure 50 HSQC spectra overlay of KF (green) and cyclo-KG **(14)** (red) in DMSO-d_6

2.4 *N*-amidation Based on The Target Delivery Approach. Target delivery of cytotoxic molecules could help to release active compounds in cancer cells selectively, avoid its degradation, thus improving the therapeutic efficacy. Hypoxia in tumor tissues leads to tumor progression by adaptive responses of tumor cells including enhanced migration of endothelial cells and therapy resistance, which results in poor prognosis and patient outcomes.[43] Cancer cells are known to express elevated levels of DT-diaphorase [NAD(P)H dehydrogenase] that catalyzes a two-electron reduction of quinones into hydroquinones. It is proposed that a benzoquinone derived KF analogue may be reduced by DT-diaphorase under hypoxia conditions, and release KF to inhibit tumor growth. Under normoxic conditions, benzoquinone reduction does not occur due to the reversible oxidation in the presence of oxygen **(Scheme 8)**. Therefore, a benzoquinone derivative of KF **(15)** was synthesized starting from the formation of an NBS-modified benzoquinone acid, followed by synthesis of its succinimide ester by reacting with 1 eq. of

HOSu using THF in the presence of 2 eq. EDCI at 0 ℃ for 12 hr. The succinimide ester of a benzoquinone derivative then reacted with 1 eq. of KF using MeCN-DMSO (8:2) for 8 hr to yield benzoquinone-KF **(15) (Scheme 9)**.

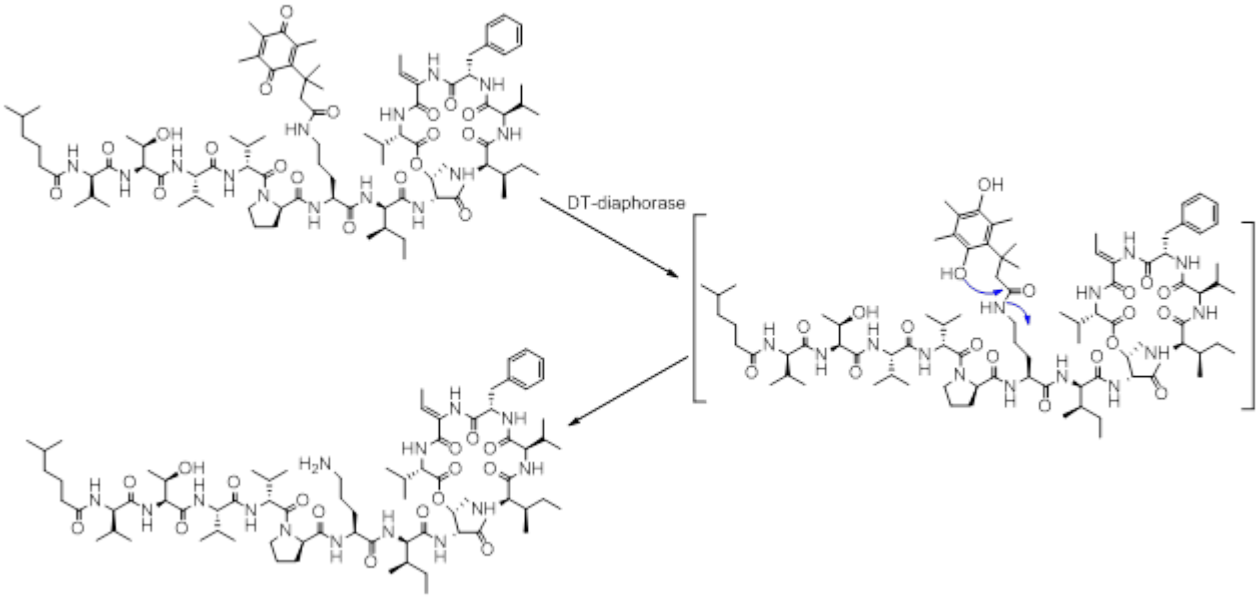

Scheme 8 Activation of KF by DT-diaphorase in hypoxic cancer cells

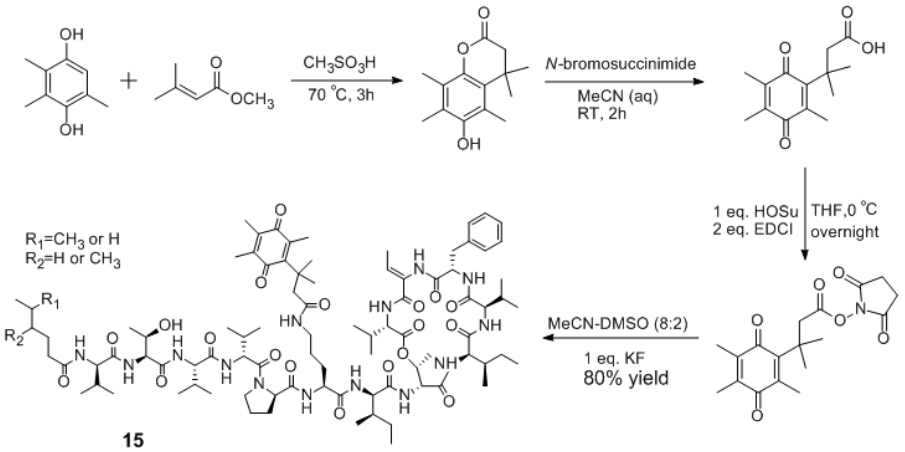

Scheme 9 Synthesis of benzoquinone-KF **(15)**

Benzoquinone-KF **(15)** provided a quasi-molecular ion of $[M+Na]^+$ at *m/z* 1732.0382 for the molecular formula of $C_{89}H_{140}N_{14}NaO_{19}$ (calc. 1732.0317, Δ +3.8 ppm) **(Figure 51)**. Comparison of ^1H NMR spectra of KF and **15** displayed that **15** has five additional methyl groups at δ_H 1.33, 1.92, 19.6, and 2.05 **(Figure 52)**. The ^{13}C NMR spectrum of **15** indicated the

presence of one benzoquinone, five methyls, one methylene, and one quaternary carbon **(Table 5)**. The proton signal of δ-C at L-Orn8 shifted downfield from δ_H 2.74 to δ_H 2.89. The addition of amide signals at δ_C 171.61, δ_H 7.82 were observed. The results indicated the formation of a new amide linkage of **15** at L-Orn8 residue **(Figures 53, 54)**. There were correlations between the new amide proton, δ-protons of L-Orn8, and β-protons of the benzoquinone residue observed in the NOESY spectrum **(Figure 55)**, which confirmed the structure of **15**.

Table 5 Additional ^{1}H and ^{13}C NMR signals of **15**[a] (δ in ppm, DMSO-d_6)

Carbon	δ_C, mult.	δ_H, mult.	Carbon	δ_C, mult.	δ_H, mult.
1	171.61, qC	(NH) 7.82, m	8	190.59, qC	
2	48.02, CH_2	2.66, s	9	136.41, qC	
3	37.66, qC		10	135.69, qC	
4	28.42, CH_3	1.33, s	11	187.22, qC	
5	28.42, CH_3	1.33, s	12	14.06, CH_3	2.05, s
6	155.32, qC		13	13.15, CH_3	1.96, s
7	144.50, qC		14	12.07, CH_3	1.92, s

[a]Assignments based on ^{1}H, ^{13}C, and HSQC NMR (100/400 MHz) experiments at room temperature.

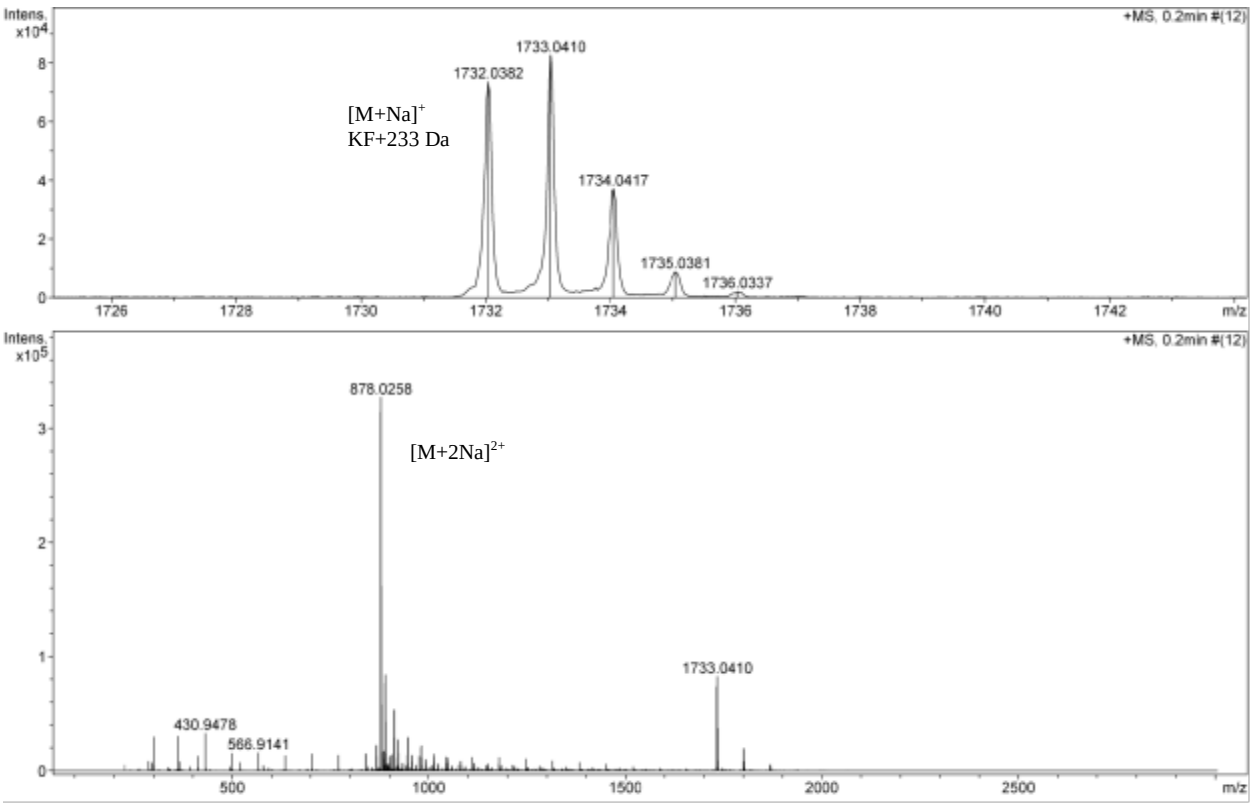

Figure 51 HRMS spectrum of benzoquinone-KF **(15)**

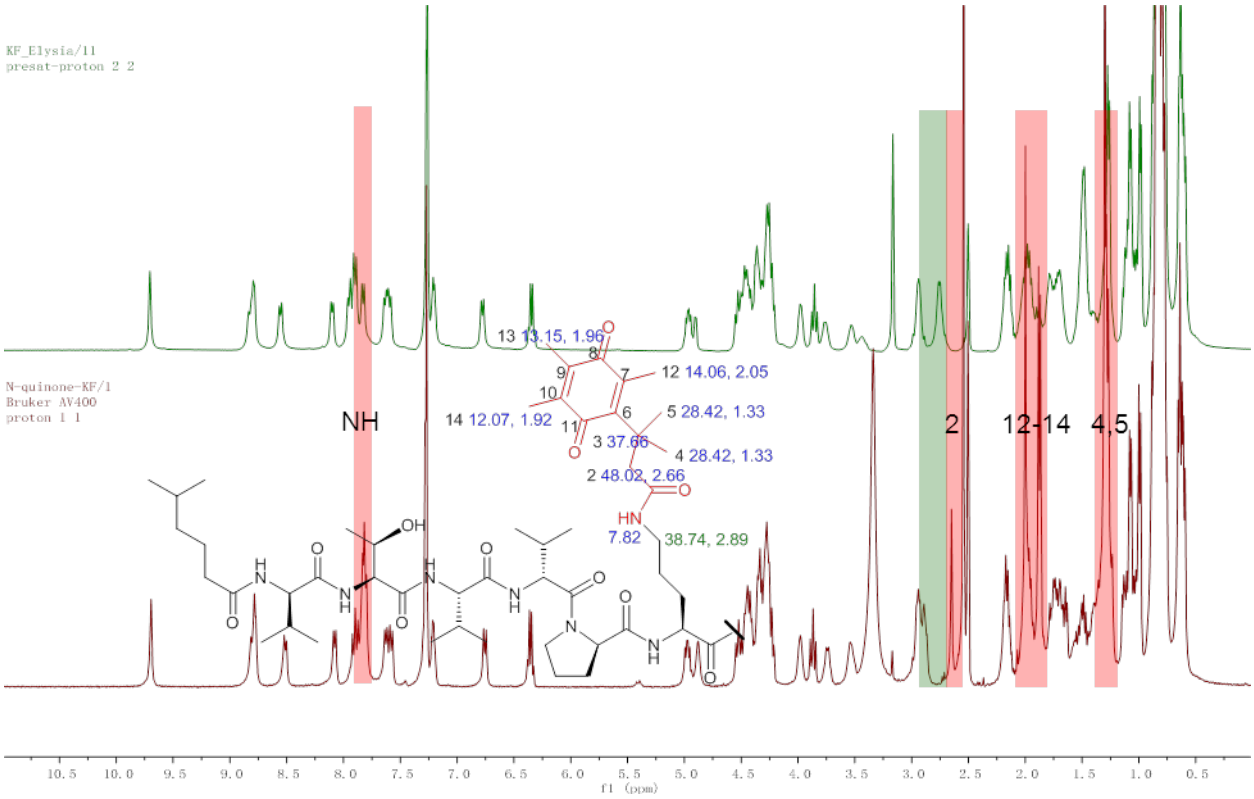

Figure 52 ^{1}H NMR spectra of KF (top) and benzoquinone-KF **(15)** (bottom) in DMSO-d_6

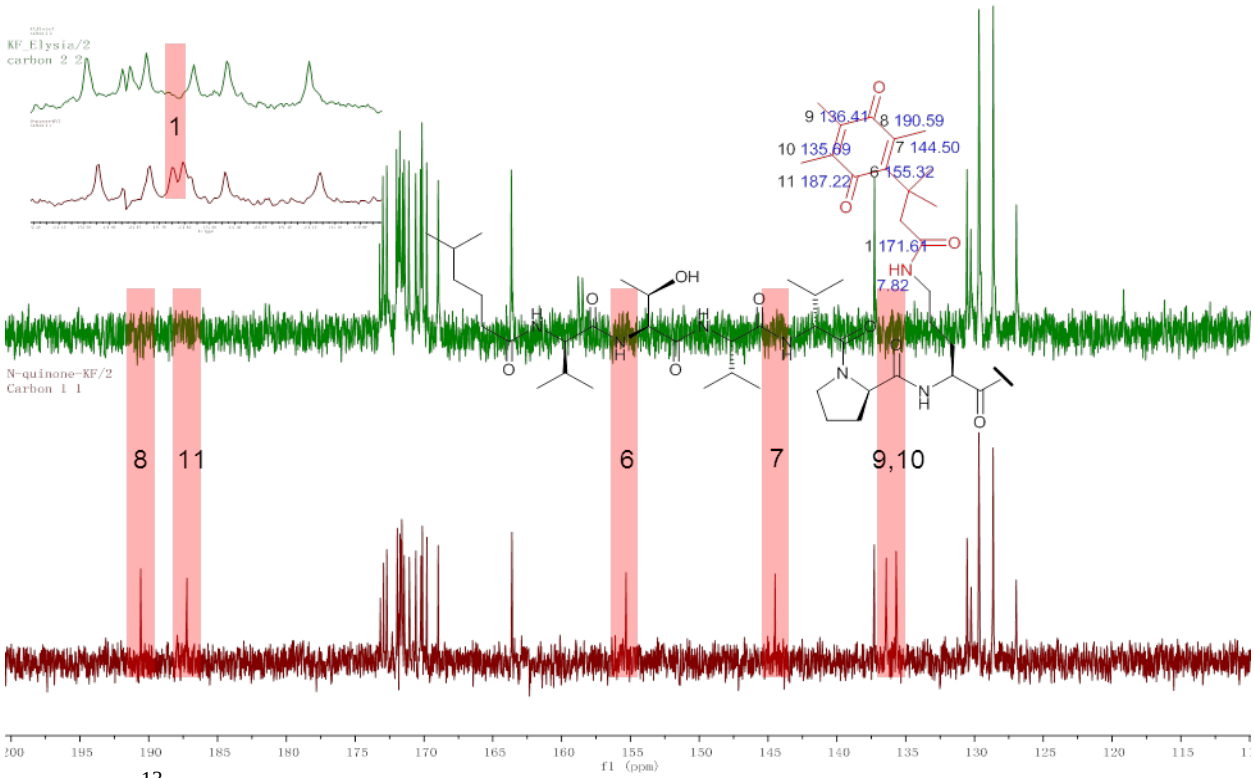

Figure 53 ^{13}C NMR spectra (δ_C 110-200) of KF (top) and benzoquinone-KF **(15)** (bottom) in DMSO-d_6

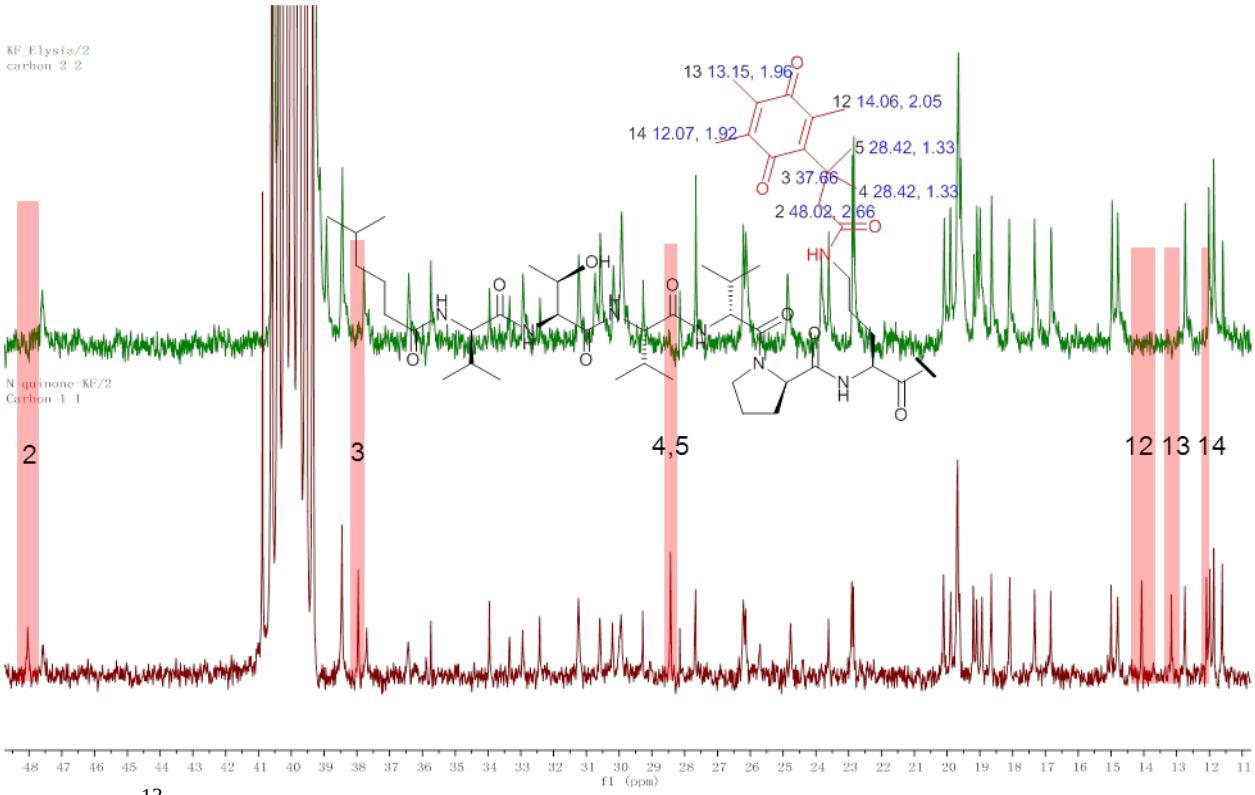

Figure 54 ^{13}C NMR spectra (δ_C 10-50) of KF (top) and benzoquinone-KF **(15)** (bottom) in DMSO-d_6

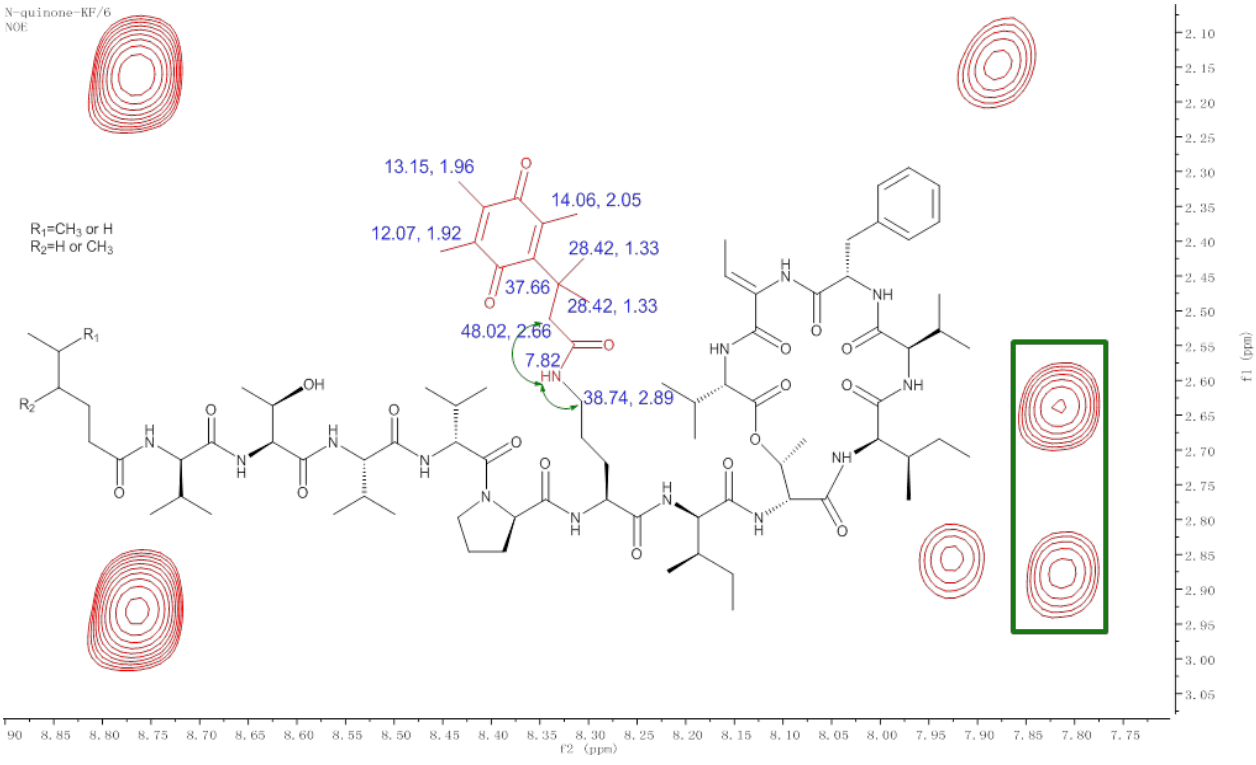

Figure 55 NOESY spectrum of benzoquinone-KF **(15)** in DMSO-d_6

3. Materials and Methods

3.1 General Experimental Procedures. NMR spectra were recorded on a Bruker Avance DRX-400 spectrometer. The ^{1}H and ^{13}C NMR chemical shifts were reported in ppm. IR spectra were measured on a PerkinElmer Spectrum 100 FT-IR spectrometer. HPLC-ESI-TOF was performed on Bruker MicroTOF spectrometer in line with an Agilent 1100 Series HPLC system and G1316A DAD detector. Preparative HPLC was carried out on a Waters PrepLC system with a single wavelength detector. Phenomenex Luna C_{18} 5 μm column (250 mm × 20.2 mm) was used. Optical rotations were measured on a JASCO DIP-370 polarimeter. The succinimide ester of bezoquinone derivative, 3-methyl-3-(2,3,5-trimethyl-1,4-benzoquinonyl)butanoic succinimide ester, was kindly provided by Dr. Seongbong Jo of the Department of Pharmaceutics, The University of Mississippi. All other reagents were purchased from Sigma-Aldrich.

3.2 Elongation of Amino Acid Chain on KF (1-8). 4-Methylhexanoic acid (1 mmol) was dissolved in 25 mL anhydrous DCM, HOSu (1 eq.) and EDCI (2 eq.) were added. The mixture was stirred at room temperature for 1 d, water (25 mL) was then added. The mixture was extracted with EtOAc three times. The combined organic layers were evapored under vacuum. The resulting residue was purified by flash silica chromatography using hexanes-EtOAc (8:2).

N-Boc protected amino acid (0.1 mmol) was dissolved in 3 mL anhydrous DMF, HOSu (1 eq.) and EDCI (2 eq.) were added. The mixture was stirred at room temperature for 2 d, and extracted with DCM-H_2O (2:1) (3×10 mL). The combined organic layers were evapored under vacuum. The second amino acid (0.1mmol) was added and dissolved in 5mL DMSO. The mixture was stirred at room temperature for 1 or 2 d and the solvent was evaporated under vacuum. The product was purified using C_{18} glass open-tubular column with MeCN-H_2O (1:1). Purified product was dissolved in TFA-H_2O (1:1) and stirred at room temperature for 1 h. The

solution was concentrated in vacuum and purified using C_{18} glass open-tubular column with H_2O to afford a dipeptide.

Purified 4-methylhexanoic ester (0.05 mmol) and dipeptide (0.05 mmol) were dissolved in 2 mL DMSO. The mixture was stirred at room temperature for 1 d and the solvent was evaporated under vacuum. The product was purified by HPLC using a C_{18} 5 μm column (250 mm × 20.2 mm) with a gradient elution of MeCN-H_2O from 20:80 to 80:20 at a flow rate of 8.0 mL/min to afford the *C*-terminal fragment.

KF (450 mg, 0.3 mmol) was dissolved in MeCN-DMSO (8:2) solution, Fmoc-OSu (1.5 eq.) was slowly added. The reaction mixture was stirred at room temperature for 8 h and the solvent was evaporated under vacuum. The product was purified by HPLC using a C_{18} 5 μm column (250 mm × 20.2 mm) with a gradient elution of MeCN-H_2O in 0.05% HCOOH from 50:50 to 100:0 at a flow rate of 8.0 mL/min to afford Fmoc-KF (90% yield). Fmoc-KF was dissolved in 6 M HCl-MeOH (1:2), and stirred under reflux at 70 ℃ for 12 h. The solvent was evaporated under vacuum and the product was purified by HPLC using a C_{18} 5 μm column (250 mm × 20.2 mm) with a gradient elution of MeCN-H_2O in 0.05% HCOOH from 20:80 to 80:20 at a flow rate of 8.0 mL/min to afford the partial hydrolyzed Fmoc-KF (70% yield).

Partial hydrolyzed Fmoc-KF (10mg, 6.7 μmol), synthesized *C*-terminal fragment (1.5 eq.), EDCI (5 eq.) and HOBt (5 eq.) were dissolved in 2 mL anhydrous DMF. The mixture was stirred at room temperature for 2 d and the solvent was evaporated under vacuum. The product was purified by HPLC using a C_{18} 5 μm column (250 mm × 20.2 mm) with a gradient elution of MeCN-H_2O in 0.05% HCOOH from 50:50 to 100:0 at a flow rate of 8.0 mL/min (80% yield). The coupling product was deprotected using 10% piperidine in 1 mL DMSO at room temperature for 2 h and the solvent was evaporated under vacuum, followed by HPLC

purification using a C_{18} 5 μm column (250 mm × 20.2 mm) with a gradient elution of MeCN-H_2O in 0.05% HCOOH from 20:80 to 80:20 at a flow rate of 8.0 mL/min to afford **1-8** (90% yield).

1 (6.2 mg) was obtained as white amorphous powder. $[\alpha]_D^{25}$ -14 (*c* 0.1, MeOH); UV λ_{max} (MeOH) 205, 224 nm; IR neat (KBr) 3280 (s, br), 2964 (s), 2932 (s), 2877 (s), 1736 (s), 1632 (s), 1514 (s), 1465 (s), 1383 (s), 1342 (s), 1227 (s), 1025 (s) cm^{-1}; HRMS *m/z* calc. for $C_{75}H_{125}N_{14}O_{16}$ $[M+H]^+$ 1477.9393, detected 1477.9453.

2 (6.5 mg) was obtained as white amorphous powder. $[\alpha]_D^{25}$ -32 (*c* 0.1, MeOH); UV (DAD) λ_{max} (MeOH) 205, 224 nm; IR neat (KBr) 3280 (s, br), 2965 (s), 2932 (s), 2876 (s), 1736 (s), 1633 (s), 1515 (s), 1464 (s), 1383 (s), 1341 (s), 1226 (s), 1024 (s) cm^{-1}; HRMS *m/z* calc. for $C_{70}H_{115}N_{13}NaO_{15}$ $[M+Na]^+$ 1400.8533, detected 1400.8471.

3 (6.1 mg) was obtained as white amorphous powder. $[\alpha]_D^{25}$ -16 (*c* 0.1, MeOH); UV (DAD) λ_{max} (MeOH) 205, 224 nm; IR neat (KBr) 3280 (s, br), 2964 (s), 2932 (s), 2876 (s), 1736 (s), 1633 (s), 1515 (s), 1464 (s), 1383 (s), 1342 (s), 1227 (s), 1025 (s) cm^{-1}; HRMS *m/z* calc. for $C_{80}H_{134}N_{15}O_{17}$ $[M+H]^+$ 1577.0077, detected 1577.0082.

4 (6.4 mg) was obtained as white amorphous powder. $[\alpha]_D^{25}$ -14 (*c* 0.1, MeOH); UV (DAD) λ_{max} (MeOH) 205, 224 nm; IR neat (KBr) 3280 (s, br), 2964 (s), 2932 (s), 2876 (s), 1736 (s), 1633 (s), 1515 (s), 1464 (s), 1383 (s), 1342 (s), 1227 (s), 1025 (s) cm^{-1}; HRMS *m/z* calc. for $C_{80}H_{134}N_{15}O_{17}$ $[M+H]^+$ 1577.0077, detected 1577.0137.

5 (5.8 mg) was obtained as white amorphous powder. $[\alpha]_D^{25}$ -30 (*c* 0.1, MeOH); UV (DAD) λ_{max} (MeOH) 205, 224 nm; IR neat (KBr) 3281 (s, br), 2964 (s), 2932 (s), 2874 (s), 1736 (s), 1633 (s), 1516 (s), 1462 (s), 1384 (s), 1343 (s), 1227 (s), 1024 (s) cm^{-1}; HRMS *m/z* calc. for $C_{81}H_{136}N_{15}O_{17}$ $[M+H]^+$ 1591.0233, detected 1591.0335.

6 (5.6 mg) was obtained as white amorphous powder. $[\alpha]_D^{25}$ -16 (*c* 0.1, MeOH); UV (DAD) λ_{max} (MeOH) 205, 224 nm; IR neat (KBr) 3281 (s, br), 2965 (s), 2932 (s), 2877 (s), 1736 (s), 1633 (s), 1515 (s), 1464 (s), 1383 (s), 1342 (s), 1227 (s), 1025 (s) cm^{-1}; HRMS *m/z* calc. for $C_{80}H_{131}N_{15}NaO_{17}$ $[M+Na]^+$ 1596.9745, detected 1596.9690.

7 (6.4 mg) was obtained as white amorphous powder. $[\alpha]_D^{25}$ -22 (*c* 0.1, MeOH); UV (DAD) λ_{max} (MeOH) 205, 224 nm; IR neat (KBr) 3284 (s, br), 2965 (s), 2932 (s), 2873 (s), 1736 (s), 1633 (s), 1525 (s), 1454 (s), 1389 (s), 1344 (s), 1230 (s), 1024 (s) cm^{-1}; HRMS *m/z* calc. for $C_{84}H_{134}N_{15}O_{17}$ $[M+H]^+$ 1625.0077, detected 1625.0131.

8 (6.2 mg) was obtained as white amorphous powder. $[\alpha]_D^{25}$ -18 (*c* 0.1, MeOH); UV (DAD) λ_{max} (MeOH) 208, 228 nm; IR neat (KBr) 3288 (s, br), 2965 (s), 2932 (s), 2877 (s), 1736 (s), 1641 (s), 1521 (s), 1455 (s), 1389 (s), 1343 (s), 1280 (s), 1233 (s), 1026 (s) cm^{-1}; HRMS *m/z* calc. for $C_{84}H_{132}F_2N_{15}O_{17}$ $[M+H]^+$ 1660.9888, detected 1660.9999.

3.3 Formation of Compounds 9-11. KF (90 mg, 60 μmol) was dissolved in MeCN-DMSO (8:2) solution, Fmoc-Cl (1.5 eq.) and DMAP (0.25 eq.) were slowly added. The reaction mixture was stirred at room temperature for 8 h and the solvent was evaporated under vacuum. The product was purified by HPLC using a C_{18} 5 μm column (250 mm × 20.2 mm) with a gradient elution of MeCN-H_2O in 0.05% HCOOH from 50:50 to 100:0 at a flow rate of 8.0 mL/min to afford **9** (73 mg) as white amorphous powder (80% yield). $[\alpha]_D^{25}$ -12 (*c* 0.1, MeOH); UV (DAD) λ_{max} (MeOH) 208, 228 nm; IR neat (KBr) 3278 (s, br), 2964 (s), 2932 (s), 2873 (s), 1738 (s), 1629 (s), 1520 (s), 1463 (s), 1385 (s), 1229 (s), 1025 (s) cm^{-1}; HRMS *m/z* calc. for $C_{76}H_{124}N_{14}NaO_{17}$ $[M+Na]^+$ 1527.9167, detected 1527.9134.

Compound **9** (45 mg, 0.03 mmol) was dissolved in 6 M HCl-MeOH (1:2), and partial hydrolyzed using the same method provided above. Its hydrolyzed product was coupled to 4-

methylhexanoic succinimide ester (1 eq.) using the same approach as described above to yield **10** (22 mg) as white amorphous powder. $[\alpha]_D^{25}$ -14 (*c* 0.1, MeOH); UV (DAD) λ_{max} (MeOH) 205, 224 nm; IR neat (KBr) 3276 (s, br), 2965 (s), 2932 (s), 2876 (s), 1736 (s), 1639 (s), 1520 (s), 1455 (s), 1382 (s), 1227 (s), 1203 (s), 1025 (s) cm^{-1}; HRMS *m/z* calc. for $C_{71}H_{115}N_{13}NaO_{16}$ $[M+Na]^+$ 1428.8482, detected 1428.8409.

KF (15 mg, 0.01 mmol) was dissolved in 6 M HCl-MeOH (1:2), and partial hydrolyzed using the same method provided above. Its hydrolyzed product was coupled to 4-methylhexanoic succinimide ester (2 eq.) using the same approach as described above to yield **11** (8 mg) as white amorphous powder. $[\alpha]_D^{25}$ -8 (*c* 0.1, MeOH); UV (DAD) λ_{max} (MeOH) 205, 224 nm; IR neat (KBr) 3281 (s, br), 2964 (s), 2932 (s), 2873 (s), 1736 (s), 1629 (s), 1582 (s), 1454 (s), 1381 (s), 1348 (s), 1227 (s), 1025 (s) cm^{-1}; HRMS *m/z* calc. for $C_{77}H_{127}N_{13}NaO_{16}$ $[M+Na]^+$ 1512.9421, detected 1512.9361.

3.4 Dehydration of KF (12). KF (30mg, 0.02 mmol) was dissolved in 2 mL anhydrous DCM-DMSO (9:1), BAST (4 eq.) was added. The reaction mixture was stirred at -78℃ for 2 h, and allowed to warm to room temperature for an additional 2 h. The solvent was evaporated under vacuum and purified by HPLC using a C_{18} 5 μm column (250 mm × 20.2 mm) with a gradient elution of MeCN-H_2O in 0.05% HCOOH from 20:80 to 80:20 at a flow rate of 8.0 mL/min to afford **12** (5.9 mg) as white amorphous powder. Yield 20%; $[\alpha]_D^{25}$ -12 (*c* 0.1, MeOH); UV (DAD) λ_{max} (MeOH) 205, 224 nm; IR neat (KBr) 3280 (s, br), 2964 (s), 2932 (s), 2877 (s), 1736 (s), 1632 (s), 1514 (s), 1465 (s), 1383 (s), 1342 (s), 1227 (s), 1025 (s) cm^{-1}; HRMS *m/z* calc. for $C_{75}H_{123}N_{14}O_{15}$ $[M+H]^+$ 1459.9287, detected 1459.9350.

3.5 Cyclization of KG (13, 14). KG (30 mg, 0.02 mmol), EDCI (2 eq.) and HOBt (2 eq.) were dissolved in 3 mL anhydrous DMF. The reaction mixture was stirred at room temperature for 2 d,

and the solvent was evaporated under vacuum. The product was purified by HPLC using a C_{18} 5 μm column (250 mm × 20.2 mm) with a gradient elution of MeCN-H_2O in 0.05% HCOOH from 20:80 to 80:20 at a flow rate of 8.0 mL/min to afford **13** and **14.**

13 (2.9 mg) was obtained as white amorphous powder. Yield 10%; $[\alpha]_D^{25}$ +30 (*c* 0.1, MeOH); UV (DAD) λ_{max} (MeOH) 205, 224 nm; IR neat (KBr) 3280 (s, br), 2964 (s), 2932 (s), 2873 (s), 1629 (s), 1516 (s), 1455 (s), 1386 (s), 1227 (s), 1025 (s) cm^{-1}; HRMS *m/z* calc. for $C_{75}H_{124}N_{14}NaO_{16}$ $[M+Na]^+$ 1499.9217, detected 1499.9186.

14 (3.2 mg) was obtained as white amorphous powder. Yield 11%; $[\alpha]_D^{25}$ +24 (*c* 0.1, MeOH); UV (DAD) λ_{max} (MeOH) 205, 224 nm; IR neat (KBr) 3280 (s, br), 2964 (s), 2932 (s), 2873 (s), 1629 (s), 1515 (s), 1454 (s), 1385 (s), 1226 (s), 1025 (s) cm^{-1}; HRMS *m/z* calc. for $C_{75}H_{124}N_{14}NaO_{16}$ $[M+Na]^+$ 1499.9217, detected 1499.9141.

3.6 Amidation of KF (15). KF (45 mg, 30 μmol) was dissolved in 15 mL solution of MeCN-DMSO (8:2), the benzoquinone derivative (1.5 eq.) was slowly added. The reaction mixture was stirred at room temperature for 8 h, and the solvent was evaporated under vacuum. The product was purified by HPLC using a C_{18} 5 μm column (250 mm × 20.2 mm) with a gradient elution of MeCN-H_2O in 0.05% HCOOH from 50:50 to 100:0 at a flow rate of 8.0 mL/min to afford **15** (42 mg) as yellow amorphous powder. Yield 80%; $[\alpha]_D^{25}$ -4 (*c* 0.1, MeOH); UV (DAD) λ_{max} (MeOH) 210, 234 nm; IR neat (KBr) 3286 (s, br), 2964 (s), 2936 (s), 2876 (s), 1736(s), 1633 (s), 1515 (s), 1465 (s), 1373 (s), 1226 (s), 1021 (s) cm^{-1}; HRMS *m/z* calc. for $C_{89}H_{140}N_{14}NaO_{19}$ $[M+Na]^+$ 1732.0317, detected 1732.0382.

3.7 Antitumor Assay. The cytotoxicity soft-agar based disc diffusion assay defines the differential cell killing among the 13 cell types examined. This unique and effective model was used to guide the discovery of novel molecular structures with anticancer potential. The screen

included 11 cell types: two leukemias (murine L1210 and human CCRF-CEM), eight solid tumors (murine Colon 38, human colon HCT116, human lung H125, human ovarian OVCAR5, Human breast MCF7, human prostate LNCaP, human pancreatic cancer PANC1 and human brain U251N), as well as two normal types, a murine and human normal cell (hematopoietic progenitor cell, CFU-GM). Differential cytotoxicity was the endpoint with four possible positive outcomes: Murine solid tumor selectivity relative to leukemia, human solid tumor selectivity relative to leukemia; and, murine or human solid tumor selectivity relative to the normal cell. Murine L1210 and human CCRF-CEM were the reference tumors of the assay.

Colon 38 gave a good monodispersed cell suspension with mechanical disruption from a murine tumor. Colon 38 (approx. 1g) was cut into small fragments in 15 mL of Hank's Balanced Salt Solution (HBSS) over a 100-mesh sieve and gently forced through by the scissors with HBSS constantly perfusing the sieve. The material was drawn into and out of a 5 mL syringe without a needle to further disperse the cell clumps. It was diluted and plated in 0.3% agarose in DMEM plus 10% heat-inactivated Bovine Calf Serum (BCS). For plating of all of the cell types other than the normal CFU, the 60 mm plates were first prepared with a hard agar bottom layer (0.6% agar in RPMI-1640 plus 15% BCS).

The human cancer cell lines were maintained in cell culture. They were removed from their cultures by a trypsin-collagenase-DNAase cocktail. Their plating efficiencies were sufficiently high that 30,000 to 60,000 cells in 3 mL produce the targeted number of colonies (over 10,000 per plate) in the 60 mm plates. This soft agar top layer (0.3% with the serum and media as above) plus the titrated tumor cells were poured into the plates and allowed to solidify.

For CFU-GM, the femoral marrow of C57Bl/6 mice was flushed with MEM-alpha; 2 mL per femur. The cells are passed through an 18-gauge needle twice and the monodispersed

suspension counted. A total of $1.5x10^6$ cells were plated in 3 mL of 0.3% agar with the addition of 10% L-cell conditioned media, which provided colony stimulating factor, in MEM-alpha plus 10% BCS. For human CFU-GM, the cells were obtained from Poietic Technologies, Inc. (Gaithersburg, MD) overnight and washed twice with PBS before being titered and added to the agar mixture. The same cell number, culture conditions and conditioning factors were used as with the murine marrow.

A volume of 15 μL of each sample was dropped onto a 6.5 mm filter disc. The disc was allowed to dry overnight and then placed close to the edge of the petri dish. The plates were incubated for 7-10 days (depending upon the cell type) and examined by an inverted stereo-microscope (10X) for measurement of the zone of inhibition measured from the edge of the filter disc to the beginning of normal-sized colony formation. The diameter of the filter disc, 6.5 mm, was arbitrarily taken as 200 units. A difference in zones between solid tumor cells and either normal or leukemia cells of 250 units defines solid tumor selective compounds. If the test material was excessively toxic at the first dosage, a range of dilutions of the agents (at either 1:4 or 1:10 decrements) against the same tumors were retested. At some dilution, quantifiable cytotoxicity was invariably obtained. The results were expressed as, for example, $_{\text{HCT-116}}\Delta_{\text{CFU}} = 350$, which indicated that there is a 350 unit zone differential between human colon HCT-116 and normal CFU-GM; such a differential ($\geq$250 units) was of a sufficient magnitude to proceed with further pharmacological studies.

CHAPTER *2*

KAHALALIDES FROM THE MOLLUSK *Elysia rufescens*

1. Introduction

Bryopsis and *Elysia* species generate a variety of depsipeptides with different activities. For example, kahalalide A shows inhibition against *Mycobacterium tuberculosis*; KF and isoKF show activities against solid tumor cell lines, HSV II, fungi, as well as leishmania; norkahalalide A (norKA) exerts inhibition of the Y_1 receptor **(Table 6)**. The MALDI-TOF mass imaging analysis of the tissue of the mollusk *Elysia rufescens* indicated the presence of kahalalide C $[M+Na]^+$ at *m/z* 936, and KF $[M+Na]^+$ at *m/z* 1500. Some new metabolites at *m/z* 761, 797, 747, and 770 were distributed on the different positions of the organism **(Figure 56)**. To acquire KF as the starting material of its analogues, both *E. rufescens* and *Bryopsis pennata* were collected. During the isolation, new peptides were identified from *E. rufescens* using a chemical dereplication approach. Further purification afforded nine new and 10 known kahalalides. In this chapter, purification and structure elucidation of the new peptides are discussed.

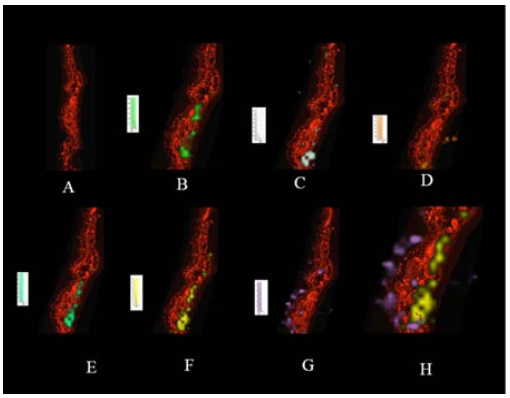

A: Epifluorescence image of a transverse 14 μm thick section across the middle of the *E. rufescens* at 590 nm; **B-G:** Epifluorescence (590 nm) image overlaid by MALDI image at *m/z* 761, 797, 936, 747, 770, 1500 indicating the localization of compounds; **H:** Epifluorescence (590 nm) image overlaid by MALDI image at m/z 770 (yellow) and 1500 (purple) showing the differential localization of the molecules.

Figure 56 MALDI imaging of the *E. rufescens*

Table 6 Kahalalide family peptides

Compounds	Mol wt	Mol formula	Activity	Reference
kahalalide A	893.49	$C_{46}H_{67}N_7O_{11}$	Antituberculosis; Antimalarial activity	12
norKA	879.47	$C_{46}H_{65}N_7O_{11}$	Y_1 receptor inhibition	44
kahalalide B	877.46	$C_{45}H_{63}N_7O_{11}$	---	12
kahalalide C	913.47	$C_{47}H_{63}N_9O_{10}$	---	12
kahalalide D	595.35	$C_{31}H_{45}N_7O_5$	---	12
kahalalide E	835.52	$C_{45}H_{69}N_7O_8$	Anti HSV II	12
kahalalide F isoKF	1476.93	$C_{75}H_{124}N_{14}O_{16}$	Anticancer *in vitro* and *in vivo* against solid tumor cell lines; Anti HSV II; Antifungal activity	12, 11
5-OHKF	1492.93	$C_{75}H_{124}N_{14}O_{17}$	Moderate antimalarial activity	44
kahalalide G	1494.94	$C_{75}H_{126}N_{14}O_{17}$	---	12
kahalalide H	1110.58	$C_{55}H_{82}N_8O_{16}$	---	45
kahalalide J	1238.67	$C_{61}H_{94}N_{10}O_{17}$	---	45
kahalalide K	891.47	$C_{46}H_{65}N_7O_{11}$	---	46
kahalalide O	932.50	$C_{48}H_{68}N_8O_{11}$	---	47
kahalalide P	1317.72	$C_{66}H_{99}N_{11}O_{17}$	Moderate inhibition on HL-60 cancer cell lines	48
kahalalide Q	1301.72	$C_{66}H_{99}N_{11}O_{16}$	Moderate inhibition on HL-60 cancer cell lines	48
kahalalide R	1518.94	$C_{77}H_{126}N_{14}O_{17}$	Anticancer activity against MCF7 human mammary carcinoma cell line	49
kahalalide S	1534.94	$C_{77}H_{126}N_{14}O_{18}$	---	49
kahalalide R2	1462.92	$C_{74}H_{122}N_{14}O_{16}$	---	50
kahalalide S2	1490.95	$C_{76}H_{126}N_{14}O_{16}$	---	50
kahalalide V	613.36	$C_{31}H_{47}N_7O_6$	---	51
kahalalide W	611.34	$C_{31}H_{45}N_7O_6$	---	51
kahalalide X	931.48	$C_{47}H_{65}N_9O_{11}$	---	51
kahalalide Y	875.48	$C_{46}H_{65}N_7O_{10}$	---	51

2. Results and Discussion

2.1 Dereplication. Dereplication approaches were used to improve the efficiency of new molecule identification. One of the typical features of peptides is that multiple charged ions, especially double charged ions $[M+2H]^{2+}$ in small peptides can be detected by LC-MS **(Figure 57)**. In the dereplication of kahalalide peptides, the LC-MS signals with both double and single charged ions were scanned to quickly determine molecular weight. Determined molecular weights were searched using Marinlit which is the library for all known marine natural products **(Figure 58)**. If the mass was not identified via this route, the peptide could be considered new and worth pursuing for further isolation and biological evaluation.

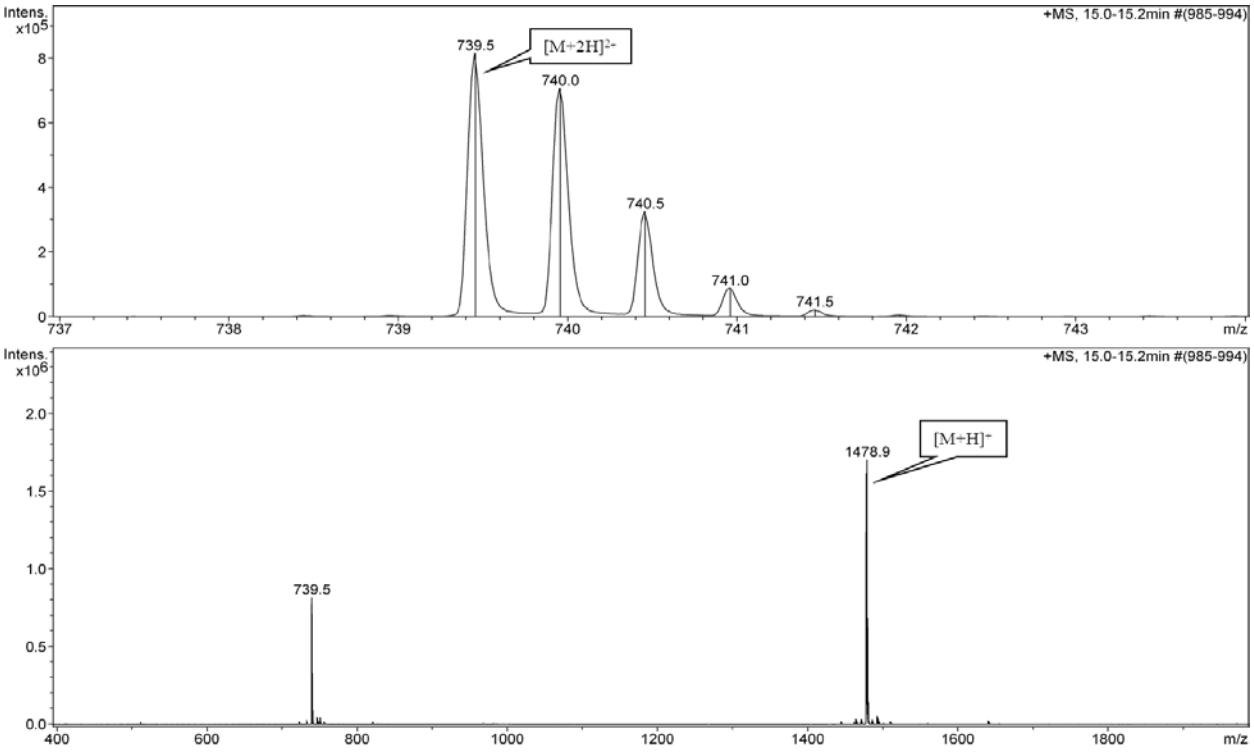

Figure 57 An example of a double charged ion in KF

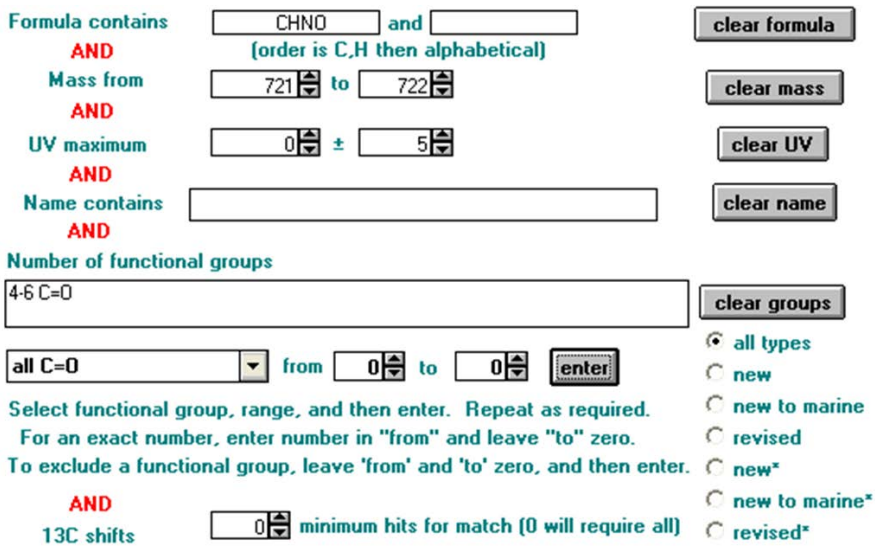

Figure 58 An example of marine product searching on Marinlit

2.2 MALDI-Imaging on *E. rufescens.* The snail sample was thawed, precut, and embedded in 1´ Dulbecco's PBS and placed in the cryostat at -20 ℃. Once the tissue and embedding block had frozen completely, 10- to 20-mm-thick coronal sections were cut and mounted onto a semithawed MALDI plate. The plate was desiccated at 38 ℃ for 10 min. The MALDI plate containing the snail tissue slices was imaged on a Zeiss Axioskop. Two sets of images were collected within the same region of the sponge tissue slice at ´400 (Image B: Zeiss filter set #14, emission 590 nm+; Image C: Zeiss filter set #2, emission 420 nm+). After gathering photomicrographs of the samples using a Nikon digital camera (2 megapixels), a matrix composed of 35 mg/mL α-cyanohydroxycinnamic acid, 35 mg/mL DHB, 78% MeCN, and 0.1% TFA was coated onto the MALDI plate by using an airbrush (www.paascheairbrush.com). The Bruker MSP 96 anchor target plate containing sample and matrix was then placed in an empty Petri dish until the sample was analyzed. A photomicrograph of the sample to be imaged by mass spectrometry was loaded onto the flexImaging command window. Three teach points were selected to align the background image with the sample target plate. After the target plate

calibration was complete, the AutoXecute command was used to analyze the samples: 350-2,000 m/z window, reflector mode, positive ion mode, 100-mV electronic gain, and real-time smooth off. The instrument was calibrated externally by using a digest of BSA as a standard. In the resulting spectra, different colors were designated to the different masses allowing the visualization of their respective distribution in the rastering window.

2.3 Extraction and Isolation. An EtOH extract of *E. rufescens* was subjected to silica gel vacuum-liquid chromatography followed by the fractionation on an HP-20 column. The LC-MS data of each fraction showed that the MeOH-H_2O (90:10) and 100% MeOH fractions mainly contained peptides. The two fractions were subjected to open column chromatography on C_{18}, followed by preparative HPLC (Phenomenex C_{18} column 21.2 × 250 mm) at a flow rate of 8 mL/min or HPLC (Phenomenex C_8 column 10.0 × 250 mm) at a flow rate of 2.5 mL/min to yield 10 known peptides kahalalide D **(16)**, kahalalide A **(21)**, kahalalide B **(22)**, kahalalide H **(23)**, kahalalide O **(24)**, kahalalide G **(28)**, kahalalide R2 **(31)**, kahalalide F **(32)**, kahalalide P **(33)**, 5-OHKF **(34)**, and nine new peptides **(17-20, 25-27, 29, 30)**, among which five peptides **(17, 20, 25-27)** were determined based on HRMS and 1D, 2D NMR spectra, while the structures of remaining four peptides could not be assigned due to their trace amounts **(Figure 59)**. It was noticed that new metabolites at *m/z* 761, 797, 747, and 770 detected using MALDI imaging were not isolated. There are several possibilities. Firstly, the metabolites are instable and degraded during the purification procedure. Secondly, those metabolites are not peptides. Hence, they were not localized when using the dereplication approach.

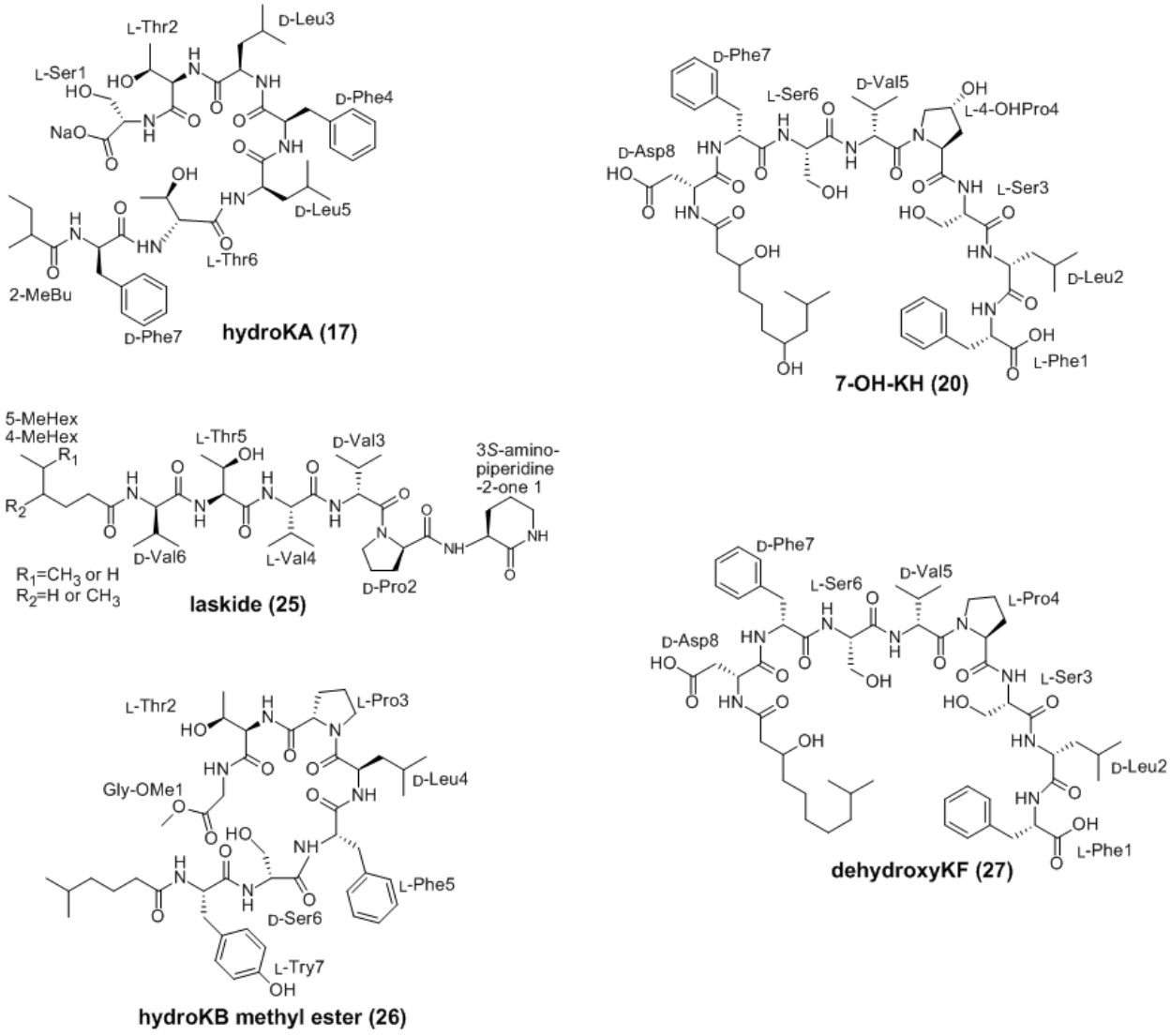

Figure 59 Structures of new kahalalides

2.4 Structure Elucidation.

HydroKA **(17)** (1.2 mg, yield 0.00012%) was obtained as white amorphous powder. HRMS provided quasi-molecular signals $[M+2Na]^{2+}$ at *m/z* 478.7487, $[M+H]^{+}$ at *m/z* 934.4843, and $[M+Na]^{+}$ at *m/z* 956.4696 **(Figure 60)** indicating the molecule is a sodium carboxylate for a molecular formula of $C_{46}H_{68}N_7Na_2O_{12}$ (calc. 956.4721, Δ -2.6 ppm). The ^{1}H, ^{13}C, and HMBC NMR spectra **(Figure 61-64)** displayed seven amide proton signals at δ_H 7.74-8.12, as well as seven amide carbonyls at δ_C 170.12, 170.16, 171.47, 171.98, 172.28, 172.34, and 175.99,

indicating the presence of seven amino acid residues. An additional carbonyl at δ_C 172.36 suggested the presence of an ester bond. The ^1H and ^{13}C NMR spectra also displayed 10 aromatic protons at δ_H 7.16-7.24, and six pairs of aromatic carbons at δ_C 126.65-138.31, demonstrating the presence of two Phe residues. The methylene group at δ_C 61.90 suggested the presence of one Ser residue. Two methine groups at δ_C 66.99 suggested the presence of two Thr residues **(Table 7)**. The assignment of amino acid residues of **17** and their correlation were identified using an HMBC experiment **(Figure 64)**. Correlations between the NH (δ_H 7.82) of Ser 1 and the carbonyl (δ_C 170.16) of Thr2, the NH (δ_H 7.66) of Thr2 and the carbonyl (δ_C 172.34) of Leu3, the NH (δ_H 8.00) of Leu3 and the carbonyl (δ_C 171.47) of Phe4, the NH (δ_H 7.96) of Phe4 and the carbonyl (δ_C 172.36) of Leu5, the NH (δ_H 7.72) of Leu5 and the carbonyl (δ_C 170.12) of Thr6, the NH (δ_H 7.76) of Thr6 and the carbonyl (δ_C 171.98) of Phe7, as well as the NH (δ_H 8.01) of Phe7 and the carbonyl (δ_C 175.99) of the 2-methylbutric acid residue, were observed **(Figure 65)**. The specific rotation $[\alpha]_D^{25}$ of **17** (*c* 0.1, MeOH) is 0. This could be attributed to the sodium carboxylate. The presence of sodium may influence the intramolecular interactions such as the H-bond formation, thus allowing sp^3 carbons on amino acid residues to rotate freely. Marfey's analysis revealed that Ser1, Thr2, Thr6 of **17** have the L- configurations, while Leu3, Phe4, Leu5, and Phe7 of **17** have the D- configurations **(Figure 66)**.

Table 7 ^{1}H and ^{13}C NMR data of hydroKA **(17)**[a] (δ in ppm, DMSO-d_6)

	Carbon	δ_C, mult	δ_H, mult.	*J* (Hz)		Carbon	δ_C, mult	δ_H, mult.	*J* (Hz)
Ser1	1	172.28, qC	(NH) 7.82 d	7.7	Leu5	1	172.36, qC	(NH) 7.72, d	7.8
	2	55.11, CH	4.36, m			2	52.09, CH	4.36, m	
	3	61.90, CH_2	3.73, dd	11.1, 3.6		3	41.30, CH_2	1.52, 1.41, m	
			3.64, dd	10.9, 4.5		4	24.57, CH	1.57, m	
Thr2	1	170.16, qC	(NH) 7.66, d	8.4		5	23.50, CH_3	0.87, m	
	2	58.48, CH	4.15, m			6	23.44, CH_3	0.87, m	
	3	66.99, CH	3.92, m		Thr6	1	170.12, qC	(NH) 7.76, d	7.8
	4	19.74, CH_3	0.91, m			2	57.90, CH	4.28, m	
Leu3	1	172.34, qC	(NH) 8.00,d	8.0		3	66.99, CH	3.97, m	
	2	51.91, CH	4.26, m			4	19.59, CH_3	1.02, d	6.3
	3	41.23, CH_2	1.52, 1.41, m		Phe7	1	171.98, qC	(NH) 8.01, d	7.7
	4	24.33, CH	1.51, m			2	54.64, CH	4.60, m	
	5	22.02, CH_3	0.82, m			3	37.67, CH_2	3.07, 2.84, m	
	6	21.93, CH_3	0.82, m			4	138.31, qC		
Phe4	1	171.47, qC	(NH) 7.96, d	8.3		5,5'	129.53, CH	7.24, m	
	2	54.64, CH	4.60, m			6,6'	128.44, CH	7.26, m	
	3	37.66, CH_2	3.07, 2.82, m			7	126.65, CH	7.17, m	
	4	138.31, qC			2Mebut	1	175.99, qC		
	5,5'	129.58, CH	7.24, m			2	41.49, CH	2.19, m	
	6,6'	128.50, CH	7.26, m			3	27.07, CH_2	1.36, 1.22, m	
	7	126.65, CH	7.17, m			4	17.87, CH_3	0.93, d	6.8
						5	11.86, CH_3	0.59, t	7.4

[a]Assignments based on ^{1}H, ^{13}C, HSQC and HMBC NMR (100/400 MHz) experiments at room temperature.

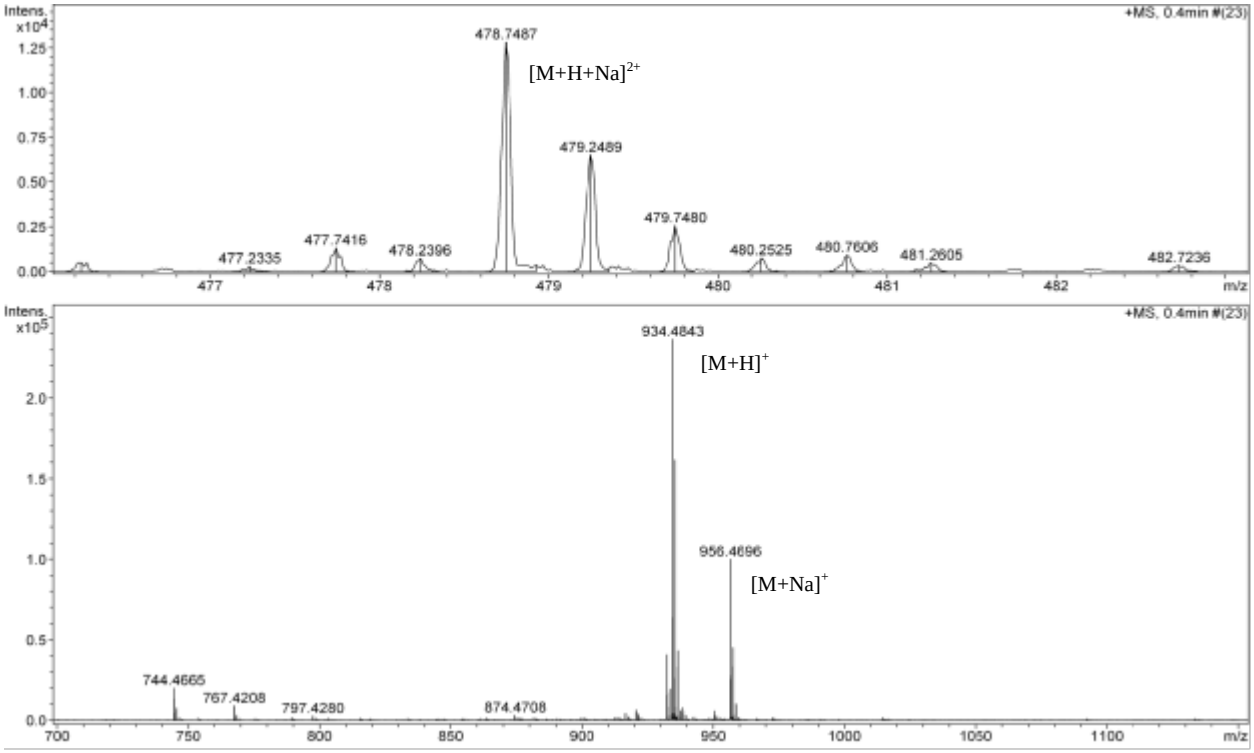

Figure 60 HRMS spectrum of hydroKA **(17)**

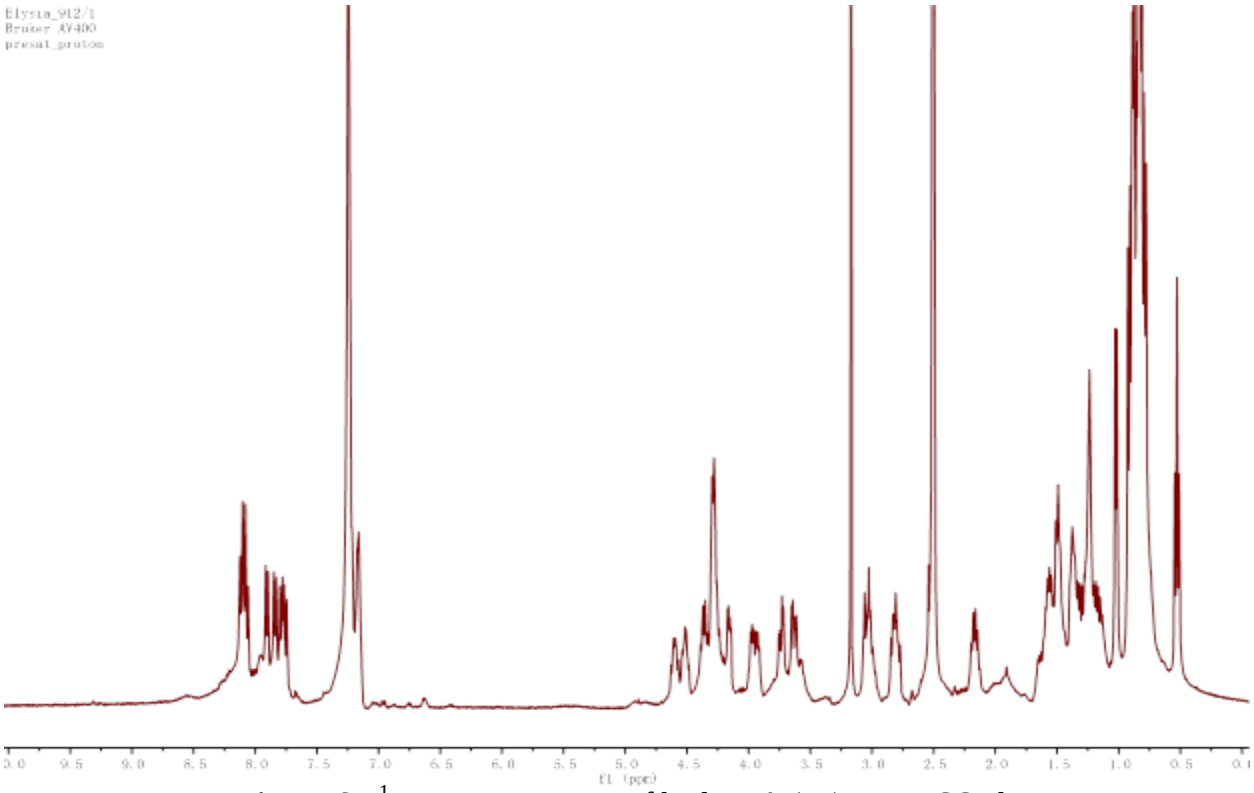

Figure 61 ^{1}H NMR spectrum of hydroKA **(17)** in DMSO-d_6

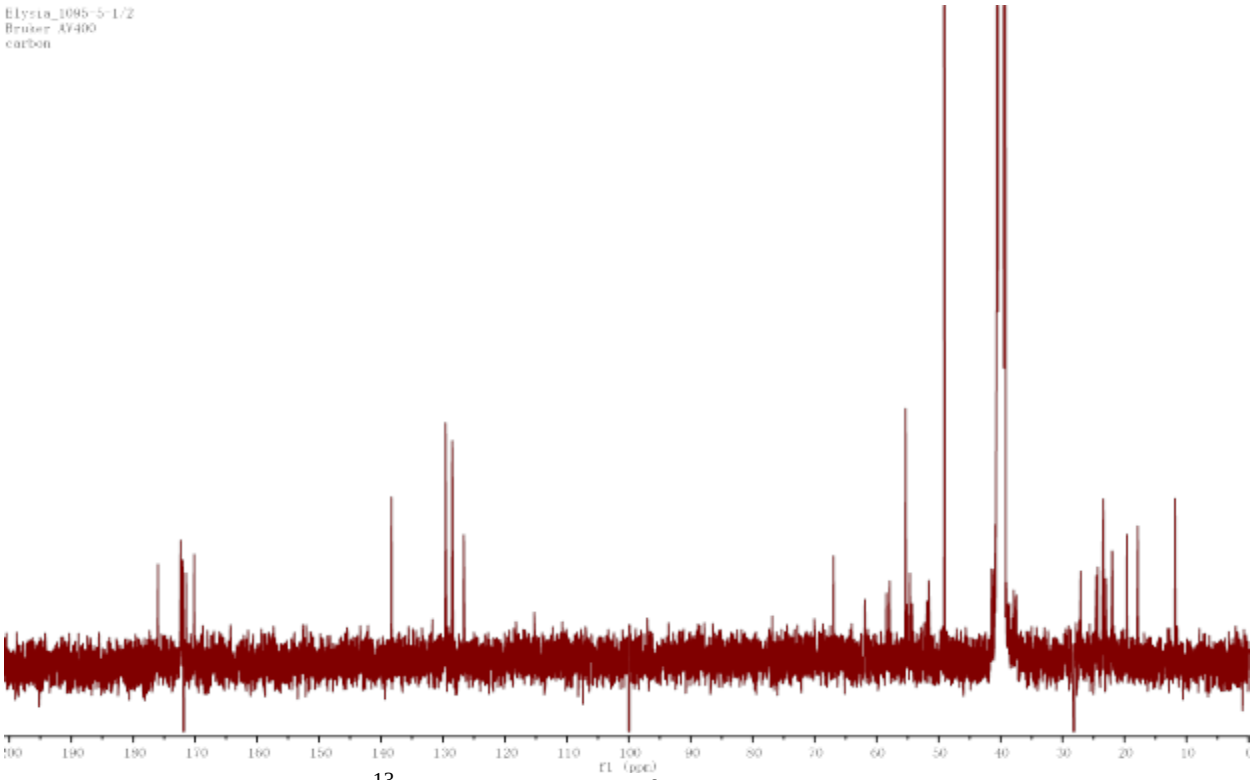

Figure 62 ^{13}C NMR spectrum of hydroKA **(17)** in DMSO-d_6

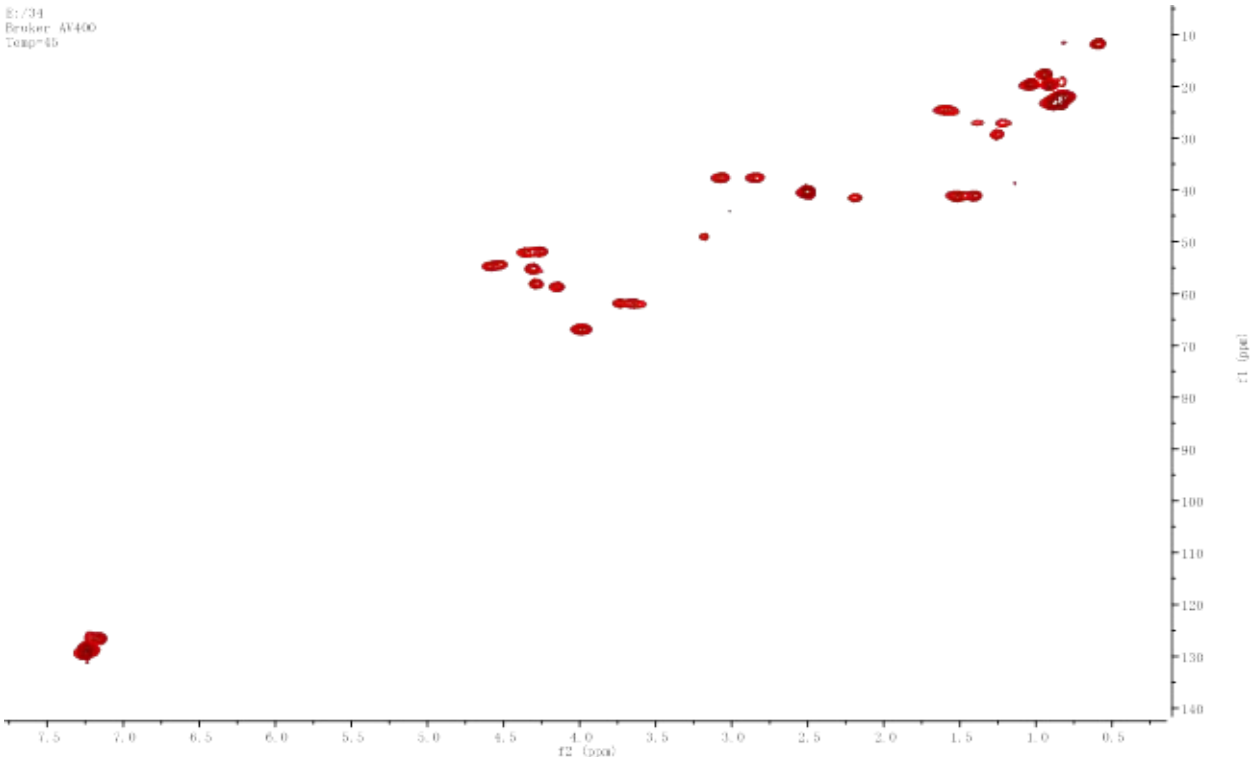

Figure 63 HSQC spectrum of hydroKA **(17)** in DMSO-d_6

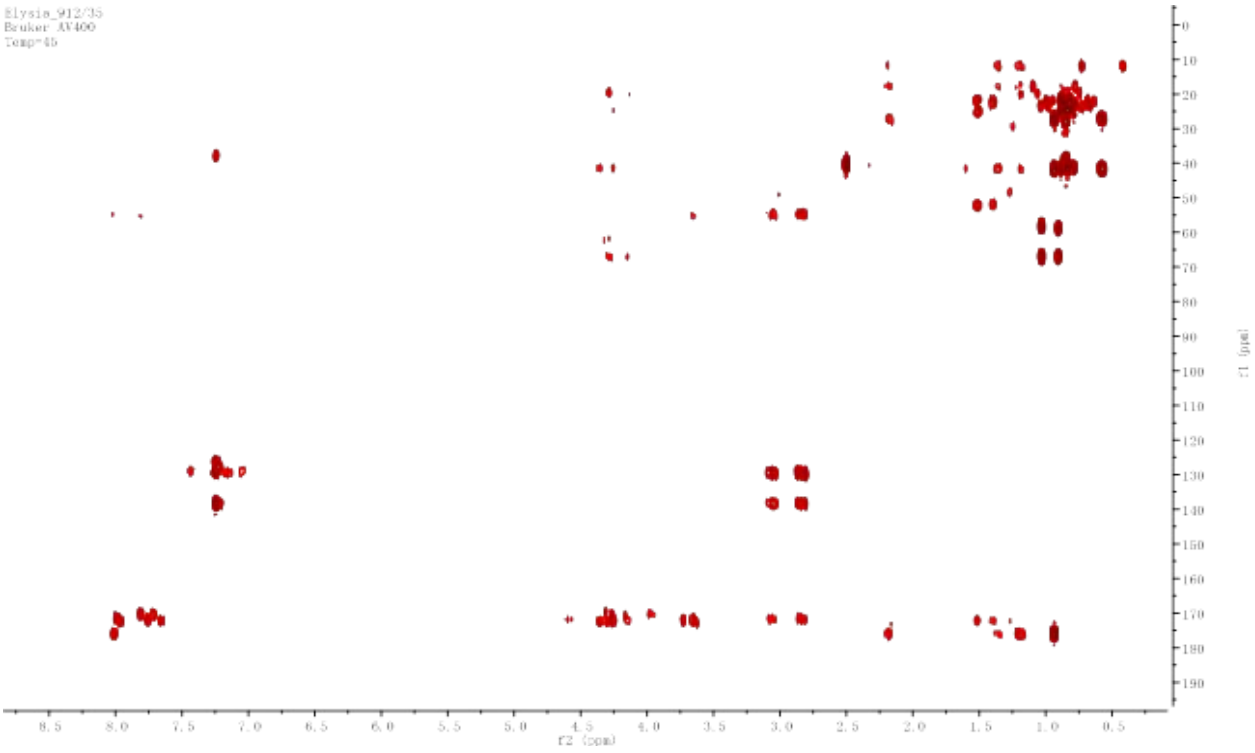

Figure 64 HMBC spectrum of hydroKA **(17)** in DMSO-d_6

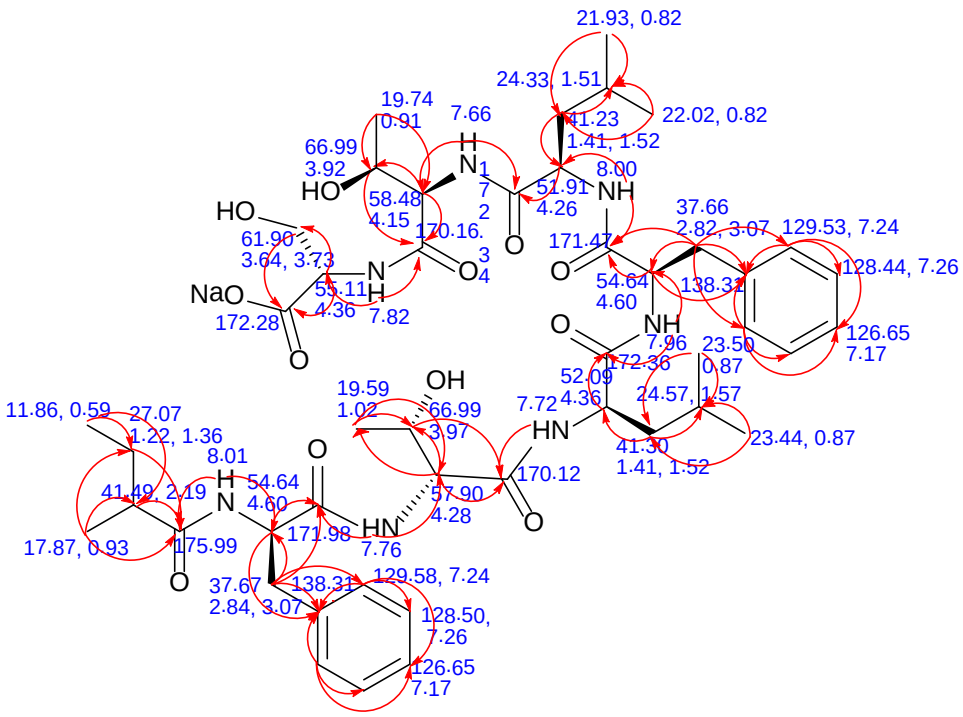

Figure 65 HMBC correlations of hydroKA **(17)**

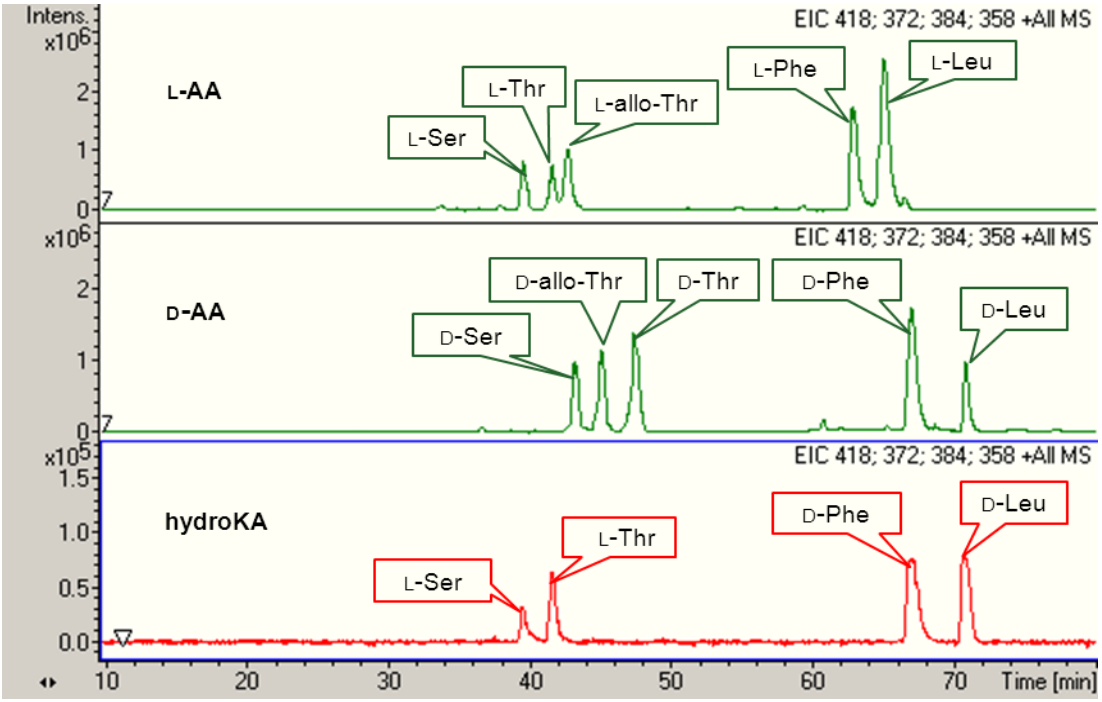

Figure 66 Marfey's analysis of hydroKA **(17)**

18 (800 μg, 0.00008%) was obtained as light yellow solid and LC-MS provided quasi-molecular signals $[M+2H]^{2+}$ at *m/z* 427.3, $[M+H]^{+}$ at *m/z* 853.6 **(Figure 67)**. The HSQC NMR spectrum showed **18** was not pure **(Figure 68)**. Future work on this new peptide will focus on the amino acid sequence analysis using FTMS.

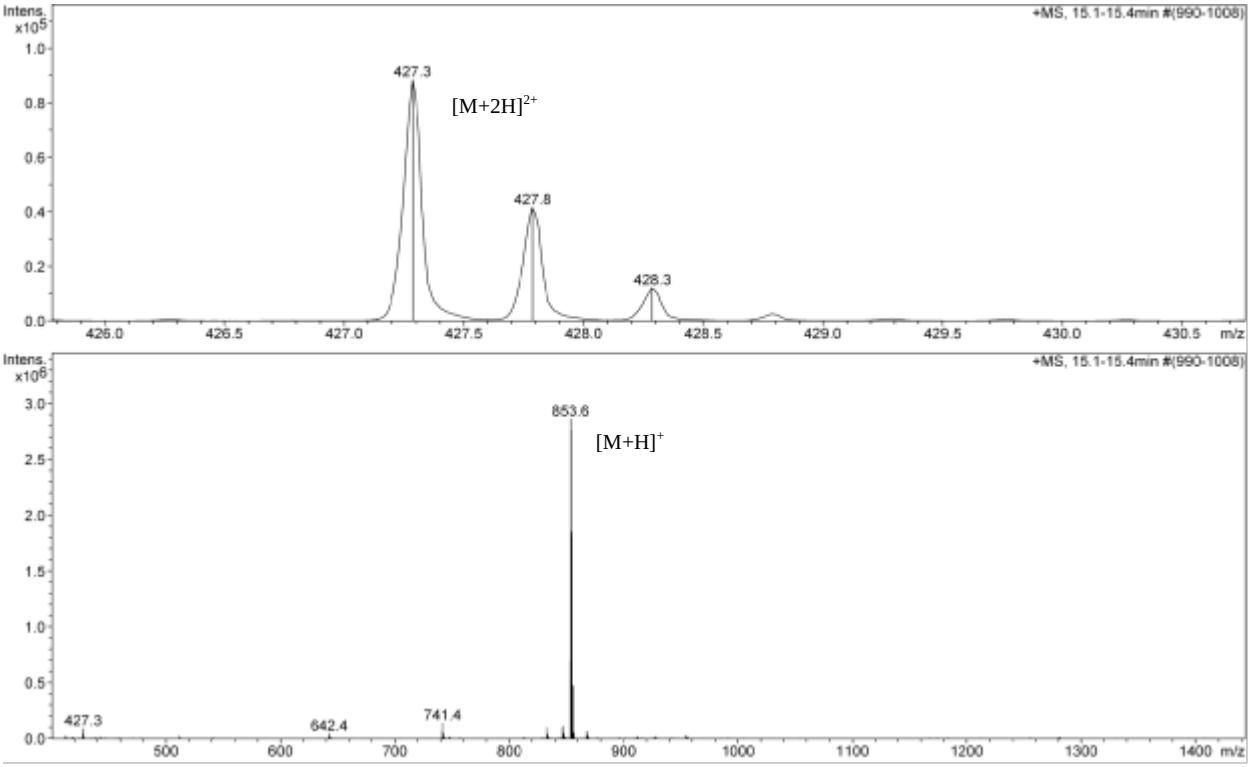

Figure 67 MS spectrum of **18**

19 (400 μg, 0.00004%) was obtained as light yellow amorphous powder and MS spectrum provided quasi-molecular signals $[M+2H]^{2+}$ at *m/z* 462.3, $[M+H]^{+}$ at *m/z* 923.5 **(Figure 69)**. However, the NMR spectra could not be acquired due to limited amount. Future FTMS analysis will be needed to assign the peptide sequence as well.

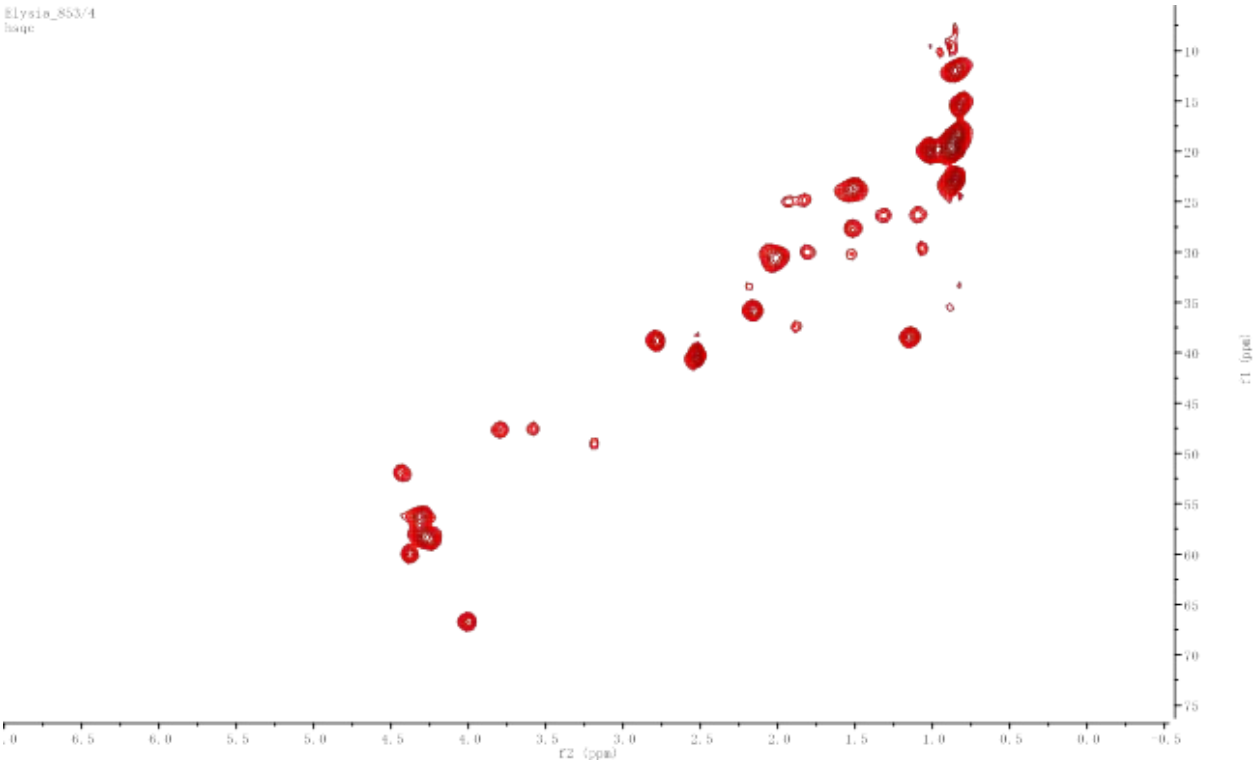

Figure 68 HSQC spectrum of **18** in DMSO-d_6

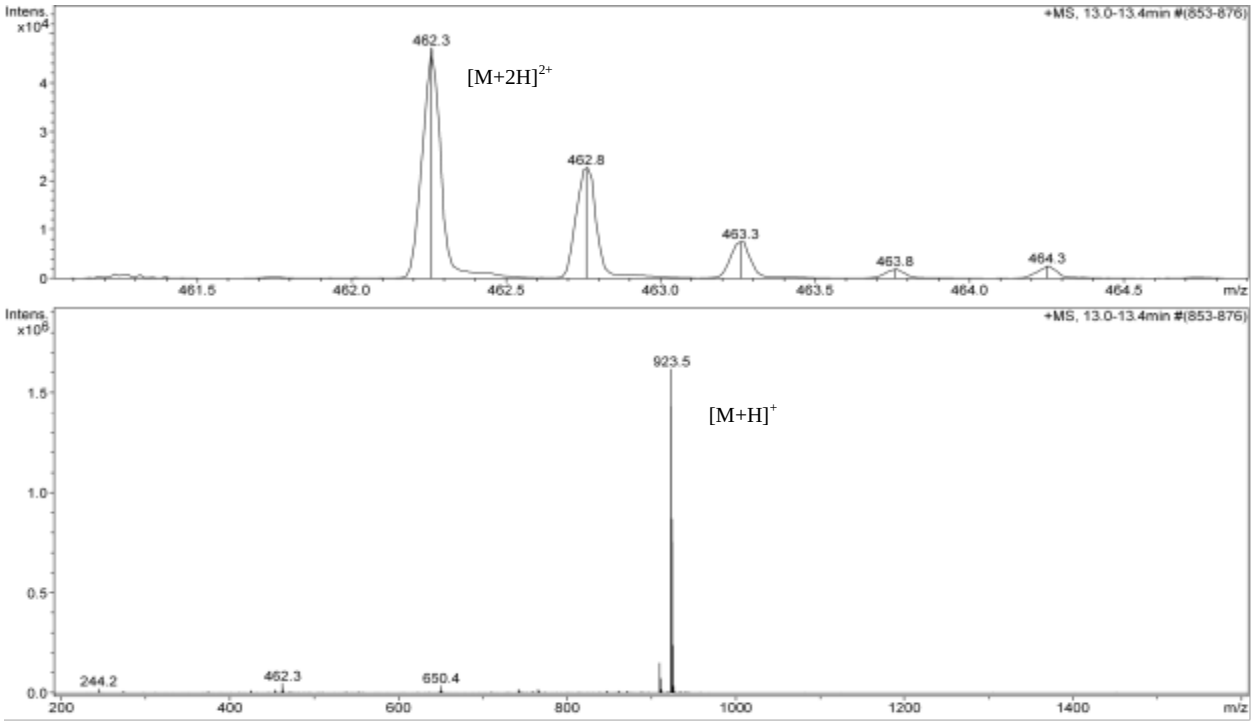

Figure 69 MS spectrum of **19**

7-OH-KH **(20)** (1.1 mg, yield 0.00011%) was obtained as colorless amorphous solid. HRMS provided a quasi-molecular signal $[M+Na]^+$ at *m/z* 1149.5712 for a molecular formula of $C_{55}H_{82}N_8NaO_{17}$ (calc. 1149.5690, Δ 1.9 ppm) **(Figure 70)**. Based on HRMS data, the mass of **20** is 16 daltons more than that of kahalalide H, which suggested that the structure could consist of one more hydroxy group than kahalalide H. Therefore, an HSQC overlay experiment was utilized to compare these two molecules. As a result, one carbon at δ_C 38.90 corresponding to the C-8 at 3-OH-9-MeDec residue of kahalalide H shifted down field to δ_C 47.03. The other four carbons of 3-OH-9-MeDec residue at δ_C 25.53, 29.83, 27.85, and 27.30 were replaced by signals at δ_C 21.87, 38.24, 68.25, and 24.27 in **20**, respectively, indicating the presence of one more hydroxy group. Based on the ^{13}C NMR chemical shifts, the lipid chain of **20** was determined as 3,7-dihydroxy-9-methyldecane **(Table 8, Figures 71, 72)**.

The relative configuration of 4-OH-Pro4 was determined using NOESY data **(Figure 73)**. There was no NOE correlation between the α-protons of Val5 and 4-OH-Pro4 observed, indicating that the 4-OH-Pro4 was *trans*- conformation. The specific rotation $[\alpha]_D^{25}$ of **20** (*c* 0.10, MeOH) is +40, which is similar to that of kahalalide H [+39, (*c* 0.45, MeOH)]. Moreover, an HSQC overlay experiment displayed that all the other amino acid residue signals overlapped well, suggesting that the absolute configuration of the amino acid residues of **20** could be the same as those of kahalalide H. Marfey's analysis of **20** confirmed that Leu2, Val5, and Asp8 are the D- configured, while Ser3, *trans*-4-OH-Pro4, and Ser6 are the L- configured, which are the same as those of kahalalide H. Both D- and L- Phe were observed in the Marfey's analysis. Considering that the optical rotation and HSQC data of **20** are closed to those of kahalalide H, the Phe residues could be L-Phe1 and D-Phe7 **(Figure 74)**.

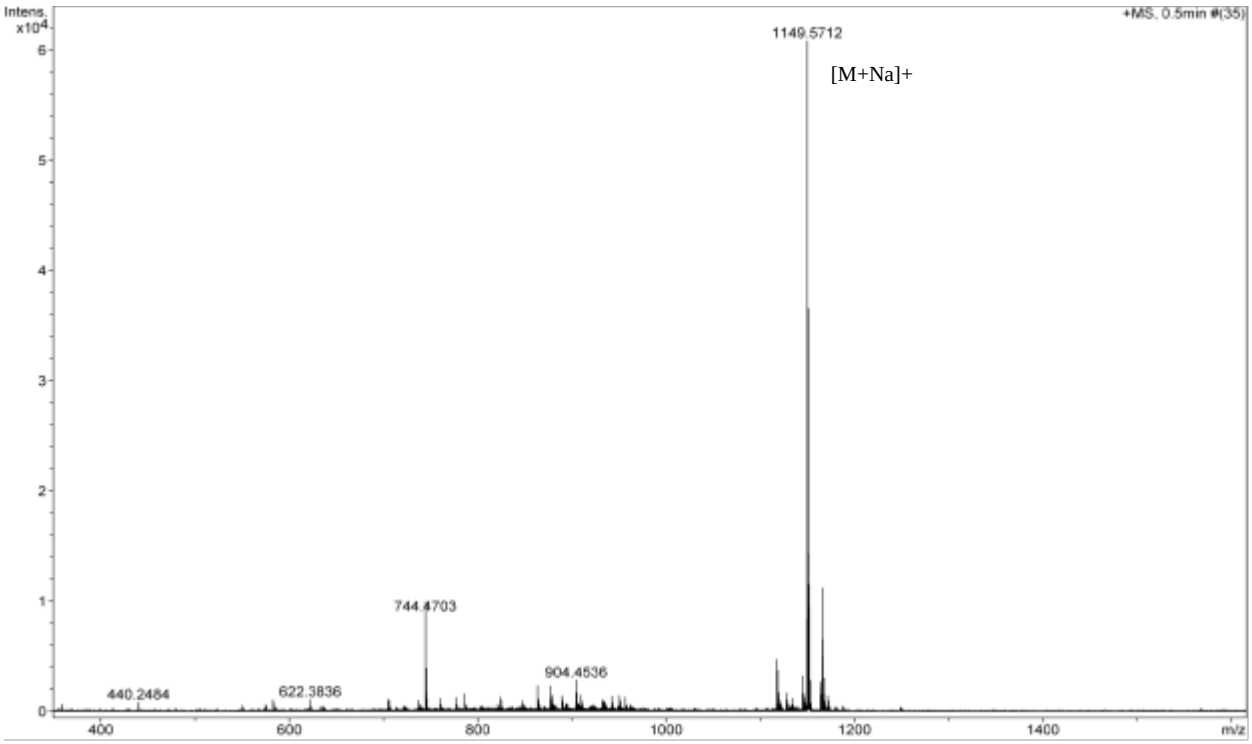

Figure 70 HRMS spectrum of 7-OH-KH **(20)**

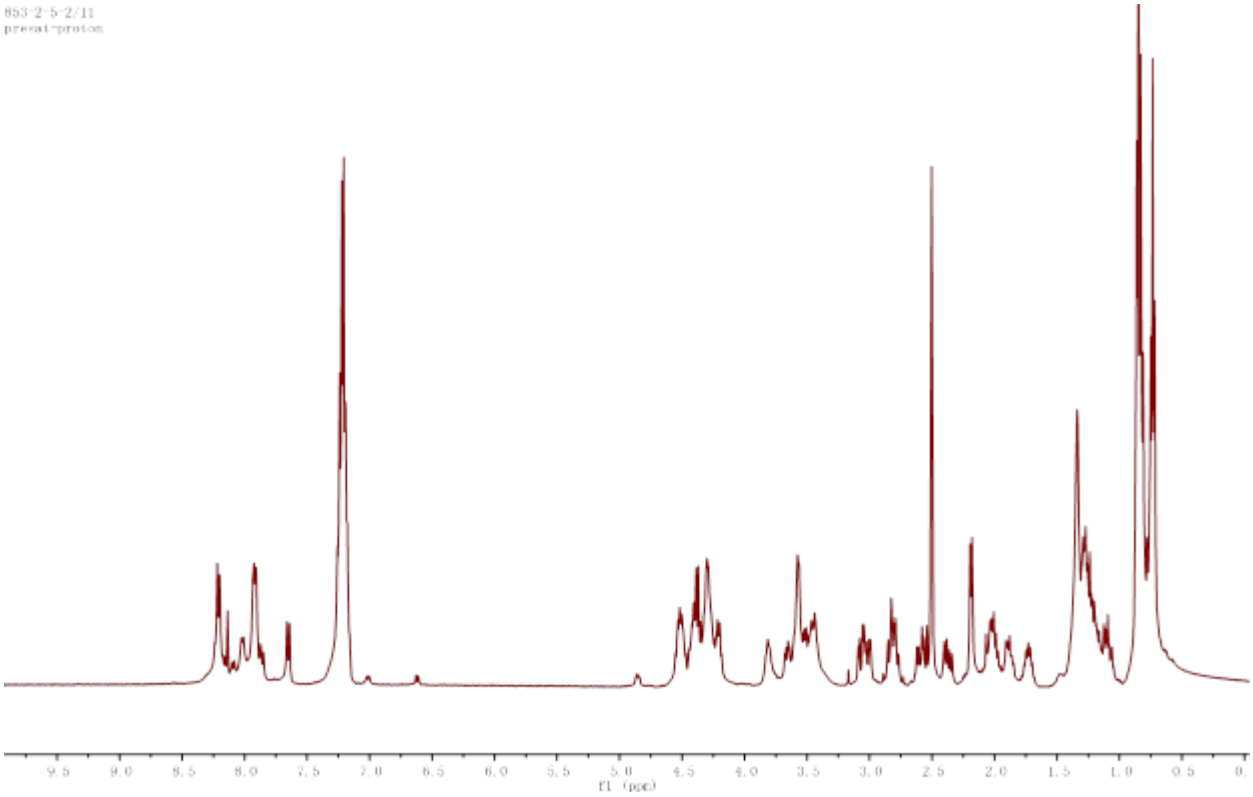

Figure 71 ^{1}H NMR spectrum of 7-OH-KH **(20)** in DMSO-d_6

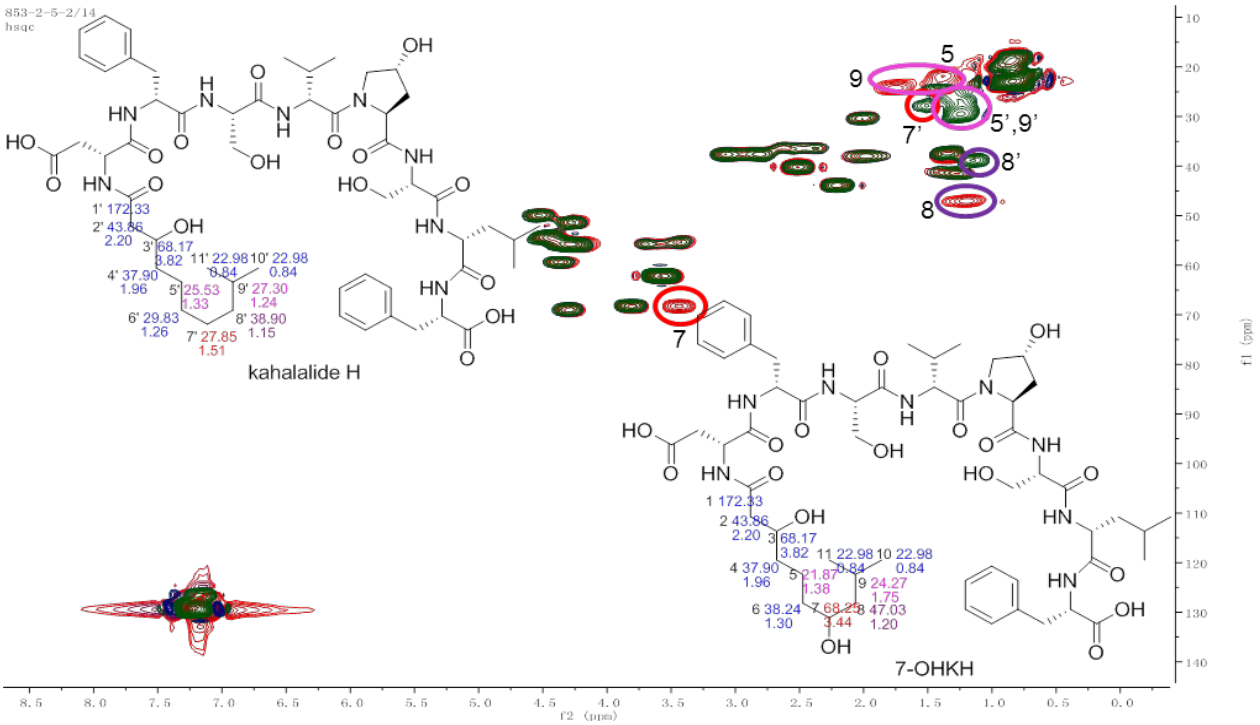

Figure 72 HSQC spectra of kahalalide H (green) and 7-OH-KH **(20)** (red) in DMSO-d_6

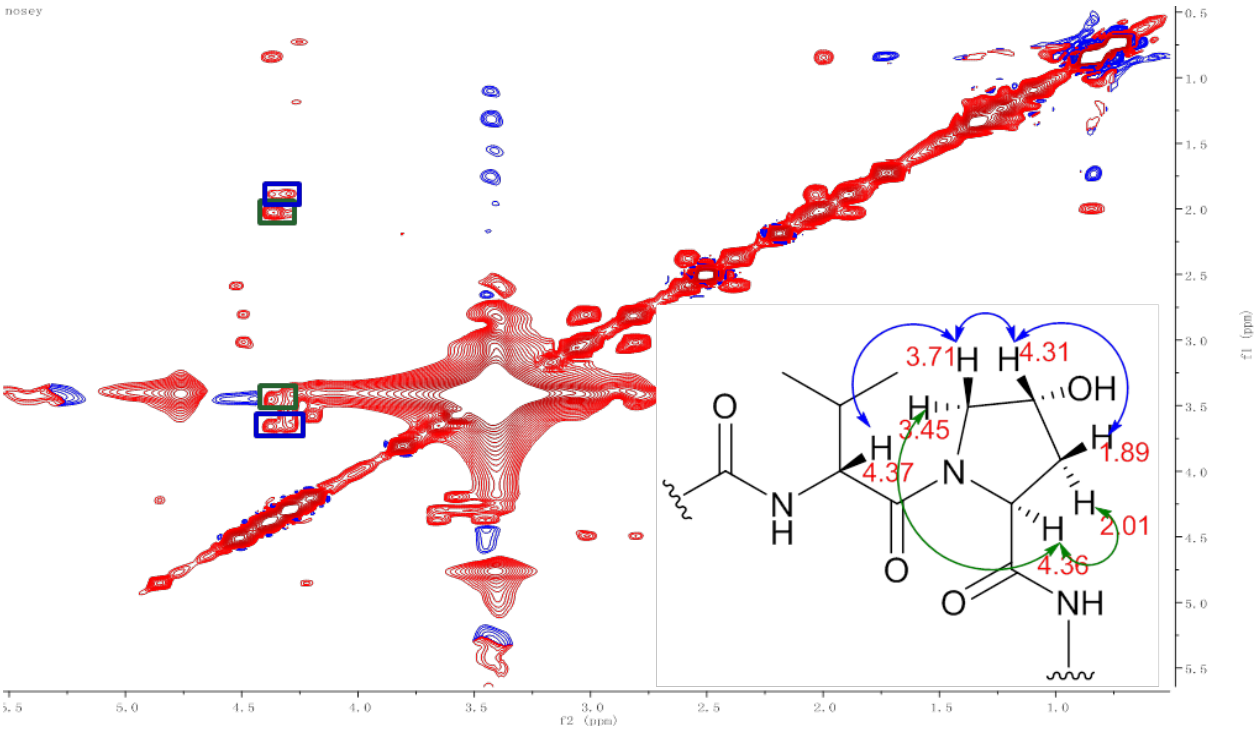

Figure 73 NOESY correlations of *trans*-4-OH-Pro in 7-OH-KH **(20)** in DMSO-d_6

Table 8 ^{1}H and ^{13}C NMR data of **20** and **27**[a] (δ in ppm, DMSO-d_6)

		20			**27**		
	Carbon	**δ_C, mult**	**δ_H, mult.**	***J* (Hz)**	**δ_C, mult**	**δ_H, mult.**	***J* (Hz)**
Phe1	1	173.47, qC	(NH) 7.86, d	7.9	173.47, qC	(NH) 7.86, d	7.9
	2	54.61, CH	4.44, m		54.61, CH	4.44, m	
	3	37.43, CH_2	3.02,dd ;2.79, m	13.6, 4.3	37.43, CH_2	3.02,dd; 2.79, m	13.6, 4.3
	4	138.11, qC			138.11, qC		
	5,5’	129.65, CH	7.20, m		129.65, CH	7.20, m	
	6,6’	128.49, CH	7.26, m		128.49, CH	7.26, m	
	7	126.73, CH	7.19, m		126.73, CH	7.19, m	
Leu2	1	170.99, qC	(NH) 7.65, d	8.2	170.99, qC	(NH) 7.65, d	8.2
	2	51.33, CH	4.28, m		51.33, CH	4.28, m	
	3	41.43, CH_2	1.27, bs		41.43, CH_2	1.27, bs	
	4	24.40, CH	1.36, m		24.40, CH	1.36, m	
	5	23.43, CH_3	0.83, m		23.43, CH_3	0.83, m	
	6	21.57, CH_3	0.79, m		21.57, CH_3	0.79, m	
Ser3	1	170.02, qC	(NH) 7.89, m		170.02, qC	(NH) 7.89, m	
	2	55.97, CH	4.31, m		55.97, CH	4.31, m	
	3	62.23, CH_2	3.58, m		62.23, CH_2	3.58, m	
OH-Pro4	1	171.29, qC			171.29, qC		
or Pro4	2	59.30, CH	4.36, m		60.99, CH	4.33, m	
	3	37.99, CH_2	1.89, 2.01, m		29.78, CH_2	1.83, m	
	4	69.01, CH	4.31, m		24.68, CH_2	1.83, m	
	5	55.74, CH_2	3.71, 3.45, m		47.58, CH_2	3.52, 3.66, m	
Val5	1	172.02, qC	(NH) 7.95, m		172.02, qC	(NH) 7.95, m	
	2	55.69, CH	4.37, m		55.69, CH	4.34, m	
	3	30.45, CH	2.01, m		30.45, CH	2.01, m	
	4	20.09, CH_3	0.83, m		20.09, CH_3	0.83, m	
	5	18.19, CH_3	0.82, m		18.19, CH_3	0.82, m	
Ser6	1	170.22, qC	(NH) 7.93, m		170.22, qC	(NH) 7.93, m	
	2	55.82, CH	4.21, m		55.82, CH	4.21, m	
	3	62.00, CH_2	3.58, m		62.00, CH_2	3.58, m	
Phe7	1	170.20, qC	(NH) 8.25, d	7.4	170.20, qC	(NH) 8.25	7.4
	2	54.06, CH	4.53, m		54.06, CH	4.53, m	
	3	37.31, CH_2	3.07,dd; 2.84, m	13.7, 4.6	37.31, CH_2	3.07,dd ;2.84, m	13.7, 4.6
	4	138.00, qC			138.00, qC		
	5,5'	129.65, CH	7.20, m		129.65, CH	7.20, m	
	6,6'	128.47, CH	7.26, m		128.47, CH	7.26, m	
	7	126.68, CH	7.19, m		126.68, CH	7.19, m	
Asp8	1	172.28, qC	(NH) 8.23, d	8.12	172.28, qC	(NH) 8.23, d	8.12
	2	50.03, CH	4.53, m		50.03, CH	4.53, m	
	3	36.34, CH_2	2.62, dd 2.36, dd	17.1, 5.6 16.8, 8.4	36.34, CH_2	2.36, dd 2.62, dd	17.1, 5.6 16.8, 8.4
	4	171.93, qC			171.93, qC		
	1	172.33, qC			172.33, qC		
3-OH-9MeDec	2	43.86, CH_2	2.20, d	6.1	43.86, CH_2	2.20, d	6.1
or 3,7-dihydroxy	3	68.17, CH	3.82, bs		68.17, CH	3.82, bs	
-9MeDec	4	37.90, CH_2	1.96, m		37.90, CH_2	1.96, m	
	5	21.87, CH_2	1.38, m		25.53, CH_2	1.33, m	
	6	38.24, CH_2	1.30, m		29.83, CH_2	1.26, bs	
	7	68.25, CH	3.44, m		27.85, CH_2	1.51, m	
	8	47.03, CH_2	1.20, m		38.90, CH_2	1.15, bs	
	9	24.27, CH	1.75, m		27.30, CH	1.24, m	
	10, 11	22.98, CH_3	0.84, m		22.98, CH_3	0.84, m	

[a]Assignments based on ^{1}H, ^{13}C, and HSQC NMR (100/400 MHz) experiments at room temperature.

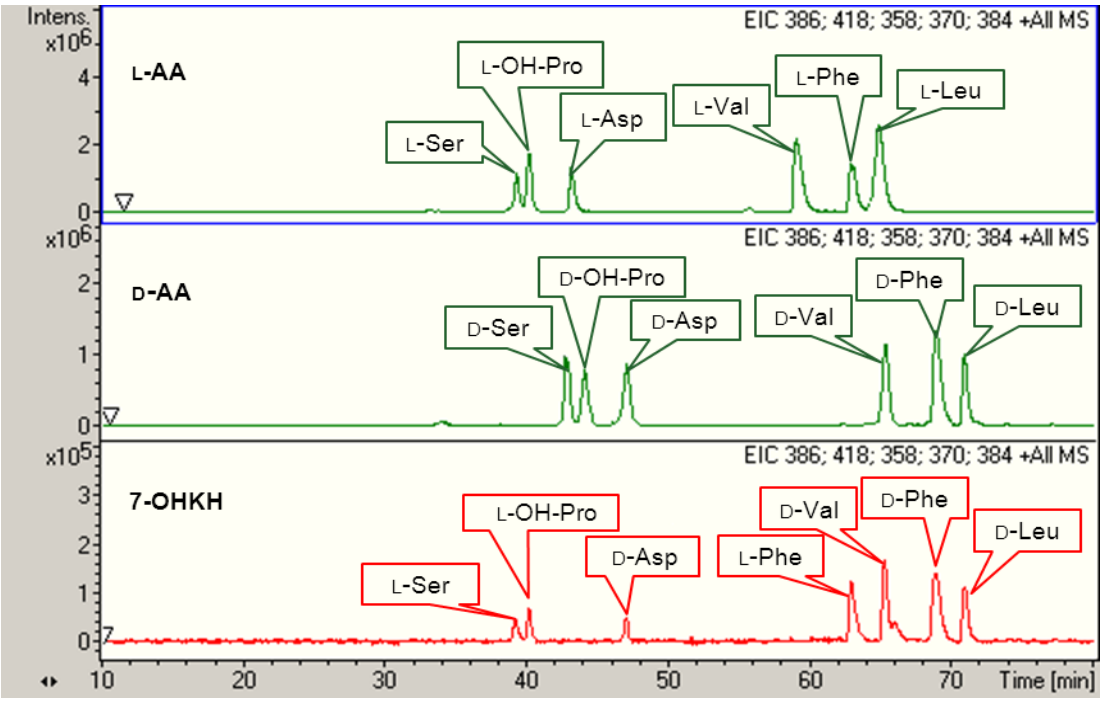

Figure 74 Marfey's analysis of 7-OHKH **(20)**

25 (10mg, yield 0.001%) possibly was a δ-lactam synthetase catalyzed kahalalide F degraded peptide (laskide). It was obtained as white amorphous powder and HRMS provided quasi-molecular signals $[2M+Na]^+$ at *m/z* 1465.8257 and $[M+Na]^+$ at *m/z* 744.4629 for a molecular formula of $C_{36}H_{63}N_7NaO_8$ (calc. 744.4630, Δ -0.1 ppm) **(Figure 75)**. The ^1H, ^{13}C, and HMBC NMR spectra displayed six amide protons at δ_H 7.58-8.08, eight carbonyls at δ_C 170.06, 170.14, 170.24, 171.09, 171.53, 172.94 and 173.18, indicating the presence of at least six amino acid residues **(Figure 76-79)**. The methine group at δ_C 66.68 suggested the presence of one Thr residue **(Table 9)**. The signals at δ_C 33.42, 33.97, 32.42, 29.26, and 11.59 in HSQC presented less intensity, suggesting the presence of a 4-MeHex isomer **(Figure 78)**. The amino acid residues and their sequence of **25** were determined using HMBC experiment. Correlation between the NH (δ_H 7.55) of 3-aminopiperidin-2-one and its carbonyl (δ_C 170.06) indicating the formation of a lactam. There was no NOESY correlation between the α-protons of Pro2 and Val3

observed. Moreover, the $\Delta\delta_{\beta\gamma}$ (differential value of ^{13}C chemical shift of β- and γ- carbons in Pro) is 5.04 ppm, which is < 8 ppm, suggested the *trans*- conformation of Pro2.[52] The absolute configuration analysis of **25** using Marfey's analysis demonstrated that **25** contains L-Thr, *trans*-D-Pro, L-Orn, D-Val, and L-Val residues **(Figure 80)**. The absolute configurations of Val3, Val4, and Val6 could not be determined. However, considering **25** is a degraded product of KF, the configuration of the Val residues could be proposed as D-Val3, L-Val4, and D-Val6.

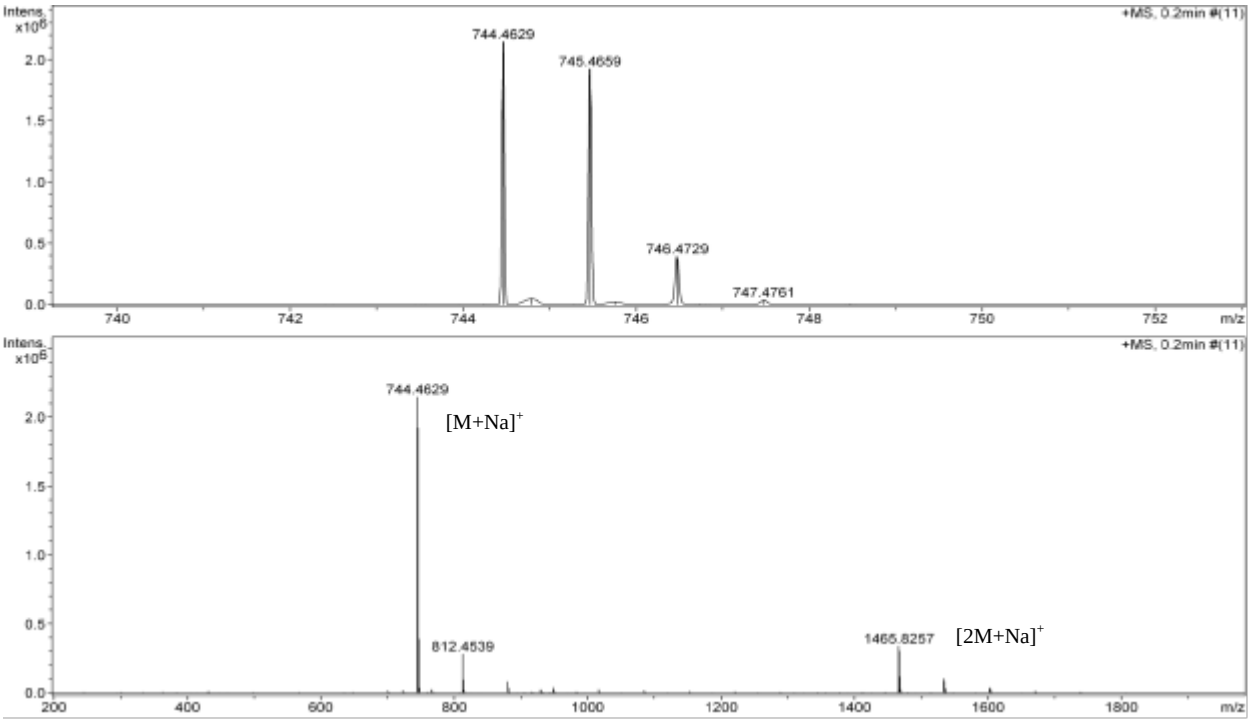

Figure 75 HRMS spectrum of laskide **(25)**

Table 9 ^{1}H and ^{13}C NMR data of laskide **(25)**[a] (δ in ppm, DMSO-d_6)

	Carbon	**δ_C, mult**	**δ_H, mult.**	***J* (Hz)**		**Carbon**	**δ_C, mult**	**δ_H, mult.**	***J* (Hz)**
3-amino piperidine -2-one	1	170.06, qC	(NH) 7.82, d	7.6	Thr 5	1	171.09, qC	(NH) 7.79, d	8.6
	2	49.65, CH	4.05, m			2	58.22, CH	4.26, m	
	3	21.21, CH_2	1.75, m			3	66.68, CH	4.01, m	
	4	27.88, CH_2	1.99, m			4	19.88, CH_3	1.02, d	6.3
	5	41.35, CH_2	3.12		Val 6	1	171.93, qC	(NH) 7.87, d	9.2
			(NH) 7.55,bs				second	(NH) 7.85, d	9.1
Pro2	1	170.14, qC				2	58.50, CH	4.23, m	
	2	59.88, CH	4.36, m			3	30.53, CH	2.02, m	
	3	29.74, CH_2	2.01, 1.82, m			4	19.69, CH_3	0.83, m	
	4	24.70, CH_2	1.91, 1.81, m			5	19.69, CH_3	0.83, m	
	5	47.48, CH_2	3.72, 3.59, m		5-MeHex	1	173.18, qC		
Val3	1	171.53, qC	(NH) 7.59, d	8.8		2	35.74, CH_2	2.17, m	
	2	57.89, CH	4.29, m			3	23.61, CH_2	1.51, m	
	3	31.16, CH	2.02, m			4	38.46, CH_2	1.13, m	
	4	18.08, CH_3	0.84, m			5	27.66, CH	1.54, m	
	5	18.08, CH_3	0.84, m			6	22.89, CH_3	0.84, m	
Val4	1	170.24, qC	(NH) 8.06, d	8.6		7	22.85, CH_3	0.84, m	
	2	56.11,CH	4.34, m		4-MeHex	1	172.94, qC		
	3	30.21, CH	2.02, m			2	33.26, CH_2	2.19, m	
	4	18.66, CH_3	0.84, m			3	32.42, CH_2	1.54, 1.29, m	
	5	18.79, CH_3	0.84, m			4	33.97, CH	1.30, m	
						5	29.26, CH_2	1.29, m	
						6	19.17, CH_3	0.80, m	
						7	11.59, CH_3	0.83, m	

[a]Assignments based on ^{1}H, ^{13}C, HSQC and HMBC NMR (100/400 MHz) experiments at room temperature.

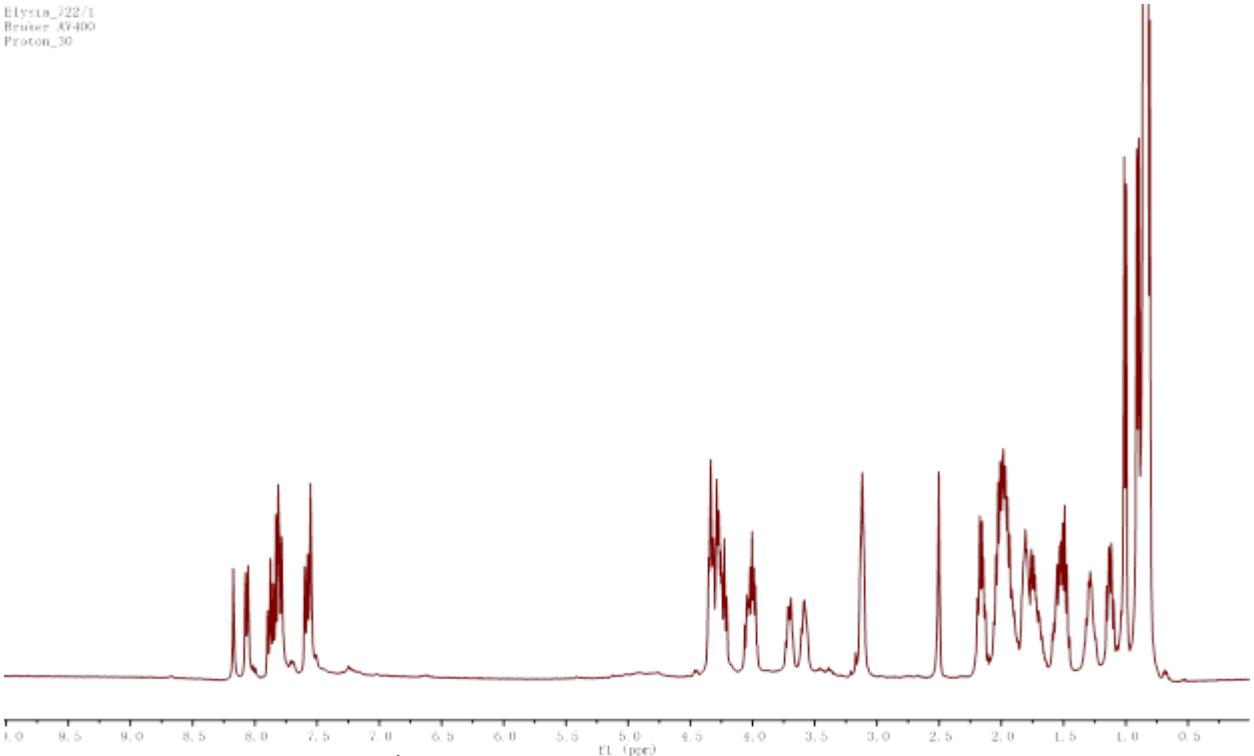

Figure 76 ^{1}H NMR spectrum of laskide **(25)** in DMSO-d_6

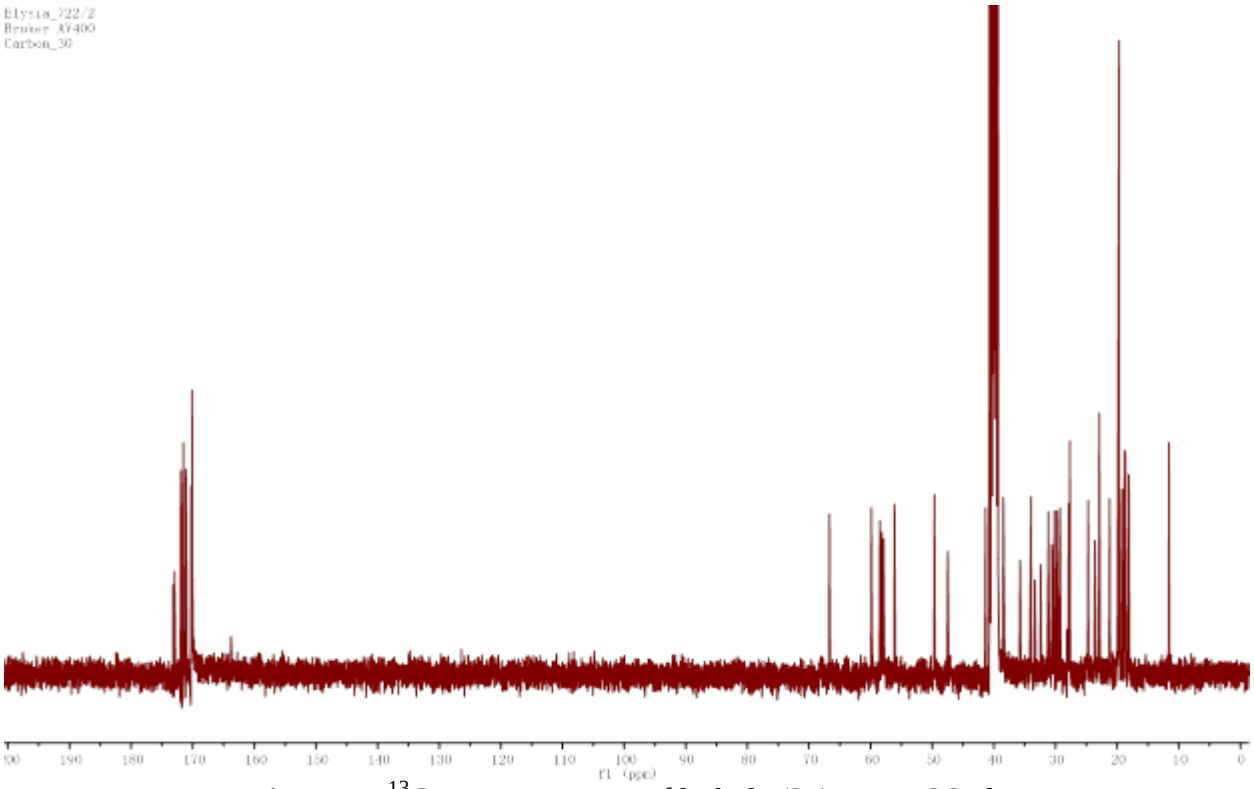

Figure 77 ^{13}C NMR spectrum of laskide **(25)** in DMSO-d_6

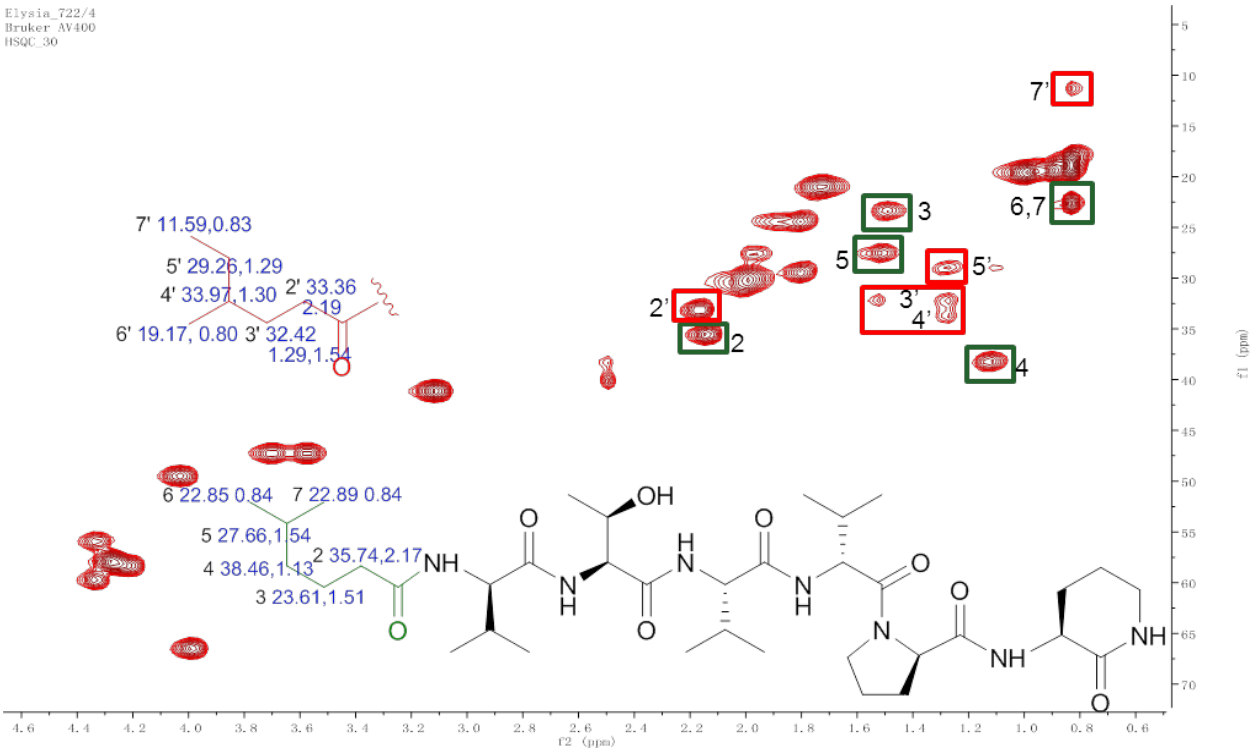

Figure 78 HSQC spectrum of laskide **(25)** in DMSO-d_6

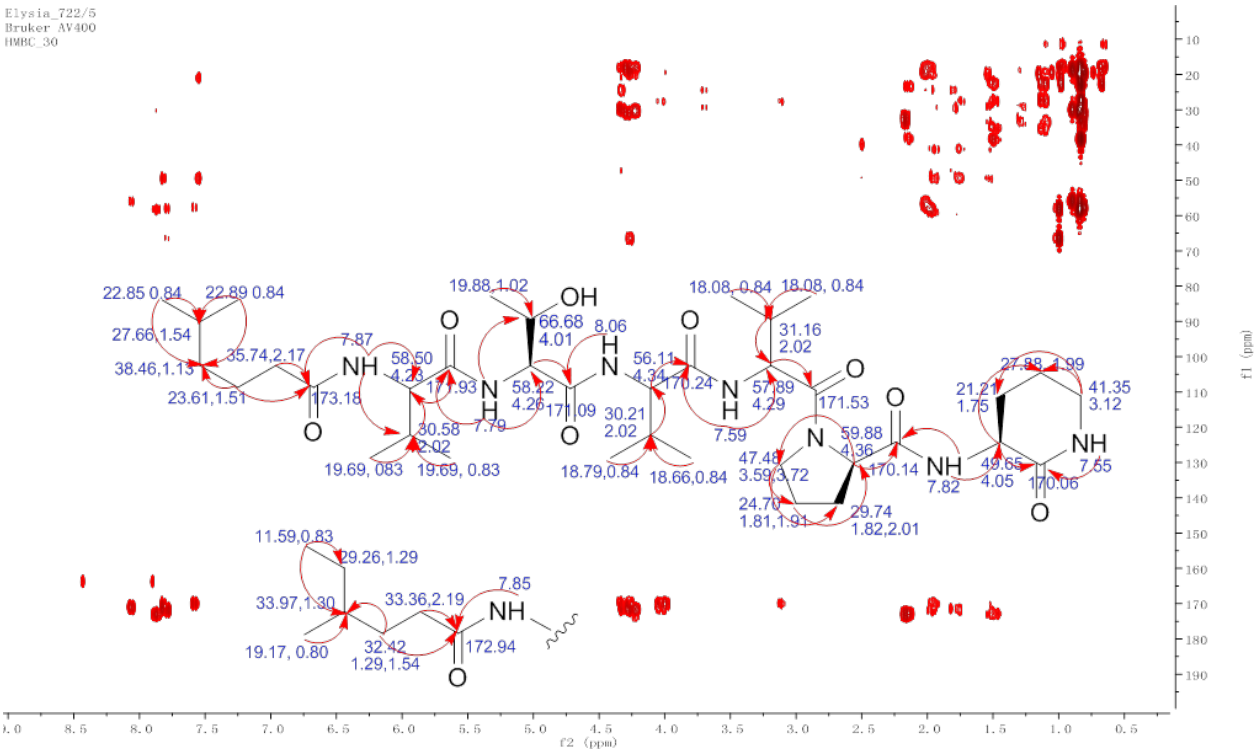

Figure 79 HMBC correlations of laskide **(25)** in DMSO-d_6

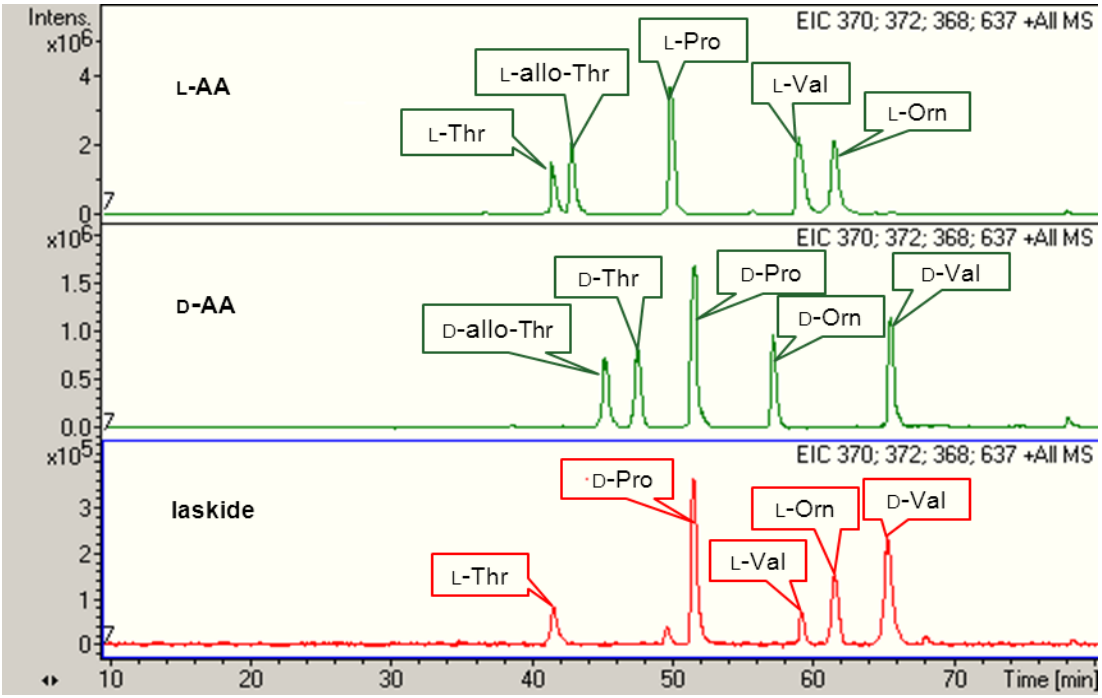

Figure 80 Marfey's analysis of laskide **(25)**

HydroKB methyl ester **(26)** (20mg, yield 0.002%) was obtained as white amorphous powder. HRMS provided quasi-molecular signals $[M+2Na]^{2+}$ at *m/z* 477.7753, $[M+Na]^{+}$ at *m/z* 933.4805 for a molecular formula of $C_{46}H_{67}N_7NaO_{12}$ (calc. 933.4818, Δ -1.4 ppm) **(Figure 81)**. The ^{1}H, ^{13}C, and HMBC NMR spectra displayed six amide protons at δ_H 6.61-7.71, eight carbonyls at δ_C 170.01, 171.76, 172.77, 171.74, 171.82, 172.33, 174.63 and 174.80, indicating the presence of at least six amino acid residues **(Figures 82-84)**. Moreover, carbons at δ_C 174.80, 31.88, 33.94, 28.99, 18.77 and 11.06 displayed less intensity in the ^{13}C NMR spectrum, demonstrating the presence of a 4-MeHex isomer. The HMBC and NOESY correlations revealed that **26** has the same amino acid sequence as kahalalide B[12] **(Table 10)**. The only difference is that the ester was hydrolyzed, and an additional methyl group was present in **26** at δ_C 52.33. It was clearly observed that the new methyl group had an HMBC correlation with the carbonyl (δ_C 175.99) of Gly1, and NOE correlations with the α-protons (δ_H 3.83, 4.13) of Gly1, thus determining that **26** is a methyl ester at Gly1 **(Figure 85)**. There was no NOE correlation between the α-protons of Pro3 and Leu4 observed. Additionally, the $\Delta\delta_{\beta\gamma}$ value of Pro3 is 4.47 ppm (< 8 ppm), indicating the Pro3 is *trans*- conformation. The specific rotation $[\alpha]_D^{25}$ of **26** (*c* 0.1, MeOH) is 0. This could be attributed to an acyclic peptide chain and the presence of a methyl ester that allow sp^3 carbons at amino acid residues to rotate freely. Marfey's analysis revealed that **26** shares the same absolute configuration as kahalalide B, which is L-Thr2, *trans*-L-Pro3, D-Leu4, L-Phe5, D-Ser6, and L-Tyr7 **(Figure 86)**.

Table 10 ^{1}H and ^{13}C NMR data of hydroKB methyl ester **(26)** [a] (δ in ppm, $CDCl_3$)

	Carbon	δ_C, mult	δ_H, mult.	*J* (Hz)		Carbon	δ_C, mult	δ_H, mult.	*J* (Hz)
GlyOMe1	1	171.01, qC	(NH) 7.63, m		Ser6	1	171.82, qC	(NH) 7.68, m	
	2	41.27, CH_2	3.83, dd	17.5, 4.1		2	55.44, CH	4.37, m	
			4.13, dd	17.2, 4.9		3	62.47, CH	3.40, d	8.7
	3	52.33, CH_3	3.63, s					4.05, d	9.6
Thr2	1	171.01, qC	(NH) 7.15, m		Try7	1	172.33, qC	(NH) 6.61,bs	
	2	59.49, CH	4.33, m			2	55.74, CH	4.55, m	
	3	66.66, CH	4.42, m			3	36.94, CH_2	2.88, dd	8.2, 4.7
	4	19.98, CH_3	1.23, d	5.3				3.06, m	
Pro3	1	171.76, qC				4	127.06, qC		
	2	61.22, CH	4.55, m			5,5’	130.14, CH	7.03, d	7.6
	3	28.99, CH_2	2.32, 2.05, bs			6,6’	116.76, CH	6.76, d	7.5
	4	24.52, CH_2	2.00, bs			7	155.91, qC		
	5	47.52, CH_2	3.98, 3.49, bs		5-MeHex	1	174.63, qC		
Leu4	1	172.77, qC	(NH) 7.35, bs			2	36.16, CH_2	2.10, t	7.2
	2	50.02, CH	4.49, m			3	23.19, CH_2	1.49, m	
	3	39.84, CH_2	1.49, 1.36, m			4	38.28, CH_2	1.06, m	
	4	24.49, CH	1.42, m			5	27.71, CH	1.42, m	
	5	23.21, CH_3	0.89, d	5.0		6	22.37, CH_3	0.78, m	
	6	21.75, CH_3	0.85, d	5.1		7	22.40, CH_3	0.78, m	
Phe5	1	171.74, qC	(NH) 7.71, bs		4-MeHex	1	174.80, qC		
	2	54.40, CH	4.69, m			2	33.71, CH_2	2.12, m	
	3	36.50, CH_2	2.97, dd	13.6, 6.2		3	31.88, CH_2	1.54, 1.33, m	
			3.21, dd	13.1, 7.3		4	33.94, CH	2.13, m	
	4	137.09, qC				5	28.99, CH_2	1.07, m	
	5,5'	129.12, CH	7.17, m			6	18.77, CH_3	0.77, m	
	6,6'	128.37, CH	7.23, m			7	11.06, CH_3	0.75, m	
	7	126.64, CH	7.17, m						

[a] Assignments based on ^{1}H, ^{13}C, HSQC and HMBC NMR (100/400 MHz) experiments at room temperature.

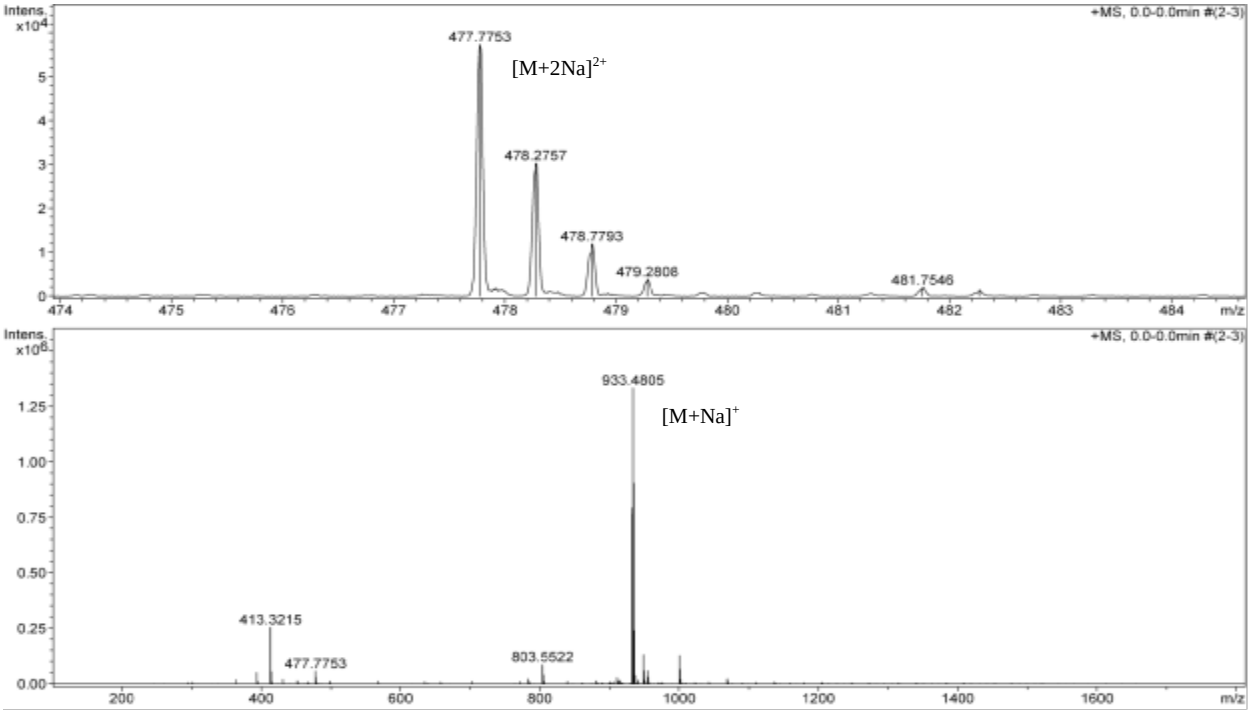

Figure 81 HRMS spectrum of hydroKB methyl ester **(26)**

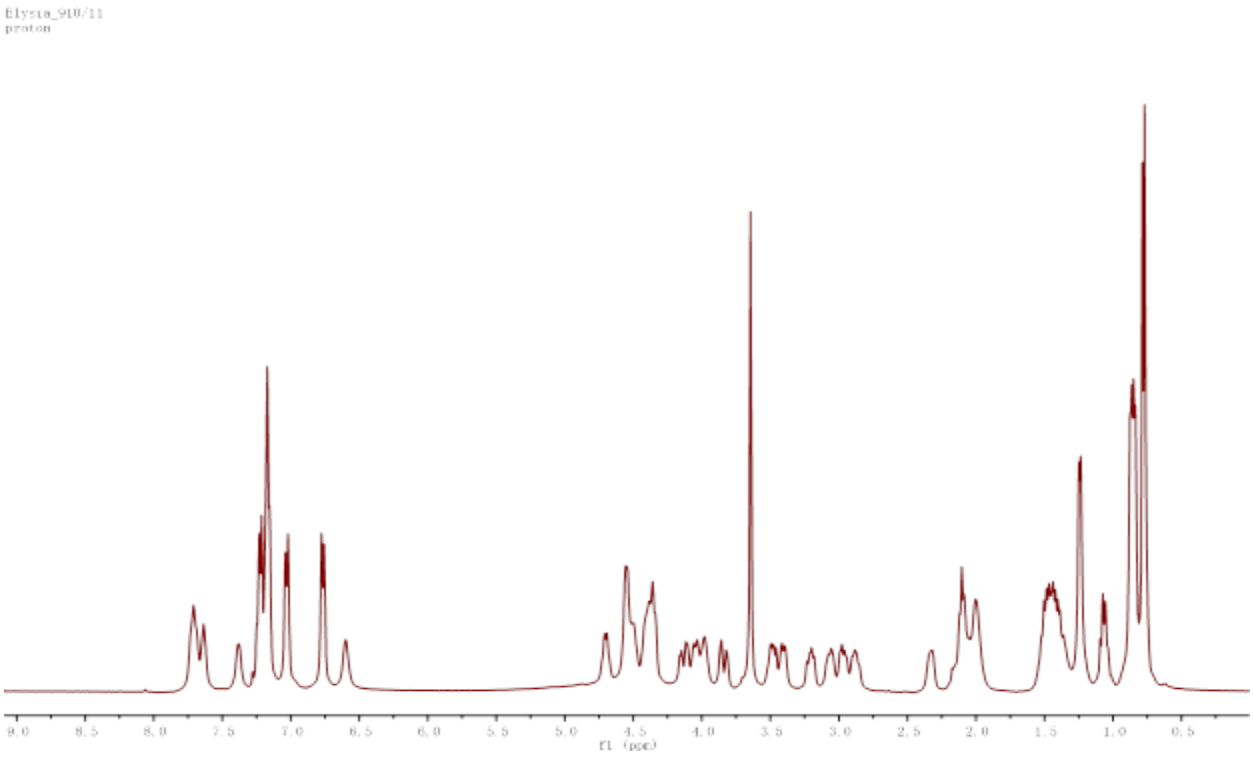

Figure 82 ^{1}H NMR spectrum of hydroKB methyl ester **(26)** in $CDCl_3$

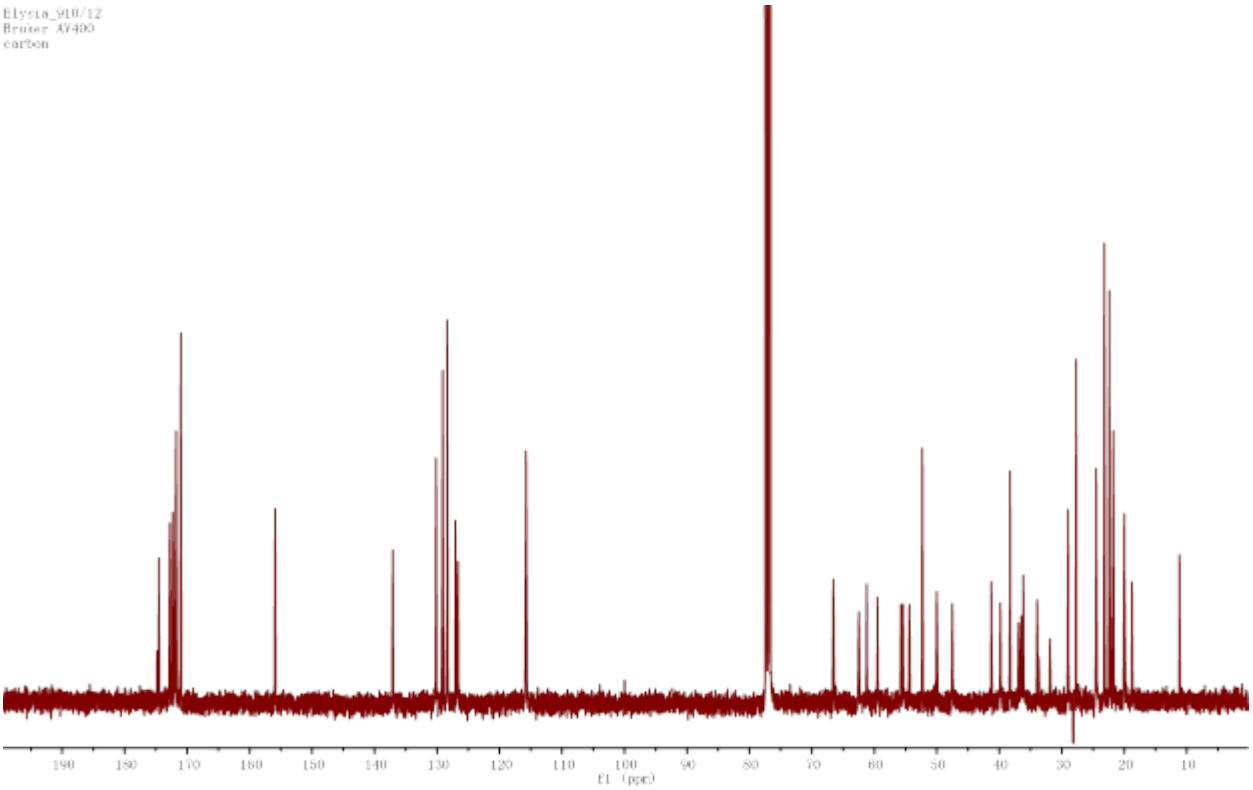

Figure 83 ^{13}C NMR spectrum of hydroKB methyl ester **(26)** in $CDCl_3$

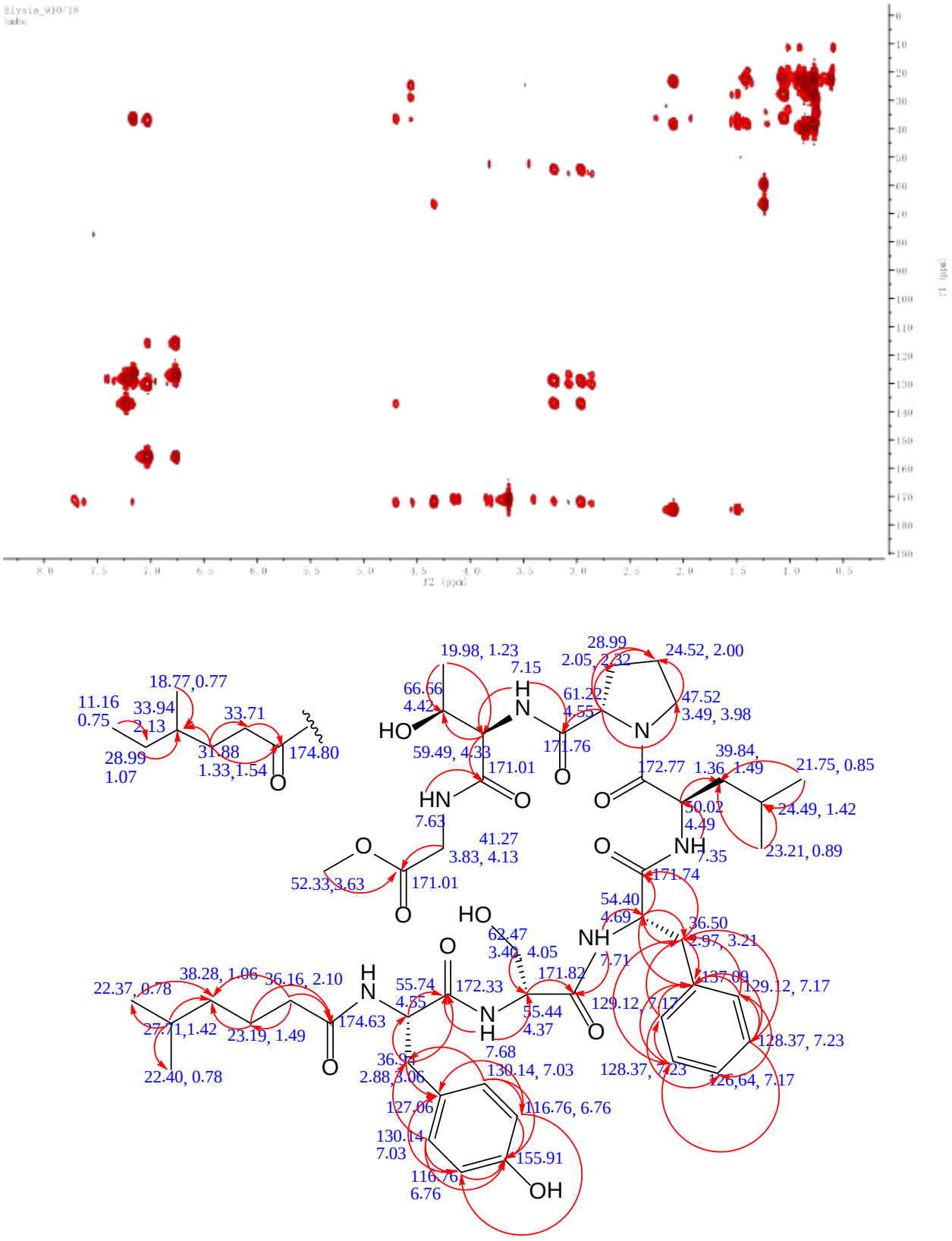

Figure 84 HMBC correlations of hydroKB methyl ester **(26)** in $CDCl_3$

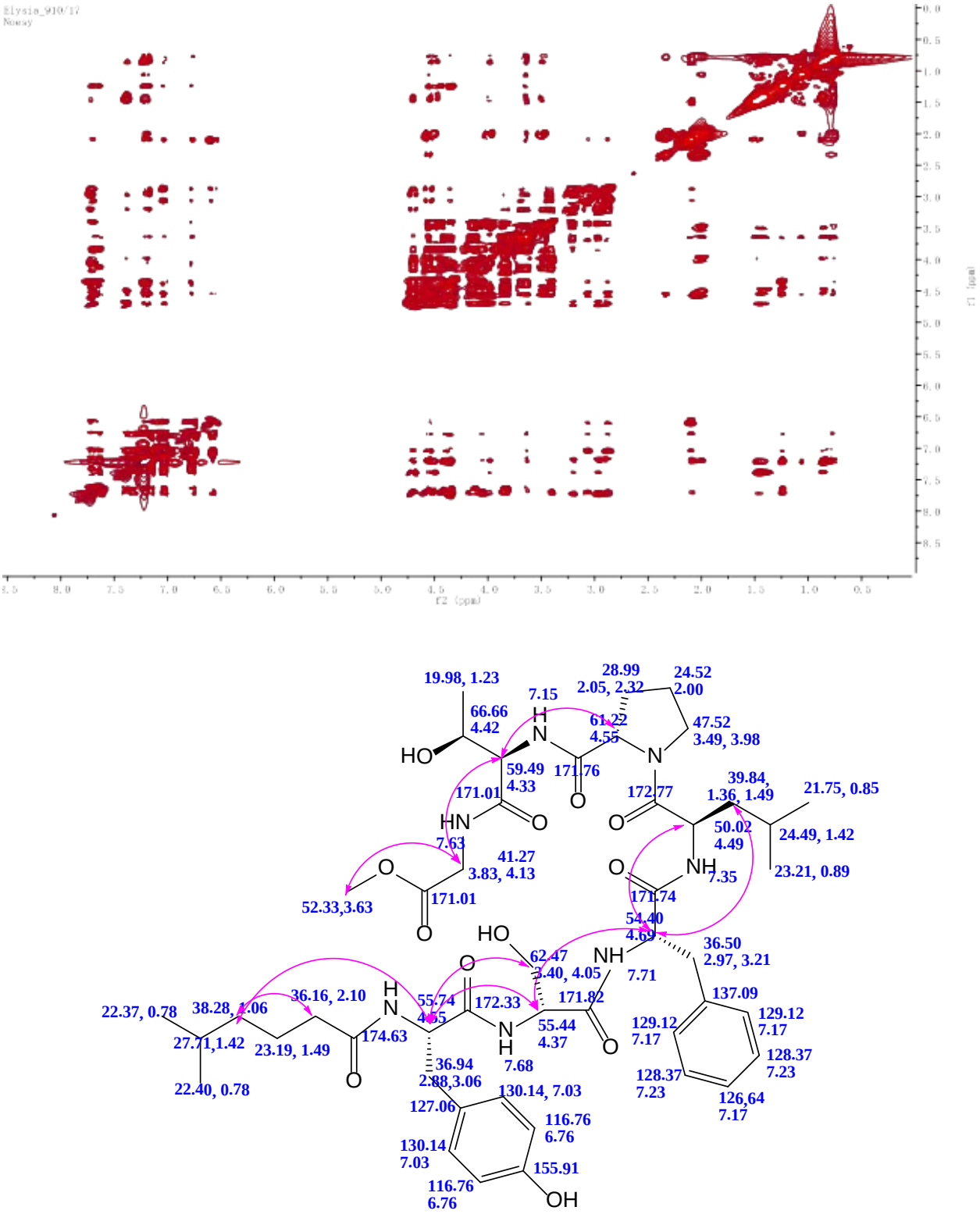

Figure 85 The key NOESY correlations of hydroKB methyl ester **(26)** in $CDCl_3$

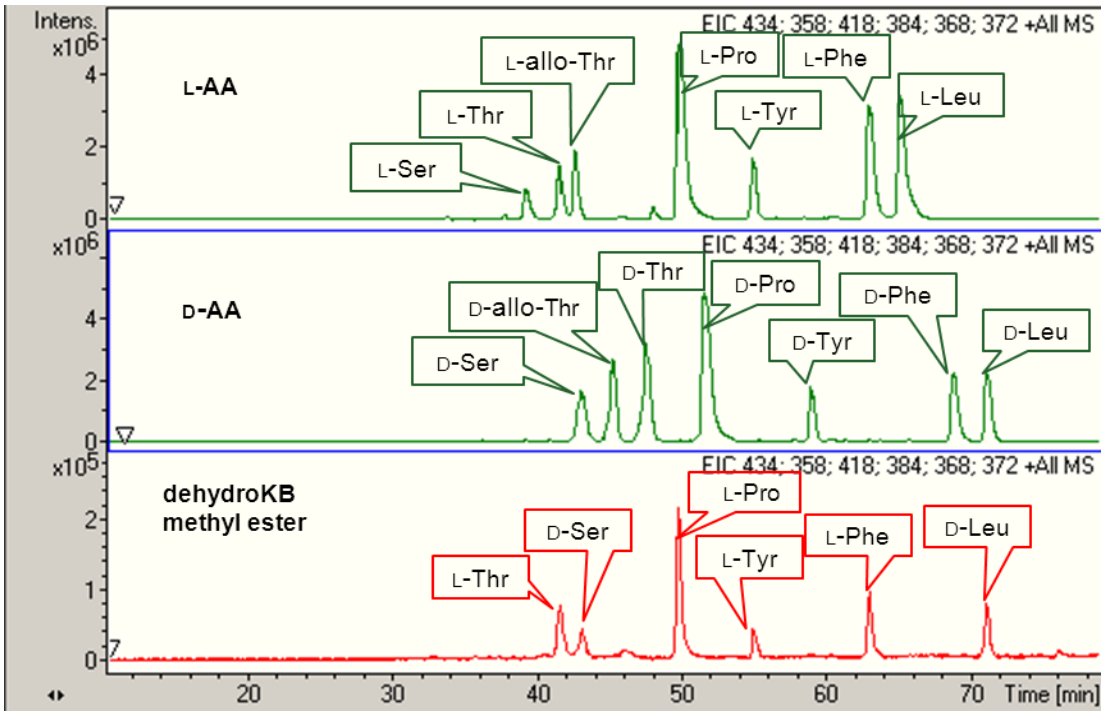

Figure 86 Marfey's analysis of dehydroKB methyl ester **(26)**

DehydroxyKH **(27)** (1.2mg, yield 0.00012%) was obtained as light yellow amorphous powder and HRMS provided quasi-molecular signals $[M+H+Na]^{2+}$ at *m/z* 559.2990, $[M+Na]^{+}$ at *m/z* 1117.5728 for a molecular formula of $C_{55}H_{82}N_8NaO_{15}$ (calc. 1117.5792, Δ -5.7 ppm) **(Figure 87)**. The mass of **27** is 16 dalton less than kahalalide H, which suggested that **27** has one less hydroxy group than kahalalide H. The HSQC overlay with kahalalide H revealed that the α-carbon of OH-Pro4 shifted slightly from δ_C 59.30 to δ_C 60.99. The other three carbon signals on OH-Pro4 at δ_C 37.99, 69.01, 55.74 shifted upfield to δ_C 29.78, 24.68, 47.58, respectively **(Figure 88, 89)**. This provided evidence that the OH-Pro4 is replaced by a Pro residue in compound **27** **(Table 8)**. The specific rotation $[\alpha]_D^{25}$ of **27** (*c* 0.1, MeOH) is +32, which is close to that of kahalalide H. Moreover, the HSQC overlay experiment displayed that all the other amino acid residues signal overlapped well, indicating that the absolute configurations of the amino acid residues of **27** are the same as those of kahalalide H. The $\Delta\delta_{\beta\gamma}$ value of Pro4 is 5.1 ppm (< 8

ppm), suggesting its *trans*- conformation. Marfey's analysis of **27** revealed that Leu2, Val5, and Asp8 are D- configured, and Ser3, *trans*-Pro4, Ser6 are L- configured. Although both D- and L-Phe were observed in **27**, considering a similar optical rotation value and HSQC data to kahalalide H, L-Phe1 and D-Phe7 could be proposed **(Figure 90)**.

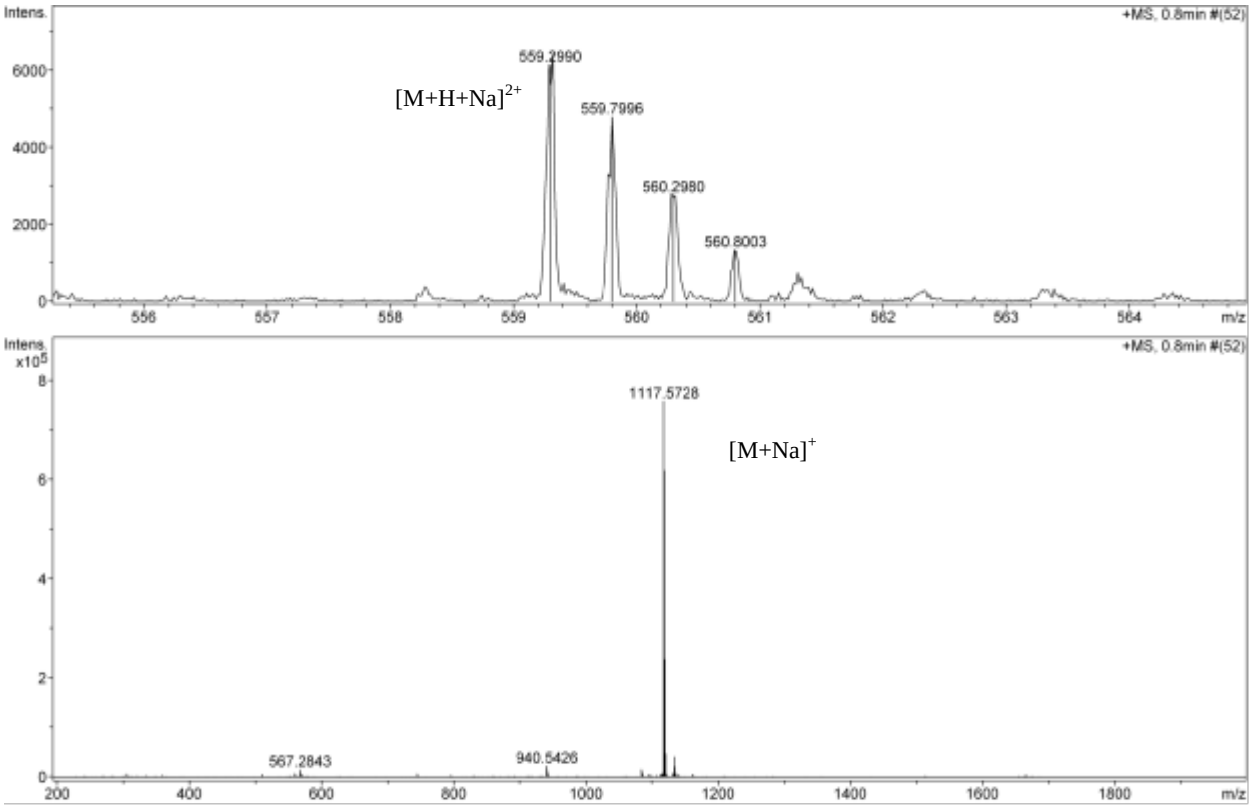

Figure 87 HRMS spectrum of dehydroxyKH **(27)**

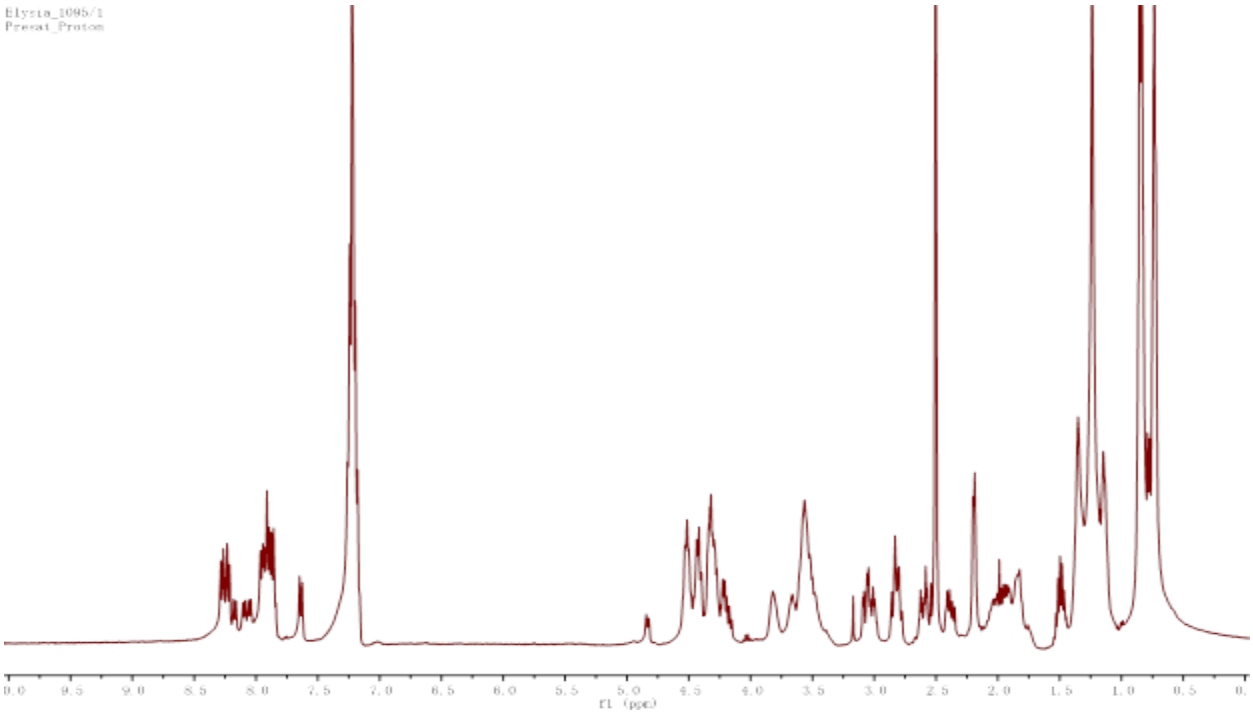

Figure 88 ^{1}H NMR spectrum of dehydroxyKH **(27)** in DMSO-d_6

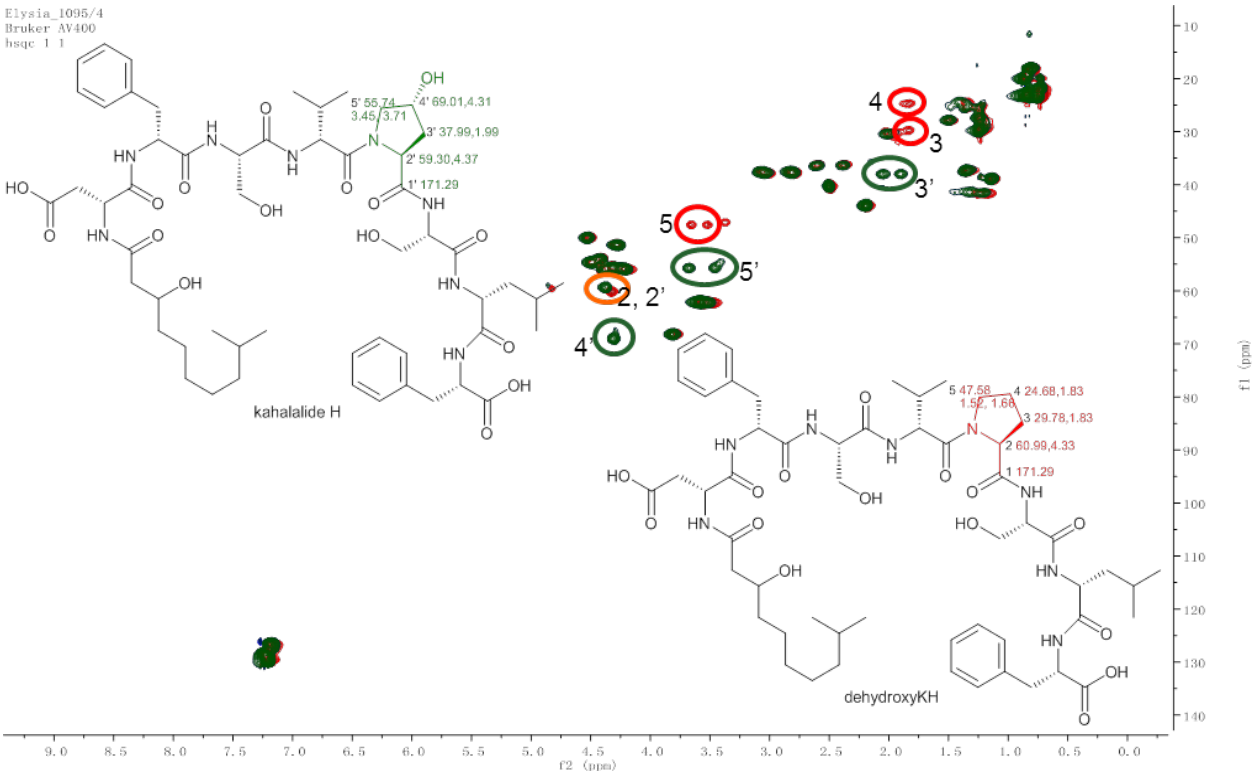

Figure 89 HSQC spectra of kahalalide H (green) and dehydroxyKH **(27)** (red) in DMSO-d_6

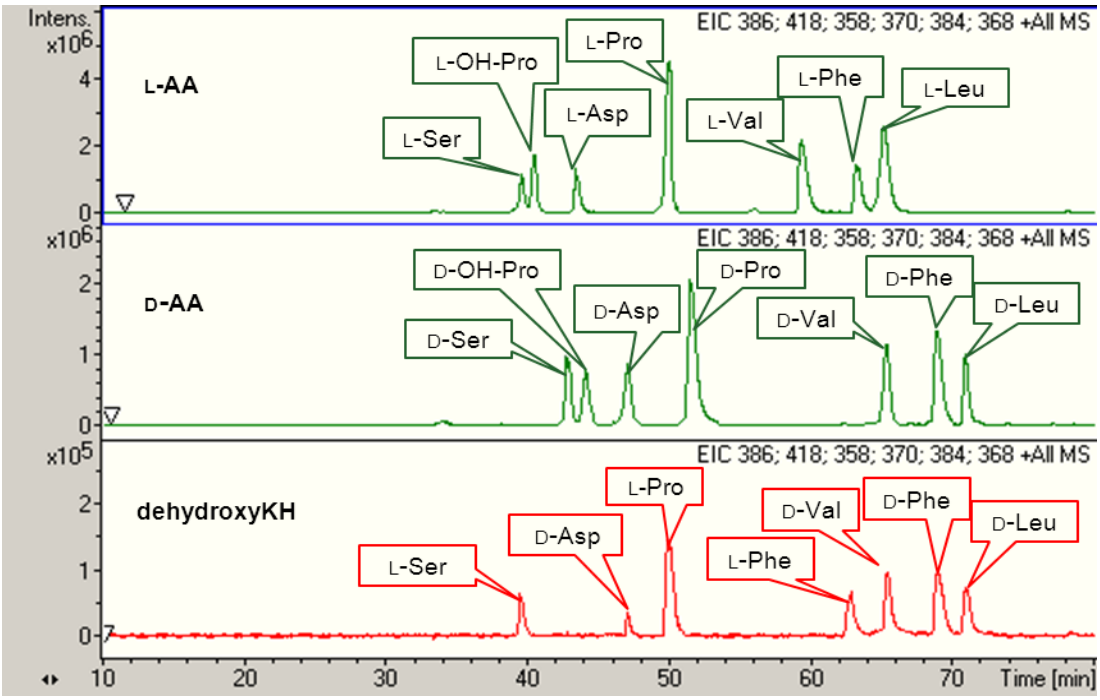

Figure 90 Marfey's analysis of dehydroxyKH **(27)**

29 (1 mg, yield 0.0001%) was obtained as light yellow amorphous powder. The LC-MS provided quasi-molecular signals $[M+2H]^{2+}$ at *m/z* 901.0, $[M+H]^{+}$ at *m/z* 1801.0 **(Figure 91)**. The ^{1}H NMR spectrum suggested the presence of 10 amide protons in **29 (Figure 92)**. However, the other NMR spectra could not be acquired due to limited amount. Future work will focus on the amino acid sequencing analysis using FTMS analysis to assign the structure.

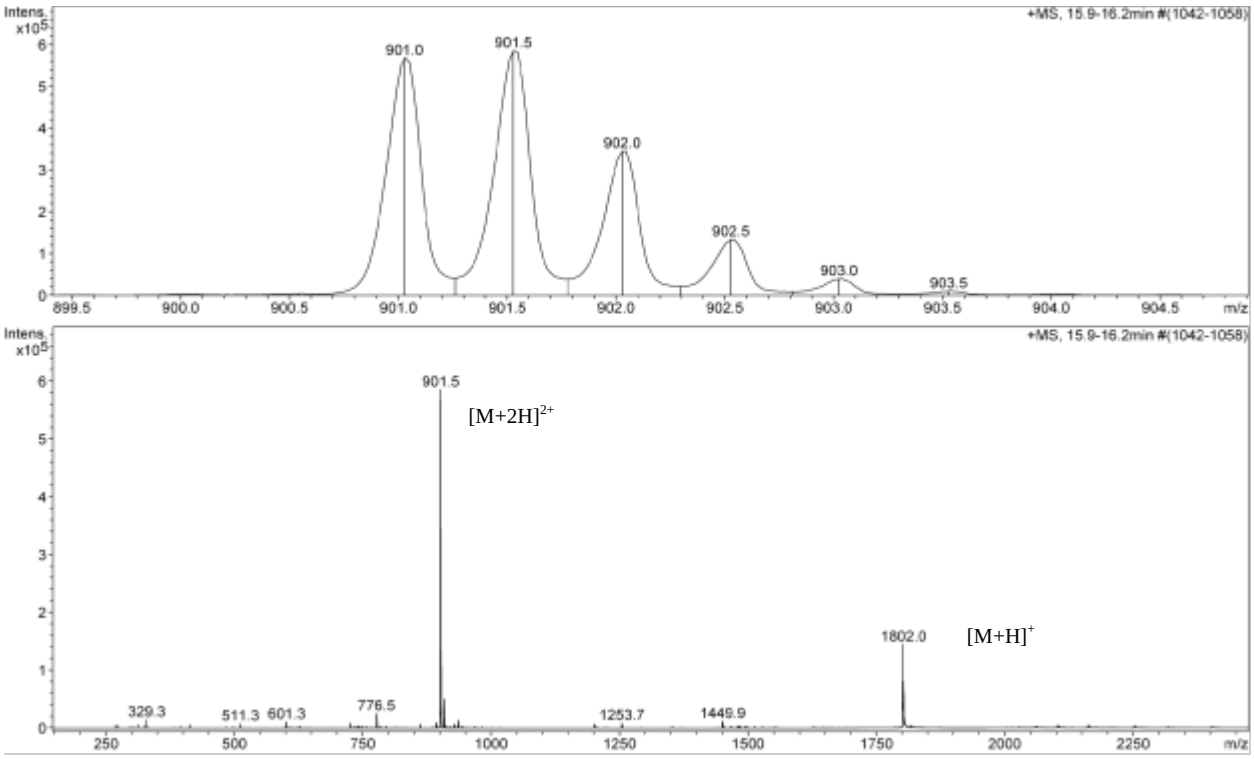

Figure 91 MS spectrum of **29**

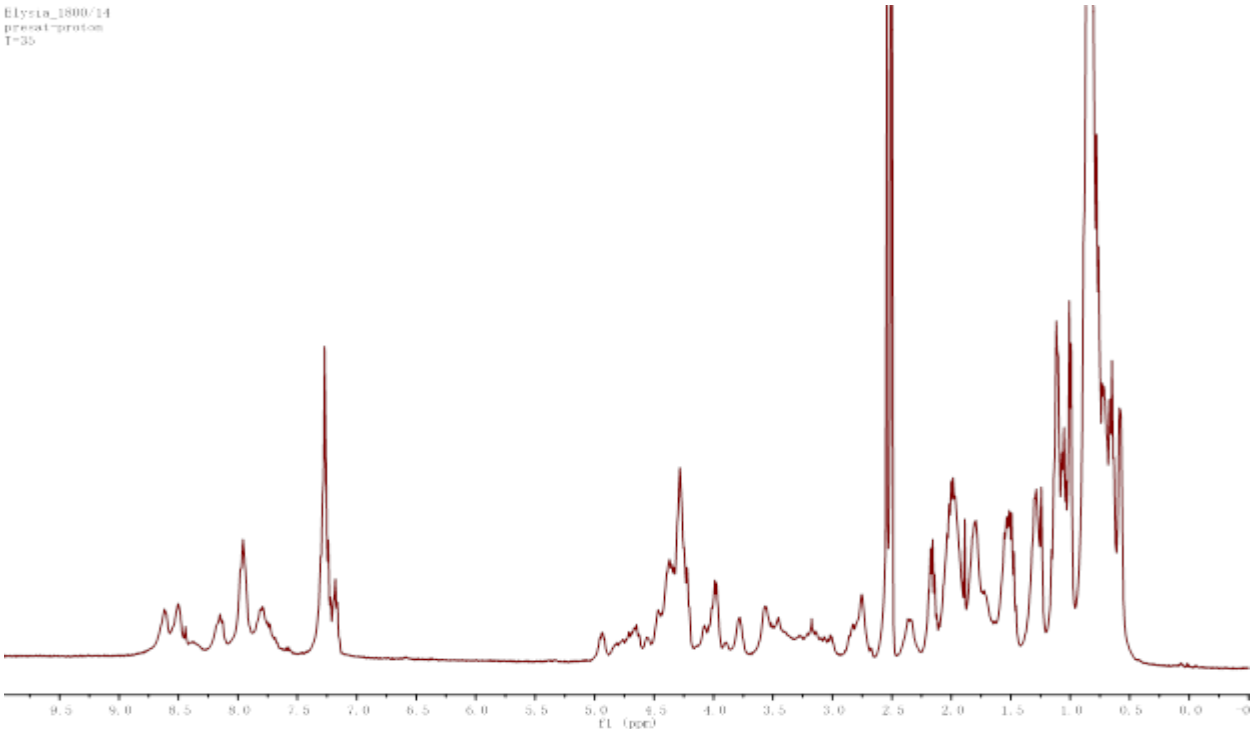

Figure 92 ^{1}H NMR spectrum of **29** in DMSO-d_6

30 (300 μg, yield 0.00003%) was obtained as white amorphous powder and LC-MS provided a quasi-molecular $[M+2H]^{2+}$ signal at *m/z* 893.0 **(Figure 93)**. The mass suggested that **30** could have one less hydroxy group than **29**. However, the NMR spectra could not be acquired due to limited amount. Further FTMS analysis of amino acid sequence will be needed to assign the structure.

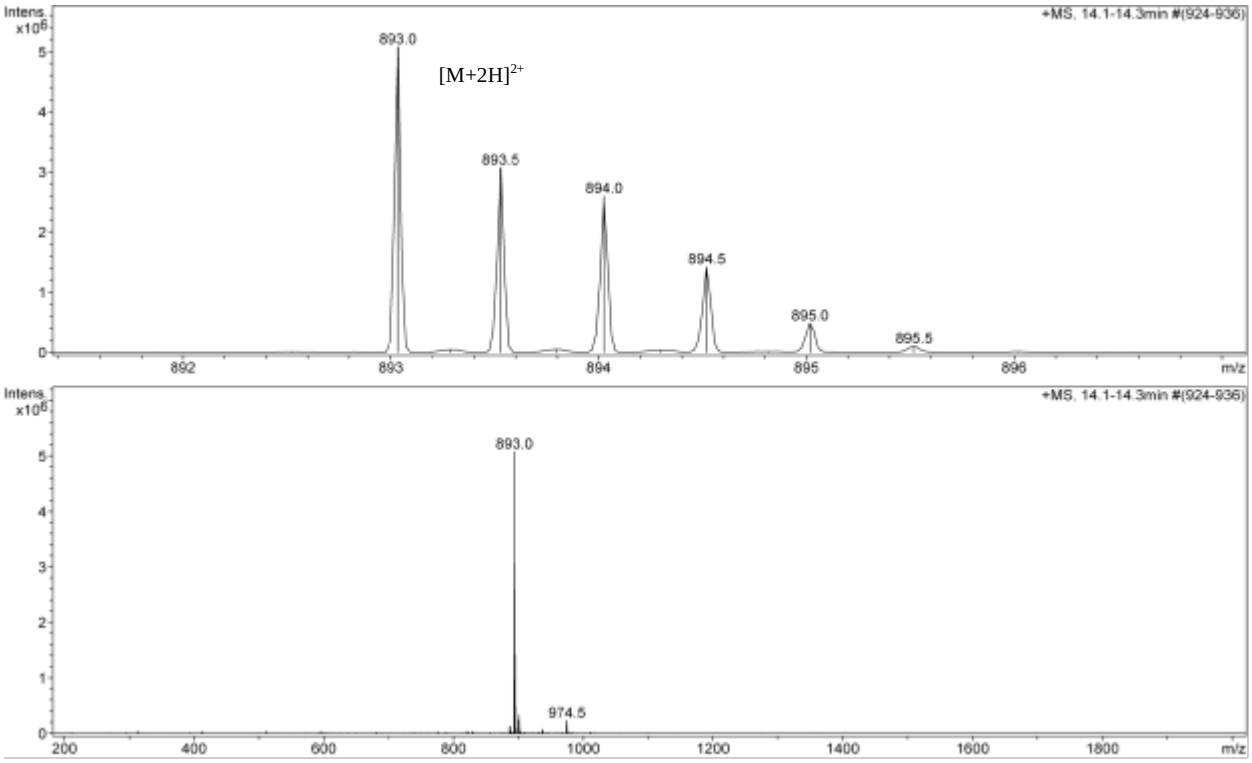

Figure 93 MS spectrum of **30**

3 Materials and Methods

3.1 General Experimental Procedures. NMR spectra were recorded on a Bruker Avance DRX-400 spectrometer. The ^{1}H and ^{13}C NMR chemical shifts were reported in ppm. The MALDI imaging was performed on the MALDI MS (Bruker microflex fitted with flexImaging 2.0 software) in positive mode, with 100-mm raster intervals in XY and approximately 35-62% laser power. HPLC-ESI-TOF was performed on Bruker MicroTOF in line with an Agilent 1100 Series HPLC system and G1316A DAD detector. Phenomenex Luna C_8 5 μm column (150 mm

× 4.6 mm) was used with a gradient elution of MeOH in 0.05% HCOOH at a flow rate of 0.6 mL/min. Preparative HPLC was carried out on a Waters PrepLC system with a single wavelength detector. Diaion HP-20 and sephadex LH-20 resins were purchased from Sigma.

3.2 Sample Collection. Samples were collected from the waters of Kahala Bay near Black Point, Oahu, during March, April and May of 2003. The collected samples were identical to voucher specimen #9507019 deposited at the Suntory Institute for Bioorganic Research, Osaka, Japan.

3.3 Sample Preparation. A dry weight of *E. rufescens* (1 kg) was blended, and the powder was extracted with EtOH for 1 hr in a sonicator. This process was repeated 5 times. The extracts were dried for further isolation.

3.4 Compound Isolation. The extract (300 g) was fractionated on a silica flash column with a gradient solvent system of hexanes-EtOAc (100:0, 50:50, 0:100) and EtOAc-MeOH (50:50, 0:100). EtOAc-MeOH fractions were found to contain peptides, and these two fractions were further eluted on HP-20 with MeOH-H_2O (50:50, 60:40, 80:20, 90:10, 100:0). The LC-MS data for each fraction showed that the MeOH-H_2O (90:10) and 100% MeOH fractions mainly contained the peptides. MeOH-H_2O (90:10) fraction was subjected to C_{18} glass open-tubular column with an isocratic solvent system of MeOH-H_2O (90:10), followed by preparative HPLC (Phenomenex C_{18} column 21.2 × 250 mm) at a flow rate of 8 mL/min or HPLC (Phenomenex C_8 column 10.0 × 250 mm) at a flow rate of 2.5 mL/min with a gradient system of MeCN-H_2O (50:50-80:20) to afford kahalalide D **(16)**. The 100% MeOH fraction was subjected to C_{18} glass open-tubular column with a gradient solvent system of MeOH-H_2O (70:30-100:0) to acquire four sub-fractions. Sub-fraction 1 was purified by preparative HPLC (Phenomenex C_{18} column 21.2 × 250 mm) at a flow rate of 8 mL/min with a gradient system of MeCN-H_2O (50:50-80:20) to afford four new peptides **(17-20)**. Sub-fraction 2 was purified using the same condition as sub-

fraction 1 to afford kahalalide A **(21)**, kahalalide B **(22)**, kahalalide H **(23)**, kahalalide O **(24)**, and three new peptides **25-27**. Sub-fraction 3 was purified by preparative HPLC (Phenomenex C_{18} column 21.2 × 250 mm) at a flow rate of 8 mL/min with a gradient system of MeCN-H_2O (60:40-90:10) to afford kahalalide G **(28)**, and two new peptides **29, 30**. Sub-fraction 4 was purified by preparative HPLC (Phenomenex C_{18} column 21.2 × 250 mm) at a flow rate of 8 mL/min or HPLC (Phenomenex C_8 column 10.0 × 250 mm) at flow rate of 2.5 mL/min with a gradient system of MeCN-H_2O (70:30-100:0) to afford kahalalide R2 **(31)**, kahalalide F **(32)**, kahalalide P **(33)**, and 5-OHKF **(34) (Scheme 10)**.

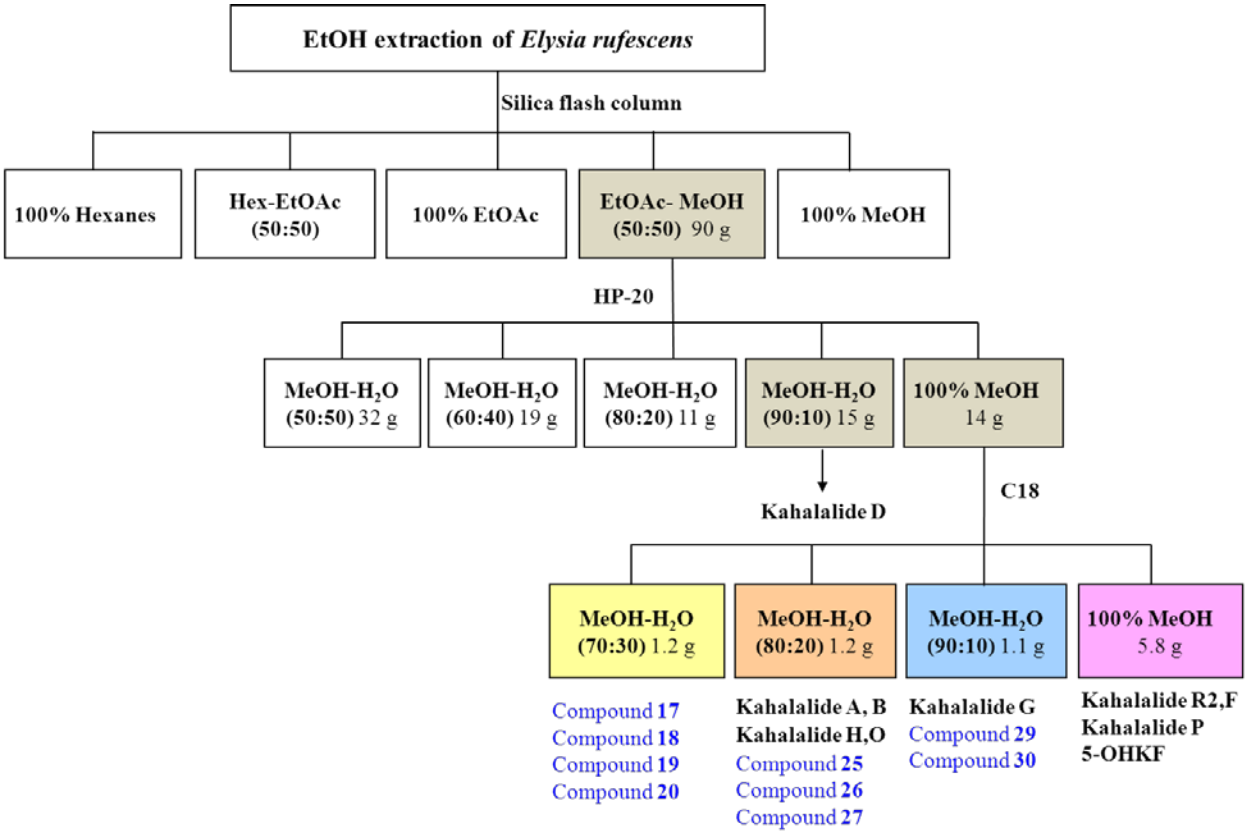

Scheme 10 Isolation scheme of kahalalides from *E. rufescens*

17 (1.2 mg) was obtained as white amorphous powder. $[\alpha]_D^{25}$ 0 (*c* 0.1, MeOH); UV λ_{max} (MeOH) 204 nm; IR neat (KBr) 3286 (s, br), 2958 (s), 2873 (s), 1744 (s), 1638 (s), 1519 (s),

1209 (s), 1025 (s) cm^{-1}; HRMS *m/z* calc. for $C_{46}H_{68}N_7Na_2O_{12}$ $[M+Na]^+$ 956.4721, detected 956.4696.

20 (1.1 mg) was obtained as colorless amorphous solid. $[\alpha]_D^{25}$ +40 (*c* 0.1, MeOH); UV λ_{max} (MeOH) 210 nm; IR neat (KBr) 3298 (s, br), 2956 (s), 2930 (s), 2869 (s), 1722 (s), 1645 (s), 1544 (s), 1440 (s), 1232 (s), 1025 (s) cm^{-1}; HRMS *m/z* calc. for $C_{55}H_{82}N_8NaO_{17}$ $[M+Na]^+$ 1149.5696, detected 1149.5712.

25 (10 mg) was obtained as white amorphous powder. $[\alpha]_D^{25}$ +42 (*c* 0.1, MeOH); UV λ_{max} (MeOH) 195 nm; IR neat (KBr) 3282 (s, br), 2960 (s), 2877 (s), 1627 (s), 1534 (s), 1025 (s) cm^{-1}; HRMS *m/z* calc. for $C_{36}H_{63}N_7NaO_8$ $[M+Na]^+$ 744.4636, detected 744.4629.

26 (20 mg) was obtained as white amorphous powder. $[\alpha]_D^{25}$ 0.0 (*c* 0.1, MeOH); UV λ_{max} (MeOH) 204 nm; IR neat (KBr) 3285 (s, br), 2956 (s), 2873 (s), 1742 (s), 1632 (s), 1514 (s), 1438 (s), 1207 (s), 1025 (s) cm^{-1}; HRMS *m/z* calc. for $C_{46}H_{67}N_7NaO_{12}$ $[M+Na]^+$ 933.4745, detected 933.4805.

27 (1.2 mg) was obtained as colorless amorphous solid. $[\alpha]_D^{25}$ +32 (*c* 0.1, MeOH); UV λ_{max} (MeOH) 210 nm; IR neat (KBr) 3298 (s, br), 2956 (s), 2929 (s), 2869 (s), 1722 (s), 1643 (s), 1544 (s), 1441 (s), 1231 (s), 1025 (s) cm^{-1}; HRMS *m/z* calc. for $C_{55}H_{82}N_8NaO_{15}$ $[M+Na]^+$ 1117.5797, detected 1117.5728.

3.5 Marfey's Analysis of New Peptides. Marfey's reaction is the most commonly used method to separate the enantiomers by introducing an additional stereogenic center, thus determining their absolute configuration **(Scheme 11)**. Peptides (0.5 μmol) were hydrolyzed using 1 mL of 6 M HCl in a sealed reaction vial at 100 ºC for 20 h. Traces of HCl was removed under vacuum. The resulting hydrolysate and amino acid standards were derivatized with 200 μL of 1% FDAA in acetone and 40 μL of 1 M $NaHCO_3$. The mixtures were heated at 40ºC for 1 h. The solution

was cooled to room temperature, neutralized with 20 μL of 2M HCl, and evaporated to dryness. LC-MS analysis of FDAA-derivatized hydrolyzates and standard FDAA-derivatized amino acids were carried out using C_8 (4.6 × 150 mm column) with a linear gradient of H_2O (0.05% HCOOH)-MeOH (0.05% HCOOH) 60:40 to 10:90 in 75 min at 0.6 mL/min. The absolute configuration of amino acid residues was determined by comparing the retention time with the standard FDAA-derivatized amino acids. The extracted ions corresponding to amino acid FDAA derivatives were listed in **Table 11**. It was noticed that Orn contains two free amine groups, the major derivative was the addition of FDAA on both amine groups in the molecule.

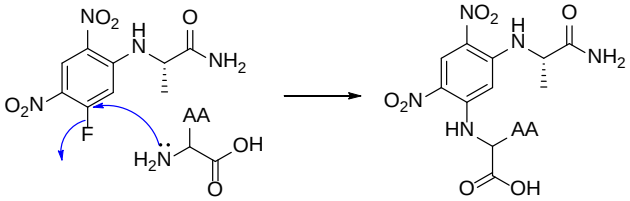

Scheme 11 The mechanism of Marfey's reaction

Table 11 Extracted ions of amino acid FDAA derivatives

Amino acid	$[M+H]^+$	Amino acid	$[M+H]^+$
Asp	386.2	allo-Thr	372.2
Leu	384.1	Tyr	434.2
Orn	637.2	Pro	368.1
Phe	418.2	OH-Pro	384.2
Ser	358.1	Val	370.2
Thr	372.2		

CHAPTER *3*

ANTICANCER LEADS FROM THE NCI REPOSITORY

1. Introduction

Since 1960, the NCI has been dedicated to the discovery of anticancer drug leads from natural sources. The Natural Products Branch of the NCI Developmental Therapeutics Program collected plants and marine organisms from around the world. During the period of 1986-1999, more than 50,000 plant samples and 10,000 marine organisms were collected from over 25 countries.[53] Each organism was extracted using DCM-MeOH (50:50), followed by H_2O. The extracts were stored in a natural product repository at -20 ℃.[53] All the extracts were prescreened in selected tumor cell lines at a rate of 20,000 samples yearly.[53,54] With bioassay-guided isolation, active molecules could be considered for further evaluation using 60 human tumor cell lines, including lung, colon, melanoma, prostate, ovarian, breast and kidney. About 2% of screened compounds with promising potency and selectivity would be recommended for in vivo assays, such as hollow fiber assay and xenografts.[55] If the candidate is selected for the next step development, NCI will provide larger-scale production, initiate preclinical studies such as collecting short and long term toxicological data, and schedule early stage clinical trials.[55] Our group has a long-term collaboration with the NCI. More than 80 extracts have been evaluated from the NCI repository. In this chapter, screening and isolation of extracts from marine organisms provided by the NCI repository are discussed.

2. Results and Discussion

2.1 Primary Screening. At the first stage, 27 extracts from the NCI repository were fractionated using standard procedure listed in the "Materials and Methods" section. All the subfractions were sent to Dr. Fred Valeriote's group at Wayne State University for prescreening in murine lymphoma L1210, colon 38, hematopoietic CFU-GM, as well as human colon HCT116, NSCLC H125, T-cell lymphoma CEM cell lines. As a result, 20 extracts were dropped due to the reduced potency or limited amount of active metabolites; four fractions were potent against several cell lines, particularly H125; three extracts showed potency, however, the materials were not provided by NCI **(Table 12)**. Four active extracts were selected for further purification.

Table 12 Current status of extracts from the NCI repository

Sample	Amount	Organism	Status
C021197-T/6	1g	*Cystodytes fuscus*	**Three known compounds** isolated
C004690	12g	*Phakellia* sp.	**Five known compounds** isolated
C023087-X/6	2g	*Phakellia cavernosa*	**Three known compounds** isolated
C012610-L/6	1g	*Didemnum rubeum*	**One known compound** isolated
C023069-180	4g	*Hyrtios erecta*	Dropped due to limited amount of active metabolites
C022471-176	2g	*Hyrtios* sp.	Dropped due to limited amount of active metabolites
C004440	20mg	*Adolphia* sp.	Dropped without selective fraction
C011316	20mg	*Nemanthus* sp.	Dropped without selective fraction
C004024	20mg	*Sclerothamnopsis* sp.	Dropped without selective fraction
C002136	20mg	Unknown	Dropped without selective fraction
C002394	20mg	Unknown	Dropped without selective fraction
C017508	20mg	Unknown	Dropped without selective fraction
C017022	20mg	*Barbatia* sp.	Dropped without selective fraction
C001119	20mg	*Batzella* sp.	Dropped without selective fraction
C017114	20mg	*Dorypleres* sp.	Dropped without selective fraction
C016326-Y/6	3g	*Eudistoma* sp.	Dropped without selective fraction
C009472	20mg	*Pchyclavularia* sp.	Dropped without selective fraction
C021336	20mg	*Stephanoscyphus* sp.	Dropped without selective fraction
C014402	20mg	*Theonella* sp.	Dropped without selective fraction
C003658	20mg	Unknown	Dropped without selective fraction
C003878	20mg	Unknown	Dropped without selective fraction
C006332	20mg	Unknown	Dropped without selective fraction
C011574	20mg	Unknown	Dropped without selective fraction
C017702	20mg	Unknown	Dropped without selective fraction
C011264	20mg	*Halichondria* sp.	Sample not provided
C013676	20mg	*Halichondria* sp.	Sample not provided
C014398	20mg	*Halichondria* sp.	Sample not provided

2.2 Identification of Active Compounds. Purification of the four potent extracts yielded 12 known compounds **(35-46)**.

2.2.1 C021197. C021197 is the extract of the ascidian *Cystodytes fuscus* collected at -10 meters from Aore Island located in the Republic of Vanuatu **(Figure 94)**. Primary activity displayed that silica EtOAc, EtOAc-MeOH (75:25, 50:50) fractions were potent against H125 and CEM cell lines. Further purification of active fractions on preparative HPLC yielded three compounds **(35-37)**. The three compounds provided quasi-molecular signals $[M+H]^+$ at *m/z* 358.1, 388.1, 431.1, respectively. Odd molecular weights of **35** and **36** suggested that they are nitrogen containing metabolites. The ^{1}H NMR chemical shifts of **35** in the regions of δ_H 7.0-9.5 and δ_H 5.58 revealed the presence of an aromatic system and olefin protons. Two vicinal methylenes at δ_H 3.32 and 3.82, as well as two methyls at δ_H 1.89 and 2.14 were observed **(Figure 95)**. Compound **36** has one more methyl group at δ_H 3.52 when compared to **35**, suggesting the presence of one *O*-methyl group. Aromatic protons and vicinal methylene protons of **37** shifted upfield when compared to **35**, indicating a change of the ring system. Searching the molecular mass using Marinlit and the comparison of acquired ^{1}H NMR spectra with published data determined these three compounds to be pyridoacridine alkaloids cystodytin A **(35)**, cystodytin F **(36)**, and shermilamine C **(37) (Figure 96)**.[56,57,58] The optical rotation of cystodytin F **(36)** is 0, indicating it is racemic.

Figure 94 The ascidian *Cystodytes fuscus*

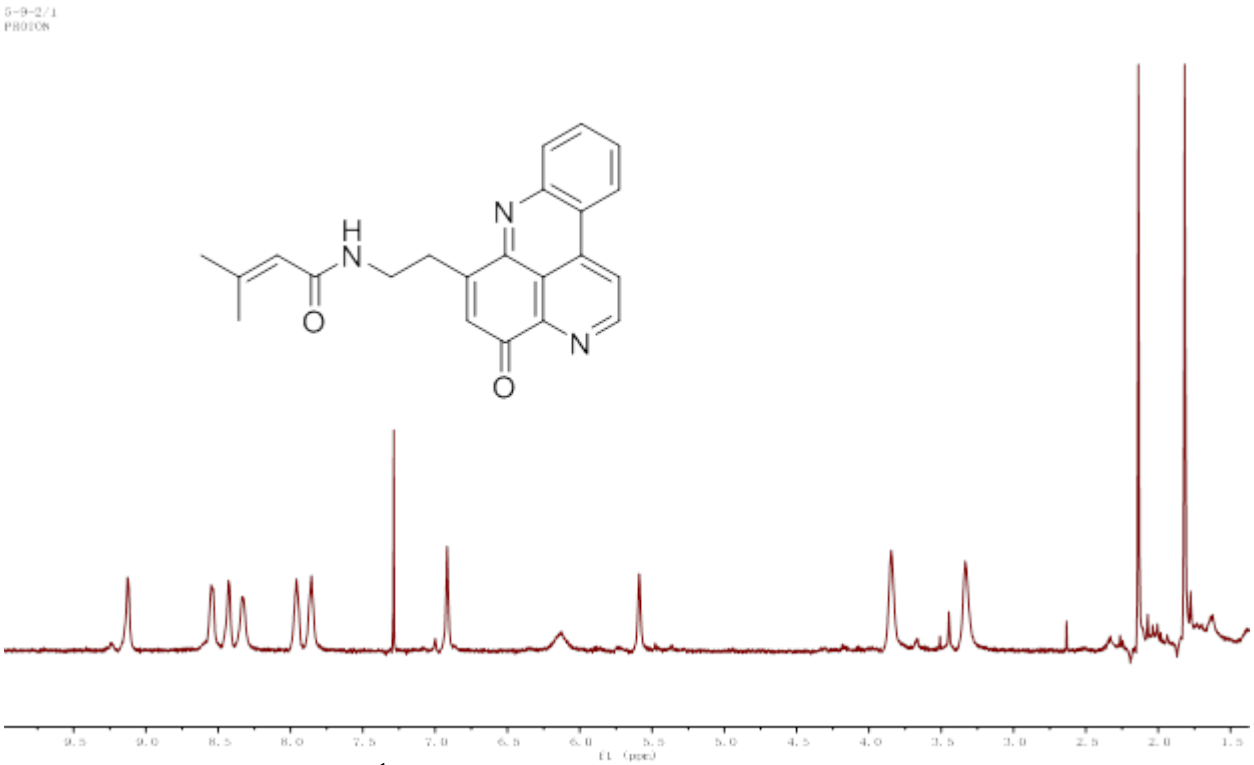

Figure 95 ^{1}H NMR spectrum of cystodytin A **(35)** in $CDCl_3$

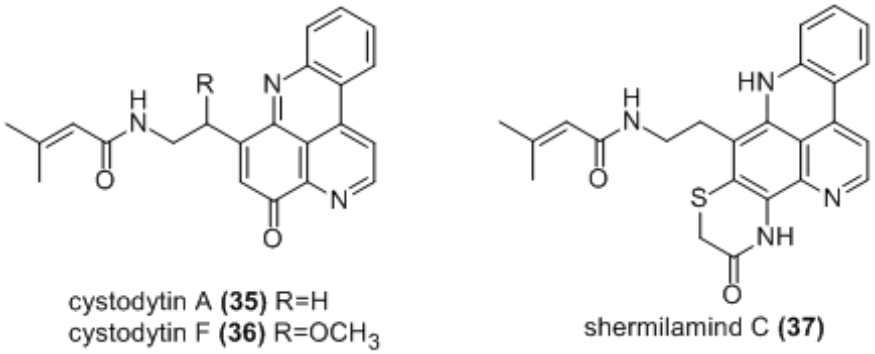

Figure 96 Structures of **35-37** isolated from *Cystodytes fuscus*

Cystodytin A **(35)** and cystodytin F **(36)** showed cytotoxicity against L1210 with IC_{50} values of 0.24 and 0.068 µg/mL, respectively.[56,57] Shermilamine C **(37)** showed inhibition of topoisomerase II catalytic activity of IC_{50} at 138 µM.[58] The cytotoxicity soft-agar based disc diffusion assay revealed cystodytin F **(36)** exerts inhibition of CFU-GM, HCT116, H125, and U251N **(Table 13)**.

Table 13 Disc diffusion assay data for compound **35-37**

Sample	Concentration (μg/mL)	Inhibition zone units			
		CFU-GM	**HCT116**	**H125**	**U251N**
DMSO		0	0	0	0
cystodytin A **(35)**	600	50	250	300	300
cystodytin F **(36)**	300	**375**	**550**	**450**	**400**
shermilamine **(37)**	1200	150	200	300	250

2.2.2 C004690. C004690 is the extract of the sponge *Phakellia* sp. Primary activity displayed that the MeOH fraction from a silica column or the H_2O fraction from a C_{18} column was potent against H125. The extract (12 g) was eluted on C_{18} glass open-tubular column using a gradient of H_2O-MeOH to generate nine subfractions. LC-MS analysis of the subfractions revealed that H_2O-MeOH (50:50, 40:60, 30:70) fractions contained brominated metabolites. Further purification on a preparative HPLC C_{18} column afforded five pure compounds **(38-42)**. The compounds provided quasi-molecular signals $[M+H]^+$ at *m/z* 327.1, 188.9, 357.1, 355.1, and 341.1, respectively. A mass ratio at M:[M+2] (1:1) was observed in all molecules, suggesting the presence of one bromine in the molecules. The ^1H NMR chemical shifts of **42** in the δ_H 6.0-7.5 region indicated the presence of an aromatic system. The ^{13}C NMR spectrum showed two carbonyls at δ_C 158.2 and 159.1 suggesting the presence of two amides or esters **(Figures 97, 98)**. One *N*-methyl at δ_H 2.6 was observed. The ^1H and ^{13}C NMR spectra of **38**, **40**, and **41** are similar to those of **42**. Compound **38** has one *N*-methyl group less than **42**. Compound **41** has one more *O*-methyl at δ_H 3.0 than **42**. One carbon signal of **40** shifted from δ_C 65.5 to 89.1 when compared to **42**, indicating the presence of a hydroxy group. Compared to these four compounds, only two aromatic protons and amide protons were observed in **39**. Marinlit searching and comparison of acquired ^1H and ^{13}C NMR spectra with published compounds confirmed the molecules are agelastatin D **(38)**, 5-bromo-1*H*-pyrrole-2-carboxamide **(39)**, agelastatin C **(40)**,

agelastatin E **(41)**, and agelastatin A **(42)** **(Figure 99)**.[59,60] The absolute configuration was determined by measuring the optical rotation values and comparing with published data.

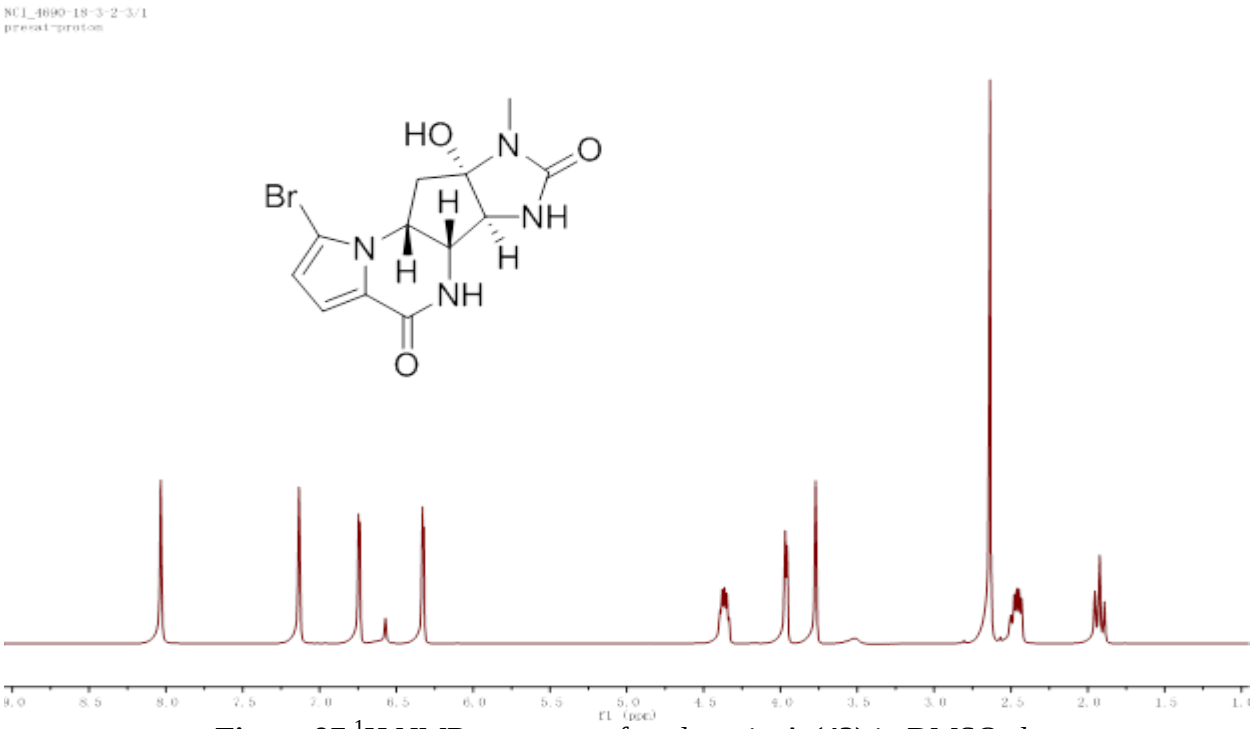

Figure 97 ^{1}H NMR spectrum of agelastatin A **(42)** in DMSO-d_6

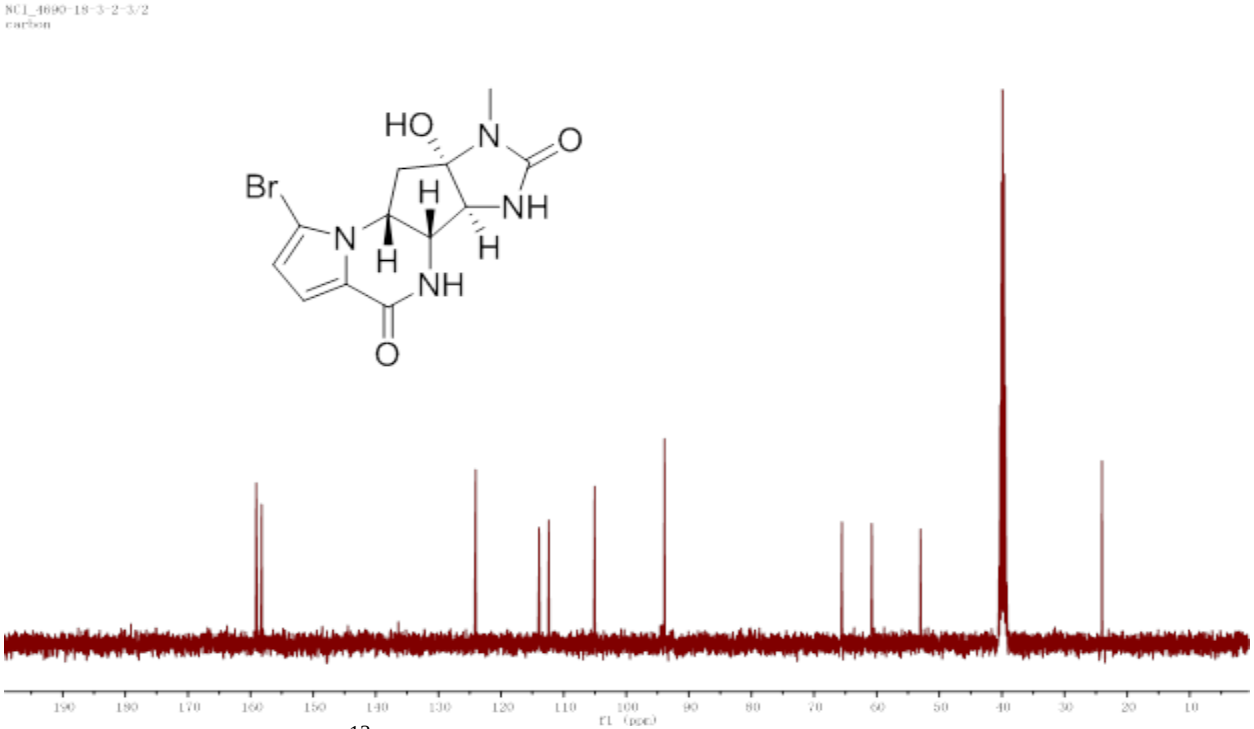

Figure 98 ^{13}C NMR spectrum of agelastatin A **(42)** in DMSO-d_6

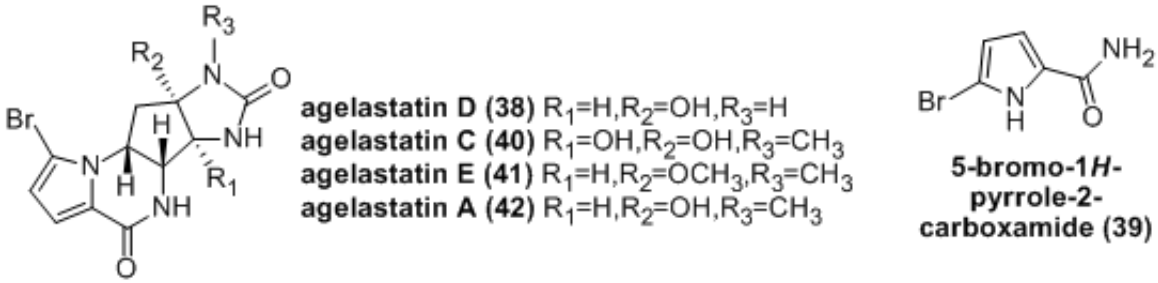

Figure 99 Structures of **38-42** isolated from *Phakellia* sp.

Agelastatin **(42)** was reported to be the most active compound in the agelastatin family. It was first isolated from the sponge *Agelas dendromorpha*.[61] **42** displayed an inhibition on GSK-3β.[61] It is totoxic against L1210 with an IC_{50} of 0.033 μg/mL, which is competitive to that of doxorubicin.[62] More than that, it showed the selectivity against human cervix carcinoma KB cell line with an IC_{50} of 0.075 μg/mL.[62] Compounds **38-42** have been sent to Wayne State for the evaluation using other cancer cell lines.

2.2.3 C023087. C023087 is the extract of the sponge *Phakellia cavernosa* (*Acanthella cavernosa*) collected at -20 meters from Guam **(Figure 100)**. Primary activity result displayed that the hexanes-EtOAc (50:50) fraction from a silica column was active against the H125 and CEM cell lines. Further purification on a preparative HPLC C_{18} column (21.2 × 250 mm) or C_8 (10.0 × 250 mm) yielded three pure compounds **(43-45)**. The compounds provided quasi-molecular signals $[M+H]^+$ at *m/z* 384.2, 411.2, and 402.3, respectively. Odd molecular weights of **43** and **45** demonstrated that they are nitrogen containing compounds. **43** has no UV absorption, while **44** and **45** have weak absorption at λ 210 nm. The ^1H and ^{13}C NMR spectra of **43** displayed a proton at δ_H 4.99 and carbons in the region of δ_C 60-90, indicating they are

Figure 100 The sponge *Phakellia cavernosa*

adjacent to oxygens. Carbons at δ_C 152.1, 152.8, and 156.7 suggested the presence of isocyano carbons. However, due to the limited sample size, insufficient pulsing, and the broadness of the signals, the response of isocynao carbons was limited **(Figures 101, 102)**. Compound **44** displayed a mass ratio of 3:1 at M:[M+2], suggesting the presence of a chlorine in the molecule. Mass searching in Marinlit and comparison of acquired ^{1}H NMR spectra with published compounds confirmed the compounds are kalihinol F **(43)**, 10-formamidokalihinol A **(44)**, and 10-formamidokalihinol F **(45) (Figure 103)**.[63,64]

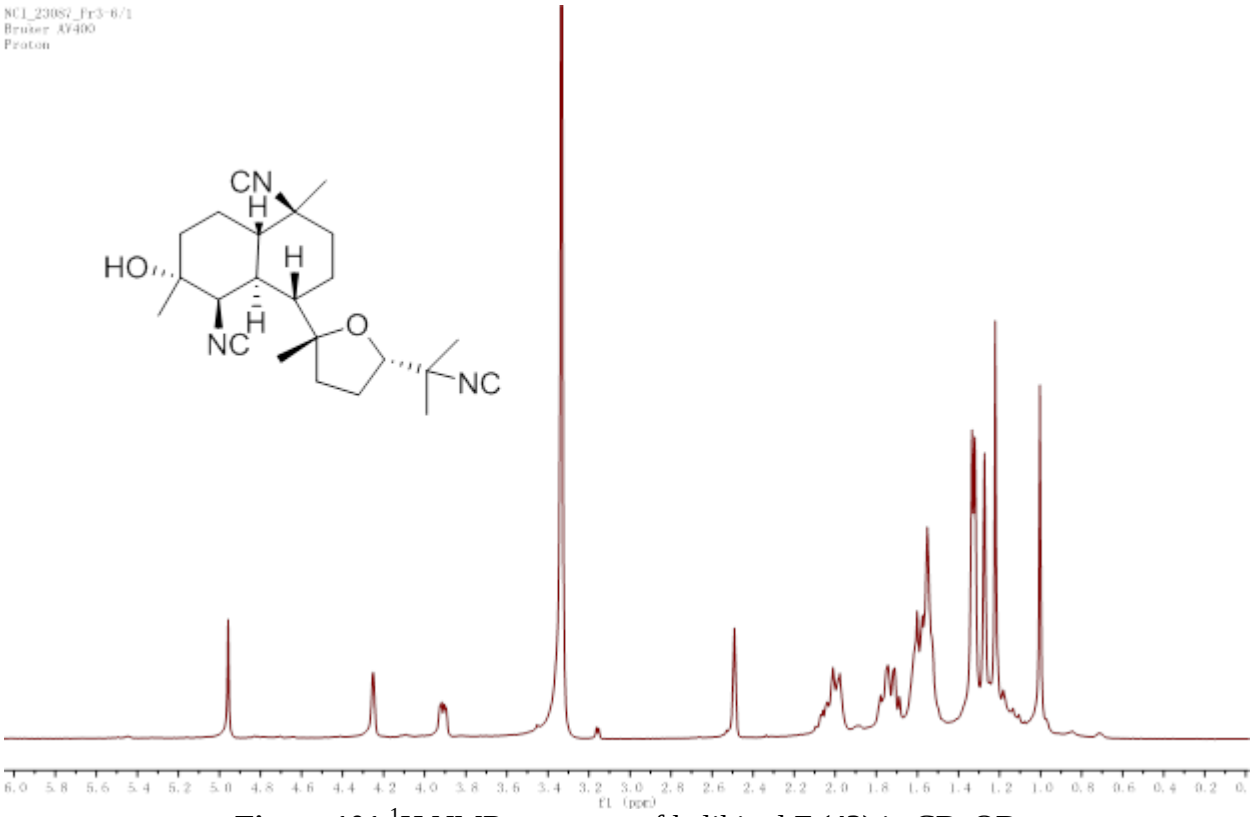

Figure 101 ^{1}H NMR spectrum of kalihinol F **(43)** in CD_3OD

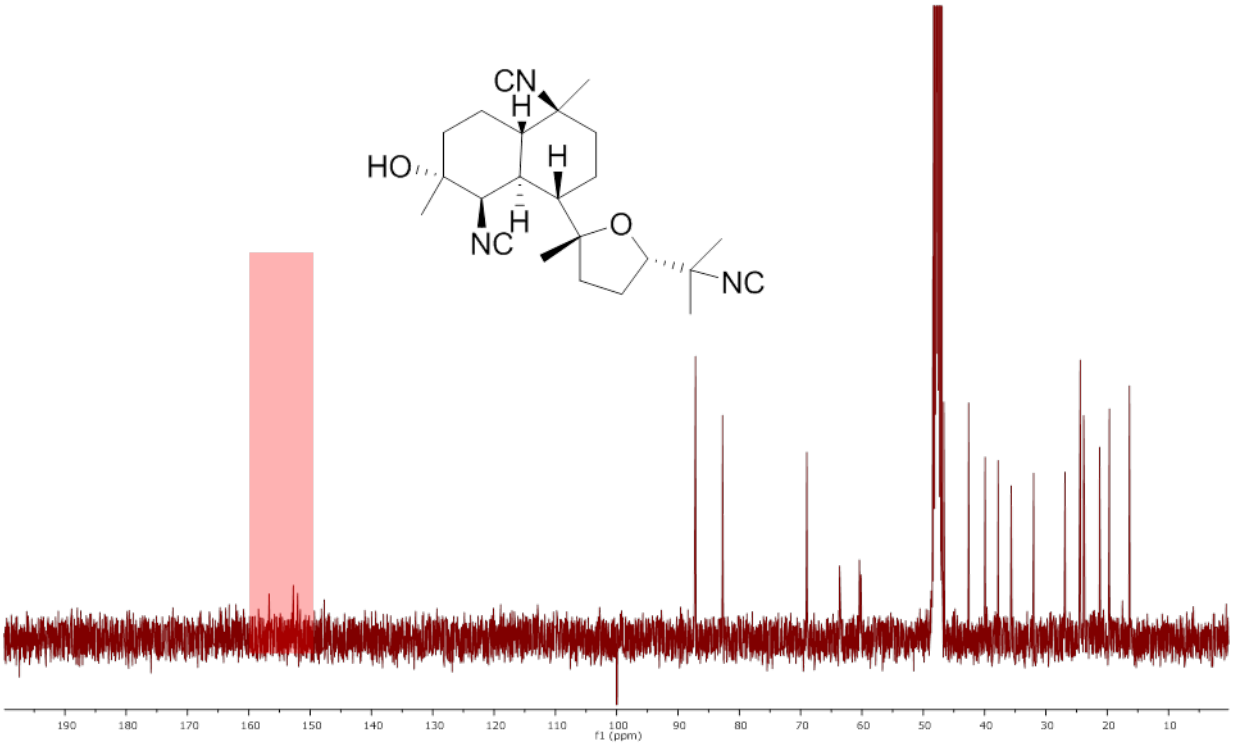

Figure 102 ^{13}C NMR spectrum of kalihinol F **(43)** in CD_3OD

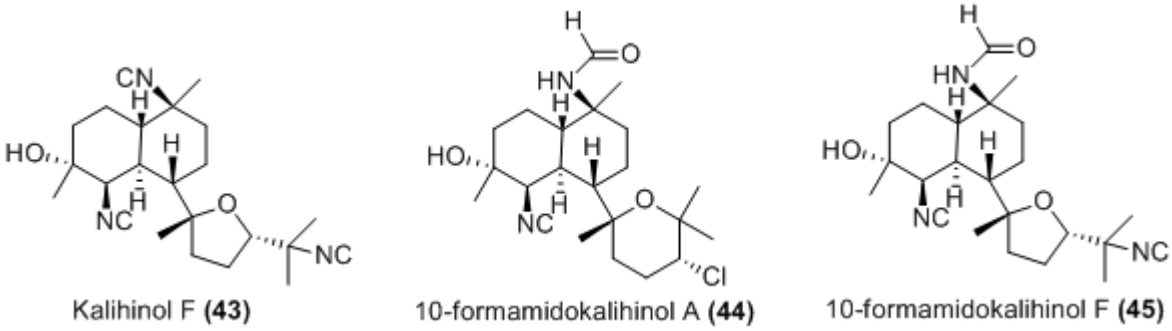

Figure 103 Structures of **43-45** isolated from *Phakellia cavernosa*

2.2.4 C012610. C012610 is the extract of the ascidian *Didemnum rubeum* collected at -10 meters from Ngerkuul in the Republic of Palau **(Figure 104)**. The primary activity result of its fractions showed the silica EtOAc-MeOH (50:50) fraction was active against the H125 cell line. Further purification on sephadex LH-20 using DCM-MeOH (1:1), followed by a preparative HPLC C_{18} column (21.2 × 250 mm) yielded compound **(46)**. The molecule gave a quasi-molecular signal $[M+H]^+$ at *m/z* 403.9. An odd molecular weight provided the evidence that it is nitrogen

containing compound. Proton and carbon signals at δ_H 7.8, δ_C 136.7, 140.1, 158.3 indicated the presence of an aromatic ring. An additional two aromatic carbons at δ_C 90.1 were observed, which was due to a shielding effect caused by the iodine. The ^{1}H NMR spectrum displayed a methyl signal at δ_H 3.81, indicating the presence of a methoxy group **(Figures 105, 106)**. Marinlit searching and comparison of acquired ^{1}H and ^{13}C NMR spectra with published data confirmed that **46** is 3,5-diiodo-4-methoxyphenethylamine **(Figure 107)**.[65]

Figure 104 The ascidian *Didemnum rubeum*

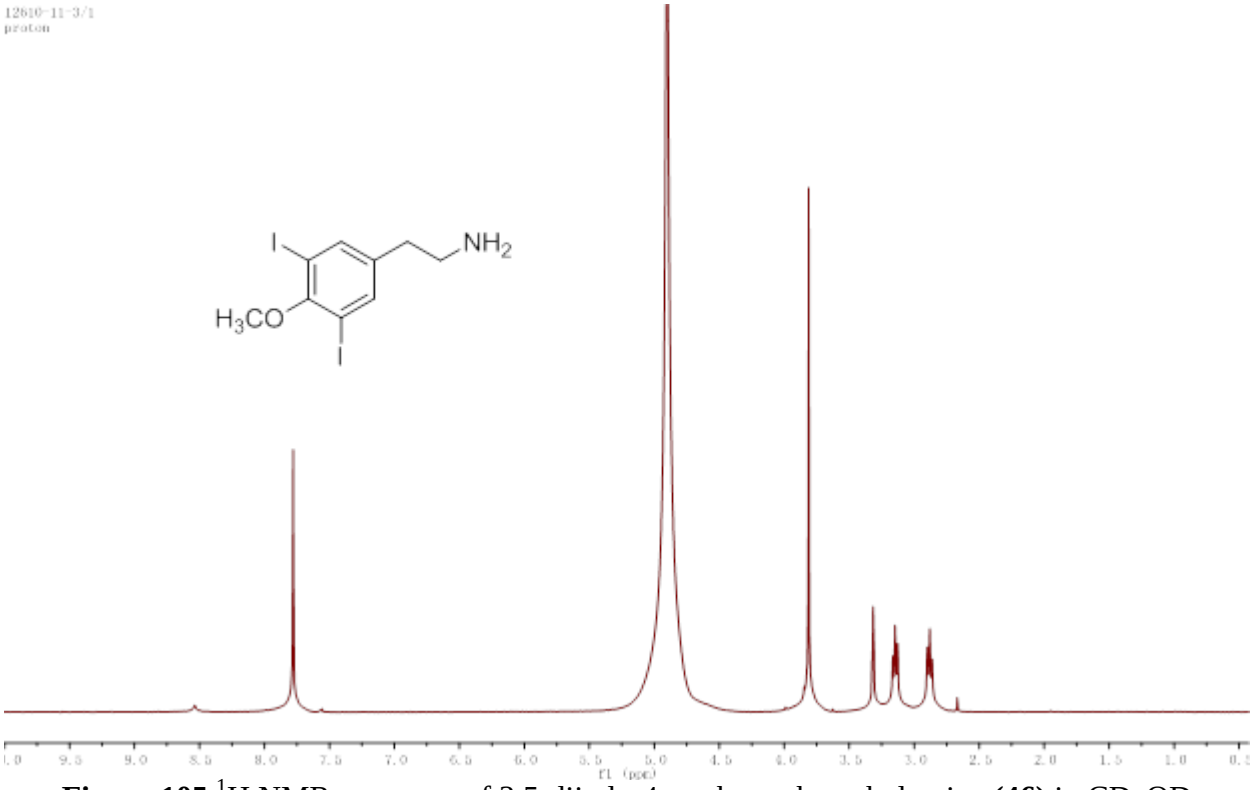

Figure 105 ^{1}H NMR spectrum of 3,5-diiodo-4-methoxyphenethylamine **(46)** in CD_3OD

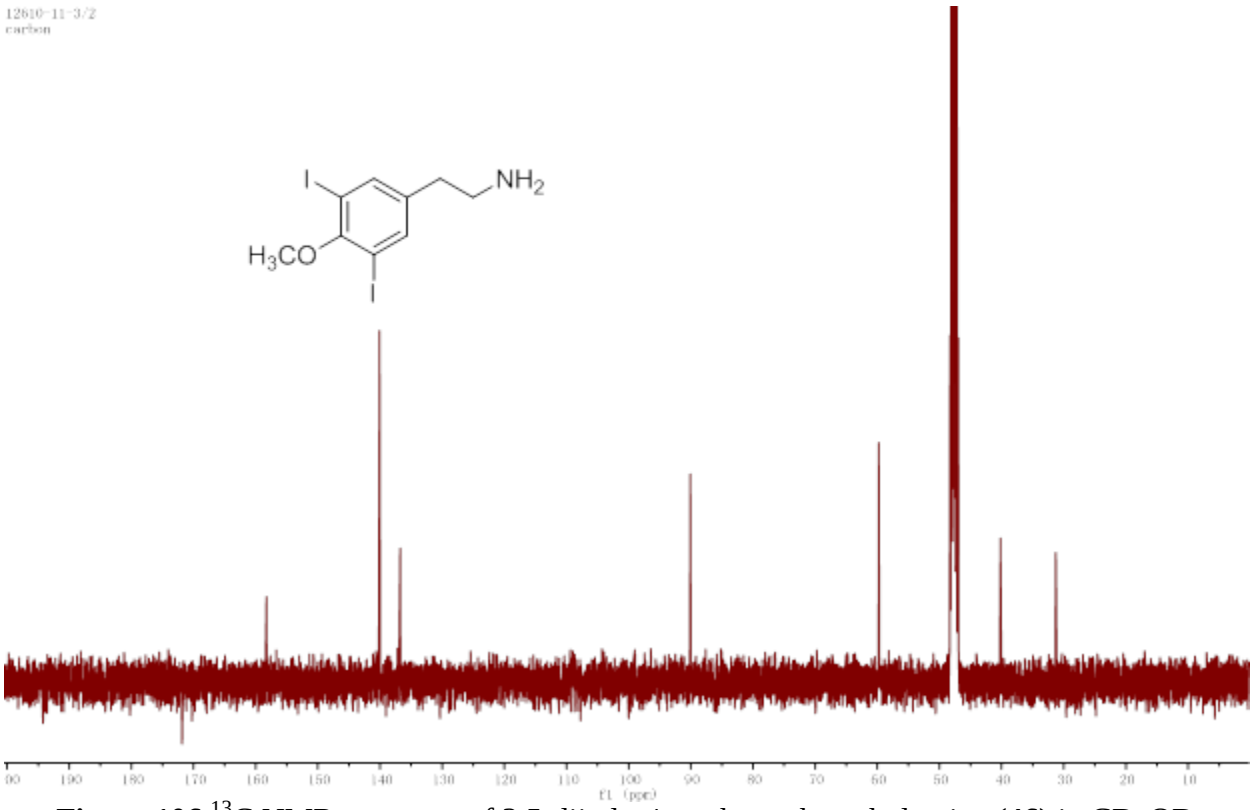

Figure 106 ^{13}C NMR spectrum of 3,5-diiodo-4-methoxyphenethylamine **(46)** in CD_3OD

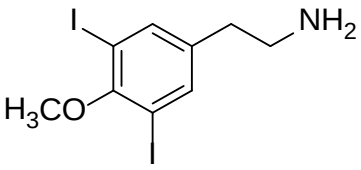

Figure 107 The structure of 3,5-diiodo-4-methoxyphenethylamine **(46)**

3. Materials and Methods

3.1 General Experimental Procedures. NMR spectra were recorded on a Bruker Avance DRX-400 spectrometer. The ^{1}H and ^{13}C NMR chemical shifts were reported in ppm. HPLC-ESI-TOF was performed on Bruker MicroTOF in line with an Agilent 1100 Series HPLC system and G1316A DAD detector. Phenomenex Luna C_8 5 μm column (150 mm × 4.6 mm) was used with a gradient elution of MeOH with 0.05% HCOOH at a flow rate of 0.6 mL/min. Preparative HPLC was carried out on a Waters PrepLC system with a single wavelength detector. C_{18} and

sephadex LH-20 resins were purchased from Sigma-Aldrich. Optical rotations were measured on a JASCO DIP-370 polarimeter.

3.2 Screening of Active extracts. A standard approach for the screening of NCI extracts was developed by our group. First, 20mg of extract is divided into four 5 mg fractions. Then 5 mg material is eluted on the silica, C_{18}, sephadex LH-20, and amino cartridges, respectively **(Scheme 12)**. All the fractions were sent to Wayne State University for bioassay. Once the activity was confirmed for the fractions, the isolation of potent extracts was performed utilizing the best separation material based on the assay data.

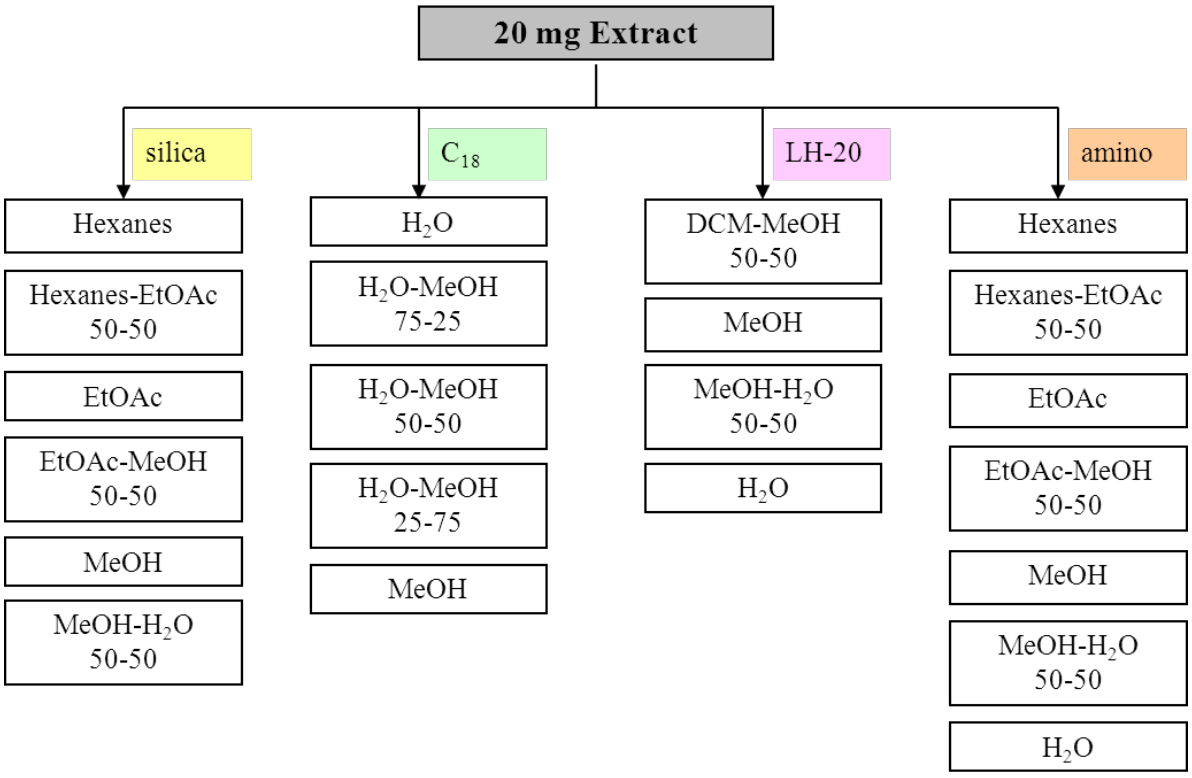

Scheme 12 A standard approach for the screening of NCI extracts

3.3 Compound Isolation.

3.3.1 C021197. The crude extract (1 g) was subjected to VLC on a silica gel column eluting with a stepwise gradient solvent of hexanes–EtOAc (100:0, 75:25, 50:50, 25:75, 0:100), and EtOAc–MeOH (75:25, 50:50, 25:75, 0:100), to yield nine fractions. Fr5-7 showing activity were

chromatographed on a preparative HPLC C_5 column (21.2 × 250 mm); C_8 column (10.0 × 250 mm using a gradient of MeOH-H_2O (0.05% HCOOH) (20:80-80:20) to afford **35** (1.5mg), **36** (1.8mg), and **37** (2.0mg).

3.3.2 C004690. The crude extract (12 g) was subjected to C_{18} glass open-tubular column eluting with a gradient solvent of H_2O-MeOH (95:5, 90:10, 75:25, 60:40, 50:50, 40:60, 30:70, 20:80, 10:90, 0:100). LC-MS data displayed that Fr5-7 contain brominated metabolites. Fr5 was chromatographed on a preparative HPLC C_{18} column (21.2 × 250 mm) using a gradient of MeCN-H_2O (10:90–50:50) to afford **38** (4.8 mg) and **39** (20 mg). Fr 6 and Fr 7 were chromatographed on a preparative HPLC C_{18} column (21.2 × 250 mm) using a gradient of MeCN-H_2O (20:80-70:30) to afford **40** (27 mg), **41** (5 mg), and **42** (150 mg).

3.3.3 C023087. The crude extract (1 g) was subjected to VLC on a silica gel column eluting with a stepwise gradient solvent of hexanes–EtOAc (100:0, 75:25, 50:50, 0:100), and EtOAc–MeOH (50:50, 0:100), to yield six fractions. The active Fr3 was subjected on a preparative HPLC C_8 column (21.2 × 250 mm) or C_8 (10.0 × 250 mm) using a gradient of MeCN-H_2O (30:70 - 100:0) to yield **43** (1.0 mg), **44** (0.8 mg), and **45** (0.8 mg).

3.3.4 C012610. The crude extract (1 g) was subjected to VLC on a silica gel column eluting with a stepwise gradient solvent of hexanes–EtOAc (100:0, 50:50, 0:100), and EtOAc–MeOH (50:50, 0:100), to yield five fractions. Active Fr4 was eluted on sephadex LH-20 using DCM-MeOH (50:50), followed by a preparative HPLC C_8 column (21.2 × 250 mm) or C_8 (10.0 × 250 mm) using a gradient of MeCN-H_2O (20:80 - 90:10) to yield **46** (1.0 mg).

3.4 Antitumor Assay. The cytotoxicity soft-agar based disc diffusion assay was described in Chapter 1.

PART II

DISCOVERY OF ANTIBIOTIC LEADS FROM MARINE ORGANISMS

CHAPTER *4*

ANTIBIOTICS FOR FOOD SAFETY FROM MARINE *Pseudomonas aeruginosa* COLLECTED IN THE GULF OF MEXICO

1. Introduction

Foodborne diseases have long been a major concern to public health. The WHO reports that there are approximately 76 million cases of foodborne illnesses annually in the U.S., and cost approximately $35 billion each year in treatment, prevention, and lost productivity.[66] Foodborne diseases are involved in high levels of morbidity and mortality, especially among infants, children, elderly, and the immunocompromised. With the growing challenges of foodborne diseases, innovative, economical, and effective controls are needed to inhibit the spread and prevent outbreaks of infectious diseases. Improving microbiological quality and safety of food is one of the most important points in this effort.

Foodborne diseases can be caused by either infections or intoxications.[67] Infections may be caused by bacteria, fungi, viruses, or parasites.[68] Intoxications can be acquired by microorganism toxins or other poisonous chemical substances found in certain plants or animals.[67] It is estimated that bacterial pathogens are responsible for more than 60% of foodborne diseases. According to the CDC, the most common bacterial pathogens leading to foodborne illnesses are *Campylobacter*, *Salmonella*, and *Escherichia coli* O157:H7.[69] In addition,

bacterial toxins produced by *Staphylococcus*, *Clostridium*, *Bacillus*, and *Vibrio* result in foodborne disease outbreaks.[67,68,69]

There are many approaches to deal with the microbiological safety of food. Except for quality assessments and controls during harvesting, processing, packaging, storage, and shipping, treating food with preservatives is another major approach. Debates on the safety of commonly used synthetic antimicrobial preservatives are ongoing. Compared to artificial presertivatives, natural ones could be safer and more readily degradable. Moreover, large-scale biosynthesis of target substances is economical, environmentally benign and achievable. Currently, only two antibiotics, the lantibiotic nisin and the bacteriocin, pediocin PA1 produced by lactic acid bacteria,[70,71] and some essential oils are used as legal food preservatives. Thus, identification of new natural products as antimicrobial preservatives is required. Marine microbes represent an unprecedented natural source for biologically active compounds. Many marine microbes belong to the same genera as terrestrial bacteria that are known producers of bioactive molecules. Many metabolites have been reported as drug-like molecules; however, molecules to be used as food preservatives have a different set of requirements than those that are destined for use as therapeutic agents. Metabolic stability is one of the major differences. A potential therapeutic product needs to be relatively stable to a variety of metabolic factors, but immediate degradation of a food additive to inactive molecules upon consumption is desirable. Therefore, discovery of antimicrobial substances from marine microorganisms is an appealing approach to reduce foodborne diseases.

Marine microbes are capable of producing distinct secondary metabolite profiles based on their need for defense, competition or a number of other environmental factors.[72] The most common approach for discovery of bioactive secondary metabolites from microbes is to screen

microbes for unique biological activities. However, a major challenge to this approach is the cultivation of microbes under laboratory conditions. Even under the best of circumstances, these experiments fail to emulate environmental conditions such as competition, diverse nutrient sources, and extreme temperature variations. The result is an artificial environment for producing secondary metabolites which may cause the silencing of certain genetic pathways since the secondary metabolites they produce are non-essential for survival. To address this problem, strategies of using epigenetic modifiers were utilized to activate the silent gene pathways. Under specific stresses, microbes can respond to stimuli, thus increasing the yield of certain secondary metabolites or producing new metabolites. Cichewicz's research group identified several new metabolites by treating the fungus *Cladosporium cladosporioides* with histone deacetylase or DNA methyltransferase inhibitors.[73] This study provided evidence that the ecological responses could be attributed to the chemical activation of gene expression corresponding to the secondary metabolite biosynthetic gene clusters. Fenical's research group also reported an increased production of emericellamides A and B when co-culturing the fungus *Emericella* sp. with an actinomycete *Salinispora arenicola*.[74] In this case, biochemical communication between microorganisms represents more complicated interactions in microbial communities.

In 2009, marine sediment microbes were collected from the Texas Gulf Coast. Based on general antimicrobial and antimalarial activities screening of their extracts, 17 antibiotic producing microbes were identified. From one of the microbes, YPD1C, which was characterized as *Pseudomonas aeruginosa*, 15 known compounds including two derivatives of phenazine **(47, 48)**, six 2-alkyl-4-quinolones **(49-54)**, and seven rhamnolipids **(55-61)** were isolated **(Figure 108)**. This isolation allowed us to understand the metabolic profile of biologically active secondary metabolites from *P. aeruginosa*, and using this as a basis for

comparison, we were able to identify the differences in metabolite production when treating *P. aeruginosa* with different modifiers and external stimuli. In the world of bacteria, stimuli can change gene expression by affecting DNA methylation,[75] transcription initiation,[76] quorum sensing,[77] kinase signaling,[78] or carbon and nitrogen metabolism.[79] In this chapter, isolation of antibiotics from *P. aeruginosa* and impacts on their production in *P. aeruginosa* are discussed using modifiers including kinase inhibitors manzamine A, kahalalide F, and sceptrin, a cell transport regulator ilimaquinone; adjustment to growth factors such as carbon sources and temperature or co-culturing with four other antibiotic producing microbes (YPD1A, YPD1D, YPD5A, and YPD5C) also collected from the Gulf of Mexico in the Fall of 2009. Interestingly, an improvement of antibiotic production was observed in a mix microbial community with the presence of the chemical modifier sceptrin.

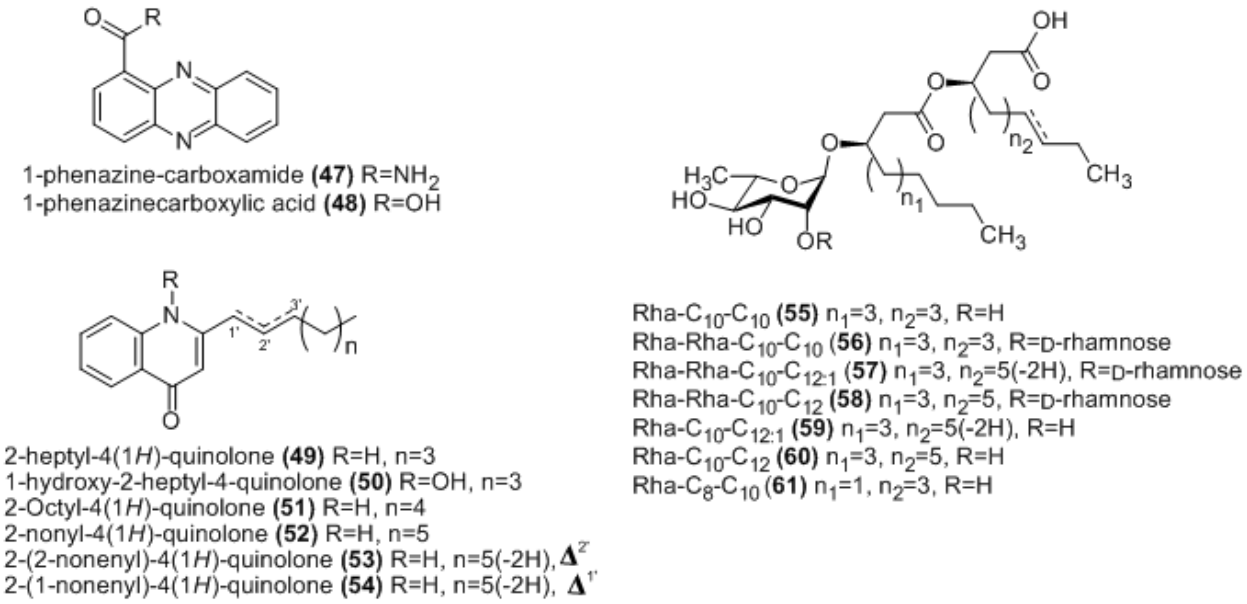

Figure 108 Structures of isolated antimicrobial agents from *P. aeruginosa*

2. Results and Discussion

2.1 Active Compounds from Fermentation of *P. aeruginosa.* The active fraction was subjected to VLC on silica gel. A disc diffusion assay revealed fractions Fr3, Fr4 (hexanes-

EtOAc 50:50, 25:75) and Fr6 EtOAc-MeOH 75:25 have activity against *Bacillus cereus* **(Figure 109)**. The LC-MS and ^{1}H NMR screening of Fr3 and Fr4 revealed signals consistent with aromatic rings. The odd molecular weight *m/z* signals suggested the presence of alkaloids. Further purification was performed using HPLC leading to the isolation of two known active compounds, 1-phenazinecarboxamide **(47)** and 1-phenazinecarboxylic acid **(48)**.

Fr6 was eluted using sephadex LH-20 with DCM-MeOH (50:50) to give 10 sub-fractions, in which Fr6-4, Fr6-6 and Fr6-7 were active using a *B. cereus* disc diffusion assay. Fr6-4 was further purified by HPLC, yielding six pure compounds. LC-MS data of compound 6-4-7-6 gave quasi-molecular ions at *m/z* 244.2 $[M+H]^+$, 266.2 $[M+Na]^+$, 487.4 $[2M+H]^+$, and 509.3 $[2M+Na]^+$, which implied the molecule contains an odd number of nitrogens. The ^{1}H and ^{13}C NMR chemical shifts of the molecule from δ_H 6.25 to δ_H 8.22, and δ_C 107.4 to δ_C 179.2, suggested that it is a quinolone derivate. The ^{1}H NMR signals from δ_H 0.8 to δ_H 1.9 indicated that the molecule contains an aliphatic chain **(Figures 110, 111)**. Based on the key HMBC correlations and comparison with known compounds in SciFinder database using a partial structure, it was determined to be the known compound 2-heptyl-4(1*H*)-quinolone **(49)**. The structures of the remaining five compounds were identified as 1-hydroxy-2-heptyl-4-quinolone **(50)**, 2-octyl-4(1*H*)-quinolone **(51)**, 2-nonyl-4(1*H*)-quinolone **(52)**, 2-(2-nonenyl)-4(1*H*)-quinolone **(53)**, and 2-(1-nonenyl)-4(1*H*)-quinolone **(54)** by the LC-MS and HMQC overlay experiments.

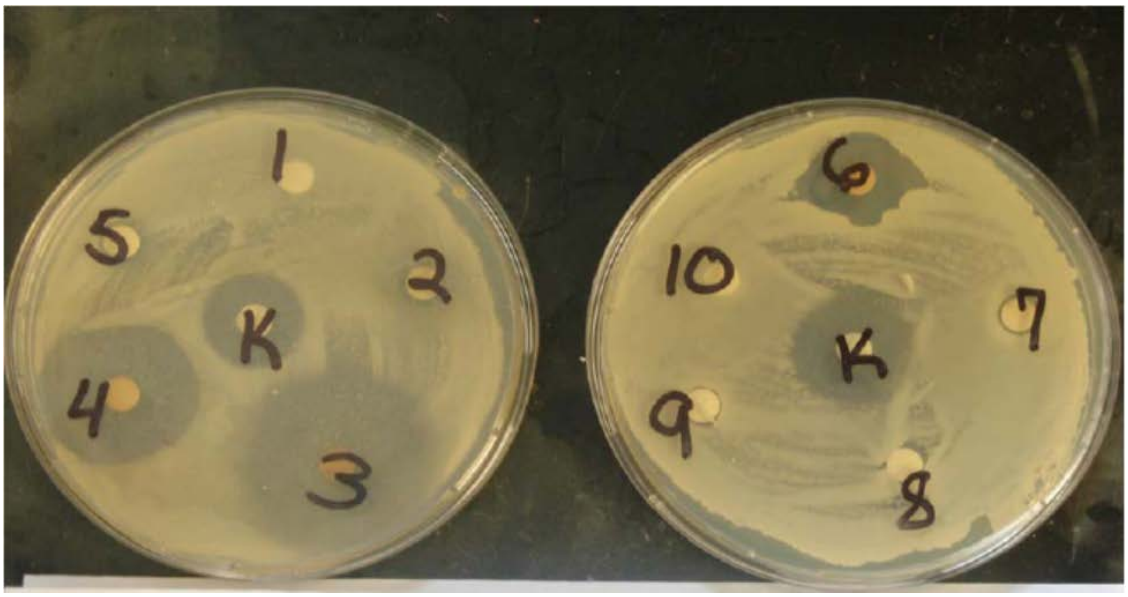

Figure 109 Bioassay result of active fractions on *Bacillus cereus*

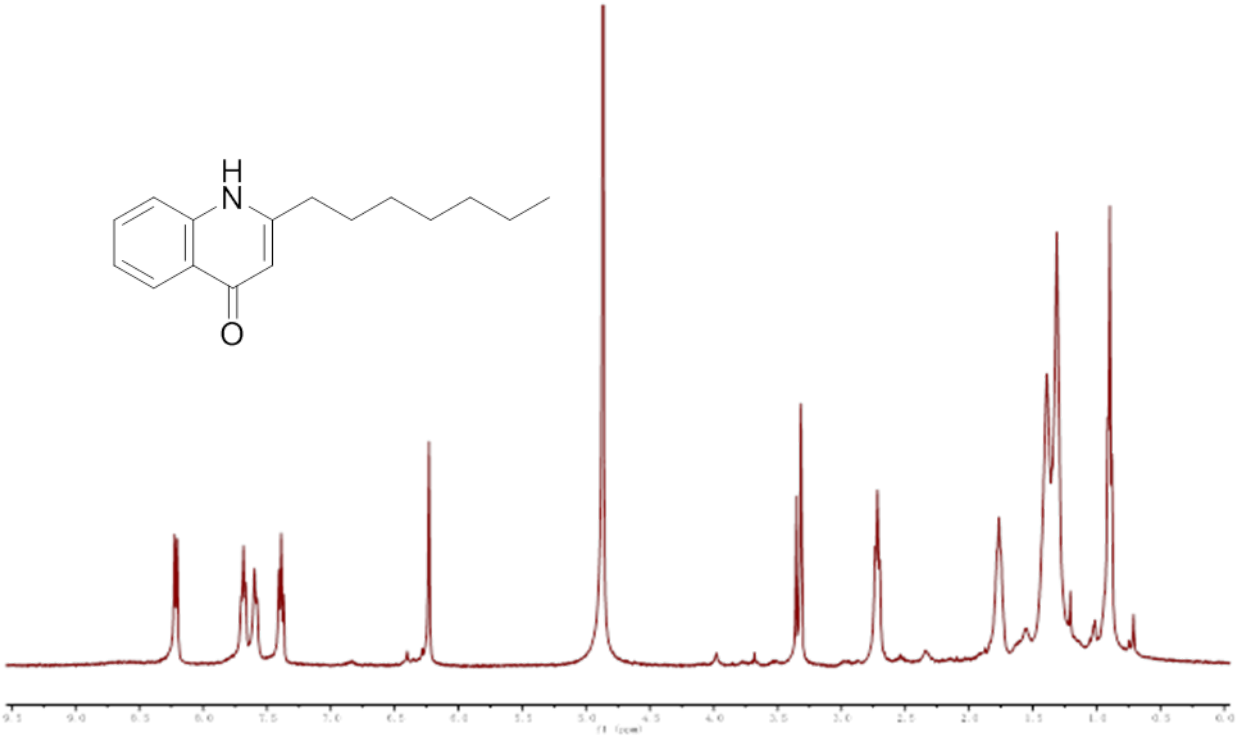

Figure 110 ^{1}H NMR spectrum of 2-heptyl-4(1*H*)-quinolone **(49)** in CD_3OD

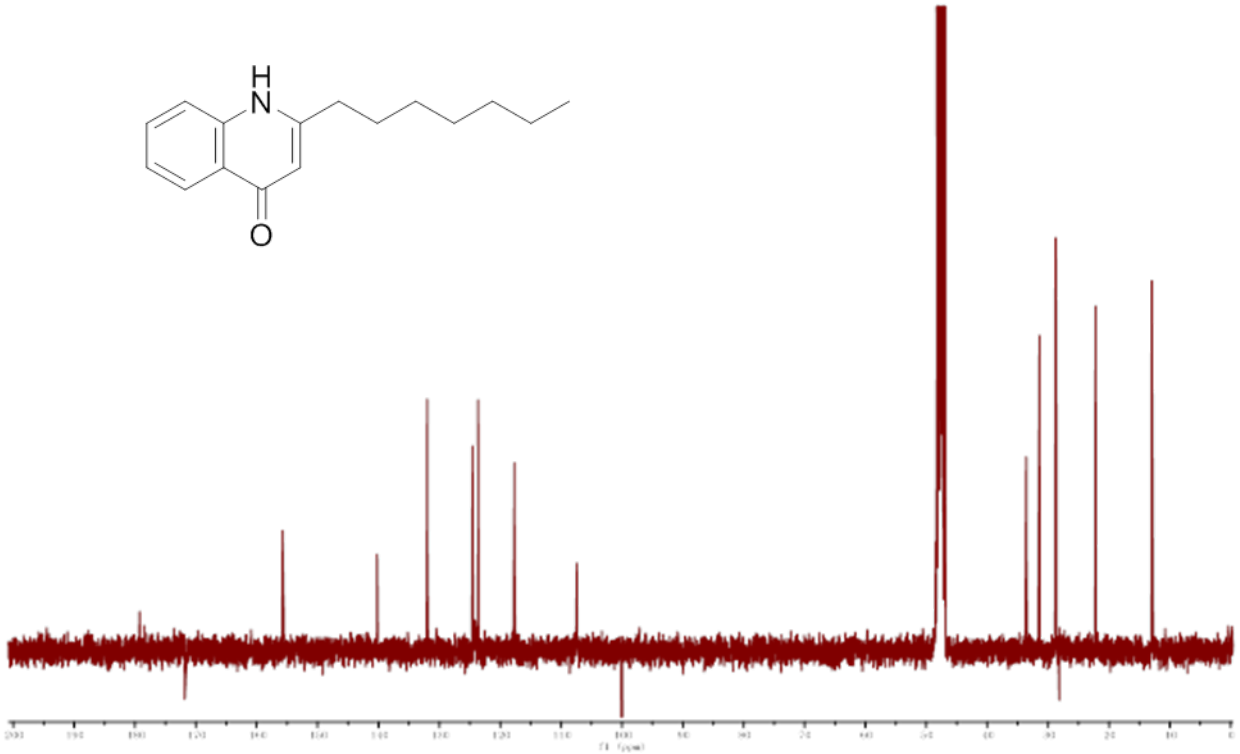

Figure 111 ^{13}C NMR of 2-heptyl-4(1*H*)-quinolone **(49)** in CD_3OD

The isolation of Fr6-6 and Fr6-7 was conducted using a C_8 (250mm×10mm, 5um) column to yield seven pure compounds. The ^{1}H NMR chemical shifts of compound 6-6-8-5-4 from δ_H 3.2 to δ_H 4.2 suggested the presence of a sugar moiety. The ^{13}C NMR spectrum showed the characteristic signals for rhamnose at δ_C 99.26, 74.13, 72.53, 71.20, 70.97, and 16.51. The ^{1}H NMR signals below δ_H 1.7 indicated the presence of an aliphatic chain **(Figures 112, 113)**. Its negative-ion mode LC-MS data gave quasi-molecular ions at *m/z* 503.3 $[M-H]^-$ and 1007.1 $[2M-H]^-$. The fragment ion at *m/z* 333.2 indicated the loss of a terminal fatty acid unit ($C_{10}H_{20}O_2$). The identity of the sugar and lipid moieties of these seven compounds and their interconnection by HMBC correlations determined they are known rhamnolipids: Rha-C_{10}-C_{10} **(55)**, Rha-Rha-C_{10}-C_{10} **(56)**, Rha-Rha-C_{10}-$C_{12:1}$ **(57)**, Rha-Rha-C_{10}-C_{12} **(58)**, Rha-C_{10}-$C_{12:1}$ **(59)**, Rha-C_{10}-C_{12} **(60)**, Rha-C_8-C_{10} **(61)**. Two D-rhamnose and two α-hydroxy fatty acid moieties were identified

by comparing characteristic spin systems from the 1D and 2D ^{1}H COSY spectra and specific rotation values to the published data.[80,81]

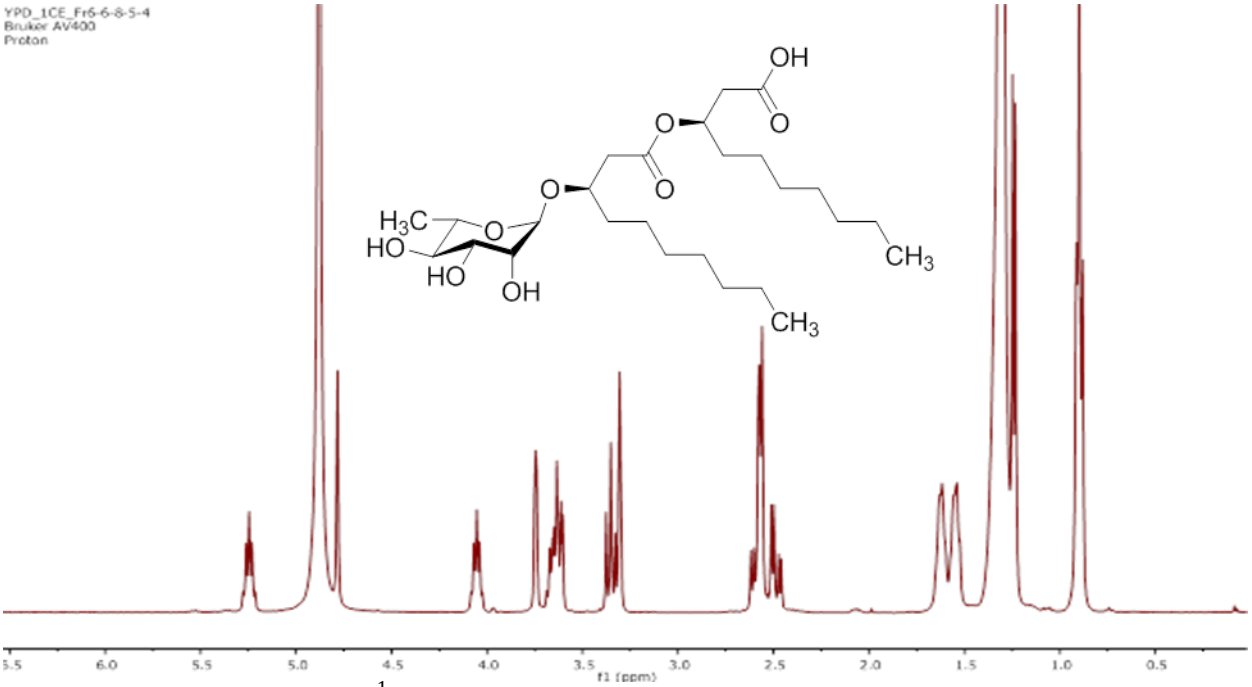

Figure 112 ^{1}H NMR spectrum of Rha-C_{10}-C_{10} **(55)** in CD_3OD

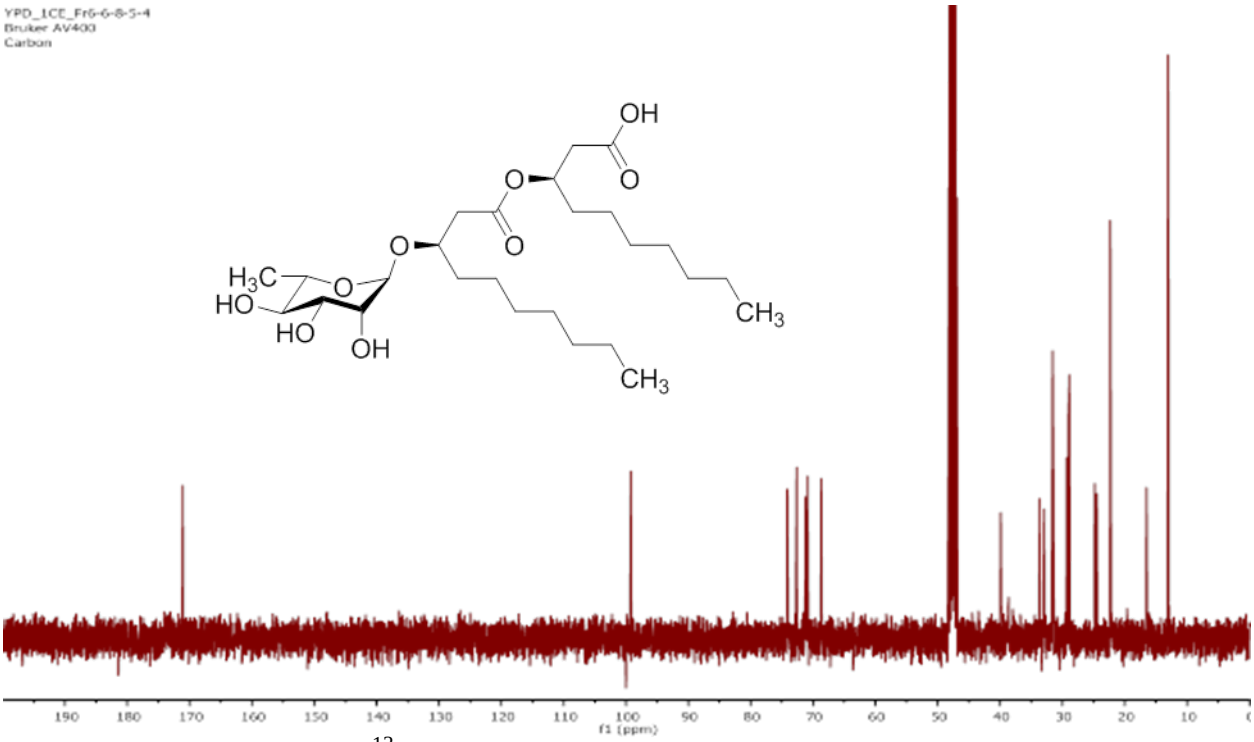

Figure 113 ^{13}C NMR spectrum of Rha-C_{10}-C_{10} **(55)** in CD_3OD

2.2 Activities. 1-Phenazinecarboxamide **(47)**, 1-phenazinecarboxylic acid **(48)**, Rha-Rha-C_{10}-$C_{12:1}$ **(57)** and Rha-Rha-C_{10}-C_{12} **(58)** showed antifungal activity against *Cryptococcus neoformans* with IC_{50} values of 6.99, 1.30, 15.67, and 5.82 μg/mL, respectively; Rha-C_{10}-$C_{12:1}$ **(59)** and Rha-C_{10}-C_{12} **(60)** showed antibacterial activity against *Staphylococcus aureus* with IC_{50} 19.88, 5.70 μg/mL, against MRS with IC_{50} at 18.89, 12.33 μg/mL, respectively; **47** and 2-(1-nonenyl)-4(1*H*)-quinolone **(54)** also displayed activity against *Mycobacterium intracellulare* with IC_{50} at 17.48, 20.00 μg/mL, respectively. In addition, 2-nonyl-4(1*H*)-quinolone **(52)** and **54** show antimalarial activity with IC_{50} at 0.13, 0.26 μg/mL in D6 strain, and 0.14, 0.36 μg/mL in W2 strain of *Plasmodium falciparum*, respectively. 1-Hydroxy-2-heptyl-4-quinolone **(50)**, 2-octyl-4(1*H*)-quinolone **(51)** and 2-(2-nonenyl)-4(1*H*)-quinolone **(53)** were not tested for activities due to the low yields.

2-Nonyl-4(1*H*)-quinolone **(52)** and 2-(1-nonenyl)-4(1*H*)-quinolone **(54)** showed potent antimalarial activity both in D6 and W2 strains of *P. falciparum*, which was first reported in this paper. Moreover, they have no cytotoxicity against Vero cells. 1-Hydroxy-2-dodecyl-4-quinolone[82] and 3-substituted 2-methyl-4(1*H*)-quinolones[83] exhibited antimalarial activity by inhibiting type II NADH dehydrogenases.[82] QSAR studies on 4(1*H*)-quinolones provided evidence that both the aromatic ring and aliphatic group are essential for the activity.[84] Since mammalian cells possess type I instead of type II NADH dehydrogenases,[82] this class of 4(1*H*)-quinolones could be potential drug leads in treating malaria.

2.3 Identification of Microorganisms. BLAST analysis demonstrated YPD1C is 99% identical to *Pseudomonas aeruginosa*. YPD1A and YPD1D were determined to be two *Bacillus* sp., YPD5A and YPD5C were two *Pseudomonas* sp..

2.4 Activities of *Pseudomonas* Extracts Treated with Different Factors. *P. aeruginosa* (YPD1C) was cultured with different carbon and nitrogen sources, regulators and co-cultured with the four other antibiotic producing microbes, YPD1A, YPD1D, YPD5A, and YPD5C. Considering the extensive number of experiments required to test all of these factors independently, an orthogonal design was used to minimize sample size. Each sample was duplicated **(Table 14)**.

Table 14 Orthogonal design of treatments on *P. aeruginosa* (n=2)

Carbon Source (400 mg/50 mL)	**Nitrogen Source (400 mg/50 mL)**	**Regulator (1 µM)**	**Temperature (°C)**	**Days**	**Microorganism**
Glucose	NH_4Cl	Sceptrin	25	2	*YPD1C*
Sodium Acetate	Urea	---	25	5	*YPD1C+1D*
Oil Mix	$NaNO_3$	Kahalalide F	25	8	*YPD1C+5A*
Starch	$NaNO_2$	Ilimaquinone	25	11	*YPD1C+1A*
Citric Acid	Peptone	Manzamine A	25	14	*YPD1C+5C*
Citric Acid	Urea	Ilimaquinone	30	2	*YPD1C+5A*
Glucose	$NaNO_3$	Manzamine A	30	5	*YPD1C+1A*
Sodium Acetate	$NaNO_2$	Sceptrin	30	8	*YPD1C+5C*
Oil Mix	Peptone	---	30	11	*YPD1C*
Starch	NH_4Cl	Kahalalide F	30	14	*YPD1C+1D*
Starch	$NaNO_3$	---	35	2	*YPD1C+5C*
Citric Acid	$NaNO_2$	Kahalalide F	35	5	*YPD1C*
Glucose	Peptone	Ilimaquinone	35	8	*YPD1C+1D*
Sodium Acetate	NH_4Cl	Manzamine A	35	11	*YPD1C+5A*
Oil Mix	Urea	Sceptrin 1uM	35	14	*YPD1C+1A*
Oil Mix	$NaNO_2$	Manzamine A	40	2	*YPD1C+1D*
Starch	Peptone	Sceptrin	40	5	*YPD1C+5A*
Citric Acid	NH_4Cl	---	40	8	*YPD1C+1A*
Glucose	Urea	Kahalalide F	40	11	*YPD1C+5C*
Sodium Acetate	$NaNO_3$	Ilimaquinone	40	14	*YPD1C*
Sodium Acetate	Peptone	Kahalalide F	45	2	*YPD1C+1A*
Oil Mix	NH_4Cl	Ilimaquinone	45	5	*YPD1C+5C*
Starch	Urea	Manzamine A	45	8	*YPD1C*
Citric Acid	$NaNO_3$	Sceptrin	45	11	*YPD1C+1D*
Glucose	$NaNO_2$	---	45	14	*YPD1C+5A*
YPD medium		Sceptrin	---	---	---
YPD medium		Ilimaquinone	---	---	---
YPD medium		Kahalalide F	---	---	---
YPD medium		Manzamine A	---	---	---

Extract activity was normalized by comparison with the activity of the regulator control in each bioassay, thus providing an accurate assessment. The direct sum in an orthogonal design was used to determine the best conditions for each modifying factor. As a result, the best conditions to produce antimicrobial compounds are oil mix (50% corn oil, 50% olive oil) as the carbon source, peptone as a nitrogen source, and incubation at 30°C for 11 days **(Table 15)**. However, only antifungal activity displayed an increase when compared to positive control. Interestingly, when treating YPD1C with sceptrin and co-culturing with YPD5A, an increase of antifungal activity against *C. neoformans*, antibacterial activity against *S. aureus* and MRS, and antimalarial activity were observed.

To further determine the significance of sceptrin and YPD5A on antibiotic production from *P. aeruginosa*, a second batch of experiments was designed using YPD media, at 30°C and 250 rpm for 7 days, different concentrations of sceptrin, and with/without YPD5A. OD_{600} values were measured to test viability of the microbe in each condition. Antimicrobial and antimalarial activities were tested for all the extracts. **(Table 16)** The activity data (T1-T6) was analyzed using the analysis of variance (ANOVA). As a result, the activities showed significant differences between all the treatments ($P<0.01$). To further determine which treatment was responsible for the major difference, a Dunnett's test was applied by comparison of treatment groups (T2-T6) with a positive control group (T1). There were no significance differences observed ($P>0.05$) between the groups singly treated with sceptrin or co-culturing (T2-T4). However, when treating sceptrin and co-culturing with YPD5A, a significant enhancement of all the activities was observed (T5, $P<0.05$; T6, $P<0.01$; **Figures 114, 115**). The antimicrobial activities of YPD5A (T7-T9) decreased significantly when adding 5 μM sceptrin (T9, $P<0.05$). Meanwhile, the OD_{600} value of T9 dropped more than five times to the same level as media

controls. It is unclear if this decline is due to a bacteriostatic or a bacteriocidal effect; however, at 1 µM there is no effect on growth. This lack of growth would also result in lack of antibiotic production.

Table 15 Orthogonal direct sum of activities in different culture conditions

		C. glabrata	*C. neoformans*	*S. aureus*	MRS	*E. coli*	Malaria
Carbon Source	Glucose	0	12	6	20	27	84
	Sodium Acetate	0	11	3	1	2	9
	Oil Mix	0	**80**	**57**	**60**	**54**	**164**
	Starch	23	10	14	18	13	90
	Citric Acid	**37**	11	12	21	22	86
Nitrogen Source	NH_4Cl	6	23	2	4	13	1
	$NaNO_3$	10	9	2	13	3	1
	Peptone	**44**	**74**	**69**	**85**	**75**	**255**
	Urea	0	3	9	10	23	172
	$NaNO_2$	0	14	11	9	5	4
Regulator	**Sceptrin**	**33**	3	21	36	7	**175**
	Manzamine A	21	8	6	4	12	4
	Ilimaquinone	0	29	4	22	48	168
	Kahalalide F	0	2	12	8	3	0
	---	6	**81**	**49**	**51**	**49**	86
Temp.	25	21	13	1	3	8	5
	30	0	**72**	**51**	**51**	**56**	**172**
	35	0	9	24	36	31	166
	40	**29**	13	13	18	6	89
	45	10	18	3	13	18	1
Days	2	0	1	2	0	12	85
	5	**23**	17	26	25	7	**94**
	8	6	19	5	23	45	88
	11	10	**78**	**51**	**62**	**49**	83
	14	21	8	9	10	6	83
Co-culture	**YPD1C**	0	**72**	**61**	**57**	**52**	83
	YPD1C+1A	6	20	12	13	13	83
	YPD1C+1D	10	8	4	30	30	87
	YPD1C+5C	21	16	1	3	11	5
	YPD1C+5A	**23**	7	15	17	12	**175**

Table 16 Antimicrobial and antimalarial activities of YPD1C with epigenetic regulation (n=3)

	Media	Temp. (°C)	Days	Sceptrin (μM)	Microorganism	OD_{600}	Antifungal (% Inh.)	Antibacterial (% Inh.)		Antimalarial (IC_{50}, μM)	
							C. neoformans	*S. aureus*	MRS	D6	W2
C1	YPD	---	---	---	---	0.60±0.004	7.72±0.96	8.98±1.04	9.17±1.16	ND	ND
C2	YPD	---	---	5	---	0.63±0.006	9.15±0.58	8.04±0.88	8.71±1.74	ND	ND
T1	YPD	30	7	---	YPD1C	4.11±0.008	18.1±4.62	55.2±5.25	57.6±3.84	7.25±0.78	9.15±1.20
T2	YPD	30	7	1	YPD1C	4.28±0.017	18.8±8.81	44.8±11.8	51.7±12.8	5.95±0.21	8.45±1.48
T3	YPD	30	7	5	YPD1C	4.30±0.072	24.4±6.89	38.3±8.29	41.4±9.27	5.43±1.25	6.80±2.09
T4	YPD	30	7	---	YPD1C+5A	3.56±0.061	6.45±1.36	6.39±2.82	15.1±4.63	ND	ND
T5	YPD	30	7	1	YPD1C+5A	3.95±0.066	45.1±12.6	65.6±16.2	81.9±13.1	2.80±1.17	3.41±0.86
T6	YPD	30	7	5	YPD1C+5A	4.12±0.005	63.5±4.43	94.1±2.49	94.3±4.00	0.89±0.10	1.10±0.14
T7	YPD	30	7	---	YPD5A	3.59±0.147	13.4±1.89	11.4±2.12	17.5±1.92	ND	ND
T8	YPD	30	7	1	YPD5A	3.59±0.101	11.7±5.46	8.43±3.50	15.3±1.40	ND	ND
T9	YPD	30	7	5	YPD5A	0.678±0.026	7.21±3.04	3.35±1.02	7.10±2.53	ND	ND

ND: IC_{50} was not tested in the secondary assay, which due to a limited inhibition (< 10%) observed in the primary assay.

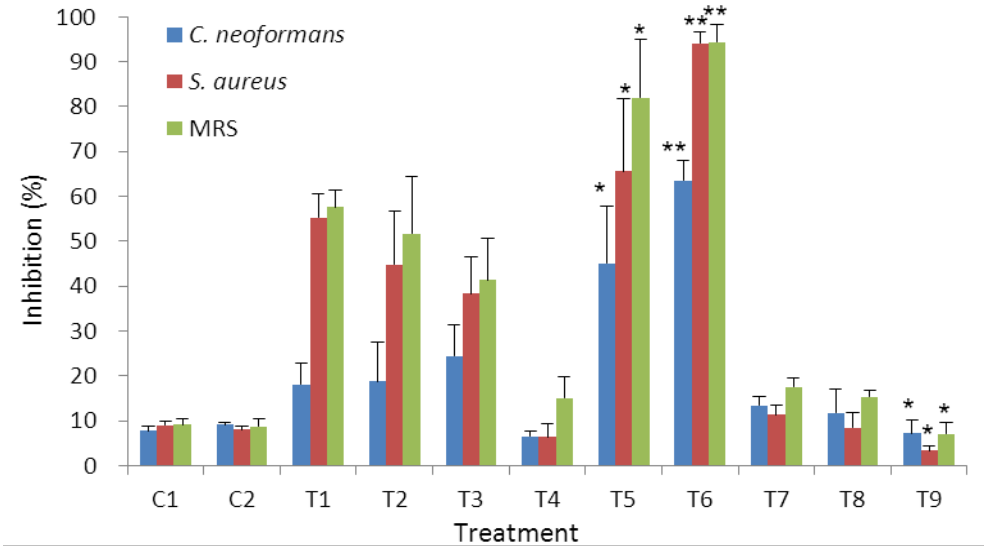

*: P<0.05; **: P<0.01

Figure 114 Antimicrobial activities of YPD1C extracts with different treatments

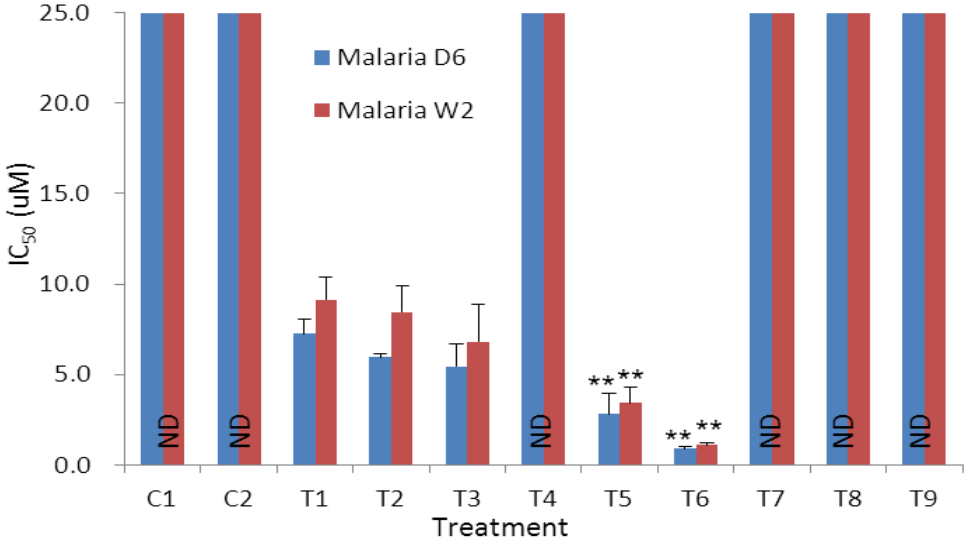

ND: IC_{50} was not tested due to less than 10% of inhibition in the primary assay

*: P<0.05; **: P<0.01

Figure 115 Antimalarial activity of YPD1C extracts with different treatments

The total ion chromatograms (TICs) of YPD5A extracts (T7-T9) displayed different profiles than those of YPD1C extracts **(Figure 116)**. Comparison of the extracted ion chromatograms (EICs) between extracts of YPD5A and YPD1C confirmed that YPD5A does not produce the same active metabolites as YPD1C. The fingerprints of groups T1, T5, and T6 were compared. The TICs showed an increase in production, especially of phenazines (R*t* 10-15 min)

and quinolones (R*t* 18-26 min) **(Figure 117)**. To further determine the variation of each class of metabolites, EICs were compared by extracting ions at *m/z*=224, 225, 244, 260, 270, 272 **(Figure 118)**, and 651, 505, 677, 679, 531, and 533 **(Figure 119)** that correspond to 1-phenazinecarboxamide **(47)** and 1-phenazinecarboxylic acid **(48)**, 2-heptyl-4(1*H*)-quinolone **(49)**, 1-hydroxy-2-heptyl-4-quinolone **(50)**, 2-(2-nonenyl)-4(1*H*)-quinolone **(53)**, 2-(1-nonenyl)-4(1*H*)-quinolone **(54)**, 2-nonyl-4(1*H*)-quinolone **(52)**, Rha-Rha-C_{10}-C_{10} **(56)**, Rha-C_{10}-C_{10} **(55)**, Rha-Rha-C_{10}-$C_{12:1}$ **(57)**, Rha-Rha-C_{10}-C_{12} **(58)**, Rha-C_{10}-$C_{12:1}$ **(59)**, and Rha-C_{10}-C_{12} **(60)**. It was noticed that the yields of **47**, **48**, **49**, **50**, **52**, **54**, **57**, **58**, and **60** increased in T5 and T6. Moreover, a new signal which could be another 2-alkyl-4-quinolone with *m/z* 298 was observed in a high intensity. Based on the MS data and retention time, it could contain two more methylenes than **53** or **54**. According to the activities, **47**, **48**, **57**, and **58** were responsible for the antifungal activity, **47**, **54**, and **60** for the antibacterial activity, and **52** and **54** for the antimalarial activity. The fingerprint comparison of T1, T5 and T6 complemented the observed bioactivity and our statistical analysis.

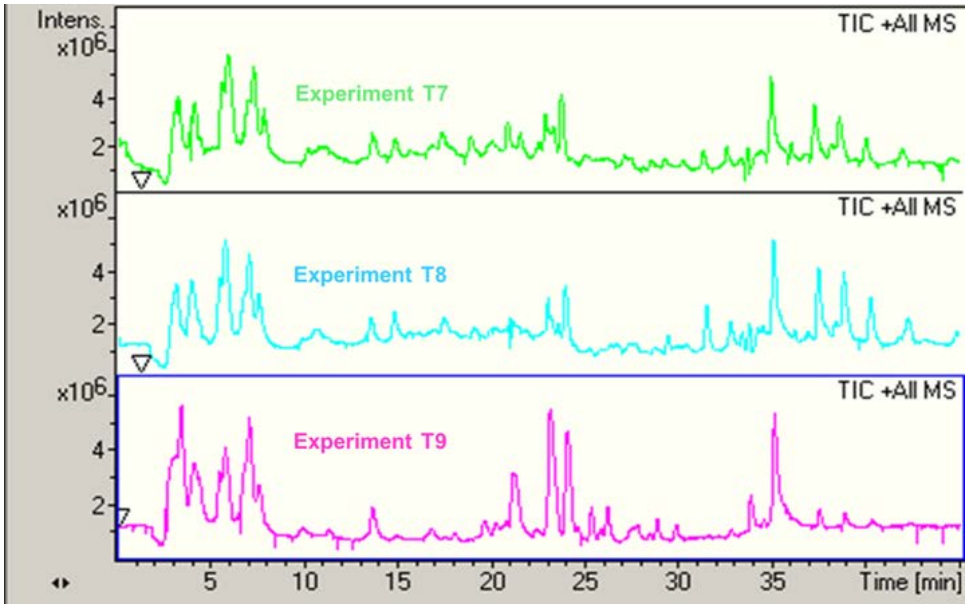

Figure 116 TIC comparison of T7-T9

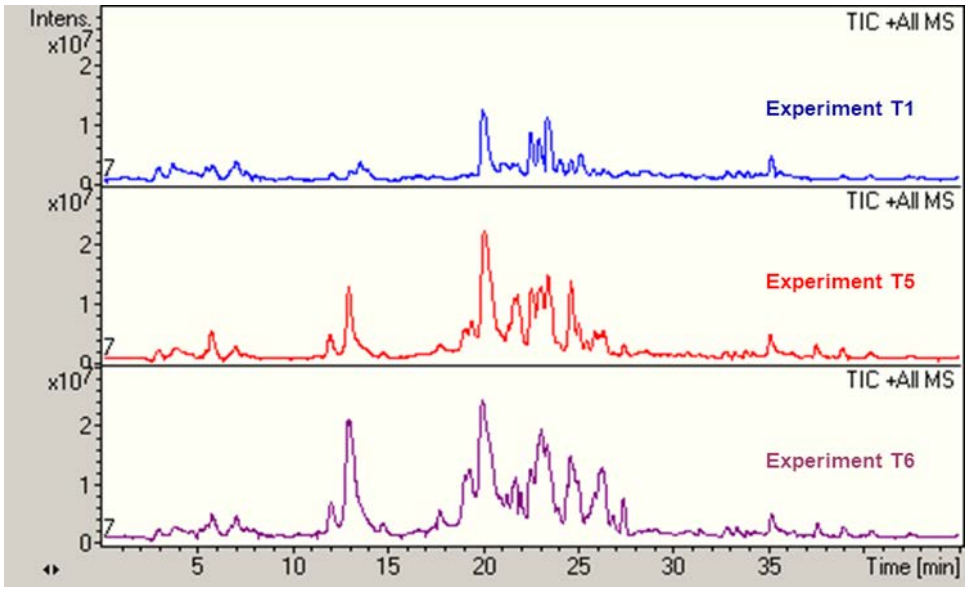

Figure 117 TIC comparison of T1, T5-T6

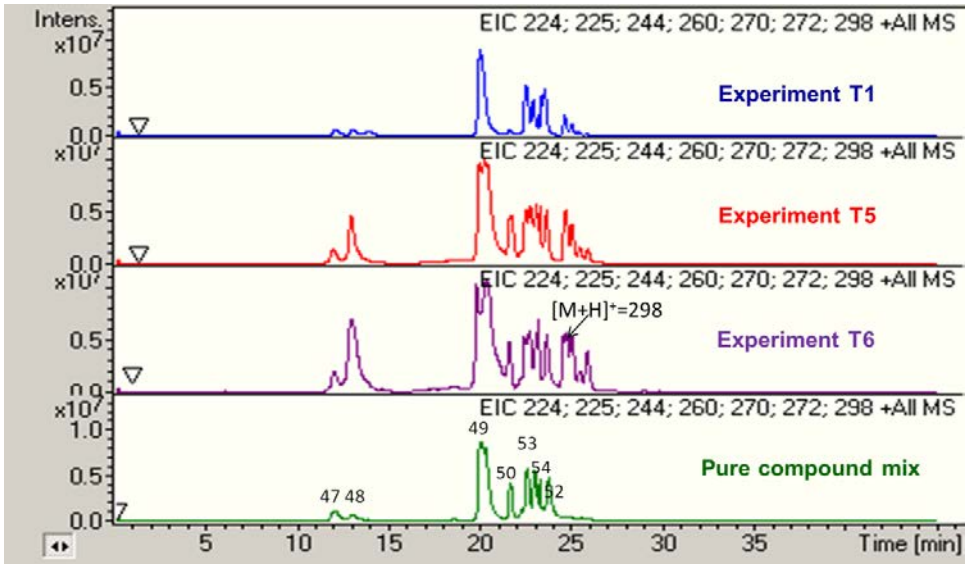

Figure 118 Quinolones EIC comparison of T1, T5-T6

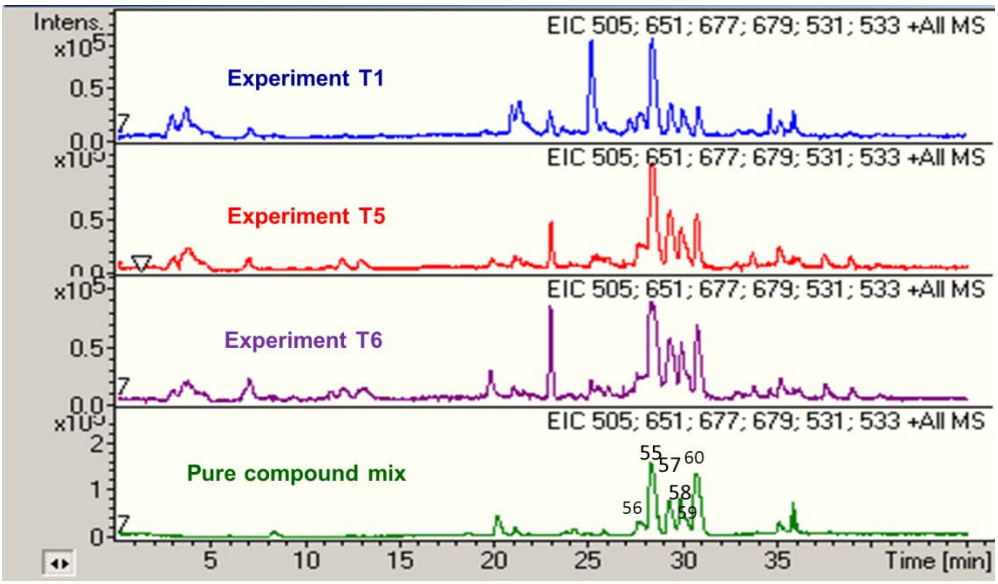

Figure 119 Rhamnolipids EIC comparison of T1, T5-T6

2.5 Role of Yeast Extract in Media. The antimicrobial activity of all the extracts indicated that the best conditions to produce antimicrobial compounds was oil mix (50% corn oil, 50% olive oil) as the carbon source, and peptone as the nitrogen source. However, antibiotic production under these conditions was far less than that of YPD medium. YPD consists of yeast extract, peptone, and dextrose, among which only yeast extract was not added during the media modifications. Hence, it was considered that yeast extract played a key role in the high yield of antibiotic production. Yeast extract is a processed product by removing the yeast cell wall. It may contain various cell contents of yeast including small RNAs. There was evidence that small RNAs in the yeast extract containing media could change bacterial protein profiles, thus influencing bacterial adaption.[85] Yeast extract serves not only as nutrient in growth media, but a stimulus to *P. aeruginosa*. It is reasonable that yeast extract induced antibiotic production in *P. aeruginosa* as a modifier.

2.6 Roles of Regulators. Manzamine A has been identified as a potent GSK-3β inhibitor.[86] Kahalalide F was shown to down-regulate the ErbB3 receptor and inhibit Akt signaling.[18] Both

of these compounds are cytotoxic. When the regulator controls were tested, manzamine A and kahalalide F displayed inhibition of all microbes. Cultures treated with manzamine A and kahalalide F lacked growth during fermentation, indicating that the compounds were cytotoxic to the bacteria.

Sceptrin has diverse activities including antifungal, antibacterial, and antihistaminic. It is an inhibitor of somatostatin and cell motility.[87] Based on our experimental data, the addition of sceptrin does not have a significant influence on *P. aeruginosa.* However, it does affect the vitality of another *Pseudomonas* species, YPD5A. The fingerprint comparison of T7-T9 suggested the yields of some metabolites were improved when YPD5A was treated with 5 μM sceptrin **(Figure 116)**. These could be degradation products of sceptrin or other metabolites released from YPD5A, which indicated that YPD5A is able to trigger a series of responses under stress conditions.

2.7 Mixed Fermentation

Usually, microbes within the same genus are able to consume the same nutrients for their survival. When co-culturing, there is potential competition for nutrients.[88,89] In our experiment, another *Pseudomonas* sp., YPD5A, was co-cultured with YPD1C. A comparison of activities as well as OD_{600} values between T1 and T4 suggested the vitality of both YPD1C and YPD5A were weakened after co-culturing. This could be proposed that some YPD1C died from an insufficient nutrient, or YPD5A released quorum sensing (QS) molecules to down-regulate the antibiotics produced from YPD1C.

Chemical communication between microbes can induce a series of interactions between species. In the experiment, another *Pseudomonas* species YPD5A was co-cultured with *P. aeruginosa*, YPD1C. The data indicates that the antibiotic production of YPD1C singly treated

with sceptrin or co-cultured with YPD5A is not sufficient to equal that of culturing all three components together. We have also established that the concentration used in this co-culture is sufficient to inhibit growth of YPD5A. This suggests several possible outcomes when co-culturing YPD1C with YPD5A. One option is that YPD5A releases a signaling molecule when exposed to 5 μM sceptrin and this molecule induces production of secondary metabolites in YPD1C. Another option is a much more complex cross-talk mechanism between the two stains involving a combination of QS molecules and sceptrin or derivatives thereof. Quinolones have been implicated in QS regulation.[90] An increase in OD_{600} as well as quinolone concentration implied a relationship between the antibiotic production of the species and microbial competition between species.

3. Materials and Methods

3.1 General Experimental Procedures. NMR spectra were recorded on a Bruker Avance DRX-400 spectrometer. The ^{1}H and ^{13}C NMR chemical shifts were reported in ppm. HPLC-ESI-TOF was performed on a Bruker MicroTOF in line with an Agilent 1100 Series HPLC system and G1316A DAD detector. A Phenomenex Luna C_{18} 5 μm column (150 mm × 4.6 mm) was used with a gradient elution of MeCN in 0.05% HCOOH at a flow rate of 0.6 mL/min. Preparative HPLC was carried out on a Waters PrepLC system with a single wavelength detector. Sephadex LH-20 and Diaion HP-20 were purchased from Sigma. Sephadex LH-20 was applied in an isocratic solvent system of MeOH-H_2O (75:25), unless otherwise stated. Optical rotations were measured on a JASCO DIP-370 polarimeter. OD values were measured on a Varian Cary 50 Bio UV/visible spectrophothmeter.

3.2 Microbial Collection and Isolation. On October 24, 2009, sediment collection was made in the tributary leading into West Galveston Bay (N29 13.349º W95 12.992º). Sediment was

collected from the bay floor using a petite ponar grabber and transferred to a sterile 50 mL conical tube. The volume of collected sediment was diluted with sterile filtered artificial sea water (2% Instant Ocean) to approximately 1.5 times the original volume. The sediment was mixed by agitation and heat shocked at 55℃ for eight minutes. The sample was allowed to rest until the sediment had settled. Volumes of 150 and 300 µL of supernatant were placed on Yeast Peptone Dextrose (YPD) (10/20/20 g/L) media with 50 µg/mL of ampicillin. The plate was left at room temperature until colonies appeared. Once colonies grew, individual colonies were chosen and streaked onto secondary plates containing no antibiotics, but still supplemented with 2% Instant Ocean. Microbes were again grown at room temperature until colonies appeared. Using these plates, pure colonies were isolated and glycerol stocked at -80℃ for preservation and large scale growth.

All organisms used for the antimicrobial assays were obtained from the American Type Culture Collection (Manassas, VA) and included the fungi *Candida albicans* ATCC 90028, *C. glabrata* ATCC 90030, *C. krusei* ATCC 6258, *Cryptococcus neoformans* ATCC 90113, and *Aspergillus fumigatus* ATCC 204305 and the bacteria *Staphylococcus aureus* ATCC 29213, methicillin-resistant *S. aureus* ATCC 33591 (MRS), *Escherichia coli* ATCC 35218, *Pseudomonas aeruginosa* ATCC 27853, and *Mycobacterium intracellulare* ATCC 23068.

3.3 16S rRNA. YPD-1A, YPD-1C, YPD-1D, YPD-5A, and YPD-5C were grown in supplemented YPD media at 30°C and 200 rpm overnight. DNA was isolated using an MoBio Ultrapure DNA purification system and following the manufacturer's instructions. 16s DNA was amplified by PCR using the published 17f and 1492r universal bacteria 16s primers. The resulting amplified DNA was cloned into the pCR2.1 vector using a topoTA (Invitrogen) ligation kit. Plasmids were purified and subsequently sequenced using the T7 and M13 sites in pCR2.1.

BLAST analysis was conducted by comparison of acquired sequences of five microorganisms with database.

3.4 Large Scale Growth and Extraction. Eight cultures of the isolate (500 mL) were grown using YPD media supplemented with 2% Instant Ocean mix in 2.5 L Fernbach flasks incubated at 30℃ and 250 rpm for 7 days. The cultures were first sonicated for 20 min and then centrifuged for 10 min at 3600 rpm in 250 mL portions. The supernatant was decanted into a flask and the cell pellet was discarded. Approximately 160 mL of HP-20 resin was added to the supernatant. The flask was placed in the incubator and left overnight at 30℃ and 250 rpm.

The HP-20 resin was extracted with a Buchner funnel, and the media was discarded. The HP-20 was then washed with 1 L of EtOH followed by 500 mL of EtOAc. The extracts were dried under vacuum, and the samples were assayed to assess biological activity.

3.5 Compound Isolation. The EtOH extract of YPD1C cultures (20 g) were loaded onto an HP-20 column and eluted with 100% H_2O, H_2O-MeOH (75:25, 50:50, 25:75), 100% MeOH, and MeOH-EtOAc (50:50). The last two fractions and EtOAc extract of YPD1C culture (2 g) acquired from the large scale extraction previously were combined. Further purifications were conducted on a silica flash column and eluted with hexanes-EtOAc (100:0, 75:25, 50:50, 25:75, 0:100), EtOAc-MeOH (75:25, 50:50; 25:75, 0:100), and MeOH-H_2O (50:50). Purifications of Fr3 and Fr4 were performed by HPLC on C_5 (250 mm×20.2 mm, 5 µm) or C_8 (250 mm×10 mm, 5 µm) columns using a gradient of MeOH with 0.05% HCOOH-H_2O with 0.05% HCOOH (from 20:80 to 100:0). Fr6 was eluted from sephadex LH-20 with DCM-MeOH (50:50) and followed by HPLC on C_5 (250 mm×20.2 mm, 5 µm), C_8 (250 mm×20.2 mm, 5 µm), or C_8 (250 mm×10 mm, 5 µm) column using gradient of MeOH with 0.05% HCOOH-H_2O with 0.05% HCOOH (from 20:80 to 100:0) or MeCN-H_2O (from 28:72 to 100:0).

3.6 Antimicrobial Assay. All organisms were tested using modified versions of the CLSI methods. Optical density was used to monitor growth for all organisms excluding *M. intracellulare* and *A. fumigatus*.[91,92] Media supplemented with 5% Alamar Blue™ (BioSource International, Camarillo, CA) is utilized for growth detection of *M. intracellulare*,[93,94] and *A. fumigatus*.[95] Samples are serially-diluted in 20% DMSO/saline and transferred (10 µL) in duplicate to 96 well flat bottom microplates. Inocula are prepared by correcting the OD_{630} of microbe suspensions in incubation broth [RPMI 1640/0.2% dextrose/0.03% glutamine/MOPS at pH 6.0 (Cellgro) for *Candida spp.*, Sabouraud Dextrose for *C. neoformans*, cation-adjusted Mueller-Hinton (Difco) at pH 7.3 for *Staphylococcus spp.*, *E. coli*, and *P. aeruginosa*, 5% Alamar Blue™ (BioSource International, Camarillo, CA) in Middlebrook 7H9 broth with OADC enrichment, pH = 7.0 for *M. intracellulare*, and 5% Alamar Blue™/RPMI 1640 broth (0.2% dextrose, 0.03% glutamine, buffered with 0.165M MOPS at pH 7.0) for *A. fumigatus* to afford an assay volume of 200 µL and final target inocula of: *Candida spp.* and *C. neoformans.*: 1.5×10^3, *M. intracellulare*: 2.0×10^6, *Staphylococcus spp.*, *E. coli*, *P. aeruginosa*: 5.0×10^5 CFU/mL, and *A. fumigatus*: 2.7×10^4 CFU/mL. Final sample test concentrations are 1% of the DMSO stock concentration. Drug controls [ciprofloxacin (ICN Biomedicals, Ohio) for bacteria and amphotericin B (ICN Biomedicals, Ohio) for fungi] are included in each assay. All organisms are read at either 530 nm using the Biotek Powerwave XS plate reader (Bio-Tek Instruments, Vermont) or 544ex/590em, (*M. intracellulare, A. fumigatus*) using the Polarstar Galaxy Plate Reader (BMG LabTechnologies, Germany) prior to and after incubation: *Candida spp.* at 35℃ for 46-50 h, *Staphylococcus spp.*, *E. coli*, and *P. aeruginosa* at 35℃ for 16-20 h, *C. neoformans* at 35℃ for 70-74 h, *A. fumigatus* at 35℃ for 46-50 h, and *M. intracellulare* at 37℃ and 10%

CO_2 for 70-74 h. IC_{50}s were calculated using XL*fit* 4.2 software (IDBS, Alameda, CA) using fit model 201.

3.7 Antimalarial Activity. Antimalarial activity was determined in vitro against chloroquine sensitive (D6, Sierra Leone) and resistant (W2, Indo China) strains of *Plasmodium falciparum* by measuring plasmodial LDH activity. Chloroquine and artemisinin were used as the positive controls. Test compounds were dissolved in DMSO (2 mg/mL). A 200 µL suspension of *P. falciparum* culture (2% parasitemia and 2% hematocrit in RPMI 1640 medium supplemented with 10% human serum and 60 µg/mL amikacin) was added to the 96-well plate containing 10 µL of serially diluted samples. The plate was flushed with a gas mixture of 90% N_2, 5% O_2, and 5% CO_2 and incubated at 37 ºC for 72 h in a modular incubation chamber. Plasmodial LDH activity was determined by using Malstat™ reagent (Flow Inc., Portland, OR).[96] The incubation mixture (20 µL) was mixed with 100 µL of the Malstat™ reagent and incubated for 30 min. A 1:1 mixture of NBT/PES (20 µL, Sigma, St. Louis, MO) were then added and the plate was further incubated for 1 h in dark. The reaction was stopped by adding 100 µL of a 5% acetic acid solution. The plate was read at 650 nm. The *in vitro* cytotoxicity to mammalian cells (Vero cells) was also tested to determine the selectivity index of antimalarial activity of compounds. Cells were seeded at a density of 25,000 cells/well and incubated for 24 h. Serially diluted samples were added and incubated for 48 h. The number of viable cells was determined by Neutral Red assay.[97] Doxorubicin was used as a positive control. IC_{50} values were obtained from dose response curves.

3.8 Disc Diffusion Assay (DDA). DDA provides a rapid, reliable method to screen fractions during purification. Considering it is one of the microbes that are responsible for the foodborne disease outbreak, and easy to grow, *B. cereus* was applied to DDA. A concentration limitation

experiment was performed with each active extract to determine the minimal amount needed to observe a zone of inhibition. Once this limit was established, this amount of each column fraction was added to a six mm filter paper disc. *B. cereus* cells (250 µL) were suspended in water and then plated onto antibiotic medium 2 (Difco) to form a bacterial lawn on the plate. The disc were added to the plate with a control of 50 µg of kanamycin and allowed to grow at 30℃ overnight. Activity was determined as a clear zone of inhibition.

3.9 Treatments of YPD1C. YPD1C was cultured at different temperatures with different carbon and nitrogen sources, regulators and co-cultured with the four other antibiotic producing microbes (YPD1A, YPD1D, YPD5A, and YPD5C). The experimental design is shown in **Table 13**. Cultures of the YPD1C isolate (50 mL) were grown using different media supplemented with 2% Instant Ocean mix in 250 mL flasks incubated at 15-45°C and 250 rpm for 3-7 days. *P. aeruginosa* grown in YPD media at 30°C and 250 rpm for 7 days was used as a positive control, while four regulators prepared in YPD media, respectively, were used as negative controls. All the cultures were sonicated for 20 min and centrifuged for 10 min at 3600 rpm. The supernatant was extracted with EtOAc (3×100 mL). The organic layers were combined for further bioassays and fingerprint analysis.

3.10 Fingerprint Setup of Each Extract. Filtered extracts were diluted with MeOH, and eluted on a C_8 column (4.6 mm×250 mm, 5 µm) using a gradient of MeOH (with 0.05% HCOOH)–H_2O (with 0.05% HCOOH) from 40:60 to 100:0 over 45 minutes at a flow rate of 0.6 mL/min. Fingerprints were acquired using a TOF-MS detector on the positive mode. A fingerprint of each extract was compared.

CHAPTER *5*

KINASES OF *Mycobacterium tuberculosis*: CLASSIFICATION, STRUCTURES, AND THE DEVELOPMENT OF INHIBITORS (A REVIEW)

1. Introduction

Tuberculosis (TB), caused by mycobacteria, especially *Mycobacterium tuberculosis* (Mtb), was responsible for 8.8 million incident cases and 1.4 million deaths in 2010.[98] With the wide spread of the human immunodeficiency virus (HIV-1), cases of HIV-associated TB have become a major concern.[99] Although TB is one of the oldest human diseases, it is still a significant health problem worldwide due to the lack of effective treatments. The primary limitations of current TB treatments include drug-resistance of Mtb by altering environmental signaling[100] and the prevalent long-term latent infections which can persist in the human host with the capability to reactivate.[101] In recent years multidrug-resistant TB and extensively drug-resistant TB have emerged. With these challenges, there is an urgent medical need for new drugs to overcome drug resistance and dormancy. Since the 1990s a number of new chemotherapeutic agents to control Mtb have entered clinical trials including cell wall, RNA, malate, ATP and protein synthesis inhibitors, as well as proton pump and DNA gyrase inhibitors.[102] No protein kinase inhibitors have entered clinical trials or been approved for treating TB thus far, though some are being investigated for this purpose.

Phosphorylation by kinases is known to regulate signal transduction pathways in cells

and kinases play critical roles in cell growth, metabolism, differentiation and apoptosis. In the past two decades, many research groups have been developing kinase inhibitors and 23 kinase inhibitors have been approved for clinical use,[103,104,105,106] some of which are proteins including trastuzumab, cetuximab, panitumumab, ranibizumab, bevacizumab, and pegaptanib. The remaining inhibitors are small molecules **(Table 17)**, including the tyrosine kinase inhibitor imatinib (Gleevec/Glivec registered by Novartis) which was the first small-molecule kinase inhibitor used as a targeted therapy to treat chronic myeloid leukemia (CML) and gastrointestinal stromal tumors (GIST).[107] In May 2001, the FDA made an exception and approved imatinib in less than three months. It was described as a "new hope for cancer". The exploration of imatinib not only disclosed the prelude of targeted cancer therapy, but promoted the development of a new class of kinase inhibitors.

Table 17 Approved small-molecule protein kinase inhibitors

Year of Approval	Name (Brand Name)	Structure	Target	Clinical use
1999	Rapamycin/ Sirolimus (Rapamune)	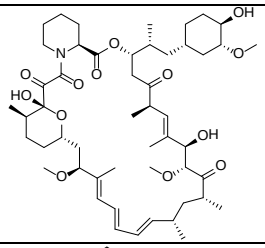	mTOR serine/ threonine kinase (STK)	Immunosuppressant
2001	Imatinib (Gleevec, USA) (Glivec, Europe)	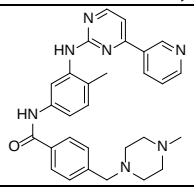	Tyrosine kinase (TK)	Chronic myelogenous leukemia (CML), gastrointestinal stromal tumors (GISTs)
2003	Gefitinib (Iressa)	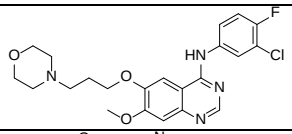	EGFR TK	Advanced or metastatic non-small cell lung cancer (NSCLC)
2004	Erlotinib (Tarceva)	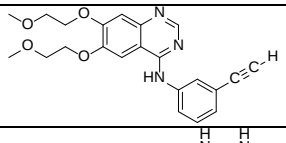	EGFR TK	NSCLC, Pancreatic cancer
2005	Sorafenib (Nexavar)	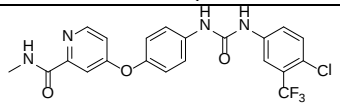	EGFR TK/ Raf STK	Renal cell carcinoma (RCC), Advanced primary liver cancer

2006	Sunitinib (Sutent)	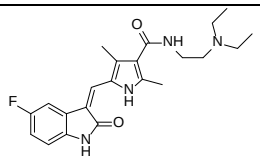	Multi-targeted TKs	RCC, imatinib-resistant GIST
2006	Dasatinib (Sprycel)	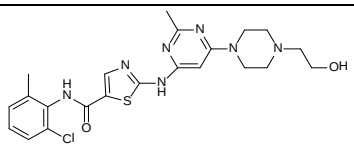	Bcr/Abl, Src TKs	Chronic myelogenous leukemia (CML), Philiadelphia chromosome -positive acute lymphoblastic leukemia (Ph+ ALL)
2007	Lapatinib (Tykerb)	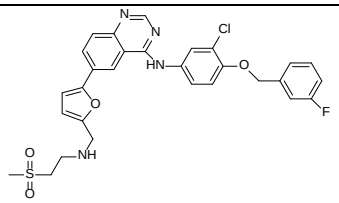	Glycogen synthase kinase (GSK)	HER2-positive Breast cancer
2007	Temsirolimus (Torisel)	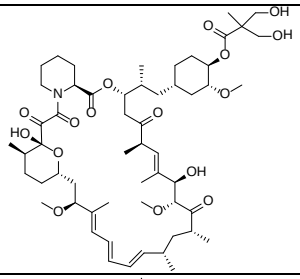	mTOR STK	RCC
2007	Nilotinib (Tasigna)	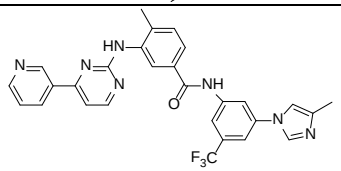	Tyrosine kinase	Drug-resistant CML
2009	Pazopanib (Votrient)	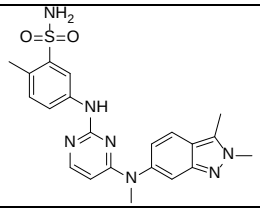	VEGFR, PDGFR TKs	RCC Soft tumor sarcoma
2009	Everolimus (Zortress, USA) (Certican, Europe)	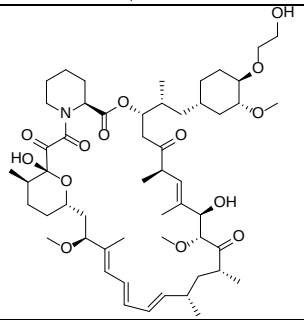	mTOR STK	Advanced kidney cancer Immunosuppressant
2011	Vandetanib (Caprelsa)	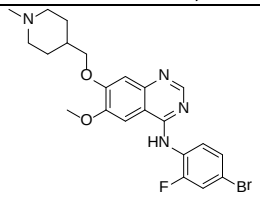	VEGFR, EGFR TKs	Metastatic medullary thyroid cancer

2011	Crizotinib (Xalkori)	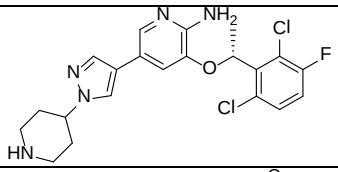	ALK, ROS1 TKs	Metastatic NSCLS
2011	Vemurafenib (Zelboraf)	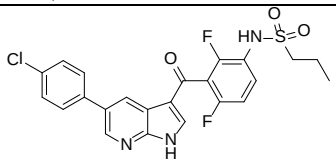	B-Raf STK	Late-stage melanoma
2011	Ruxolitinib (Jakafi)	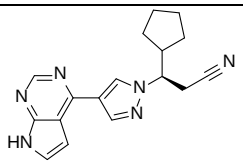	Janus TK	Intermediate or high-risk myelofibrosis
2012	Axitinib (Inlyta)	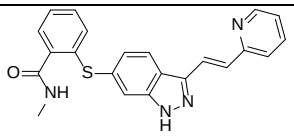	VEGFR, c-Kit TKs	Metastatic RCC

With the whole genome sequence of the Mtb strain H37Rv having been completed,[108] it helped to reveal the kinases in Mtb. In Mtb, prokaryotic two-component systems and eukaryotic-like serine/threonine protein kinases are used to transmit signals and control complex processes. Other kinases acting on small molecules take part in biochemical reactions including small molecule degradation, energy metabolism, central intermediary metabolism, amino acid biosynthesis, nucleotide biosynthesis, and serving as cofactors and carriers of these reactions. With many crystal structures of Mtb kinases completed, it is now possible to explore the potential of Mtb kinase inhibitors. Based on the kinase inhibitor scaffolds, various types of candidates, more than 26,000 in total, against the whole bacterium have been screened. Several classes of compounds, such as 2-acylaminothiophenes, 2-aminobenzothiazoles, benzopyran-2-ones, and 1,3,4-oxadiazoles displayed a significant inhibition on Mtb growth **(Figure 120)**.[109] Many research groups have designed and screened inhibitors targeting specific kinases. In this review, we summarized the classification, function, crystal structures of kinases in Mtb, as well as Mtb kinase inhibitor design. SciFinder Scholar, Pubmed, Google Scholar, and protein data bank (PDB) are the major searching utilities used to finish the review.

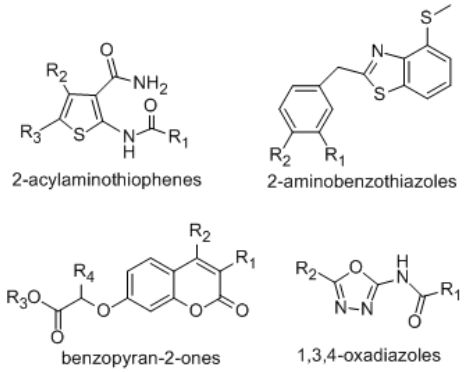

Figure 120 Scaffolds of Mtb growth inhibitors

2. Histidine Kinases in Two-Component Systems

The primary environmental signal transduction pathways in prokaryotes feature two-component systems (TCS) which include a sensor histidine kinase (HK) and a response regulator (RR).[110] An external or internal stimulus can lead to the transfer of a phosphoryl group from adenosine triphosphate (ATP) to a conserved histidine of HK. Right after the phosphorylation, the histidine kinase catalyses the transfer of the phosphate group from the phosphorylated histidine residue to the receiver domain on an aspartate residue of the RR. The RR mediates an appropriate response, mainly by activating transcription.[111]

Mtb has 14 sensor HKs and 16 RRs to form 12 HK/RR pairs and RR orphans,[108,112] Microbial HKs shares five conserved motifs denoted as the H-box, N-box, G1-box, F-box and G2-box.[113] Depending upon the conservation of amino acids in and around the H-box, bacterial HKs are classified into five different types, types I-IV and CheA.[113] All Mtb HKs belong to either Type IA (MtrB, MprB, PrrB, PhoR, KdpD, SenX3, TcrY, TrcS and Rv601c/Rv600c) or Type III (DevS, DevT, PdtaS and NarS).[113] Members of Mtb HKs that belong to Type IA have four orthodox type motifs, the N-Box, G1-Box, F-Box and G2-Box, referred to as the catalytic ATP (CA) binding domain,[114] while those belonging to Type III have unorthodox type motifs, where one or more motifs are missing (the F-box and part of the G2-box are missing in the

amino acid sequences of DevS, DevT, PdtaS and NarS) or they are otherwise different from the orthodox type.

A typical HK is composed of three domains: the sensor, dimerization and catalytic domains. The sensor domain, which can be of different types, senses the external/internal signal [e.g. cyclic GMP binding-Adenyl cyclase-FhlA (GAF) domain of DevS and DosT[115,116]; osmosensitive K^+ channel sensor domain of KdpD[117]; Per-Arnt-Sim (PAS) domain of SenX3[118] and PdtaS[119]]. Since the functional form of the HKs is a dimer, HKs dimerize using a dimerization domain. The dimerization domain is composed of two helices, the first of which houses the H-box whose conserved histidine gets phosphorylated during phosphotransfer. The catalytic domain is composed of four motifs, the N-box, G1-box, F-box and G2-box. This domain catalyzes the transfer of a phosphate from ATP to the conserved histidine in the H-box.[114,120] Several pairs of HK/RR of Mtb have been studied to date. However the only crystal structures available are for the sensor domain (GAF domain) of DosS and DosT, and for the CA domain of PrrB.

The DosS(DevS)/DosT/DosR system controls the Mtb dormancy regulon. DosS and DosR deletion mutants of Mtb showed a growth defect in mouse and guinea pig models, suggesting that these proteins are required for full virulence.[121] DosS and DosT are HKs that transduce signals on to the response regulator DosR by phosphotransfer.[122] The activation of DosS and DosT is controlled by the heme binding of O_2, nitrogen monoxide (NO), or carbon monoxide (CO).[123,124] Both DosS and DosT are essential. They play different roles in oxygen sensing. DosT is more important at the early stage of hypoxic conditions, it induces the DosR regulon with its DosS, then the predominance is switched to DosS when O_2 is limited.[125] Hence, DosS was reported to serve as a redox sensor, which is activated when the Met(Fe^{3+}) form under

the rapid oxidation by O_2 is reduced to the Fe^{2+} form;[124,126] while DosT is a hypoxia sensor, autophosphorylation activity of which will increase when it is deoxygenated.[124] However, the most recent study indicated that in vivo, DosS is more preferably a hypoxia sensor, since DosS is active in the ferrous unligated form, and turned off upon oxygen binding to the ferrous complex.[127] These conflicting results have been replenished by that DosS serves as an oxygen sensor at off switch, and redox sensor at on switch.[128] The N-terminal input domains of the DosS and DosT sensors have been shown to contain two GAF domains. The first GAF domain (GAF-A) contains the residue which coordinates the heme iron.[126,115] The C-terminal domain is responsible for autophosphorylation and phosphotransfer to DosR.[115] It has been determined that His149 in the DosS GAF-A domain,[115] and His147 in the DosT GAF-A domain,[116] which is at the same position as His149 in a sequence alignment of DosT with DosS, are the residues which coordinated the heme iron. Tyr171 in DosS[127] and Tyr169 in DosT[116] play a key role in the ligand-binding site. The Tyr forms a stacking interaction with heme, and its hydroxy group provides a H-bond to stabilize oxygen-binding to the heme iron.[116,129] The complementary functionality of DosS and DosT is related to the structural difference in their GAF-A domain. The Glu87 side chain of DosS and the corresponding residues of DosT respond to functionality conversion between DosS and DosT.[130, 131]

MtrA, an RR of the two complement system MtrB/MtrA, was reported to be essential for the viability of bacteria.[132,133] However, unlike other two-component systems requiring both an RR and its cognate HK, MtrB was found not to be essential for the growth of Mtb in vitro. It has been shown that levels of phosphorylated and non-phosphorylated MtrA are tightly regulated in virulent Mtb, hence factors interfering with this regulation may limit proliferation.[134]

MprB/MprA is a stress responsive signal-transducing pair mainly by activating a sigma

factor SigE.[135,136] MprB/MprA also display a dual regulation with TrcS/TrcR on a β-propeller protein Rv1057 which could stabilize the envelope.[137] MprA, the RR, is required for the maintenance of persistence.[138] MprA can be phosphorylated by either MprB or by a small, nonprotein phosphodonor like acetyl phosphate.[139] Residues His249 of MprB, which is the key histidine of the H-box that has been shown to be phosphorylated for several bacterial HKs, and Asp48 in His-MrpA have been proven to be important not only in MprB/MprA activity in vitro, but also for biological function in vivo.[139]

PdtaR was determined to be a phosphorylation dependent transcriptional antitermination regulator. Later on, it was confirmed to be activated by the protein Rv3220c with Mg^{2+} as a cofactor after autophosphorylation.[119] Rv3220c, which has also been called PdtaS, possesses four domains with GAF-PAS-HisKA (histidine kinase domain)-HATpase. The sequence and structure of C-terminal HisKA and HATPas, together with in vitro phosphorylation assays defined it to be the cognate HK of PdtaR.[119] The N-terminal GAF-PAS domains form a dimer with PAS-PAS, GAF-GAF, and PAS-GAF interfaces. The PAS domain is responsible to transmit signals to the HisKA. A flexible inter-domain linker between GAF and PAS could regulate the orientation of two domains to change the conformation of the dimer, thus affecting the dimerization of HisKA .[140]

The PrrB/PrrA system is important in adaption to the intracellular environment, and essential for the viability of Mtb.[141,142] They are transiently required in the early stages for intracellular multiplication in mouse macrophages, indicating their role in the infection.[143] The C-terminal domain of PrrB includes an HAMP linker (H domain), H-box domain, and CA domain.[144] Nowak *et al*. described solution structures of $PrrB^{HDC}$ and $PrrB^{DC}$, and a high-resolution crystal structure of $PrrB^{C}$.[145] The phosphorylation assay in the presence of Mg^{2+}

showed $PrrB^{HDC}$ is active for both autophosphorylation and phosphotransfer. The solution structure of $PrrB^{HDC}$ is dimeric, and the CA domain is closer to the dimerization domain than what is observed in the model development using the dimerization domain of CheA, in the crystal structure of PrrB and in the crystal structure of CheA. The crystal structure of the CA domain of PrrB does not have a bound ligand (ATP), while the residues around the ATP binding site partially occupy the putative ATP binding site as deduced from the structure of PhoQ bound to ADPNP and Mg^{2+}. The PrrB-dependent RR PrrA belongs to the OmpR/PhoB family and its crystal structure have been described.[146]

The Rv0600c(HK1)/Rv0601c(HK2)/TcrA system is different from traditional two component systems. It is composed of three proteins, two HKs, HK1 (Rv0600c) and HK2 (Rv0601c), that together phosphorylate a single RR TcrA.[147] The function of this three-protein system is still unclear. However, HK2 can be upregulated in the presence of an antibiotic, tetrahydrolipstatin, suggesting its role in metabolism of small molecules.[148] HK1 contains the CA domain (with N-, G1-, F- and G2-boxes), while HK2 possesses a histidine containing H-box. Together, HK1/HK2 forms a complete HK. HK2 forms a dimer. HK1 phosphorylates His131 on HK2, then HK2 transfers the phosphoryl group to the conserved Asp residue on TrcA.[149,150] Homology modeling and subsequent docking of HK1 and HK2 has shown that Arg64, Arg73, Asp81, Gly118, and Arg134 of HK1 form hydrogen bonds with Glu43, Glu145, Arg134, Arg17, and Trp103 of HK2. [147, 149]

TrcS, a HK, and TrcR, a RR, constitute another two-complement system of Mtb. Autophosphorylation of TrcS needs Mn^{2+} or Ca^{2+} as a cofactor, and a phosphoryl group is presumed to be transferred from His287 to Asp82 in the N-terminal receiver domain of TrcR.[151] As the genes of TrcS and TrcR are expressed during the log phase of growth in the broth culture

and initial stages of infection in macrophages transiently, they may play a role in the intracellular adaptation, although the possibility of their role in extracellular replication and at the end of the latency period or initiation of reactivation stage cannot be ignored.[152]

The PhoR/PhoP system is related to complex lipids biosynthesis and Mtb virulence. A PhoR/PhoP knock-out mutant of Mtb results in a deficiency in polyketide-derived lipids, such as sulfolipid (SL), diacyltrehaloses (DAT), and polyacyltrehaloses (PAT), which play roles in virulence.[153, 154] However, only PhoP, the RR, but not HK PhoR, has been proven to be required for the biosynthesis of polyketide-derived lipids.[153] In addition to synthesis of lipids, PhoP is involved in regulation of hypoxia response through DosR crosstalking, stress response, respiratory metabolism, secretion of T-cell antigen EAST-6,[155] and specific T-cell recognition.[155,156] More recently, there is evidence that PhoP is a key regulator of Mtb, and its mutants can be used as live vaccines to treate Mtb.[157] The structure and binding site of PhoP have been discussed in some other studies.[158,159,160 ,161]

The SenX3/RegX3 system, in which His167 and Asp52 are the sites for phosphorylation and phosphotransfer, respectively, is required for Mtb virulence.[162,118] Based on the model of SenX3/RegX3 regulating phosphate-dependent gene expression in *M. smegmatis*, SenX3 carries out autophosphorylation, phosphotransfer onto RegX3 when inorganic phosphate (Pi) concentration is limited.[163] SenX3, as an HK, has a PAS-similar domain which is related to oxygen or redox sensing. When compared with a modeled PAS domain, it lacks two helices in its N-terminal region which makes the structure more open and easier to target.[118] However, RegX3 is reported to be able to acquire phosphate from another phosphodonor than SenX3, though the phosphodonor is still unknown.[163]

KdpD/KdpE is reported to regulate kdpFABC expression in bacteria, which encodes for

K^+-translocating P-type ATPase.[164] In Mtb, the N-terminal domain of the HK KdpD interacts with the membrane lipoproteins LprF and LprJ, and its C-terminal domain forms a ternary complex with N-KdpD/LprF and N-KdpD/LprJ. This protein complex regulates the expression of kdpFABC, controlled by RR KdpE.[165]

Other two complement systems, NarS/NarL and TcrY/TcrX, are not well characterized. Parish *et al*. constructed mutants of TcrY/TcrX and NarL.[133] Infection with mutant NarL in SCID mice showed no difference relative to the wild-type strain, while infection with mutant TcrY/TcrX showed hypervirulence. Their functions are still not known.

3. Serine/Threonine Protein Kinases of Mtb

Mtb does not have many two-component regulatory systems when compared with other prokaryotes (e.g. *E. coli* has 25 orthodox sensory kinases and 32 RRs).[166] This deficiency is replenished by eukaryotic-like serine/threonine protein kinases (STPKs). The Mtb genome contains 11 STPKs named PknA, PknB, and PknD-PknL.[108] Two (PknG and PknL) out of 11 are soluble proteins, while the others are membrane bound.[167] Based on sequence analysis, the receptor-like (membrane bound) STPKs are divided into three groups PknA/B/L, PknD/E/H, and PknF/I/J. The two soluble kinases do not cluster with others.[168,169,170] The N-terminal domains of the receptor-like STPKs connect through a single transmembrane helix to one or more C-terminal domains that serve as signal sensors. The kinase domain is intracellular while the sensor domain is extracellular. STPKs are involved in many functions, such as cell division,[171] membrane transport,[172] amino acid uptake,[173] and transcription.[174] The STPKs of Mtb have been extensively reviewed. A bioinformatics analysis and overall view of STPK family members of mycobacterium has been reviewed in several publications,[167,168,175,176,177] and a comprehensive view of substrates of STPKs have been given by Chao *et al*.[178]

A transposon insertion experiment has shown that PknA is one of the three STPKs (PknA, PknB and PknG) required for growth in culture, indicating its role in proper function of Mtb. PknA is predominantly expressed in the exponential growth phase in experiments performed in culture. Since a partial depletion of PknA results in narrower and elongated cells, it was suggested to be involved in regulation of cell shape and in cell division in Mtb.[179] PknA phosphorylates mtFabH, beta-ketoacyl-ACP synthase III, which is involved in mycolic acid biosynthesis;[180] mMurD, mycobacterial UDP-*N*-acetylmuramoyl-L-alanine: D-glutamate-ligase, which is involved in peptidoglycan biosynthesis;[181] Wag31, which is involved in regulation of cell shape and cell wall synthesis;[179,182,183] mFtsZ, which is involved in septum formation during cell division;[184] EmbR, which is further required for the transcriptional regulation of embCAB operon involved in cell wall arabinosyltransferases;[185] Rv1422, a conserved protein of unknown function;[179] KasA, KasB, and *mt*FabD, three type II fatty acid synthase (FAS-II) components;[186] and Ser/Thr phosphatase.[187] Recombinant PknA was reported to be phosphorylated at seven sites in the intracellular domain.[188] Although PknA has shown to be important for mycobacterium survival, no efforts have been reported for developing PknA inhibitors.

As for PknA, a transposon insertion experiment highlighted the importance of PknB in the regulation of cell shape and in cell division in Mtb.[179] K-252-b, a natural indolecarbazole protein kinase inhibitor which inhibits PknB in vitro, inhibited growth of slow- and fast-growing mycobacterial strains. Overexpression of Mtb PknB in *M. smegmatis* led to a two-fold increase in resistance to inhibitor K-252-b, revealing PknB as a target of inhibitor K-252-b.[189] This observation further demonstrated the importance of PknB in Mtb survival. The substrates of PknB include PBPA, a penicillin binding protein which is involved in cell division;[190] Forkhead-Associated (FHA) domain-containing proteins, such as Rv0020c and Rv1747 (demonstrated in

vitro);[191,192,193] GarA (Rv1827),[194] EmbR,[184] and Rv0019c,[195] which are responsible for cell cycle regulation, protein degradation, DNA damage response, and signal transduction;[196] polyketide-associated protein PapA5;[195] Wag31;[179,182,183] Rv1422, a conserved protein of unknown function (demonstrated in vivo); [179] SigH, a sigma factor which is a regulator of transcription of several genes during stress and RshA, an anti sigma factor, which negatively regulates SigH in vivo;[197] and N-acetylglucosamine-1-phosphate uridyltransferase (GluM), which is involved in the biosynthesis of peptidoglycan.[198]

There have been some efforts to understand the structural basis of the function, autophosphorylation and interactions with inhibitors for PknB. The structure of PknB was solved in the presence of an ATP analogue,[199,200] with ATP competitive inhibitors mitoxantrone[201] and KT5720 in complex with a mutant PknB,[202] providing valuable resources for protein structure-based drug discovery efforts. The X-ray structures of PknB highlighted its remarkable similarities with protein kinases of eukaryotic origin.[199] The kinase domain of PknB consists of N- and C- lobes that bracket the ATP binding site **(Figure 121A)**. In this structure, PknB takes on the closed conformation which results from the movement of the hinge region between the N- and C-lobes.[199] The autophosphorylation of PknB is thought to depend on activation of the kinase domain by N-lobe dimerization[203] and mediation of substrate recognition by the G-helix in the C-lobe.[202] Moreover, the extracytoplasmic penicillin binding proteins and serine/threonine kinase (PASTA) domain serves as a sensor for signaling molecules. The ligand-dependent dimerization of the PknB-PASTA domain promotes cell growth by binding to the exogenous peptidoglycan fragment.[204,205]

Considering the importance of PknB for Mtb survival, drug discovery efforts have been initiated. Nine hundred and seventy compounds from a protein kinase inhibitor library (Vichem's

Nested Chemical Library, NCL) were tested for PknB inhibitory activity in vitro[206] and a few compounds with submicromolar inhibitory activity were identified. For further effort to explore potentially useful agents, a docking model was setup to screen 19033 compounds, among which VI-15662 and VI-17494 showed a dual inhibition on PknB and PknG, while VI-12177 displayed a promising activity with an IC_{50} of 88 nM[207] **(Figure 121B)**. Recently, more than 50,000 compounds including 45,000 commercial available and 6,400 synthetic molecules were screened using "kinase Glo" assay kit. Aminopyrimidine compounds MRT67127, MRT67153, and MRT67150 displayed the best activity thus far with an IC_{50} of 53, 56, and 55 nM, respectively.[208] An SAR investigation on the aminopyrimidine analogues revealed that the induction of a basic amine side chain facilitated the binding affinity, while the replacement of the pyrazole head group with pyridine could improve the selectivity.[209]

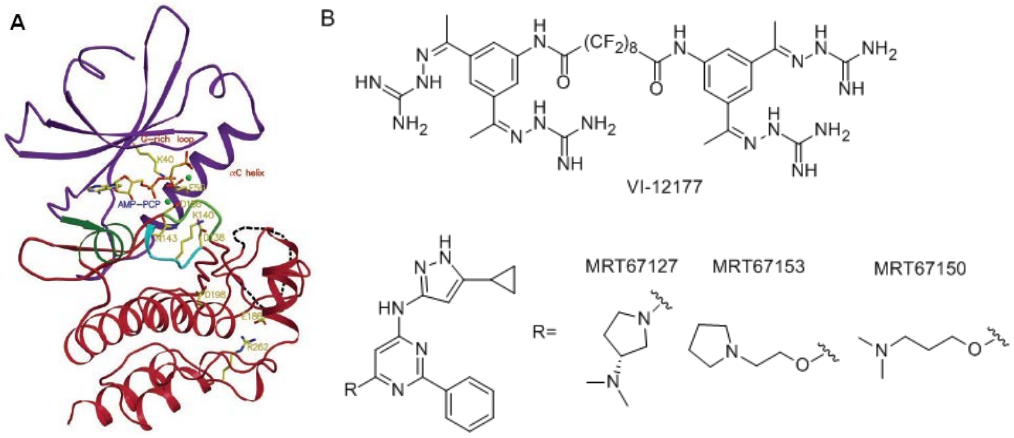

Figure 121 (A) Overall structure of the catalytic domain of PknB in complex with a nucleotide triphosphate analogue; (B) Inhibitors of PknB
The figure was reprinted from reference 199 with the permission of the American Society for Biochemistry and Molecular Biology

Similar to PknA and PknB, PknL might be involved in cell division as well.[168] The study of the protein-protein interactions (PPI) network of Mtb provided the evidence that PknL interacts with two cell division protein, FtsE and FtsH.[210] It is reported to phosphorylate a DNA-binding protein, Rv2175c, of which the structure was determined by NMR methods.[211] The

Thr173 and Thr175 residues which correspond to Thr171 and Thr173 in PknB have been proven to be phosphorylation sites in the activation loop.[212] This indicates that PknL's phosphorylation mode is similar to that of PknB. Rv2175c, KasA, KasB, and *mt*FabD[186] as well as GroEL1[213] are substrates of PknL.

The exact in vivo function and importance of protein kinase PknD is not well characterized. Some preliminary studies have shown that the PknD knockout strain shows no attenuation in growth compared to wild type in mice.[214] The latest research pointed out that PknD is crucial for invasion and virulence in central nervous system tuberculosis.[215] As the gene of PknD is located next to the gene encoding phosphate transporter, it was suggested to be involved in phosphate transport.[167] The unphosphorylated MtPknD kinase domain can be activated by dimerization through the N-lobe, which suggested a similar interface to that by which PknB regulates PknD.[216] However, the rate of phosphate uptake in a PknD knockout was observed to be comparable to that of wild type.[214] The putative substrates for PknD were shown to be MmpL7,[217] which is involved in deposition of components of the cell wall; Rv0516c, a putative sigma factor;[174] and the FHA-A domain of Rv1747,[191] an ATP-binding cassette (ABC) transporter which is required by Mtb for infection (demonstrated in a murine model).[218] The crystal structure of the MtPknD sensor domain has been determined. It forms a β-propeller with six blades that are arranged cyclically. The sensor domain mediates signaling by changing the quaternary structure of the intracellular kinase domain.[219]

PknE showed an increased nitric oxide-mediated apoptosis of host macrophages.[220,221] However, this protein is not absolutely required for the Mtb in vitro[220] or in a murine model.[222] The substrates of PknE include EmbR2, a homologue of EmbR, a transcription factor;[223] the FHA domain of Rv1747,[191] and GarA.[194] The structure of apo-PknE has been solved. The PknE

kinase-domain forms a back-to-back dimer similar to that observed in the crystal structure of the PknB kinase-domain, supporting the idea of regulation of STPKs through dimerization.[224] The regulation of kinase activity through dimer formation via this interface has been validated experimentally for PknD.[216]

A deletion mutant of PknH showed enhanced survival and replication in murine models, especially during stages of chronic infection, compared to wild type and to a PknE deletion mutant, indicating the role of PknH in regulation of downstream pathways responsible for in vivo growth.[222] PknH was reported to mediate phosphorylation of the FHA domain of the transcriptional regulatory protein EmbR;[225] transcription factor Rv0681 and penicillin binding protein DacB1;[226] and the hypoxia- and NO-inducible dormancy regulon DosR.[227] The activity of PknH can be inhibited by staurosporine.[228] Staurosporine **(Figure 122)**, isolated from bacterium *Streptomyces staurosporeus*, is an ATP-competitive inhibitor of both tyrosine and serine/threonine protein kinases. It binds to many kinases with high affinity and lacks specificity,[229] however, it could serve as a precursor of many new kinase-selective agents.

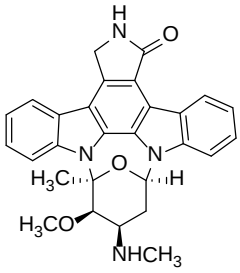

Figure 122 PknH inhibitor staurosporine

PknF is able to regulate different stages of cell division.[172] It also modulates phosphorylation of two FHA domains of the adjacent Rv1747,[230,191] and an advanced study showed it down-regulates glucose transport.[172] Considering that Rv1747 can serve as a substrate of PknD and PknE,[191] and that another ABC transporter EmbR can be phosphorylated by

PknH,[225] the PknF might be cross-regulated together with the cluster of PknD/PknE/PknH. In addition, like PknA/PknB/PknE, PknF phosphorylates the GroEL1 chaperone which plays an essential role in cytokine-dependent granulomatous response during Mtb infection.[213]

Unlike other transmembrane domain-containing STPK, PknI is reported to be localized mainly in the cytosol, which indicates it might not be involved in host protein modification.[231] Similar to PknH, PknI serves as a downregulator during infection of Mtb both in vitro and in immunodeficient mice.[231,232] The PknI mutant was shown to grow better under host mediated signals such as low pH and limited oxygen availability, suggesting its role in sensing the macrophage environment and slowing Mtb growth within the infected host.[232] The substrates of PknI and the regulatory pathways initiated by PknI have not been characterized.

Few studies have been completed on PknJ. PknJ is only present in Mtb among all sequenced mycobacterial species, which implies its specificity.[168] In a PPI map, PknJ showed the ability to interact with FadE proteins suggesting it may be involved in fatty acid metabolism, which is similar to PknA/PknB/PknL.[210] Thr168, Thr171, and Thr173 form the autophosphorylation sites of PknJ.[233] PknJ is able to phosphorylate EmbR; methyltransferase MmaA4/Hma, which is responsible for mycolic acid biosynthesis; dipeptidase PepE, whose encoding gene is adjacent to PknJ;[233] and pyruvate kinase A (MtPykA, Rv1617).[234]

PknK is a member of a cluster of soluble kinases. It regulates the growth of Mtb during both the early and persistent stages of infection.[235] The PPI network showed it to be like PknL, in that it interacts with FtsE and FtsH,[210] and ABC transporters.[210] Another recent study showed that a transcription factor VirS and four mycobacterial monooxygenase (mym) operon proteins, Mym, LipR, Rv3085, and Rv3088, are substrates of PknK. The PknK-induced phosphorylation on VirS promotes 2-3 fold mym promoter activity.[236] Mutations on Lys55 and two threonines in the

activation loop, Thr178 and Thr180, result in a loss of phosphorylation, which demonstrates that these residues are necessary to the activity of PknK.[236] Unlike for transmembrane STPKs, PknK is tied to the cell membranes by its PDZ domain or C-terminal domain in order to be able to function.

Unlike most of STPKs, PknG lacks a critical arginine residue in the kinase-domain which plays a key role in the activation of kinase activity. Its autophosphorylation is conducted on six Thr residues near the N-terminus, however, the autophosphorylation is not necessary to activate PknG kinase activity.[237] Instead, it is crucial for PknG to be able to inhibit phagosome-lysosome fusion,[237,238] thus promoting Mtb survival in macrophages, which results from downregulation of protein kinase C-α controlled by PknG.[239] In addition, PknG participates in glutamine and glutamate metabolism under stress conditions, thereby sustaining Mtb survival. [173,178] It is required for Mtb intrinsic antibiotic resistance to multiple antibiotics as well.[240] The essential roles of PknG in maintaining Mtb virulence and resistance make it a potential target for antituberculosis drug design.

Scherr *et al*. reported a crystal structure of PknG in complex with inhibitor AX20017 **(Figure 123A)**.[241] PknG has three structural domains: the C-terminal contains a tetratricopeptide repeat (TPR) domain to mediate protein-protein interactions; the N-terminal moiety contains the rubredoxin domain that regulates PknG activity; the kinase domain is between the rubredoxin and TPR domains, and it adopts the typical two-lobed structure of eukaryotic protein kinases.[241,242] PknG is able to phosphorylate GarA, and it is more active under oxidizing conditions.[242] Unlike PknB and PknE which dimerize through the N-terminal domain, PknG dimerizes using the TPR domain. The AX20017 inhibitor **(Figure 123B)** has been determined to bind deep within a narrow pocket formed by the kinase lobes and a unique N-terminal peptide

segment of PknG.[241] Inhibitor AX20017 was shown to be specific for PknG when tested against other Mtb kinases[238] and a panel of 28 human protein kinases.[241] Székely *et al*. screened 1000 compounds to identify PknG inhibitors. As a result, AX20017 was confirmed to be a potent PknG inhibitor. Chemical modification of lead AX20017 led to identification of AX35510 with an IC_{50} of 200 nM, which was also found to be active in a macrophage assay.[206] Based on these data, Hegymegi-Barakonyi *et al*. continued the optimization, and screened compounds against PknB, PknG, NAD kinase, and NAD synthetase as multiple targets with PknG as the primary one.[207] As a result, eight analogues showed promising inhibition, and the most potent one with low toxicity was VI-16315 **(Figure 123B)** with an IC_{50} of 10 nM.

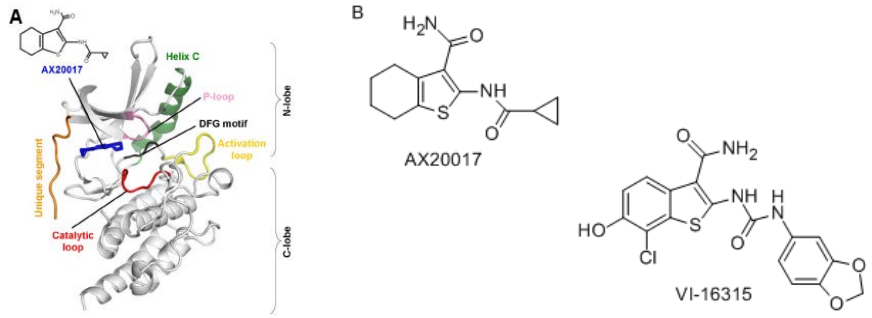

Figure 123 (A) Crystal structure of PknG-AX20017 complex; (B) PknG inhibitors
The figure was reprinted from reference 241 with the permission of the National Academy of Sciences, U.S.A

4. Tyrosine Kinase of Mtb

It was thought that protein tyrosine kinases (PTKs) only exist in eukaryotes. In the last two decades, however, PTKs have been identified in various strains of bacteria and recognized to play important roles in biosynthesis of polysaccharides,[243,244] stress response,[245] DNA metabolism,[246] and antibiotic resistance.[247] Bacterial PTKs have an external domain, trans-membrane α-helices, and an intracellular catalytic domain with the ATP-binding Walker A and B motifs which are required for kinase activity. The end of the C-terminus possesses a Tyr-rich cluster that is responsible for multiple phosphorylation.[248,249]

There was no PTK found in Mtb until the identification of the protein encoded by

Rv2232, named PtkA, which is able to use ATP or GTP as phosphate donors and functions as a PTK to phosphorylate protein tyrosine phosphatase PTPA.[250] Although the roles of PtkA are still not clear, considering that PTPA is essential to maintain virulence in host macrophages,[251] it could be a potential target for treatment of Mtb.

5. Other Kinases of Mtb

In addition to signal transduction, many other different types of kinases participate in the biochemical reactions of Mtb. Some of them were discussed in this review. Some others have not been well studied thus far **(Table 18)**.

Table 18 Some other not well studied kinases in Mtb

Kinase	Accession	Characterization reference	Structure
Acetate kinase	P63409	Whole genome	---
Acetylglutamate kinase	P0A4Y6	Whole genome	2AP9
Galactokinase	P96910	Whole genome	---
Glycerol kinase	O69664	Whole genome	---
2-Amino-4-hydroxy-6-hydroxymethyldihydropteridine Pyrophosphokinase	P64143	Whole genome	---
6-Phosphofructokinase	P65690	Whole genome	---
Homoserine kinase	P65224	Whole genome	---
Ribose-phosphate pyrophosphokinase	P65232	Whole genome	---
Pyruvate kinase	O06134	Whole genome	---
Phosphoglycerate kinase	P65700	Whole genome	---
Phosphoenolpyruvate carboxykinase	P65686	Whole genome	---
Polyphosphate glucokinase	Q59568	PMID:8617763	---
Inorganic polyphosphate/ATP- NAD kinase	P0A5S6	PMID:11006082	---
Glutamate 5-kinase	P71910	Whole genome	---
Probable GTP pyrophosphokinase	P66014	Whole genome	---
Phosphomethylpyrimidine kinase	P66913	Whole genome	---
Ribokinase	Q7D752	Whole genome	---
Pyruvate, phosphate dikinase	Q7D8T1	Whole genome	---

Whole genome reference-PMID:12218036, 9634230

5.1 Polyphosphate Kinase

Inorganic polyphosphate (polyP) plays a number of critical roles in bacterial persistence, stress, and virulence. PolyP intracellular metabolism is regulated by the polyphosphate kinase (PPK) protein families. The enzyme PPK catalyses the reversible transfer of the terminal c-Pi of

ATP to form a long chain polyphosphate. The vulnerability of this gene was evaluated by antisense knockdown experiments in Mtb using an IPTG inducible mycobacterial vector.[252] Expression profiling studies demonstrated that down regulation of PPK causes a rapid bacterial cidality during the late growth phase. PPK thus seems to be a suitable antitubercular drug target. Recently, a class II MtPPK, MtPPK2 was biochemically characterized.[253] The role of MtPPK2 is to catalyze polyP-dependent phosphorylation from ADP to ATP. To develop inhibitors of MtPPk2, high affinity DNA aptamers were screened. One G-quadruplex aptamer was highly selective to MtPPK2 with an IC_{50} at 39.3 ± 10 nM. The crystal structure of MtPPK2 is not characterized yet. However, based on the crystal structures of the *Pseudomonas aeruginosa* and *Sinorhizobium meliloti* PPKs, as well as a similar secondary structure of MtPPK2 as those proteins, it is proposed that the conserved Walker A (P-loop) and B motifs could be responsible for the polyphosphate binding.[253]

5.2 4-Diphosphocytidyl-2-C-methyl-D-erythritol Kinase

Isoprenoid precursors, which are a large group of natural products playing key roles in many biological pathways, can only be biosynthesized by the 2-*C*-methyl-D-erythritol 4-phosphate pathway in Mtb.[254] The 4-diphosphocytidyl-2-*C*-methyl-D-erythritol kinase (IspE), which is an essential enzyme in the isoprenoid precursor biosynthesis pathway, catalyzes ATP-dependent phosphorylation of 4-diphosphocytidyl-2-*C*-methyl-D-erythritol (CDP-ME) to 4-diphosphocytidyl-2-*C*-methyl-D-erythritol-2-phosphate and plays a crucial role in Mtb survival.[255,256] Therefore, IspE is an attractive and potential target for antimicrobial drug discovery. The MtIspE contains an N-terminal ATP binding domain and a C-terminal substrate binding domain. Three motifs creating the catalytic center are present in the MtIspE. Motif A participates in the formation of substrate binding site, motif B is the P-loop, and motif C stabilizes the

conformations of motifs A and B.[257] ADP, 4-diphosphocytidyl-2-*C*-methyl-D-erythritol (CDP-ME) and an ATP analogue adenosine 5'-(β,γ-imino)triphosphate (AMP-PNP) were used as MtIspE substrates to study the binding sites. A π-π interaction between Tyr28 and Tyr158 at the substrate binding site was found to be crucial to stabilize the substrate. The same interaction was observed in *E. coli* between Tyr and Phe. In the ATP binding site, a glycine-rich loop formed seven H bonds with water to stabilize the phosphate.[257] All the results provided an implication for MtIspE inhibitor design.

5.3 Aspartokinase

Aspartokinase (AsK) is responsible for the biosynthesis of 4-phospho-L-aspartate that involved in the metabolic pathway of lysine, threonine, methionine and isoleucine.[258] Since an intermediate of the lysine biosynthesis from 4-phospho-L-aspartate, mesodiaminopimelate, is a major component of the bacterial cell wall, an inhibition on AsK could decrease the production of lysine, thus interfering with the formation of the bacterial cell wall.[258] Due to its selectivity on the bacterial cell wall, AsK could be another potential target for the development of nontoxic inhibitors.

All the AsKs that have been studied contain an N-terminal kinase domain, coming together with different number of regulatory ACT domains originally characterized in AsK, chorismate mutase, and TyrA (prehenate dehydrogenase).[259] Depending on the protein-protein interaction in the regulatory domain, AsKs are classified into three types. Type I and II are homo-dimeric. Each monomer contains two or four ACT domains. Type III is hetero-tetrameric ($\alpha_2\beta_2$-). Each α- or β- subunit contains two ACT domains.[259] The MtAsK belongs to type III AsK. Its N-terminal α-subunit forms the catalytic domain, and its two β-subunits as well as C-terminal α-subunits form the regulatory domain.[260,261] Molecular docking studies with natural

substrates, products and feedback inhibitors are in agreement with the published data and showed that ACT domains play an important role in binding to ligands.[258] An enzymatic assay revealed an inhibition of MtAsK activity when it bond to threonine. The residues Asp274, Gln298, Ile126, Asn125, Thr59, Ile61, Ala30, Ala31, Gly28, and Val124 could be responsible for the formation of the binding pocket.[261] Based on the docking conformations, a pharmacophore model can be developed by probing the common features of ligands.

5.4 Nucleoside Kinases

Nucleoside kinases form a family which includes adenosine kinase (AK), guanosine kinase (GK), cytidine kinase (CK), thymidine kinase (TK), and uridine kinase (UK). Only AK of Mtb has been studied so far.

AK, which belongs to the phosphofructokinase B (PfkB) family of carbohydrate kinases, is responsible for the phosphorylation of adenosine (Ado) to adenosine monophosphate (AMP) by using ATP as cofactor. AK was not found in bacteria until it was identified and characterized in Mtb by Long *et al*.[262] MtAK is a dimer, while human AK is a monomer. Their overall structures are similar when comparing apo-MtAK to the human AK·$(Ado)_2$ complex.[263] However, the Ado binding pocket of MtAK is quite different from that of human AK.[263] Moreover, only 24% of its sequence is identical to the known AKs, and it is structurally and biochemically unique from other known AKs, including having higher optimum pH profile, lower pI, quaternary structure as a dimer, no stimulation by inorganic phosphate (Pi), and different specificities of substrate and phosphate donor.[262] These aspects suggest that AK inhibitors against Mtb might have high selectivity versus human AK. This hypothesis has been confirmed by Gupta's group. When treating MtAK with some non-nucleoside inhibitors of HsAK, the inhibition was attenuated from the micromolar range to 1 mM. The same tendency was found for their substrate

specificity.[264] Some Ado analogues such as 2-methyl-Ado and fluorinated 3-deaza-Ado analogues **(Figure 124)** are proinhibitors of Mtb, which can be activated and become toxic to mycobacteria by phosphorylation. 2-Methyl-Ado shows a moderate inhibition on Mtb with a 95% MIC of 3 μg/mL,[265] while 2-fluoro-3-deaza-Ado and 2,3-difluoro-3-deaza-Ado are much better substrates for MtAK than for human AK with specific activity of 63 and 81 nmol/mg/min, respectively.[266] More modifications to the adenine moiety were produced **(Figure 124)**.[267,268] As a result, the most potent inhibitors are N^1-benzyl-Ado, 6-cyclopentyloxypurine riboside, and 7-iodo-7-deaza-Ado with Ki of 0.19, 0.15, and 0.21 μM, respectively. Since MtAK preferred the β-D-ribofuranosyl conformation or modifications that closely resembled this conformation, the modifications on the ribofuranosyl moiety have been studied as well.[269] Twenty-eight of the 63 compounds showed inhibition. The most potent inhibitor is 5'-amino-5'-deoxy-Ado with a Ki of 0.8 μM, which was shown to have an ATP-competitive mode of inhibition.

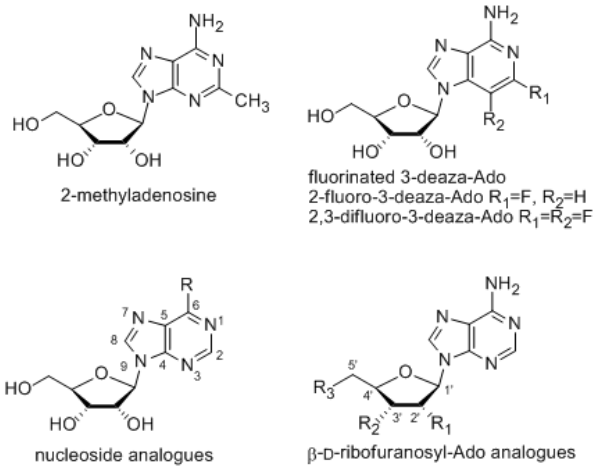

Figure 124 MtAK inhibitors

5.5 Nucleoside-Phosphate Kinases

Nucleoside-phosphate kinases are a family of nucleoside monophosphate (NMP) kinases (NMPK), including adenylate kinase (ADK), guanosine monophosphate kinase (GMPK), cytidylate kinase (cytidine monophosphate kinase, CMPK), thymidylate kinase (thymidine

monophosphate kinase, TMPK), uridylate kinase (uridine monophosphate kinase, UMPK) which catalyze ATP dependent phosphorylation of NMP/dNMP to NDP/dNDP, and all nucleotide diphosphate kinases (NdKs).

5.5.1 Nucleoside Monophosphate Kinases (NMPKs)

NMPKs catalyze the phosphorylation of NMP/dNMP to NDP/dNDP. They consist of CORE, LID, and NMP-binding domains. ADKs were grouped into long variants of bacteria, yeast and mitochondria, and short variants of eukaryote cytosolic enzymes, differing in the length of amino acids in the LID domain. Later on, some ADKs of bacteria including Mtb have been grouped into a new subfamily called short bacterial forms.[270] The crystal structure of MtADK showed that the overall structure is similar to the other ADKs, while the LID only contains 10 residues.[271] There were obvious conformational differences when comparing free and complexed ADK structures.[270,271] In addition, unlike for ADKs from either eukaryotes or other bacteria, MtADK has low catalytic activity, which results in low growth and low survival under nutritionally deprived conditions.[270]

Hible *et al*. reported the crystal structures of apo, GMP-bound, and GDP-bound GMPK.[272] Some properties of MtGMPK are significantly different from those of other GMPKs. The MtGMPK has an open domain conformation no matter if it is in the apo state or binding to GMP or GDP, while conformations of other GMPKs closed when they bound to either substrate. The GMP binding site of MtGMPK has unique interactions relative to other GMPKs. For example, it lacks a conserved Tyr81, which binds with α-phosphate of GMP in other GMPKs like GMPK of mouse. The corresponding residue to Tyr81 in MtGMPK is Ser99 which cannot form a hydrogen bond with the α-phosphate of GMP due to its shorter side chain, and instead interacts with water in the binding site. The length and sequence of the MtGMPK β5/β6 loop are also

distinct, which provides a unique binding pocket. The specificity in structure could be helpful for drug design. A typical GMPK structure from Mtb is shown in **Figure 125**.

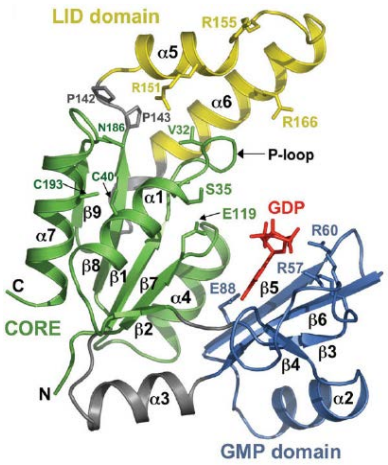

Figure 125 Crystal structure of reduced GMPK-GMP in Mtb
The CORE domain is in green, the LID domain is in yellow, and the GMP domain is in blue.
Reprinted from reference 272 with the permission of John Wiley & Sons, Inc.

In the genome of H37Rv strain, Rv1712 is identified as a putative *cmk* gene, and it has been confirmed to function as a CMPK.[273] CMPK is involved in the biosynthesis of pyrimidine ribonucleotide. No crystal structure of MtCMPK is available, but a homology model based on *E.coli* CMPK was made and refined using molecular dynamics.[274] *E. coli* CMPK contains a short LID domain and an insertion of 40 amino acid residues in its NMP-binding domain, which makes it different from other NMP kinases.[273] MtCMPK shares many common features with *E.coli* CMPKs, which could be used to guide design of inhibitors specific for MtCMPK. The LID and NMP-binding domains and also the phosphate donor site have low motion in the CMP-bound form compared to in the unbound CMPK suggesting that CMP-binding is responsible for stabilizing the protein. Moreover, the mode of action of MtCMPK is similar to that of shikimate kinase in Mtb.[274]

The TMPKs have been grouped into type I and type II TMPKs. For type I, mostly found in eukaryotes, the active-site arginine residues are in the P-loop, while for type II, usually found

in bacteria, those Args are in the LID. However, MtTMPK does not belong to either type, since arginine residues from both the P-loop and LID can be involved in catalyzing phosphoryl transfer.[275,276] Also, the Mg^{2+} ion located in the TMP-binding site is unique, since no Mg^{2+} was observed in TMPK of yeast or *E. coli*, and the Mg^{2+} in TMPK of human is far from the binding site.[275] 3'-Azido-3'-deoxythymidine 5'-*O*-monophosphate (AZTMP) is an MtTMPK inhibitor, which can explain the importance of Mg^{2+} in MtTMPK, since its mechanism of action may involve its azido group preventing Mg^{2+} ion binding.[277] Moreover, the sequence of amino acids in MtTMPK is only 22% identical to that of human TMPK.[275] These factors make MtTMPK one of the best potential targets for the design of new antitubercular drugs.

Many researchers have focused on screening of selective, competitive inhibitors of TMPK. Modifications of dTMP at 2'-, 3'-, 5'-, 5- positions displayed better affinities than those of nucleotides, and the inhibition of nucleosides was equal to those of their 5'-*O*-monosphate esters, which indicated that the ribose moiety is more important to maintain in the modified structures.[278,279,280,281,282] Later, the 3D-pharmacophore sites of those 81 thymidine analogues using 4D-QSAR method were mapped.[283] It was proposed that regions between the C-5' of the sugar ring and the nitrogen of the thiourea moiety can be good modification sites. 2',3'-bicyclic nucleosides[284,285] and 5'-thiourea-substituted α-thymidine analogues[286] were designed as TMPK inhibitors **(Figure 126)**. The analogue which contains a 3-trifluoromethyl-4-chlorophenyl-thiourea moiety showed a better activity with K_i of 0.6 μM and MIC_{50} of 6.25 μg/mL. Modifications to replace the ribose moiety with units, such as N^1-(4-substituted-benzyl)-pyrimidines[287,288] and acyclic nucleoside analogues[289,290] were synthesized as well **(Figure 126)**. Some derivatives had low K_i between 0.27–0.93 μM. However, none of them displayed great inhibition of bacterial growth. Because of the unsatisfactory bioactivity of the thymidine-based

analogues, Siddiqi's group searched for novel inhibitors by first developing a pharmacophore model, and using it to help in identifying potential inhibitors from the Maybridge database using protein structure-based virtual screening against MtTMPK.[291] As a result, three compounds were identified **(Figure 126)** which showed promising inhibition with MIC of 3.12 μg/mL. In an effort to identify more potent and selective inhibitors of MtTMPK, a study of small peptide inhibitors as potential lead compounds was undertaken.[292] Based on the crystal structures of MtTMPK and human TMPK complexed with AZTMP, respectively, a rational structure-based approach has been employed to design small peptides as MtTMPK inhibitors. By comparing their differential binding at the active site using *in silico* docking and selectivity analysis, a set of Trp- containing tripeptides, particularly Trp-Pro-Asp, was found to be most potent and selective for MtTMPK with K_d of 0.018 nM (compared to human TMPK with K_d of 0.43 μM).[292] The inhibition of tripeptide is attractive enough as a drug candidate. As for the other peptide drugs,[293] however, enzymatic unstability might cause less efficacy in vivo. Therefore, modifications on the tripeptide should be considered.

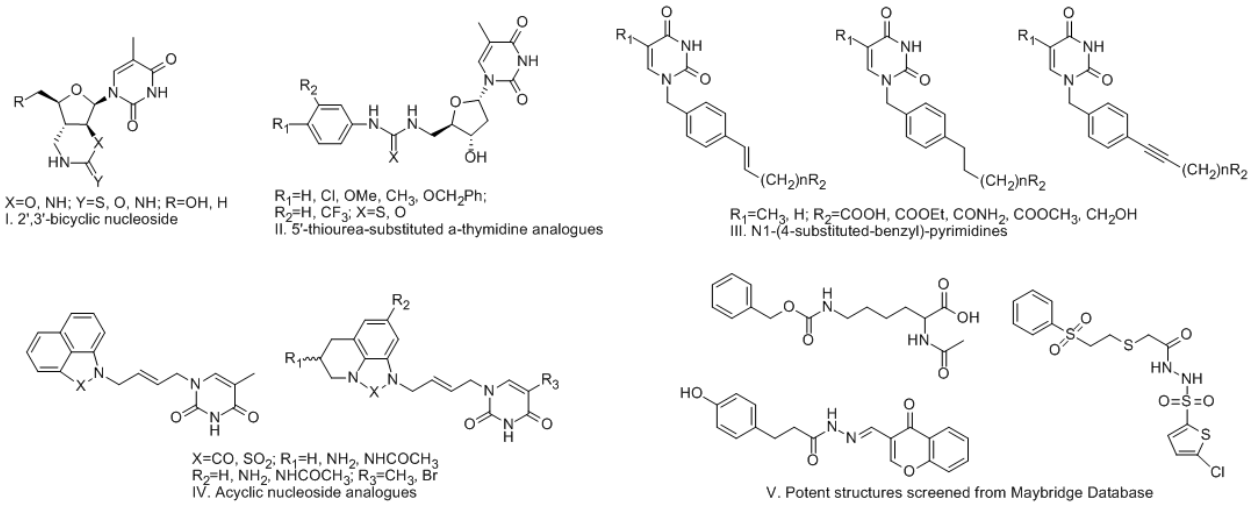

Figure 126 TMPK inhibitors

MtUMPK (encoding gene pyrH) has been proven to be essential in Mtb.[294] Considering the primary amino acid sequence and 3D structure of bacterial UMPKs are different from those of eukaryotes, the structure of UMPK is it also could be an attractive target.[295] The structure of MtUMPK is homo-tetrameric. ATP and UMP serve as specific substrates of MtUMPK. It was suggested that Lys36, Asp166, Lys185, Phe191, and Asp221 are the key residues involved in ATP binding by comparing with *E.coli* UMPK. Using the same method, Gly77, Gly78, Arg82, Gly83, Asp97, Met158, and Leu169 were suggested to participate in the UMP binding.[295] Based on the kinetic study, GTP exerts upregulation on MtUMPK. Opposite to GTP, UTP has noncompetitive inhibition towards MtUMPK. Two mechanisms were proposed for their regulation: GTP/UTP could bind onto the ATP binding site, or they possibly bind onto the third nucleotide-binding site, thus regulating MtUMPK.[295] The hypothesis of an allosteric pocket was confirmed by the crystal structure of MtUMPK in complex with GTP. The nucleotide binding only affects a small region with 30 residues. When GTP binding into the allosteric pocket, Pro139 plays a key role in the regulation of MtUMPK.[296] The structural and functional characterization provided evidence for the inhibitor design.

5.5.2 Nucleoside Diphosphate Kinase (NdK)

NdK plays a key role in the maintenance of intracellular ratios of NTPs and dNTPs. Tiwari et al. reported autophosphorylation as well as phosphotransfer activities of MtNdK through structure-function analysis.[297] Mutation studies showed that His53 plays a significant role in autophosphorylation. Furthermore, Tyr50 and Arg86 were found to maintain phosphotransfer capabilities.[297]

5.6 Shikimate Kinase

The shikimate pathway of Mtb is required for biosynthesis of aromatic compounds and is

essential for all aromatic amino acids, as well as other metabolites such as folic acid and ubiquinone.[298] Shikimate kinase (SK) is responsible for the phosphate transfer from ATP onto the 3-hydroxy group of shikimic acid.[299] SK has been found in bacteria, fungi, algae, and higher plants, but not in mammals,[300] so it has the potential to be a valuable target for antibacterial drugs. The structures of shikimate kinases are similar to those of NMP kinases. The crystal structure of MtSK has been elucidated as an unliganded form;[301,302] a binary complex with MgADP,[303] MgATP,[301] shikimic acid;[302] a ternary complex of SK with shikimic acid as one substrate and ADP,[304] MgADP,[305] or ATP analogue[302] as another substrate; or a ternary complex with shikimate-3-phosphate and ADP.[301] Based on most of these crystal structures of MtSK, many efforts have been made to explain the mechanisms of protein binding and design the MtSK inhibitors. The Bartunik group set up a model for the transition state and provided a putative mechanism of phosphoryl transfer by MtSK **(Figure 127)**.[301] The conformational changes caused by binding shikimate, magnesium and chloride ions to MtSK are also helpful to understand the catalytic mechanism.[306] Another kinetics and structural dynamic study of MtSK was performed. The measurement of hydrogen/deuterium (H/D) exchange on the amide bonds of protein using MS/MS is able to track energy transfer, thus facilitating the studies of protein dynamics and protein-ligand interaction.[307]

Pyrazolone derivatives **(Figure 128A)**, which are patented by AstraZeneca, have been reported as potential inhibitors of MtSK, and most of these analogues have $IC_{50} < 20$ μM.[308] More recently, *in silico* high-throughput screenings on MtSK inhibitors have been completed.[309,310] Drug-like compounds from the online service Free ADME/Tox Filtering (FAF)-drugs exhibited better docking scores were screened based on Lipinski's Rule of Five or other rules. The key interactions between top-scoring compounds and MtSK suggested that a five-

membered heteroaromatic system (triazole or tetrazole) is crucial in drug development, in which the inhibitor asxe1 showed the best binding affinity **(Figure 128B)**.[309] Since small peptide inhibitors show several advantages compared to these small molecules in treating diseases, such as high specificity and affinity to target proteins, greater potency, and lower toxicity, they are appealing to scientists and to the pharmaceutical industry, though they are likely to be metabolically unstable. Kaur's group developed dipeptides using a structure-based *in silico* approach. A dipeptide Arg-Asp displayed the best binding affinity by far with K_d of 5.49 nM, which is 10 times lower than that of asxe1.[311]

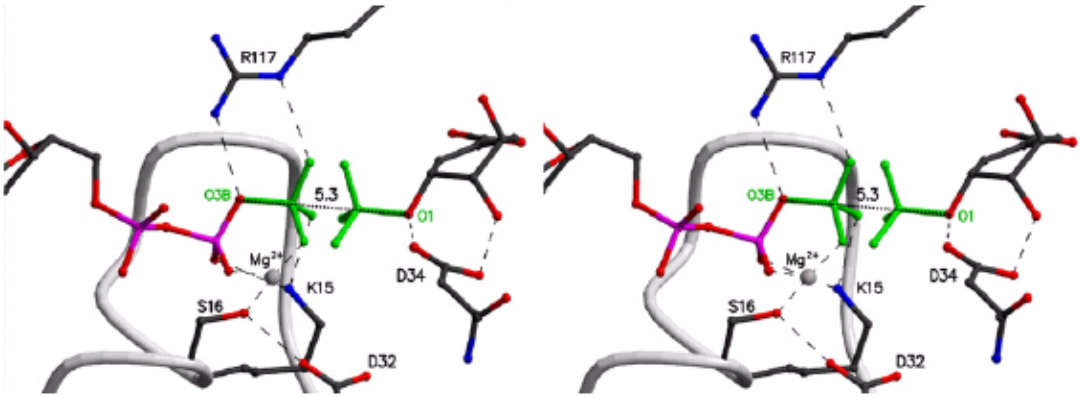

Figure 127 Structure model of the transition state for in-line associative phosphoryl transfer
Reprinted from reference 301 with the permission of Elsevier B.V.

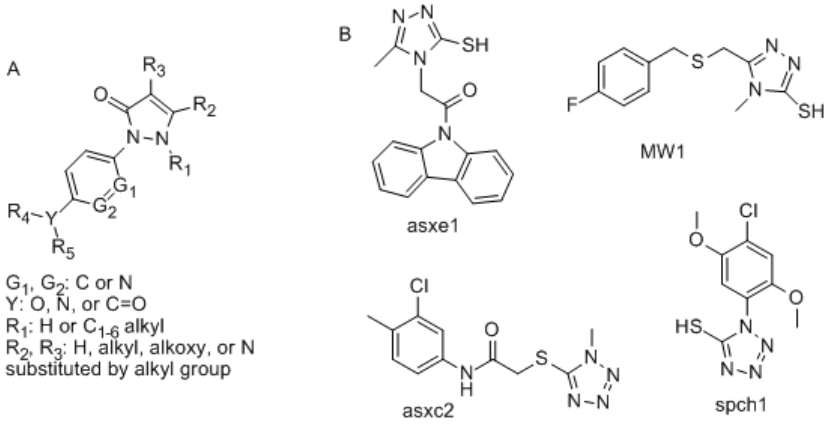

Figure 128 (A) Pyrazolone derivatives; (B) Inhibitors with heteroaromatic system

5.7 NAD Kinase

Mtb NAD kinase carries out the phosphorylation of NAD to form NADP and hence is important for the control of essential cellular processes. The Mtb NAD kinase was identified being able to utilize either inorganic polyphosphate [poly(P)] or ATP as a phosphate donor.[312] The kinetic analysis showed that it has a higher affinity for poly(P) than ATP,[313] whereas human NAD kinase only utilizes ATP.[314] Additionally, the full length of MtNAD kinase has an allosteric aspect which was not observed in the human NAD kinase.[313] In a synthetic study completed by Bonnac *et al*., the NAD^+ analogue benzamide adenine dinucleotide (BAD) displayed a weak inhibition on human NAD kinase but not on Mtb enzyme,[315] which also provided the evidence to support the difference between Mtb and the human NAD kinases. The crystal structure of MtNAD kinase has been solved as apo or using NAD as a substrate.[316,317] Modeling studies confirmed that the GGDG motif and residues 189-210 are crucial in catalysis, which was identified by comparing activity with mutants.[313] In addition, the importance of an NE/D short motif in NAD-binding was observed.[317] Although MtNAD has the potential to be a good target, the development of inhibitor for it seems difficult. When screening was completed using PknB, PknG, NAD kinase, and NAD synthetase as multiple targets, as discussed previously, only one compound, VI-13632, exhibited inhibition at IC_{50} of 53 μM.[207] Some other reported analogues showing inhibition of MtNAD are not selective. They are able to inhibit human NAD kinase as well.[318]

5.8 Pantothenate Kinase

Pantothenate kinase (PanK, CoaA) is a key regulatory enzyme for coenzyme-A (CoA) biosynthesis.[319] It phosphorylates pantothenate at its 4'-position forming 4'-phosphopantothenate, which is involved in the CoA biosynthetic pathway. The prokaryotic PanKs are classified in the P-loop kinase family, whereas the eukaryotic PanKs are identified as a member of the

ribonuclease H-like family.[320] This classification indicates their sequence and structural disparity. There are three isoforms of PanK found: most bacteria have type I PanK, a few bacteria and eukaryotes possess type II Pank, and type III enzyme was identified in several bacteria recently. Mtb has both type I and type III enzymes; however, only type I was found to be crucial for the function of Mtb in a gene inactivation study.[321] The crystal structure of type I MtPanK was solved by using CoA,[322,323] citrate, nonhydrolysable ATP analogue AMPPCP, ADP and pantothenate,[323] GMPPCP, GDP, GDP or GMPPCP with pantothenate, GDP with phosphopantothenate[324] as substrates. MtPanK presents a dual substrate specificity for both ATP and GTP.[324,325] When compared with the crystal structure of *E. coli* PanK and analyzing other known sequences of bacterial PanKs, there are some small differences in the N-terminal stretch, C-terminal region of H4, the subsequent loop, and another region involving the loop between S6 and H10, which are related to the intersubunit interface in the dimeric molecule **(Figure 129)**.[322] All the differences can be considered in inhibitor design to improve the selectivity. It is reported that the activity of murine pantothenate kinase isoform PanK3 is feedback-regulated by acetyl-CoA (IC_{50}=1 μM) and palmitoyl-CoA (IC_{50}=2 μM) through competitively binding to the ATP.[326] However, their inhibitory activities on Mtb are not known. Pantothenol was reported to exert inhibition on bacterial PanK as well.[327,328] The inhibition could be attributed to the formation of 4'-phosphopatothenol when pantothenol serving as a substrate of PanK, thus competitively inhibiting 4'-phosphopantothenoylcysteine decarboxylase (CoaBC) to utilize 4'-phosphopatothenate.[329] A high-throughput screening of MtPanK inhibitors was performed by measuring the protein thermal stability. This assay reveals the mode of the inhibition such as competitive or noncompetitive. Among all the compounds screened, a triazole compound displayed an ATP-competitive inhibition with IC_{50} at 0.07 μM; a thiazole compound showed an

uncompetitive inhibition with IC_{50} at 2.57 μM; and a biaryl acetic acid compound exerted mixed inhibitions with the best IC_{50} at 0.12 μM **(Figure 130)**.[330]

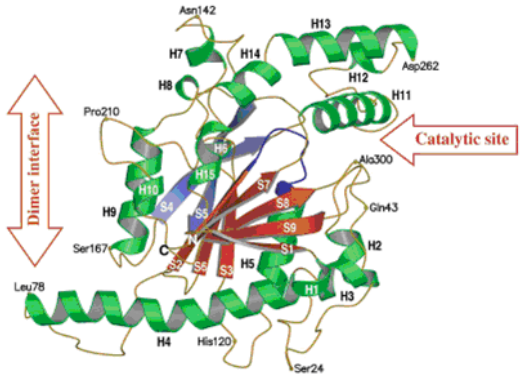

Figure 129 The PanK subunit
N-terminus and C-terminus are marked as N and C.
Reprinted from reference 322 with the permission of The International Union of Crystallography

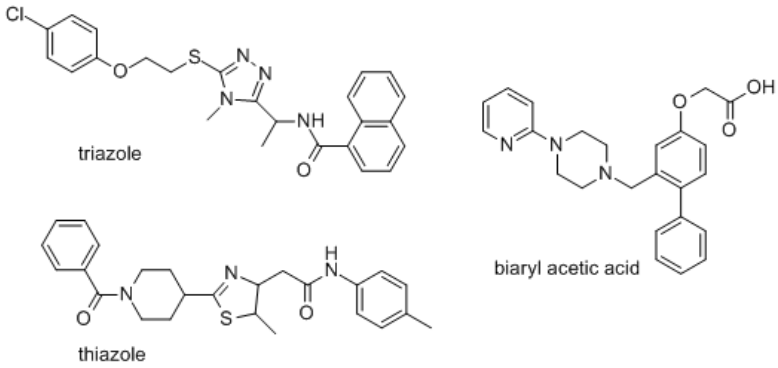

Figure 130 Structures of MtPanK inhibitors

5.9 Dephosphocoenzyme A Kinase

Dephosphocoenzyme A kinase (CoaE), participating in the last step of the mycobacterial CoA biosynthesis pathway, is crucial to the Mtb's survival as well. Its sequence similarity to that of human is as low as 15%.[331] Therefore, it could be another potential target for Mtb inhibitors. The dephosphocoenzyme A (DCoA) and CTP are substrates of CoaE.[331] MtCoaE belongs to P-loop containing NMPK family, which has mobile LID and CoA domains. The enzyme presents as a mixture of the monomer and trimer. The trimer form restricts the mobility of LID and CoA domains due to its spatial constraints, thus keeping the enzyme inactive. When binding to its

specific substrate DCoA, the conformation of CoaE changed, and the spatial constraints are released, thus leading its active monomer become predominant.[332] The activation, however, could be prevented in the presence of CTP. The oligomeric equilibrium suggests that CTP analogues could be potent MtCoaE inhibitors.[332]

6. Conclusion and Perspectives

Protein kinases are one of the largest protein families, and are essential in regulating cell activities. Kinase inhibitors have been attracting attention because of their potential therapeutic utility. However, no inhibitor of Mtb histidine kinases targeting two-component system has been generated to date. As we discussed above, some HKs such as MtrB, PhoR are not essential for the growth of Mtb. In some two-component systems such as SenX3-RegX3, a phosphoryl group can also be transferred from other small phosphodonor compounds to RR.[163] Hence, more studies focused on structural analysis of RRs instead of HKs.[146,333,334,335,336] However, considering the characteristics of two-component systems, histidine kinases in Mtb still can be good targets. Firstly, two-component systems regulate antimicrobial resistance. The resistances of some drugs such as vancomycin, β-lactams, polymixin, and tetracycline are all related to two-component systems.[337] Secondly, pairs including DosS/DosT/DosR, MprB/MprA, SenX3/RegX3, are absolutely required for mycobacterium growth and persistence, while eukaryotes do not use a two-component system for signal transduction. Inhibitors targeting these HK/RR pairs therefore should possess good selectivity. Moreover, the autophosphorylation of HKs always occurs in the catalytic domain with the conserved histidine residue, indicating that an inhibitor might be able to target multiple two-component systems. A recent study on a noncognate HK/RR interaction between DosS/NarL provided a clue of cross interaction between HK/RR,[338] which also suggest the possibility of multiple targets on the two-component system. In previous reviews, many HKs

including AlgR2, CheA, NRII, KinA, HpkA, YycG have been studied as targets for antimicrobial agents.[337,339] However, the functions of some two-component systems in Mtb, such as SenX3/RegX3, NarS/NarL and TcrY/TcrX are not well characterized. To develop HK inhibitors, more studies need to be conducted.

Unlike other prokaryotes, many serine/threonine protein kinases take the place of two-component systems in signal transduction in Mtb. **Table 19** shows the sequence identity/similarity for the kinase domains for pairs of the STPKs, with the lowest identity ~19% and the highest ~70%. It has been shown that *M. tuberculosis* STPKs form a distinct cluster close to human CK1.[169] The sequence identity with human CK1a of the Mtb Pkns varies from 9.9-16.5%, which is significantly lower than the identity within Pkns. These STPKs can be good targets because of the good selectivity. As we discussed above, some inhibitors of PknB and PknG have already shown potential in treating TB. Except for STPKs, PTKs could be interesting, even if there is only one tyrosine kinase found in Mtb until now. With the studies and knowledge on this family increasing, PTKs might be becoming more attractive targets.

Table 19 Sequence identity in the kinase domain of STPKs and human CK1a computed from multiple sequence alignment[#]

	PknA	**PknB**	**PknD**	**PknE**	**PknF**	**PknG**	**PknH**	**PknI**	**PknJ**	**PknK**
PknB	41.5									
PknD	36.1	37.3								
PknE	37.4	35.9	65.1							
PknF	32.7	38.6	39	36.9						
PknG	23.5	21.1	22	20.2	19.3					
PknH	36.9	35.4	69.3	69.6	39	20.2				
PknI	26.2	27.2	32.9	30.4	49.2	19.7	32.9			
PknJ	33	41.5	40.9	38.3	48.3	19.1	38.7	39.1		
PknK	32.5	34.9	35.2	31.4	31.6	20.2	32.1	27.6	34.2	
PknL	40.2	44.7	34.2	34.7	32.2	22	32.3	23.6	32.2	34.7

Multiple sequence alignment was carried using ClustalW [340] and sequence identity matrix was calculated using BioEdit [341]

The mechanism of action employed by nucleoside analogues differs from existing antitubercular drugs, which might help to avoid cross-resistance. To use the best studied ADK

and TMPK as examples, both of them have low sequence and structural homology to eukaryotes which suggests they are potential antibacterial targets. Other kinases in Mtb display different characteristics from those in humans as well, such as AspK and SK are observed in bacteria, fungi, algae, or higher plants, but not in mammals; MtNAD is [poly(P)]/ATP dependent of which poly(P) has higher affinity, while that of human is only ATP-dependent; MtPanK shows sequence and structural disparity from both human and other bacteria, all these aspects can be used to develop highly selective and less toxic antibacterial agents.

Natural products, especially marine organisms which are widely distributed over 70% of the earth's surface, provide a major source of new drug candidates. All the species are able to produce secondary metabolites with different activities due to defense, competition, or a number of other environmental reasons.[72] Many potent kinase inhibitors **(Table 20)** have been isolated to date. One of the major tools used in new drug development is the screening of drug leads from natural products. With the development of bioassays, many techniques are utilized for the screening of Mtb kinase inhibitors: The measurement of protein thermal stability was applied into screening of MtPanK;[330] A high-throughput screening using the measurement of phosphorylation status via detecting the remaining ATP was utilized to explore PknB inhibitors;[208] To improve the accuracy of the assay, a method using western blot coupling to mass spectrometry was designed to identify the substrates of PknB;[342] Additionally, with the well characterized protein structures, as well as computational prediction of drug targets using a complete proteome level comparisons between Mtb and other species,[343] the development of Mtb kinase inhibitors could benefit from combinatorial and rational drug designs. Natural and synthetic products screening can provide antitubercular leads, and with the use of computer aided drug design (CADD), we are confident that Mtb kinase inhibitors with high selectivity will

indeed be developed.

Table 20 Typical kinase inhibitors from marine natural products

Compound	Structure	Origin	Activity	Reference
Stypoquinonic acid	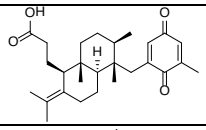	Brown alga *Stypopodium zonale*	Tyrosine kinase inhibitor	344
Xestoquinone	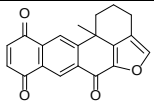	Sponge *Xestospongia* sp.	Antimalarial Pfnek-1 inhibitor	345
B-5354C	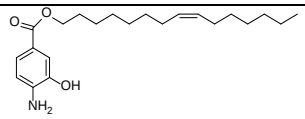	Marine bacterium SANK 71896	Sphingosine kinase inhibitor	346
Halenaquinone	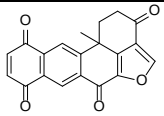	Sponge *X. exigua*	Phosphatidylinositol 3-kinase inhibitor	347
Hymenialdisine	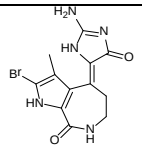	Sponge *Axinella damicornis*	GSK-3β and CK1 inhibitor	348
Microxine	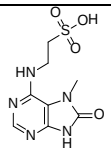	Sponge *Microxina* sp.	CDC2 kinase inhibitor	349
Pheophytin	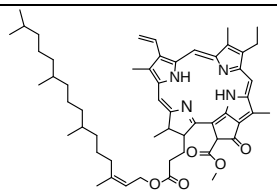	Brown alga *Sargassum fulvellum*	A representative mitogen-activated protein kinase inhibitor	350
Variolin B	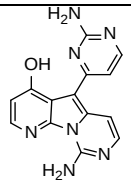	Sponge *Kirkpatrickia variolosa*	Cyclin-dependent kinases inhibitor	351
Deoxyvariolin B	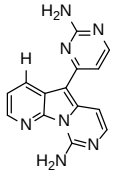	Variolin B derived		

BIBLIOGRAPHY

1. (a) American Cancer Society, Cancer Facts and Figures 2006. *Atlanta: American Cancer Society* **2006,** *2006*; (b) American Cancer Society, Cancer Facts and Figures 2007. *Atlanta: American Cancer Society* **2007,** *2007*; (c) American Cancer Society, Cancer Facts and Figures 2008. *Atlanta: American Cancer Society* **2008,** *2008*; (d) American Cancer Society, Cancer Facts and Figures 2009. *Atlanta: American Cancer Society* **2009,** *2009*; (e) American Cancer Society, Cancer Facts and Figures 2010. *Atlanta: American Cancer Society* **2010,** *2010*; (f) American Cancer Society, Cancer Facts and Figures 2011. *Atlanta: American Cancer Society* **2011,** *2011*; (g) American Cancer Society, Cancer Facts and Figures 2012. *Atlanta: American Cancer Society* **2012,** *2012*.

2. National Cancer Institute Types of treatment. http://www.cancer.gov/cancertopics/treatment/types-of-treatment (accessed April 18, 2011).

3. Engelman, J. A.; Settleman, J., Acquired resistance to tyrosine kinase inhibitors during cancer therapy. *Curr. Opin. Genet. Dev.* **2008,** *18*, 73-79.

4. Newman, D. J.; Cragg, G. M., Natural products as sources of new drugs over the last 25 years. *J. Nat. Prod.* **2007,** *70*, 461-477.

5. Valoti, G.; Nicoletti, M. I.; Pellegrino, A.; Jimeno, J.; Hendriks, H.; D'Incalci, M.; Faircloth, G.; Giavazzi, R., Ecteinascidin-743, a new marine natural product with potent antitumor activity on human ovarian carcinoma xenografts. *Clin. Cancer Res.* **1998,** *4*, 1977-1983.

6. Mayer, A. M. S.; Glaser, K. B.; Cuevas, C.; Jacobs, R. S.; Kem, W.; Little, R. D.; McIntosh, J. M.; Newman, D. J.; Potts, B. C.; Shuster, D. E., The odyssey of marine pharmaceuticals: a current pipeline perspective. *Trends Pharmacol. Sci.* **2010,** *31*, 255-265.

7. Madden, T.; Tran, H. T.; Beck, D.; Huie, R.; Newman, R. A.; Pusztai, L.; Wright, J. J.; Abbruzzese, J. L., Novel marine-derived anticancer agents: a phase I clinical, pharmacoglogical, and pharmacodynamic study of dolastatin 10 (NSC 376128) in patients with advanced solid tumors. *Clin. Cancer Res.* **2000,** *6*, 1293-1301.

8. Von Mehren, M.; Balcerzak, S. P.; Kraft, A. S.; Edmonson, J. H.; Okuno, S. H.; Davey, M.; McLaughlin, S.; Beard, M. T.; Rogatko, A., Phase II trial of dolastatin-10, a novel anti-tubulin aget, in metastatic soft tissue sarcomas. *Sarcoma* **2004,** *8*, 107-111.

9. Kindler, H. L.; Tothy, P. K.; Wolff, R.; McCormack, R. A.; Abbruzzese, J. L.; Mani, S.; Wade-Oliver, K. T.; Vokes, E. E., Phase II trials of dolastatin-10 in advanced pancreaticobiliary cancers. *Invest. New Drugs* **2005,** *23*, 489-493.

10. Watanabe, J.; Minami, M.; Kobayashi, M., Antitumor activity of TZT-1027 (soblidotin). *Anticancer Res.* **2006,** *26*, 1973-1982.

11. Hamann, M. T.; Scheuer, P. J., Kahalalide F: a bioactive depsipeptide from the sacoglossan mollusk *Elysia rufescens* and the green alga *Bryopsis* sp. *J. Am. Chem. Soc.* **1993,** *115*, 5825-5826.

12. Hamann, M. T.; Otto, C. S.; Scheuer, P. J.; Dunbar, D.C. Kahalalides: bioactive peptides from a marine mollusk *Elysia rufescens* and its algal diet *Bryopsis* sp. *J. Org. Chem.* **1996,** *61*, 6594-6600.

13. Hill, R. T.; Hamann, M. T.; Enticknap, J.; Rao, K. V. Kahalalide-producing bacteria. WO 2005/042720 A2, 2005.

14. Faircloth, G.; Carmen Cuevas Marchante, M., Kahalalide F and ES285: potent anticancer agents from marine molluscs. *Prog. Mol. Subcell. Biol.* **2006,** *43*, 363-379.

15. Suárez, Y.; González, L.; Cuadrado, A.; Berciano, M.; Lafarga, m.; Muñoz, A., Kahalalide F, a new marine-derived compound, induces oncosis in human prostate and breast cancer cells. *Mol. Cancer Ther.* **2003,** *2*, 863-872.

16. Hamann, M. T., Technology evaluation: kahalalide F, PharmaMar. *Curr. Opin. Mol. Ther.* **2004,** *6*, 657-665.

17. García-Rocha, M.; Bonay, P.; Jesús, A., The antitumoral compound kahalalide F acts on cell lysosomes. *Cancer Lett.* **1996,** *99*, 43-50.

18. Janmaat, M. L., Kahalalide F induces necrosis-like cell death that involves depletion of ErbB3 and inhibition of Akt signaling. *Mol. Pharmacol.* **2005,** *68*, 502-510.

19. Hynes, N. E.; Lane, H. A., ERBB receptors and cancer: the complexity of targeted inhibitors. *Nat. Rev. Cancer* **2005,** *5*, 341-354.

20. Tsujioka, H.; Yotsumoto, F.; Shirota, K.; Horiuchi, S.; Yoshizato, T.; Kuroki, M.; Miyamoto, S., Emerging strategies for ErbB ligand-based targeted therapy for cancer. *Anticancer Res.* **2010,** *30*, 3107-3112.

21. Cai, Z.; Zhang, H.; Liu, J.; Berezov, A.; Murali, R.; Wang, Q.; Greene, M. I., Targeting erbB receptors. *Semin. Cell Dev. Biol.* **2010,** *21*, 961-966.

22. Pfizer. Dacomitinib (pf-00299804) 2011. http://www.pfizer.com/files/news/esmo/dacomitinib_pf_00299804_fact_sheet.pdf (accessed June 13, 2012).

23. Pardo, B.; Paz-Ares, L.; Tabernero, J.; Ciruelos, E.; Garcia, M.; Salazar, R.; Lopez, A.; Blanco, M.; Nieto, A.; Jimeno, J.; Izquierdo, M. A.; Trigo, J. M., Phase I clinical and pharmacokinetic study of kahalalide F administered weekly as a 1-hour infusion to patients with advanced solid tumors. *Clin. Cancer Res.* **2008,** *14*, 1116-1123.

24. Rademaker-Lakhai, J. M.; Horenblas, S.; Meinhardt, W.; Stokvis, E.; de Reijke, T. M.; Jimeno, J. M.; Lopez-Lazaro, L.; Lopez Martin, J. A.; Beijnen, J. H.; Schellens, J. H., Phase I clinical and pharmacokinetic study of kahalalide F in patients with advanced androgen refractory prostate cancer. *Clin. Cancer Res.* **2005,** *11*, 1854-1862.

25. Martín-Algarra, S.; Espinosa, E.; Rubió, J.; López, J. J. L.; Manzano, J. L.; Carrión, L. A.; Plazaola, A.; Tanovic, A.; Paz-Ares, L., Phase II study of weekly kahalalide F in patients with advanced malignant melanoma. *Eur. J. Cancer* **2009,** *45*, 732-735.

26. Izquierdo, M. A. Use of KF in psoriasis. WO 2004/075910 A1, 2004.

27. Jiménez, J. C.; López-Macià, A.; Gracia, C.; Varón, S.; Carrascal, M.; Caba, J. M.; Royo, M.; Francesch, A. M.; Cuevas, C.; Giralt, E.; Albericio, F., Structure-activity relationship of kahalalide F synthetic analogues. *J. Med. Chem.* **2008,** *51*, 4920-4931.

28. López-Macià, À.; Jiménez, J. C.; Royo, M.; Giralt, E.; Albericio, F., Synthesis and structure determination of kahalalide F. *J. Am. Chem. Soc.* **2001,** *123*, 11398-11401.

29. University of Hawaii *Bryopsis pennata*. http://www.hawaii.edu/reefalgae/invasive_algae/chloro/bryopsis_pennata.htm (accessed June 14, 2012).

30. Shilabin, A. G.; Kasanah, N.; Wedge, D. E.; Hamann, M. T., Lysosome and HER3 (ErbB3) selective anticancer agent kahalalide F: semisynthetic modifications and antifungal lead-exploration studies. *J. Med. Chem.* **2007,** *50*, 4340-4350.

31. Shilabin, A. G.; Hamann, M. T., In vitro and in vivo evaluation of select kahalalide F analogs with antitumor and antifungal activities. *Bioorg. Med. Chem.* **2011,** *19*, 6628-6632.

32. Jiménez, J. C.; López-Macià, A.; Gracia, C.; Varón, S.; Carrascal, M.; Caba, J. M.; Royo, M.; Francesch, A. M.; Cuevas, C.; Giralt, E.; Albericio, F., Structure-activity relationship of kahalalide F synthetic analogues. *J. Med. Chem.* **2008,** *51*, 4920-4931.

33. Ruffles, G. K. Preparation of kahalalide F analogs as antitumor agents. WO 2005/023846 A1, 2005.

34. Yamage, M.; Yoshiyama, M.; Grab, D. J.; Kubo, M.; Iwasaki, T.; Kitani, H.; Ishibashi, J.; Yamakawa, M., Characteristics of novel inset difensin-based membrane-disrupting trypanocidal peptides. *Biosci. Biotechnol. Biochem.* **2009,** *73*, 1520-1526.

35. Valivaveetil, F. I.; Sekedat, M.; Mackinnon, R.; Muir, T. W., Glycine as a D-amino acid surrogate in the K^+-selectivity filter. *Proc. Natl. Acad. Sci. U. S. A.* **2004,** *101*.

36. Tugyi, R.; Uray, K.; Iyán, D.; Fellinger, E.; Perkins, A.; Hudecz, F., Partial D-amino acid substitution: improved enzymatic stability and preserved Ab recognition of a MUC2 epitope peptide. *Proc. Natl. Acad. Sci. U. S. A.* **2005,** *102*.

37. Koichi, I.; Toshio, A., N-O acyl rearrangement. *Methods Enzymol.* **1967,** *11*, 262-282.

38. Singh, R. P.; Shreeve, J. n. M., Recent advances in nucleophilic fluorination reactions of organic compounds using Deoxofluor and DAST. *Synthesis* **2002,** *17*, 2561-2578.

39. Phillips, A. J.; Uto, Y.; Wipf, P.; Reno, M. J.; Williams, D. R., Synthesis of functionalized oxazolines and oxazoles with DAST and Deoxo-Fluor. *Org. Lett.* **2000,** *2*, 1165-1168.

40. L'Heureux, A. L.; Beaulieu, F.; Bennett, C.; Bill, D. R.; Clayton, S.; LaFlamme, F.; Mirmehrabi, M.; Tadayon, S.; Tovell, D.; Couturier, M., Aminodifluorosulfinium salts: selective fluorination reagents with enhanced thermal stability and ease of handling. *J. Org. Chem.* **2010,** *75*, 3401-3411.

41. Sutherland, A.; Vederas, J. C., The first isolation of an alkoxy-*N*,*N*-dialkylaminodifluorosulfane from the reaction of an alcohol and DAST: an efficient synthesis of (2S,3R,6S)-3-fluoro-2,6-diaminopimelic acid. *Chem. Commun.* **1999**, 1739-1740.

42. Sparidans, R. W.; Stokvis, E.; Jimeno, J. M.; López-Lázaro, L.; Schellens, J. H.; Beijnen, J. H., Chemical and enzymatic stability of a cyclic depsipeptide, the novel, marine-derived, anti-cancer agent kahalalide F. *Anti Cancer Drugs* **2001,** *12*, 575-582.

43. Mikhaylova, M.; Mori, N.; Wildes, F. B.; Walczak, P.; Gimi, B.; Bhujwalla, Z. M., Hypoxia increase breast cancer cell-induced lymphatic endothelial cell migration. *Neoplasia* **2008,** *10*, 380-389.

44. Gao, J.; Caballero-George, C.; Wang, B.; Rao, K. V.; Shilabin, A. G.; Hamann, M. T., 5-OHKF and norKA, depsipeptides from a Hawaiian collection of *Bryopsis pennata*: binding properties for norKA to the human neuropeptide Y Y_1 receptor. *J. Nat. Prod.* **2009,** *72*, 2172-2176.

45. Goetz, G.; Nakao, Y.; Scheuer, P. J., Two acyclic kahalalides from the sacoglossan mollusk *Elysia rufescens*. *J. Nat. Prod.* **1997,** *60*, 562-567.

46. Kan, Y.; Fujita, T.; Sakamoto, B.; Hokama, Y.; Nagai, H., Kahalalide K, a new cyclic depsipeptide from the Hawaiian green alga *Bryopsis* species. *J. Nat. Prod.* **1999,** *62*, 1169-1172.

47. Horgen, F. D.; delos Santos, D. B.; Goetz, G.; Sakamoto, B.; Kan, Y.; Nagai, H.; Scheuer, P. J., A new depsipeptide from the sacoglossan mollusk *Elysia ornata* and the green alga *Bryopsis* species. *J. Nat. Prod.* **2000,** *63*, 152-154.

48. Dmitrenok, A.; Iwashita, T.; Nakajima, T.; Sakamoto, B.; Namikoshi, M.; Nagai, H., New cyclic depsipeptides from the green alga *Bryopsis* species; application of a carboxypeptidase hydrolysis reaction to the structure determination. *Tetrahedron* **2006,** *62*, 1301-1308.

49. Ashour, M.; Edrada, R.; Ebel, R.; Wray, V.; Wätjen, W.; Padmakumar, K.; Müller, W. E. G.; Lin, W. H.; Proksch, P., Kahalalide derivatives from the Indian sacoglossan mollusk *Elysia grandifolia*. *J. Nat. Prod.* **2006,** *69*, 1547-1553.

50. Tilvi, S., Tandem mass spectrometry of kahalalides: identification of two new cyclic depsipeptides, kahalalide R and S from *Elysia grandifolia*. *J. Mass Spectrom.* **2007,** *42*, 70-80.

51. Rao, K. V.; Na, M.; Cook, J. C.; Peng, J.; Matsumoto, R.; Hamann, M. T., Kahalalides V–Y isolated from a Hawaiian collection of the sacoglossan mollusk *Elysia rufesens*. *J. Nat. Prod.* **2008,** *71*, 772-778.

52. Mohammed, R.; Peng, J.; Kelly, M.; Hamann, M. T., Cyclic heptapeptides from the Jamaican sponge *Stylissa caribica*. *J. Nat. Prod.* **2006,** *69*, 1739-1744.

53. NCI. Natural products repository. http://dtp.nci.nih.gov/branches/npb/repository.html (accessed July 1, 2012).

54. Boyd, M. R. The NCI in vitro anticancer drug discovery screen: concept, implementation and operation, 1985-1995. http://home.ncifcrf.gov/mtdp/catalog/full_text/paper309/Paper309.pdf (accessed July 1, 2012).

55. NCI. Drug Discovery at the National Cancer Institute: Fact Sheet. http://www.cancer.gov/cancertopics/factsheet/NCI/drugdiscovery (accessed July 1, 2012).

56. Kobayashi, J.; Cheng, J.-F.; Wälchli, M. R.; Nakamura, H.; Hirata, Y.; Sasaki, T.; Ohizumi, Y., Cystodytins A, B, and C, novel tetracyclic aromatic alkaloids with potent antineoplastic activity from the Okinawan tunicate *Cystodytes dellechiajei*. *J. Org. Chem.* **1988,** *53*, 1800-1804.

57. Kobayashi, J.; Tsuda, M.; Tanabe, A.; Ishibashi, M.; Cheng, J.-F.; Yamamura, S.; Sasaki, T., Cystodytins D-I, new cytotoxic tetracyclic aromatic alkaloids from the Okinawan marine tunicate *Cystodytes dellechiaje*. *J. Nat. Prod.* **1991,** *54*, 1634-1638.

58. McDonald, L. A.; Eldredge, G. S.; Barrows, L. R.; Ireland, C. M., Inhibition of topoisomerase II catalytic activity by pyridoacridine alkaloids from a *Cystodytes* sp. ascidian: a mechanism for the apparent intercalator-induced inhibition of topoisomerase II. *J. Med. Chem.* **1994,** *37*, 3819-3827.

59. Hong, T. W.; Jímenez, D. R.; Molinski, T. F., Agelastatins C and D, new pentacyclic bromopyrroles from the sponge *Cymbastela* sp., and potent arthropod toxicity of (-)-agelastatin A. *J. Nat. Prod.* **1998,** *61*, 158-161.

60. Tilvi, S.; Moriou, C.; Martin, M.-T.; Gallard, J.-F.; Sorres, J.; Patel, K.; Petek, S.; Debitus, C.; Ermolenko, L.; Al-Mourabit, A., Agelastatin E, agelastatin F, and benzosceptrin C from the marine sponge *Agelas dendromorpha*. *J. Nat. Prod.* **2010,** *73*, 720-723.

61. D'Ambrosio, M.; Guerriero, A.; Debitus, C.; Ribes, O.; Pusset, J.; Leroy, S.; Pietra, F., Agelastatin A, a new skeleton cytotoxic alkaloid of the oroidin family. Isolation from the axinellid sponge *Agelas dendromorpha* of the Coral Sea. *J. Chem. Soc. Chem. Commun.* **1993,** *16*, 1305-1306.

62. D'Ambrosio, M.; Guerriero, A.; Ripamonti, M.; Debitus, C.; Waikedre, J.; Pietra, F., The activity centres of agelastatin A, a strongly cytotoxic alkaloid of the Coral Sea axinellid sponge *Agelas dendromorpha*, as determined by comparative bioassays with semisynthetic derivatives. *Helv. Chim. Acta* **1996,** *79*, 727-735.

63. Chang, C. W. J.; Patra, A.; Baker, J. A.; Scheuer, P. J., Kalihinols, multifunctional diterpenoid antibiotics from marine sponges *Acanthella* spp. *J. Am. Chem. Soc.* **1987,** *109*, 6119-6123.

64. Yang, L. H.; Lee, O. O.; Jin, T.; Li, X. C.; Qian, P. Y., Antifouling properties of 10β-formamidokalihinol-A and kalihinol A isolated from the marine sponge *Acanthella cavernosa*. *Biofouling* **2006,** *22*, 23-32.

65. Ford, P. W.; Davidson, B. S., Plakinidine D, a new pyrroloacridine alkaloid from the ascidian *Didemnum rubeum*. *J. Nat. Prod.* **1997,** *60*, 1051-1053.

66. World Health Organization Media Center. Food safety and foodborne illness. Fact Sheet No.237 2007. http://www.who.int/mediacentre/factsheets/fs237/en/. (accessed August 19, 2010).

67. Bureau of Medicine and Surgery. Manual of naval preventive medicine. http://www.tpub.com/content/aviation2/P-5010-1/P-5010-10128.htm (accessed Sepetember 19, 2010).

68. U.S Department of Agriculture. Bacterial foodborne disease: medical costs and productivity losses. http://www.ers.usda.gov/publications/aer741/aer741.pdf (accessed August 20, 2010).

69. Center for Disease Control and Prevention. Foodborne illness: most common foodborne diseases
2005. http://www.cdc.gov/ncidod/dbmd/diseaseinfo/foodborneinfections_g.htm#mostcommon (accessed August 19, 2010).

70. McAuliffe, O.; Ross, R. P.; Hill, C., Lantibiotics: structure, biosynthesis and mode of action. *FEMS Microbiol. Rev.* **2001,** *25*, 285-308.

71. Cotter, P. D.; Hill, C.; Ross, R. P., Bacteriocins: developing innate immunity for food. *Nat. Rev. Microbiol.* **2005,** *3*, 777-788.

72. Engel, S.; Jensen, P.; Fenical, W., Chemical ecology of marine microbial defense. *J. Chem. Ecol.* **2002,** *28*, 1971-1985.

73. Williams, R. B.; Henrikson, J. C.; Hoover, A. R.; Lee, A. E.; Cichewicz, R. H., Epigenetic remodeling of the fungal secondary metabolome. *Org. Biomol. Chem.* **2008,** *6*, 1895.

74. Oh, D.-C.; Kauffman, C. A.; Jensen, P. R.; Fenical, W., Induced production of emericellamides A and B from the marine-derived fungus *Emericella* sp. in competing co-culture. *J. Nat. Prod.* **2007,** *70,* 515-520.

75. Casadesus, J.; Low, D., Epigenetic gene regulation in the bacterial world. *Microbiol. Mol. Biol. Rev.* **2006,** *70,* 830-856.

76. Turnbough, J. C. L., Regulation of bacterial gene expression by the NTP substrates of transcription initiation. *Mol. Microbiol.* **2008,** *69,* 10-14.

77. Daniels, R.; Vanderleyden, J.; Michiels, J., Quorum sensing and swarming migration in bacteria. *FEMS Microbiol. Rev.* **2004,** *28,* 261-289.

78. Mikami, K.; Kanesaki, Y.; Suzuki, I.; Murata, N., The histidine kinase Hik33 perceives osmotic stress and cold stress in *Synechocystis* sp. PCC 6803. *Mol. Microbiol.* **2002,** *46*, 905-915.

79. Martín, J.-F.; Liras, P., Engineering of regulatory cascades and networks controlling antibiotic biosynthesis in Streptomyces. *Curr. Opin. Microbiol.* **2010,** *13*, 263-273.

80. Edwards, J. R.; Hayashi, J. A., Structure of a rhamnolipid from *Pseudomonas aeruginosa*. *Arch. Biochem. Biophys.* **1965,** *111*, 415-421.

81. Sharma, A.; Jansen, R.; Nimtz, M.; Johri, B. N.; Wray, V., Rhamnolipids from the Rhizosphere bacterium *Pseudomonas* sp. GRP_3 that reduces damping-off disease in Chilli and tomato nurseries. *J. Nat. Prod.* **2007,** *70,* 941-947.

82. Saleh, A.; Friesen, J.; Baumeister, S.; Gross, U.; Bohne, W., Growth inhibition of *Toxoplasma gondii* and *Plasmodium falciparum* by nanomolar concentrations of 1-hydroxy-2-dodecyl-4(1*H*)quinolone, a high-affinity inhibitor of alternative (Type II) NADH dehydrogenases. *Antimicrob. Agents Chemother.* **2007,** *51*, 1217-1222.

83. Cross, R. M.; Monastyrskyi, A.; Mutka, T. S.; Burrows, J. N.; Kyle, D. E.; Manetsch, R., Endochin optimization: structure-activity and structure-property relationship studies of 3-substituted-2-methyl-4(1*H*)-quinolones with antimalarial activity. *J. Med. Chem.* **2010,** *53*, 7076-7094.

84. Basak, S. C.; Mills, D.; Hawkins, D. M.; Bhattacharjee, A. K., Quantitative structure–activity relationship studies of antimalarial compounds from their calculated mathematical descriptors. *SAR QSAR Environ. Res.* **2010,** *21,* 103-125.

85. Pavankumar, A. R.; Ayyappasamy, S. P.; Sankaran, K., Small RNA fragments in complex culture media cause alterations in protein profiles of three species of bacteria. *Biotechniques* **2012,** *52*, 167-172.

86. Hamann, M. T.; Alonso, D.; Martin-Aparicio, E.; Fuertes, A.; Perez-Puerto, M. J.; Castro, A.; Morales, S.; Navarro, M. L.; Del Monte-Millan, M.; Medina, M.; Pennaka, H.; Balaiah, A.; Peng, J.; Cook, J. C.; Wahyuono, S.; Martinez, A., Glycogen synthase kinase-2 (GSK-3) inhibitory activity and structure-activity relationship (SAR) studies of the manzamine alkaloids. Potential for Alzheimer's disease. *J. Nat. Prod.* **2007,** *70*, 1397-1405.

87. Cipre, A.; O'Malley, D. P.; Finlay, D.; Baran, P. S.; Vuori, K., Sceptrin, a marine natural compound, inhibits cell motility in a variety of cancer cell lines. *ACS Chem. Biol.* **2010,** *5*, 195-202.

88. Pettit, R. K., Mixed dermentation for natural product drug discovery. *Appl. Microbiol. Biotechnol.* **2009,** *83*, 19-25.

89. Slattery, M.; Rajbhandari, I.; Wesson, K., Competition-mediated antibiotic induction in the marine bacterium *Strepomyces tenjimariensis*. *Microb. Ecol.* **2001,** *41*, 90-96.

90. Fletcher, M. P.; Stephen, P. D.; Shanika, A. C.; Chhabra, S. R.; Miguel, C.; Paul, W., A dual biosensor for 2-alkyl-4-quinolone quorum-sensing signal molecules. *Environ. Microbiol.* **2007,** *9*, 2683-2693.

91. NCCLS, Reference method for broth dilution antifungal susceptibility testing of yeasts: approved standard M27-A2. *National Committee on Clinical Laboratory Standards* **2002,** *22*, 15.

92. NCCLS, Methods for diultion antimicrobial susceptibility test for bacteria that grow aerobically: approved standard seventh edition M7-A7. *National Committee on Clinical Laboratory Standards* **2006,** *26*, 2.

93. NCCLS, Susceptibility testing of mycobacteria, nocardia, and other aerobic actinomycetes: tentative standard-approved standard, M24-A. *National Committee on Clinical Laboratory Standards* **2003,** *23*, 18.

94. Franzblau, S. G.; Witzig, R. S.; Mclaughlin, J. C.; Torres, P.; Madico, G.; Hernandez, A.; Degnan, M. T.; Cook, M. B.; Quenzer, V. K.; Ferguson, R. M., Rapid, low-technology MIC determination with clinical *Mycobacterium tuberculosis* isolates by using the microplate alamar blue assay. *J. Clin. Microbiol.* **1998,** *36*, 362-366.

95. NCCLS, Reference method for broth dilution antifungal susceptibility testing of filamentous fungi: approved standard M38-A. *National Committee on Clinical Laboratory Standards* **2002,** *22*, 16.

96. Makler, M. T.; Ries, J. M.; Williams, J. A.; Bancroft, J. E.; Piper, R. C.; Gibbins, B. L.; Hinrichs, D. J., Parasite lactate dehydrogenase as an assay for *Plasmodium falciparum* drug sensitivity. *Am. J. Trop. Med. Hyg.* **1993,** *48*, 739-741.

97. Borenfreund, E.; Babich, H.; Martin-Alguacil, N., Rapid chemosensitivity assay with human normal and tumor cells in vitro. *In Vitro Cell. Dev. Biol.* **1990,** *26*, 1030-1034.

98. NIH. Tuberculosis. Fact sheet N^{o}104. http://www.who.int/mediacentre/factsheets/fs104/en/ (accessed July 2, 2012).

99. Corbett, E. L.; Watt, C. J.; Walker, N.; Maher, D.; Williams, B. G.; Raviglione, M. C.; Dye, C., The growing burdern of tuberculosis: global trends and interactions with the HIV. *Arch. Intern. Med.* **2003,** *163*, 1009-1021.

100. Johnson, R.; Streicher, E. M.; Louw, G. E.; Warren, R. M.; Van Helden, P. D.; Victor, T. C., Drug resistance in *Mycobacterium tuberculosis*. *Curr. Issues Mol. Biol.* **2006,** *8*, 97-112.

101. Cardona, P.-J., New insights on the nature of latent tuberculosis infection and its treatment. *Inflamm. Allergy Drug Targets* **2006,** *6*, 27-39.

102. Laurenzi, M.; Ginsberg, A.; Spigelman, M., Challenges associated with current and future TB treatment. *Infect. Disord. Drug Targets* **2007,** *7*, 105-119.

103. Rabindran, S. K., Antitumor activity of HER-2 inhibitors. *Cancer Lett.* **2005,** *227*, 9-23.

104. Landry, Y.; Gies, J.-P., Drugs and their molecular targets: an updated overview. *Fundam. Clin. Pharmacol.* **2008,** *22*, 1-18.

105. Petrelli, A.; Giordano, S., From single- to multi- target drugs in cancer therapy: when aspecificity becomes an advantage. *Curr. Med. Chem.* **2008,** *15*, 422-432.

106. FDA, Orange Book: Approved Drug Products with Therapeutic Equivalence Evaluations. http://www.accessdata.fda.gov/scripts/cder/ob/docs/queryai.cfm (accessed Jul 2th, 2012).

107. Radford, I. R., Imatinib. Novartis. *Curr. Opin. Investig. Drugs* **2002,** *3*, 492-499.

108. Cole, S. T.; Brosch, R.; Parkhill, J.; Garnier, T.; Churcher, C.; Harris, D.; Gordon, S. V.; Eiglmeier, K.; Gas, S.; Barry III, C. E.; Tekaia, F.; Badcock, K.; Basham, D.; Brown, D.; Chillingworth, T.; Connor, R.; Davies, R.; Devlin, K.; Feltwell, T.; Gentles, S.; Hamlin, N.; Holroyd, S.; Hornsby, T.; Jagels, K.; Krogh, A.; McLean, J.; Moule, S.; Murphy, L.; Oliver, K.; Osborne, J.; Quail, M. A.; Rajandream, M. A.; Rogers, J.; Rutter, S.; Seeger, K.; Skelton, J.; Squares, R.; Squares, S.; Sulston, J. E.; Taylor, K.; Whitehead, S.; Barrell, B. G., Deciphering the biology of *Mycobacterium tuberculosis* from the complete genome sequence. *Nature* **1998,** *393*, 537-544.

109. Reynolds, R. C.; Ananthan, S.; Faaleolea, E.; Hobrath, J. V.; Kwong, C. D.; Maddox, C.; Rasmussen, L.; Sosa, M. I.; Thammasuvimol, E.; White, E. L.; Zhang, W.; Secrist, J. A., High throughput screening of a library based on kinase inhibitor scaffolds against *Mycobacterium tuberculosis* H37Rv. *Tuberculosis* **2012,** *92*, 72-83.

110. Stock, A. M.; Robinson, V. L.; Goudreau, P. N., Two-component signal transduction. *Annu. Rev. Biochem.* **2000,** *69*, 183-215.

111. Hoch, J. A., Two-component and phosphorelay signal transduction. *Curr. Opin. Microbiol.* **2000,** *3*, 165-170.

112. Tuberculosis and the Tubercle Bacillus. Cole, S. T.; Eisenach, K. D.; McMurray, D. N.; Jacobs, W. R., Eds. American Society for Microbiology: 2005; p 360.

113. Kim, D.-j.; Forst, S., Genomic analysis of the histidine kinase family in bacteria and archaea. *Microbiology* **2001,** *147*, 1197-1212.

114. Dutta, R.; Qin, L.; Inouye, M., Histidine kinases: diversity of domain organization. *Mol. Microbiol.* **1999,** *34*, 633-640.

115. Sardiwal, S.; Kendall, S. L.; Movahedzadeh, F.; Rison, S. C. G.; Stoker, N. G.; Djordjevic, S., A GAF domain in the hypoxia/NO-inducible *Mycobacterium tuberculosis* DosS protein binds Haem. *J. Mol. Biol.* **2005,** *353*, 929-936.

116. Podust, L. M.; Ioanoviciu, A.; Ortiz de Montellano, P. R., 2.3 Å X-ray structure of the heme-bound GAF domain of sensory histidine kinase DosT of *Mycobacterium tuberculosis*. *Biochemistry (Mosc.)* **2008,** *47*, 12523-12531.

117. Heermann, R.; Lippert, M.-L.; Jung, K., Domain swapping reveals that the N-terminal domain of the sensor kinase KdpD in *Escherichia coli* is important for signaling. *BMC Microbiol.* **2009,** *9*, 133.

118. Rickman, L.; Saldanha, J. W.; Hunt, D. M.; Hoar, D. N.; Colston, M. J.; Millar, J. B. A.; Buxton, R. S., A two-component signal transduction system with a PAS domain-containing sensor is required for virulence of *Mycobacterium tuberculosis* in mice. *Biochem. Biophys. Res. Commun.* **2004,** *314*, 259-267.

119. Morth, J. P.; Gosmann, S.; Nowak, E.; Tucker, P. A., A novel two-component system found in *Mycobacterium tuberculosis*. *FEBS Lett.* **2005,** *579*, 4145-4148.

120. Yamada, S.; Shiro, Y., Structural basis of the signal transduction in the two-component system. *Adv. Exp. Med. Biol.* **2008,** *631*, 22-39.

121. Converse, P. J.; Karakousis, P. C.; Klinkenberg, L. G.; Kesavan, A. K.; Ly, L. H.; Allen, S. S.; Grosset, J. H.; Jain, S. K.; Lamichhane, G.; Manabe, Y. C.; McMurray, D. N.; Nuermberger, E. L.; Bishai, W. R., Role of the dosR-dosS two-component regulatory system in *Mycobacterium tuberculosis* virulence in three animal models. *Infect. Immun.* **2009,** *77*, 1230-1237.

122. Roberts, D. M., Two sensor kinases contribute to the hypoxic response of *Mycobacterium tuberculosis*. *J. Biol. Chem.* **2004,** *279*, 23082-23087.

123. Kumar, A.; Deshane, J. S.; Crossman, D. K.; Bolisetty, S.; Yan, B. S.; Kramnik, I.; Agarwal, A.; Steyn, A. J. C., Heme oxygenase-1-derived carbon monoxide induces the *Mycobacterium tuberculosis* dormancy regulon. *J. Biol. Chem.* **2008,** *283*, 18032-18039.

124. Kumar, A.; Toledo, J. C.; Patel, R. P.; Lancaster, J. R.; Steyn, A. J. C., *Mycobacterium tuberculosis* DosS is a redox sensor and DosT is a hypoxia sensor. *Proc. Natl. Acad. Sci. U. S. A.* **2007,** *104*, 11568-11573.

125. Honaker, R. W.; Leistikow, R. L.; Bartek, I. L.; Voskuil, M. I., Unique roles of dosT and dosS in dosR regulon induction and *Mycobacterium tuberculosis* dormancy. *Infect. Immun.* **2009,** *77*, 3258-3263.

126. Cho, H. Y.; Cho, H. J.; Kim, Y. M.; Oh, J. I.; Kang, B. S., Structural insight into the heme-based redox sensing by DosS from *Mycobacterium tuberculosis*. *J. Biol. Chem.* **2009,** *284*, 13057-13067.

127. Ioanoviciu, A.; Meharenna, Y. T.; Poulos, T. L.; Ortiz de Montellano, P. R., DevS oxy complex stability identifies this heme protein as a gas sensor in *Mycobacterium tuberculosis* dormancy. *Biochemistry (Mosc.)* **2009,** *48*, 5839-5848.

128. Honaker, R. W.; Dhiman, R. K.; Narayanasamy, P.; Crick, D. C.; Voskuil, M. I., DosS responds to a reduced electron transport system to induce the *Mycobacterium tuberculosis* Dos R regulon. *J. Bacteriol.* **2010,** *192*, 6447-6455.

129. Vos, M. H.; Bouzhir-Sima, L.; Lambry, J.-C.; Luo, H.; Eaton-Rye, J. J.; Ioanoviciu, A.; Ortiz de Montellano, P. R.; Liebl, U., Ultrafast ligand dynamics in the heme-based GAF sensor domains of the histidine kinases DosS and DosT from *Mycobacterium tuberculosis*. *Biochemistry (Mosc.)* **2012,** *51*, 159-166.

130. Kim, M.-J.; Park, K.-J.; Ko, I.-J.; Kim, Y. M.; Oh, J.-I., Different roles of DosS and DosT in the hypoxic adaptation of mycobacteria. *J. Bacteriol.* **2010,** *192*, 4868-4875.

131. Cho, H. Y.; Cho, H. J.; Kim, M. H.; Kang, B. S., Blockage of the channel to heme by the E87 side chain in the GAF domain of *Mycobacterium tuberculosis* DosS confers the unique sensitivity of DosS to oxygen. *FEBS Lett.* **2011,** *585*, 1873-1878.

132. Zahrt, T. C.; Deretic, V., An essential two-component signal transduction system in *Mycobacterium tuberculosis*. *J. Bacteriol.* **2000,** *182*, 3832-3838.

133. Parish, T.; Smith, D. A.; Kendall, S.; Casali, N.; Bancroft, G. J.; Stoker, N. G., Deletion of two-component regulatory systems increases the virulence of *Mycobacterium tuberculosis*. *Infect. Immun.* **2003,** *71*, 1134-1140.

134. Fol, M.; Chauhan, A.; Nair, N. K.; Maloney, E.; Moomey, M.; Jagannath, C.; Madiraju, M. V. V. S.; Rajagopalan, M., Modulation of *Mycobacterium tuberculosis* proliferation by MtrA, an essential two-component response regulator. *Mol. Microbiol.* **2006,** *60*, 643-657.

135. He, H.; Hovey, R.; Kane, J.; Singh, V.; Zahrt, T. C., MprAB is a stress-responsive two-component system that directly regulates expression of sigma factors SigB and SigE in *Mycobacterium tuberculosis*. *J. Bacteriol.* **2006,** *188*, 2134-2143.

136. Pang, X.; Vu, P.; Byrd, T. F.; Ghanny, S.; Soteropoulos, P.; Mukamolova, G. V.; Wu, S.; Samten, B.; Howard, S. T., Evidence for complex interactions of stress-associated regulons in an mprAB deletion mutant of *Mycobacterium tuberculosis*. *Microbiology* **2007,** *153*, 1229-1242.

137. Pang, X.; Cao, G.; Neuenschwander, P. F.; Haydel, S. E.; Hou, G.; Howard, S. T., The β-propeller gene Rv1057 of *Mycobacterium tuberculosis* has a complex promoter directly regulated by both the MprAB and TrcRS two-component systems. *Tuberculosis* **2011,** *91*, S142-S149.

138. Zahrt, T. C., *Mycobacterium tuberculosis* signal transduction system required for persistent infections. *Proc. Natl. Acad. Sci. U. S. A.* **2001,** *98*, 12706-12711.

139. Zahrt, T. C.; Wozniak, C.; Jones, D.; Trevett, A., Functional analysis of the *Mycobacterium tuberculosis* MprAB two-component signal transduction system. *Infect. Immun.* **2003,** *71*, 6962-6970.

140. Preu, J.; Panjikar, S.; Morth, P.; Jaiswal, R.; Karunakar, P.; Tucker, P. A., The sensor region of the ubiquitous cytosolic sensor kinase, PdtaS, contains PAS and GAF domain sensing modules. *J. Struct. Biol.* **2012,** *177*, 498-505.

141. Ewann, F., Intracellular autoregulation of the *Mycobacterium tuberculosis* PrrA response regulator. *Microbiology* **2004,** *150*, 241-246.

142. Haydel, S. E.; Malhotra, V.; Cornelison, G. L.; Clark-Curtiss, J. E., The prrAB two-component system is essential for *Mycobacterium tuberculosis* viability and is induced under nitrogen-limiting conditions. *J. Bacteriol.* **2011,** *194*, 354-361.

143. Ewann, F., Transient requirement of the PrrA-PrrB two-component system for early intracellular multiplication of *Mycobacterium tuberculosis*. *Infect. Immun.* **2002,** *70*, 2256-2263.

144. Bateman, A.; Coin, L.; Durbin, R.; Finn, R. D.; Hollich, V.; Griffiths-Jones, S.; Khanna, A.; Marshall, M.; Moxon, S.; Sonnhammer, E. L. L., The Pfam protein families database. *Nucleic Acids Res.* **2004,** *32*, D138-141.

145. Nowak, E.; Panjikar, S.; Morth, J. P.; Jordanova, R.; Svergun, D. I.; Tucker, P. A., Structural and functional aspects of the sensor histidine kinase PrrB from *Mycobacterium tuberculosis*. *Structure* **2006,** *14*, 275-285.

146. Nowak, E., The structural basis of signal transduction for the response regulator PrrA from *Mycobacterium tuberculosis*. *J. Biol. Chem.* **2006,** *281*, 9659-9666.

147. Shrivastava, R.; Das, D. R.; Wiker, H. G.; Das, A. K., Functional insights from the molecular modelling of a novel two-component system. *Biochem. Biophys. Res. Commun.* **2006,** *344*, 1327-1333.

148. Waddell, S. J.; Stabler, R. A.; Laing, K.; Kremer, L.; Beynolds, R. C.; Besra, G. S., The use of microarray analysis to determine the gene expression profiles of *Mycobacterium tuberculosis* in response to anti-bacterial compounds. *Tuberculosis* **2004,** *84*, 263-274.

149. Shrivastava, R.; Ghosh, A. K.; Das, A. K., Probing the nucleotide binding and phosphorylation by the histidine kinase of a novel three-protein two-component system from *Mycobacterium tuberculosis*. *FEBS Lett.* **2007,** *581*, 1903-1909.

150. Shrivastava, R.; Ghosh, A. K.; Das, A. K., Intra- and intermolecular domain interactions among novel two-component system proteins coded by Rv0600c, Rv0601c and Rv0602c of *Mycobacterium tuberculosis*. *Microbiology* **2009,** *155*, 772-779.

151. Haydel, S. E.; Dunlap, N. E.; Benjamin, W. H., In vitro evidence of two-component system phosphorylation between the *Mycobacterium tuberculosis* TrcR/TrcS proteins. *Microbioal Pathogenesis* **1999,** *26*, 195-206.

152. Haydel, S. E.; Benjamin, W. H.; Dunlap, N. E.; Clark-Curtiss, J. E., Expression, autoregulation, and DNA binding properties of the *Mycobacterium tuberculosis* TrcR response regulator. *J. Bacteriol.* **2002,** *184*, 2192-2203.

153. Gonzalo-Asensio, J.; Maia, C.; Ferrer, N. L.; Barilone, N.; Laval, F.; Soto, C. Y.; Winter, N.; Daffe, M.; Gicquel, B.; Martin, C.; Kackson, M., The virulence-associated two-component PhoP-PhoR system controls the biosynthesis of polyketide-derived lipids in *Mycobacterium tuberculosis*. *J. Biol. Chem.* **2006,** *281*, 1313-1316.

154. Chesne-Seck, M. L.; Barilone, N.; Boudou, F.; Asensio, J. G.; Kolattukudy, P. E.; Martin, C.; Cole, S. T.; Gicquel, B.; Gopaul, D. N.; Jackson, M., A point mutation in the two-component regulator PhoP-PhoR accounts for the absence of polyketide-derived acyltrehaloses but not that of phthiocerol dimycocerosates in *Mycobacterium tuberculosis* H37Ra. *J. Bacteriol.* **2007,** *190*, 1329-1334.

155. Gonzalo-Asensio, J.; Mostowy, S.; Harders-Westerveen, J.; Huygen, K.; Hernández-Pando, R.; Thole, J.; Behr, M.; Gicquel, B.; Martín, C., Phop: a missing piece in the intricate puzzle of *Mycobacterium tuberculosis* virulence. *PLoS ONE* **2008,** *3*, e3496.

156. Frigui, W.; Bottai, D.; Majlessi, L.; Monot, M.; Josselin, E.; Brodin, P.; Garnier, T.; Gicquel, B.; Martin, C.; Leclerc, C.; Cole, S. T.; Brosch, R., Control of *M. tuberculosis* ESAT-6 secretion and specific T cell recognition by PhoP. *PLoS Pathog.* **2008,** *4*, e33.

157. Gonzalo-Asensio, J. A.; Arbués, A.; Pérez, E.; Gicquel, B.; Martin, C., Live tuberculosis vaccines based on phoP mutants: a step towards clinical trials. *Expert Opinion on Vaccines & Antibiodies* **2008,** *8*, 201-211.

158. Pathak, A.; Goyal, R.; Sinha, A.; Sarkar, D., Domain structure of virulence-associated response regulator PhoP of *Mycobacterium tuberculosis*: role of the linker region in regulator-promoter interaction(s). *J. Biol. Chem.* **2010,** *285*, 34309-34318.

159. Das, A. K.; Pathak, A.; Sinha, A.; Datt, M.; Singh, B.; Karthikeyan, S.; Sarkar, D., A single-amino-acid substitution in the C terminus of PhoP determines DNA-binding specificity of the virulence-associated response regulator from *Mycobacterium tuberculosis*. *J. Mol. Biol.* **2010,** *398*, 647-656.

160. Sinha, A.; Gupta, S.; Bhutani, S.; Pathak, A.; Sarkar, D., PhoP-PhoP interaction at adjacent PhoP binding sites is influenced by protein phosphorylation. *J. Bacteriol.* **2007,** *190*, 1317-1328.

161. Gupta, S.; Pathak, A.; Sinha, A.; Sarkar, D., *Mycobacterium tuberculosis* PhoP recognizes two adjacent direct-repeat sequences to form head-to-head dimers. *J. Bacteriol.* **2009,** *191*, 7466-7476.

162. Himpens, S.; Locht, C.; Supply, P., Molecular characterization of the mycobacterial SenX3-RegX3 two-component system: evidence for autoregulation. *Microbiology* **2000,** *146*, 3091-3098.

163. Glover, R. T.; Kriakov, J.; Garforth, S. J.; Baughn, A. D.; Jacobs, W. R., The two-component regulatory system senX3-regX3 regulates phosphate-dependent gene expression in *Mycobacterium smegmatis*. *J. Bacteriol.* **2007,** *189*, 5495-5503.

164. Kremling, A.; Heermann, R.; Centler, F.; Jung, K.; Gilles, E. D., Analysis of two-component signal transduction by mathematical modeling using the KdpD/KdpE system of *Escherichia coli*. *Biosystems* **2004,** *78*, 23-37.

165. Steyn, A. J. C.; Joseph, J.; Bloom, B. R., Interaction of the sensor module of *Mycobacterium tuberculosis* H37Rv KdpD with members of the Lpr family. *Mol. Microbiol.* **2003,** *47*, 1075-1089.

166. Mizuno, T., Compilation of all genes encoding two-component phosphotransfer signal transducers in the genome of *Escherichia coli*. *DNA Res.* **1997,** *4*, 161-168.

167. Av-Gay, Y.; Everett, M., The eukaryotic-like Ser/Thr protein kinase of *Mycobacterium tuberculosis*. *Trends Microbiol.* **2000,** *8*, 238-244.

168. Narayan, A.; Sachdeva, P.; Sharma, K.; Saini, A. K.; Tyagi, A. K.; Singh, Y., Serine threonine protein kinase of mycobacterial genus: phylogeny to function. *Physiol. Genomics* **2007,** *29*, 66-75.

169. Wehenkel, A.; Bellinzoni, M.; Graña, M.; Duran, R.; Villarino, A.; Fernandez, P.; Andre-Leroux, G.; England, P.; Takiff, H.; Cerveñansky, C.; Cole, S. T.; Alzari, P. M., Mycobacterial Ser/Thr protein kinases and phosphatases: Physiological roles and therapeutic potential. *Biochim. Biophys. Acta* **2008,** *1784*, 193-202.

170. Manning, G.; Whyte, D. B.; Martinez, R.; Hunter, T.; Sudarsanam, S., The protein kinase complement of the human genome. *Science* **2002,** *298*, 1912-1934.

171. Chaba, R.; Raje, M.; Chakraborti, P. K., Evidence that a eukaryotic-type serine/threonine protein kinase from *Mycobacterium tuberculosis* regulates morphological changes associated with cell division. *Eur. J. Biochem.* **2002,** *269*, 1078-1085.

172. Deol, P.; Vohra, R.; Saini, A. K.; Singh, A.; Chandra, H.; Chopra, P.; Das, T. K.; Tyagi, A. K.; Singh, Y., Role of *Mycobacterium tuberculosis* Ser/Thr kinase PknF: implications in glucose transport and cell division. *J. Bacteriol.* **2005,** *187*, 3415-3420.

173. Cowley, S.; Ko, M.; Pick, N.; Chow, R.; Downing, K. J.; Gordhan, B. G.; Betts, J. C.; Mizrahi, V.; Smith, D. A.; Stokes, R. W.; Av-Gay, Y., The *Mycobacterium tuberculosis* protein serine/threonine kinase PknG is linked to cellular glutamate/glutamine levels and is important for growth in vivo. *Mol. Microbiol.* **2004,** *52*, 1691-1702.

174. Greenstein, A. E.; MacGurn, J. A.; Baer, C. E.; Falick, A. M.; Cox, J. S.; Alber, T., *M. tuberculosis* Ser/Thr protein kinase D phosphorylates an anti-anti–sigma factor homolog. *PLoS Pathog.* **2007,** *3*, e49.

175. Greenstein, A. E.; Grundner, C.; Echols, N.; Gay, L. M.; Lombana, T. N.; Miecskowski, C. A.; Pullen, K. E.; Sung, P.-y.; Alber, T., Structure/function studies of Ser/Thr and Tyr protein phosphorylation in *Mycobacterium tuberculosis*. *J. Mol. Microbiol. Biotechnol.* **2005,** *9*, 167-181.

176. Alber, T., Signaling mechanisms of the *Mycobacterium tuberculosis* receptor Ser/Thr protein kinases. *Curr. Opin. Struct. Biol.* **2009,** *19*, 650-657.

177. Danilenko, V. N.; Osolodkin, D. I.; Lakatosh, S. A.; Preobrazhenskaya, M. N.; Shtil, A. A., Bacterial eukaryotic type serine-threonine protein kinases, from structural biology to targeted anti-infective drug design. *Curr. Top. Med. Chem.* **2011,** *11*, 1352-1369.

178. Chao, J.; Wong, D.; Zheng, X.; Poirier, V.; Bach, H.; Hmama, Z.; Av-Gay, Y., Protein kinase and phosphatase signaling in *Mycobacterium tuberculosis* physiology and pathogenesis. *Biochim. Biophys. Acta* **2010,** *1804*, 620-627.

179. Kang, C. M., The *Mycobacterium tuberculosis* serine/threonine kinases PknA and PknB: substrate identification and regulation of cell shape. *Genes Dev.* **2005,** *19*, 1692-1704.

180. Veyron-Churlet, R.; Molle, V.; Taylor, R. C.; Brown, A. K.; Besra, G. S.; Zanella-Cleon, I.; Futterer, K.; Kremer, L., The *Mycobacterium tuberculosis* β-ketoacyl-acyl carrier protein synthase III activity is inhibited by phosphorylation on a single threonine residue. *J. Biol. Chem.* **2009,** *284*, 6414-6424.

181. Thakur, M.; Chakraborti, Pradip K., Ability of PknA, a mycobacterial eukaryotic-type serine/threonine kinase, to transphosphorylate MurD, a ligase involved in the process of peptidoglycan biosynthesis. *Biochem. J.* **2008,** *415*, 27.

182. Kang, C. M.; Nyayapathy, S.; Lee, J. Y.; Suh, J. W.; Husson, R. N., Wag31, a homologue of the cell division protein DivIVA, regulates growth, morphology and polar cell wall synthesis in mycobacteria. *Microbiology* **2008,** *154*, 725-735.

183. Jani, C.; Eoh, H.; Lee, J.; Hamasha, K.; Sahana, M.; Han, J.-S.; Nyayapathy, S.; Lee, J.-Y.; Suh, J.-W.; Lee, S.; Rehse, S. J.; Crick, D. C.; Kang, C.-M., Regulation of polar peptidoglycan biosynthesis by Wag31 phosphorylation in mycobacteria. *BMC Microbiol.* **2010,** *10*, 327.

184. Thakur, M.; Chakraborti, P. K., GTPase activity of mycobacterial FtsZ is impaired due to its transphosphorylation by the eukaryotic-type Ser/Thr kinase, PknA. *J. Biol. Chem.* **2006,** *281*, 40107-40113.

185. Sharma, K.; Gupta, M.; Krupa, A.; Srinivasan, N.; Singh, Y., EmbR, a regulatory protein with ATPase activity, is a substrate of multiple serine/threonine kinases and phosphatase in *Mycobacterium tuberculosis*. *FEBS J.* **2006,** *273*, 2711-2721.

186. Molle, V., The condensing activities of the *Mycobacterium tuberculosis* type II fatty acid synthase are differentially regulated by phosphorylation. *J. Biol. Chem.* **2006,** *281*, 30094-30103.

187. Sajid, A.; Arora, G.; Gupta, M.; Upadhyay, S.; Nandicoori, V. K.; Singh, Y., Phosphorylation of *Mycobacterium tuberculosis* Ser/Thr phosphatase by PknA and PknB. *PLoS ONE* **2011,** *6*, e17871.

188. Molle, V.; Zanella-Cleon, I.; Robin, J.-P.; Mallejac, S.; Cozzone, A. J.; Becchi, M., Characterization of the phosphorylation sites of *Mycobacterium tuberculosis* serine/threonine protein kinases, PknA, PknD, PknE, and PknH by mass spectrometry. *Proteomics* **2006,** *6*, 3754-3766.

189. Fernandez, P.; Saint-Joanis, B.; Barilone, N.; Jackson, M.; Gicquel, B.; Cole, S. T.; Alzari, P. M., The Ser/Thr protein kinase PknB is essential for sustaining mycobacterial growth. *J. Bacteriol.* **2006,** *188*, 7778-7784.

190. Dasgupta, A., The serine/threonine kinase PknB of *Mycobacterium tuberculosis* phosphorylates PBPA, a penicillin-binding protein required for cell division. *Microbiology* **2006,** *152*, 493-504.

191. Grundner, C.; Gay, L. M.; Alber, T., *Mycobacterium tuberculosis* serine/threonine kinases PknB, PknD, PknE, and PknF phosphorylate multiple FHA domains. *Protein Sci.* **2005,** *14*, 1918-1921.

192. Roumestand, C.; Leiba, J.; Galophe, N.; Margeat, E.; Padilla, A.; Bessin, Y.; Barthe, P.; Molle, V.; Cohen-Gonsaud, M., Structural insight into the *Mycobacterium tuberculosis* Rv0020c protein and its interaction with the PknB kinase. *Structure* **2011,** *19*, 1525-1534.

193. Spivey, V. L.; Molle, V.; Whalan, R. H.; Rodgers, A.; Leiba, J.; Stach, L.; Walker, K. B.; Smerdon, S. J.; Buxton, R. S., Forkhead-associated (FHA) domain containing ABC transporter Rv1747 is positively regulated by Ser/Thr phosphorylation in *Mycobacterium tuberculosis*. *J. Biol. Chem.* **2011,** *286*, 26198-26209.

194. Villarino, A.; Duran, R.; Wehenkel, A.; Fernandez, P.; England, P.; Brodin, P.; Cole, S. T.; Zimny-Arndt, U.; Jungblut, P. R.; Cerveñansky, C.; Alzari, P. M., Proteomic identification of *M. tuberculosis* protein kinase substrates: PknB recruits GarA, a FHA domain-containing protein, through activation loop-mediated interactions. *J. Mol. Biol.* **2005,** *350*, 953-963.

195. Gupta, M.; Sajid, A.; Arora, G.; Tandon, V.; Singh, Y., Forkhead-associated domain-containing protein Rv0019c and polyketide-associated protein PapA5, from substrates of serine/threonine protein kinase PknB to interacting proteins of *Mycobacterium tuberculosis*. *J. Biol. Chem.* **2009,** *284*, 34723-34734.

196. Mahjan, A.; Yuan, C.; Lee, H.; Chen, E. S.; Wu, P.-Y.; Tsai, M.-D., Structure and function of the phosphothreonine-specific FHA domain. *Sci. Signal.* **2009,** *1*, re12.

197. Park, S. T.; Kang, C. M.; Husson, R. N., Regulation of the SigH stress response regulon by an essential protein kinase in *Mycobacterium tuberculosis*. *Proc. Natl. Acad. Sci. U. S. A.* **2008,** *105*, 13105-13110.

198. Parikh, A.; Verma, S. K.; Khan, S.; Prakash, B.; Nandicoori, V. K., PknB-mediated phosphorylation of a novel substrate, *N*-acetylglucosamine-1-phosphate uridyltransferase, modulates its acetyltransferase activity. *J. Mol. Biol.* **2009,** *386*, 451-464.

199. Ortiz-Lombardia, M., Crystal structure of the catalytic domain of the PknB serine/threonine kinase from *Mycobacterium tuberculosis*. *J. Biol. Chem.* **2003,** *278*, 13094-13100.

200. Young, T. A.; Delagoutte, B.; Endrizzi, J. A.; Falick, A. M.; Alber, T., Structure of *Mycobacterium tuberculosis* PknB supports a universal activation mechanism for Ser/Thr protein kinases. *Nat. Struct. Biol.* **2003,** *10*, 168-174.

201. Wehenkel, A.; Fernandez, P.; Bellinzoni, M.; Catherinot, V.; Barilone, N.; Labesse, G.; Jackson, M.; Alzari, P. M., The structure of PknB in complex with mitoxantrone, an ATP-competitive inhibitor, suggests a mode of protein kinase regulation in mycobacteria. *FEBS Lett.* **2006,** *580*, 3018-3022.

202. Miecskowski, C. A.; Lavarone, A. T.; Alber, T., Auto-activation mechanism of the *Mycobacterium tuberculosis* PknB receptor Ser/Thr kinase. *The EMBO Journal* **2008,** *27*, 3186-3197.

203. Lombana, T. N.; Echols, N.; Good, M. C.; Thomsen, N. D.; Ng, H.-L.; Greenstein, A. E.; Falick, A. M.; King, D. S.; Alber, T., Allosteric activation mechanism of the *Mycobacterium tuberculosis* receptor Ser/Thr protein kinase, PknB. *Structure* **2010,** *18*, 1667-1577.

204. Barthe, P.; Mukamolova, G. V.; Roumestand, C.; Cohen-Gonsaud, M., The structure of PknB extracellular PASTA domain from *Mycobacterium tuberculosis* suggests a ligand-dependent kinase activation. *Structure* **2010,** *18*, 606-615.

205. Bishai, W. R.; Mir, M.; Asong, J.; Li, X.; Cardot, J.; Boons, G.-J.; Husson, R. N., The extracytoplasmic domain of the *Mycobacterium tuberculosis* Ser/Thr kinase PknB binds specific muropeptides and is required for PknB localization. *PLoS Pathog.* **2011,** *7*, e1002182.

206. Székely, R.; Wáczek, F.; Szabadkai, I.; Németh, G.; Hegymegi-Barakonyi, B.; Erős, D.; Szokol, B.; Pató, J.; Hafenbradl, D.; Satchell, J.; Saint-Joanis, B.; Cole, S. T.; Őrfi, L.; Klebl, B. M.; Kéri, G., A novel drug discovery concept for tuberculosis: Inhibition of bacterial and host cell signalling. *Immunol. Lett.* **2008,** *116*, 225-231.

207. Hegymegi-Barakonyi, B.; Székely, R.; Varga, Z.; Kiss, R.; Borbély, G.; Németh, G.; Bánhegyi, P.; Pató, J.; Greff, Z.; Horváth, Z.; Mészáros, G.; Marosfalvi, J.; Erős, D.; Szántai-Kis, C.; Breza, N.; Garavaglia, S.; Perozzi, S.; Rizzi, M.; Hafenbradl, D.; Ko, M.; Av-Gay, Y.; Klebl, B. M.; Őrfi, L.; Kéri, G., Signalling inhibitors anainst *Mycobacterium tuberculosis* - early days of a new therapeutic concept in tuberculosis. *Curr. Med. Chem.* **2008,** *15*, 2760-2770.

208. Lougheed, K. E. A.; Osborne, S. A.; Saxty, B.; Whalley, D.; Chapman, T.; Bouloc, N.; Chugh, J.; Nott, T. J.; Patel, D.; Spivey, V. L.; Kettleborough, C. A.; Bryans, J. S.; Taylor, D. L.; Smerdon, S. J.; Buxton, R. S., Effective inhibitors of the essential kinase PknB and their potential as anti-mycobacterial agents. *Tuberculosis* **2011,** *91*, 277-286.

209. Chapman, T. M.; Bouloc, N.; Buxton, R. S.; Chugh, J.; Lougheed, K. E. A.; Osborne, S. A.; Saxty, B.; Smerdon, S. J.; Taylor, D. L.; Whalley, D., Substituted aminopyrimidine protein kinase B (PknB) inhibitors show activity against *Mycobacterium tuberculosis*. *Bioorg. Med. Chem. Lett.* **2012,** *22*, 3349-3353.

210. Cui, T.; Zhang, L.; Wang, X.; He, Z.-G., Uncovering new signaling proteins and potential drug targets through the interactome analysis of *Mycobacterium tuberculosis*. *BMC Genomics* **2009,** *10*, 118.

211. Cohen-Gonsaud, M.; Barthe, P.; Canova, M. J.; Stagier-Simon, C.; Kremer, L.; Roumestand, C.; Molle, V., The *Mycobacterium tuberculosis* Ser/Thr kinase substrate Rv2175c is a DNA-binding protein regulated by phosphorylation. *J. Biol. Chem.* **2009,** *284*, 19290-19300.

212. Canova, M. J.; Veyron-Churlet, R.; Zanella-Cleon, I.; Cohen-Gonsaud, M.; Cozzone, A. J.; Becchi, M.; Kremer, L.; Molle, V., The *Mycobacterium tuberculosis* serine/threonine kinase PknL phosphorylates Rv2175c. *Proteomics* **2008,** *8*, 521-533.

213. Canova, M. J.; Kremer, L.; Molle, V., The *Mycobacterium tuberculosis* GroEL1 chaperone is a substrate of Ser/Thr protein kinases. *J. Bacteriol.* **2009,** *191*, 2876-2883.

214. Peirs, P.; Lefevre, P.; Boarbi, S.; Wang, X. M.; Denis, O.; Braibant, M.; Pethe, K.; Locht, C.; Huygen, K.; Content, J., *Mycobacterium tuberculosis* with disruption in genes encoding the phosphate binding proteins PstS1 and PstS2 is deficient in phosphate uptake and demonstrates reduced in vivo virulence. *Infect. Immun.* **2005,** *73*, 1898-1902.

215. Be, N. A.; Bishai, W. R.; Jain, S. K., Role of *Mycobacterium tuberculosis* pknD in the pathogenesis of central nervous system tuberculosis. *BMC Microbiol.* **2012,** *12*, 7.

216. Greenstein, A. E.; Echols, N.; Lombana, T. N.; King, D. S.; Alber, T., Allosteric activation by dimerization of the PknD receptor Ser/Thr protein kinase from *Mycobacterium tuberculosis*. *J. Biol. Chem.* **2007,** *282*, 11427-11435.

217. Pérez, J.; Garcia, R.; Bach, H.; de Waard, J. H.; Jacobs, W. R.; Av-Gay, Y.; Bubis, J.; Takiff, H. E., *Mycobacterium tuberculosis* transporter MmpL7 is a potential substrate for kinase PknD. *Biochem. Biophys. Res. Commun.* **2006,** *348*, 6-12.

218. Curry, J. M.; Whalan, R.; Hunt, D. M.; Gohil, K.; Strom, M.; Rickman, L.; Colston, M. J.; Smerdon, S. J.; Buxton, R. S., An ABC transporter containing a forkhead-associated domain interacts with a serine-threonine protein kinase and is required for growth of *Mycobacterium tuberculosis* in mice. *Infect. Immun.* **2005,** *73*, 4471-4477.

219. Good, M. C.; Greenstein, A. E.; Young, T. A.; Ng, H.-L.; Alber, T., Sensor domain of the *Mycobacterium tuberculosis* receptor Ser/Thr protein kinase, PknD, forms a highly symmetric β propeller. *J. Mol. Biol.* **2004,** *339*, 459-469.

220. Jayakumar, D.; Jacobs, W. R.; Narayanan, S., Protein kinase E of *Mycobacterium tuberculosis* has a role in the nitric oxide stress response and apoptosis in a human macrophage model of infection. *Cell. Microbiol.* **2008,** *10*, 365-374.

221. Kumar, D.; Narayanan, S., pknE, a serine/threonine kinase of *Mycobacterium tuberculosis* modulates multiple apoptotic paradigms. *Infect. Genet. Evol.* **2012,** *12*, 737-747.

222. Papavinasasundaram, K. G.; Chan, B.; Chung, J. H.; Colston, M. J.; Davis, E. O.; Av-Gay, Y., Deletion of the *Mycobacterium tuberculosis* pknH gene confers a higher bacillary load during the chronic phase of infection in BALB/c mice. *J. Bacteriol.* **2005,** *187*, 5751-5760.

223. Molle, V.; Reynolds, Robert C.; Alderwick, Luke J.; Besra, Gurdyal S.; Cozzone, Alain J.; Fütterer, K.; Kremer, L., EmbR2, a structural homologue of EmbR, inhibits the *Mycobacterium tuberculosis* kinase/substrate pair PknH/EmbR. *Biochem. J.* **2008,** *410*, 309.

224. Gay, L. M.; Ng, H.-L.; Alber, T., A conserved dimer and global conformational changes in the structure of apo-PknE Ser/Thr protein kinase from *Mycobacterium tuberculosis*. *J. Mol. Biol.* **2006,** *360*, 409-420.

225. Molle, V.; Kremer, L.; Girard-Blanc, C.; Besra, G. S.; Cozzone, A. J.; Prost, J.-F., An FHA phosphoprotein recognitio domain mediates protein EmbR phosphorylation by PknH, a Ser/Thr protein kinase from *Mycobacterium tuberculosis*. *Biochemistry (Mosc.)* **2003,** *42*, 15300-15309.

226. Zhang, X. J.; Papavinasasundaram, K. G.; Av-Gay, Y., Novel substrates of *Mycobacterium tuberculosis* PknH Ser/Thr kinase. *Biochem. Biophys. Res. Commun.* **2007,** *355*, 162-168.

227. Chao, J. D.; Papavinasasundaram, K. G.; Zheng, X.; Chavez-Steenbock, A.; Wang, X.; Lee, G. Q.; Av-Gay, Y., Convergence of Ser/Thr and two-component signaling to coordinate expression of the dormancy regulon in *Mycobacterium tuberculosis*. *J. Biol. Chem.* **2010,** *285*, 29239-29246.

228. Sharma, K.; Chandra, H.; Gupta, P. K.; Pathak, M.; Narayan, A.; Meena, L. S.; d'Souza, R. C. J.; Chopra, P.; Ramachandran, S.; Singh, Y., PknH, a transmembrane Hank's type serine/threonine kinase from *Mycobacterium tuberculosisis* differentially expressed under stress conditions. *FEMS Microbiol. Lett.* **2004,** *233*, 107-113.

229. Karaman, M. W.; Herrgard, S.; Treiber, D. K.; Gallant, P.; Atteridge, C. E.; Campbell, B. T.; Chan, K. W.; Ciceri, P.; Davis, M. I.; Edeen, P. T.; Faraoni, R.; Floyd, M.; Hunt, J. P.; Lockhart, D. J.; Mianov, Z. V.; Morrison, M. J.; Pallares, G.; Patel, H. K.; Pritchard, S.; Wodicka, J. M.; Zarrinkar, P. P., A quantitative analysis of kinase inhibitor selectivity. *Nat. Biotechnol.* **2008,** *26*, 127-132.

230. Molle, V., Two FHA domains on an ABC transporter, Rv1747, mediate its phosphorylation by PknF, a Ser/Thr protein kinase from *Mycobacterium tuberculosis*. *FEMS Microbiol. Lett.* **2004,** *234*, 215-223.

231. Singh, A.; Singh, Y.; Pine, R.; Shi, L.; Chandra, R.; Drlica, K., Protein kinase I of *Mycobacterium tuberculosis*: cellular localization and expression during infection of macrophage-like cells. *Tuberculosis* **2006,** *86*, 28-33.

232. Gopalaswamy, R.; Narayanan, S.; Chen, B.; Jacobs, W. R.; Av-Gay, Y., The serine/threonine protein kinase PknI controls the growth of *Mycobacterium tuberculosis* upon infection. *FEMS Microbiol. Lett.* **2009,** *295*, 23-29.

233. Jang, J.; Stella, A.; Boudou, F.; Levillain, F.; Darthuy, E.; Vaubourgeix, J.; Wang, C.; Bardou, F.; Puzo, G.; Gilleron, M.; Burlet-Schiltz, O.; Monsarrat, B.; Brodin, P.; Gicquel, B.; Neyrolles, O., Functional characterization of the *Mycobacterium tuberculosis* serine/threonine kinase PknJ. *Microbiology* **2010,** *156*, 1619-1631.

234. Arora, G.; Sajid, A.; Gupta, M.; Bhaduri, A.; Kumar, P.; Basumodak, S.; Singh, Y., Understanding the role of PknJ in *Mycobacterium tuberculosis*: biochemical characterization and identification of novel substrate pyruvate kinase A. *PLoS ONE* **2010,** *5*, e10772.

235. Malhotra, V.; Arteaga-Cortes, L. T.; Clay, G.; Clark-Curtiss, J. E., *Mycobacterium tuberculosis* protein kinase K confers survival advantage during early infection in mice and regulates growth in culture and during persistent infection: implications for immune modulation. *Microbiology* **2010,** *156*, 2829-2841.

236. Kumar, P.; Kumar, D.; Parikh, A.; Rananaware, D.; Gupta, M.; Singh, Y.; Nandicoori, V. K., The *Mycobacterium tuberculosis* protein kinase K modulates activation of transcription from the promoter of mycobacterial monooxygenase operon through phosphorylation of the transcriptional regulator VirS. *J. Biol. Chem.* **2009,** *284*, 11090-11099.

237. Scherr, N.; Muller, P.; Perisa, D.; Combaluzier, B.; Jeno, P.; Pieters, J., Survival of pathogenic mycobacteria in macrophages is mediated through autophosphorylation of protein kinase G. *J. Bacteriol.* **2009,** *191*, 4546-4554.

238. Walburger, A.; Koul, A.; Ferrari, G.; Nguyen, L.; Prescianotto-Baschong, C.; Huygen, K.; Klebl, B.; Thompson, C.; Bacher, G.; Pieters, J., Protein kinase G from pathogenic mycobacteria promotes survival within macrophages. *Science* **2004,** *304*, 1800-1804.

239. Chaurasiya, S. K.; Srivastava, K. K., Downregulation of protein kinase C-alpha enhances intracellular survival of mycobacteria: role of PknG. *BMC Microbiol.* **2009,** *9*, 271.

240. Wolff, K. A.; Nguyen, H. T.; Cartabuke, R. H.; Singh, A.; Ogwang, S.; Nguyen, L., Protein kinase G is required for intrinsic antibiotic resistance in mycobacteria. *Antimicrob. Agents Chemother.* **2009,** *53*, 3515-3519.

241. Scherr, N.; Honnappa, S.; Kunz, G.; Mueller, P.; Jayachandran, R.; Winkler, F.; Pieters, J.; Steinmetz, M. O., From the cover: structural basis for the specific inhibition of protein kinase G, a virulence factor of *Mycobacterium tuberculosis*. *Proc. Natl. Acad. Sci. U. S. A.* **2007,** *104*, 12151-12156.

242. Tiwari, D.; Singh, R. K.; Goswami, K.; Verma, S. K.; Prakash, B.; Nandicoori, V. K., Key residues in *Mycobacterium tuberculosis* protein kinase G play a role in regulating kinase activity and survival in the host. *J. Biol. Chem.* **2009,** *284*, 27467-27479.

243. Vincent, C.; Duclos, B.; Grangeasse, C.; Vaganay, E.; Riberty, M.; Cozzone, A. J.; Doublet, P., Relationship between exopolysaccharide production and protein-tyrosine phosphorylation in gram-negative bacteria. *J. Mol. Biol.* **2000,** *304*, 311-321.

244. Wugeditsch, T., Phosphorylation of Wzc, a tyrosine autokinase, is essential for assembly of group 1 capsular polysaccharides in *Escherichia coli*. *J. Biol. Chem.* **2001,** *276*, 2361-2371.

245. Klein, G.; Dartigalongue, C.; Raina, S., Phosphorylation-mediated regulation of heat shock response in *Escherichia coli*. *Mol. Microbiol.* **2003,** *48*, 269-285.

246. Mijakovic, I., Bacterial single-stranded DNA-binding proteins are phosphorylated on tyrosine. *Nucleic Acids Res.* **2006,** *34*, 1588-1596.

247. Lacour, S.; Bechet, E.; Cozzone, A. J.; Mijakovic, I.; Grangeasse, C., Tyrosine phosphorylation of the UDP-glucose dehydrogenase of *Escherichia coli* is at the crossroads of colanic acid synthesis and polymyxin resistance. *PLoS ONE* **2008,** *3*, e3053.

248. Lee, D. C.; Jia, Z., Emerging structural insights into bacterial tyrosine kinases. *Trends Biochem. Sci.* **2009,** *34*, 351-357.

249. Grangeasse, C.; Terreux, R.; Nessler, S., Bacterial tyrosine-kinases: structure–function analysis and therapeutic potential. *Biochim. Biophys. Acta* **2010,** *1804*, 628-634.

250. Bach, H.; Wong, D.; Av‐Gay, Y., *Mycobacterium tuberculosis* PtkA is a novel protein tyrosine kinase whose substrate is PtpA. *Biochem. J.* **2009,** *420*, 155-160.

251. Bach, H.; Papavinasasundaram, K. G.; Wong, D.; Hmama, Z.; Av-Gay, Y., *Mycobacterium tuberculosis* virulence is mediated by PtpA dephosphorylation of human vacuolar protein sorting 33B. *Cell Host Microbe* **2008,** *3*, 316-322.

252. Jagannathan, V.; Kaur, P.; Datta, S., Polyphosphate kinase from *M. tuberculosis*: an interconnect between the genetic and biochemical role. *PLoS ONE* **2010,** *5*, e14336.

253. Shum, K. T.; Lui, E. L. H.; Wong, S. C. K.; Yeung, P.; Sam, L.; Wang, Y.; Watt, R. M.; Tanner, J. A., Aptamer-mediated inhibition of *Mycobacterium tuberculosis* polyphosphate kinase 2. *Biochemistry (Mosc.)* **2011,** *50*, 3261-3271.

254. Rohdich, F.; Kis, K.; Bacher, A.; Eisenreich, W., The non-mevalonate pathway of isoprenoids: genes, enzymes, and intermediates. *Curr. Opin. Chem. Biol.* **2001,** *5*, 535-540.

255. Eisenreich, W.; Bacher, A.; Arigoni, D.; Rohdich, F., Biosynthesis of isoprenoids via the non-mevalonate pathway. *Cell. Mol. Life Sci.* **2004,** *61*, 1401-1426.

256. Brennan, P. J.; Crick, D. C., The cell-wall core of *Mycobacterium tuberculosis* in the context of drug discovery. *Curr. Top. Med. Chem.* **2007,** *7*, 475-488.

257. Shan, S.; Chen, X.; Liu, T.; Rao, Z.; Lou, Z., Crystal structure of 4-diphosphocytidyl-2-C-methyl-D-erythritol kinase (IspE) from *Mycobacterium tuberculosis*. *FASEB J.* **2011,** *25*, 1577-1584.

258. Chaitanya, M.; Babajan, B.; Anuradha, C. M.; Naveen, M.; Rajasekhar, C.; Madhusudana, P.; Kumar, C. S., Exploring the molecular basis for selective binding of *Mycobacterium tuberculosis* Asp kinase toward its natural substrates and feedback inhibitors: a docking and molecular dynamics study. *J. Mol. Model.* **2010,** *16*, 1357-1367.

259. Robin, A. Y.; Cobessi, D.; Curien, G.; Robert-Genthon, M.; Ferrer, J.-L.; Dumas, R., A new mode of dimerization of allosteric enzymes with ACT domains revealed by the crystal structure of the aspartate kinase from cyanobacteria. *J. Mol. Biol.* **2010,** *399*, 283-293.

260. Schuldt, L.; Suchowersky, R.; Veith, K.; Mueller-Dieckmann, J.; Weiss, M. S., Cloning, expression, purification, crystallization and preliminary X-ray diffraction analysis of the regulatory domain of aspartokinase (Rv3709c) from *Mycobacterium tuberculosis*. *Acta Crystallograph. Sect. F Struct. Biol. Cryst. Commun.* **2011,** *67*, 380-385.

261. Yang, Q.; Yu, K.; Yan, L.; Li, Y.; Chen, C.; Li, X., Structural view of the regulatory subunit of aspartate kinase from *Mycobacterium tuberculosis*. *Protein Cell* **2011,** *2*, 745-754.

262. Long, M. C.; Escuyer, V.; Parker, W. B., Identification and characterization of a unique adenosine kinase from *Mycobacterium tuberculosis*. *J. Bacteriol.* **2003,** *185*, 6548-6555.

263. Reddy, M. C. M.; Palaninathan, S. K.; Shetty, N. D.; Owen, J. L.; Watson, M. D.; Sacchettini, J. C., High resolution crystal structures of *Mycobacterium tuberculosis* adenosine kinase: Insights into the mechanisn and specificity of this novel prokaryotic enzyme. *J. Biol. Chem.* **2007,** *282*, 27334-27342.

264. Park, J.; Singh, B.; Gupta, R. S., Mycobacterial adenosine kinase is not a typical adenosine kinase. *FEBS Lett.* **2009,** *583*, 2231-2236.

265. Barrow, E. W., Antimycobacterial activity of 2-methyladenosine. *J. Antimicrob. Chemother.* **2003,** *52*, 801-808.

266. Long, M. C.; Allan, P. W.; Luo, M. Z.; Liu, M. C.; Sartorelli, A. C.; Parker, W. B., Evaluation of 3-deaza-adenosine analogues as ligands for adenosine kinase and inhibitors of *Mycobacterium tuberculosis* growth. *J. Antimicrob. Chemother.* **2007,** *59*, 118-121.

267. Long, M. C.; Parker, W. B., Structure–activity relationship for nucleoside analogs as inhibitors or substrates of adenosine kinase from *Mycobacterium tuberculosis*. *Biochem. Pharmacol.* **2006,** *71*, 1671-1682.

268. Spáčilová, P.; Nauš, P.; Pohl, R.; Votruba, I.; Snášel, J.; Zábranská, H.; Pichová, I.; Ameral, R.; Birkuš, G.; Cihlář, T.; Hocek, M., CycloSal-phosphate pronucleotides of cytostatic 6-(Het)aryl-7-deazapurine ribonucleosides: synthesis, cytostatic activity, and inhibition of adenosine kinases. *Chemmedchem* **2010,** *5*, 1386-1396.

269. Long, M. C.; Shaddix, S. C.; Moukha-Chafiq, O.; Maddry, J. A.; Nagy, L.; Parker, W. B., Structure–activity relationship for adenosine kinase from *Mycobacterium tuberculosis*. *Biochem. Pharmacol.* **2008,** *75*, 1588-1600.

270. Munier-Lehmann, H.; Burlacu-Miron, S.; Craescu, C. T.; Mantsch, H. H., A new subfamily of short bacterial adenylate kinase with the *Mycobacterium tuberculosis* enzyme as a model: a predictive and experimental study. *Proteins* **1999,** *36*, 238-248.

271. Bellinzoni, M.; Haouz, A.; Graña, M.; Munier-Lehmann, H.; Shepard, W.; Alzari, P. M., The crystal structure of *Mycobacterium tuberculosis* adenylate kinase in complex with two molecules of ADP and Mg^{2+} supports an associative mechanism for phosphoryl transfer. *Protein Sci.* **2006,** *15*, 1489-1493.

272. Hible, G.; Christova, P.; Renault, L.; Seclaman, E.; Thompson, A.; Girard, E.; Munier-Lehmann, H.; Cherfils, J., Unique GMP-binding site in *Mycobacterium tuberculosis* guanosine monophosphate kinase. *Proteins* **2005,** *62*, 489-500.

273. Thum, C.; Schneider, C. Z.; Palma, M. S.; Santos, D. S.; Basso, L. A., The Rv1712 locus from *Mycobacterium tuberculosis* H37Rv codes for a functional CMP kinase that preferentially phosphorylates dCMP. *J. Bacteriol.* **2009,** *191*, 2884-2887.

274. Caceres, R. A.; Timmers, L. F. S. M.; Vivan, A. L.; Schneider, C. Z.; Basso, L. A.; De Azevedo, W. F. J.; Santos, D. S., Molecular modeling and dynamics studies of cytidylate kinase from *Mycobacterium tuberculosis* H37Rv. *J. Mol. Model.* **2008,** *14*, 427-434.

275. de la Sierra, L. I.; Munier-Lehmann, H.; Gilles, A. M.; Bârzu, O.; Delarue, M., X-ray structure of TMP kinase from *Mycobacterium tuberculosis* complexed with TMP at 1.95 Å resolution. *J. Mol. Biol.* **2001,** *311*, 87-100.

276. Munier-Lehmann, H.; Chaffotte, A.; Pochet, S.; Labesse, G., Thymidylate kinase of *Mycobacterium tuberculosis*: a chimera sharing properties common to eukaryotic and bacterial enzymes. *Protein Sci.* **2001,** *10*, 1195-1205.

277. Fioravanti, E.; Adam, V.; Munier-Lehmann, H.; Bourgeois, D., The crystal structure of *Mycobacterium tuberculosis* thymidylate kinase in complex with 3'-azidodeoxythymidine monophosphate suggests a mechanism for competitive inhibition. *Biochemistry (Mosc.)* **2005,** *44*, 130-137.

278. Vanheusden, V.; Van Rompaey, P.; Munier-Lehmann, H.; Pochet, S.; Herdewijn, P.; Van Calenbergh, S., Thymidine and thymidine-5′-*O*-monophosphate analogues as inhibitors of *Mycobacterium tuberculosis* thymidylate kinase. *Bioorg. Med. Chem. Lett.* **2003,** *13*, 3045-3048.

279. Van Rompaey, P.; Nauwelaerts, K.; Vanheusden, V.; Rozenski, J.; Munier-Lehmann, H.; Herdewijn, P.; Van Calenbergh, S., *Mycobacterium tuberculosis* thymidine monophosphate kinase inhibitors: biological evaluation and conformational analysis of 2′- and 3′-modified thymidine analogues. *Eur. J. Org. Chem.* **2003,** *2003*, 2911-2918.

280. Haouz, A., Enzymatic and structural analysis of inhibitors designed against *Mycobacterium tuberculosis* thymidylate kinase. New insights into the phosphoryl transfer mechanism. *J. Biol. Chem.* **2002,** *278*, 4963-4971.

281. Vanheusden, V.; Munier-Lehmann, H.; Froeyen, M.; Busson, R.; Rozenski, J.; Herdewijn, P.; Van Calenbergh, S., Discovery of bicyclic thymidine analogues as selective and high-affinity inhibitors of *Mycobacterium tuberculosis* thymidine monophosphate kinase. *J. Med. Chem.* **2004,** *47*, 6187-6194.

282. Vanheusden, V.; Munier-Lehmann, H.; Froeyen, M.; Dugué, L.; Heyerick, A.; De Keukeleire, D.; Pochet, S.; Busson, R.; Herdewijn, P.; Van Calenbergh, S., 3'-*C*-branched-chain-substituted nucleoside and nucleotides as potent inhibitors of *Mycobacterium tuberculosis* thymidine monophosphate kinase. *J. Med. Chem.* **2003,** *46*, 3811-3821.

283. Andrade, C. H.; Pasqualoto, K. F. M.; Ferreira, E. I.; Hopfinger, A. J., 3D-Pharmacophore mapping of thymidine-based inhibitors of TMPK as potential antituberculosis agents. *J. Comput. Aided Mol. Des.* **2010,** *24*, 157-172.

284. Van Daele, I.; Munier-Lehmann, H.; Hendrickx, P. M. S.; Marchal, G.; Chavarot, P.; Froeyen, M.; Qing, L.; Martins, J. C.; Van Calenbergh, S., Synthesis and biological evaluation of bicyclic nucleosides as inhibitors of *Mycobacterium tuberculosis* thymidylate kinase. *Chemmedchem* **2006,** *1*, 1081-1090.

285. Frecer, V.; Seneci, P.; Miertus, S., Computer-assisted combinatorial design of bicyclic thymidine analogs as inhibitors of *Mycobacterium tuberculosis* thymidine monophosphate kinase. *J. Comput. Aided Mol. Des.* **2010,** *25*, 31-49.

286. Van Daele, I.; Munier-Lehmann, H.; Froeyen, M.; Balzarini, J.; Van Calenbergh, S., Rational design of 5'-thiourea-substituted α-thymidine analogues as thymidine monophosphate

kinase inhibitors capable of inhibiting mycobacterial growth. *J. Med. Chem.* **2007,** *50*, 5281-5292.

287. Gasse, C.; Douguet, D.; Huteau, V.; Marchal, G.; Munier-Lehmann, H.; Pochet, S., Substituted benzyl-pyrimidines targeting thymidine monophosphate kinase of *Mycobacterium tuberculosis*: Synthesis and in vitro anti-mycobacterial activity. *Bioorg. Med. Chem.* **2008,** *16*, 6075-6085.

288. Chitre, T. S.; Kathiravan, M. K.; Bothara, K. G.; Bhandari, S. V.; Jalnapurkar, R. R., Pharmacophore optimization and design of competitive inhibitors of thymidine monophosphate kinase through molecular modeling studies. *Chem. Biol. Drug Des.* **2011,** *78*, 826-834.

289. Familiar, O.; Munier‐Lehmann, H.; Negri, A.; Gago, F.; Douguet, D.; Rigouts, L.; Hernández, A. I.; Camarasa, M. J.; Pérez‐Pérez, M. J., Exploring acyclic nucleoside analogues as inhibitors of *Mycobacterium tuberculosis* thymidylate kinase. *Chemmedchem* **2008,** *3*, 1083-1093.

290. Familiar, O.; Munier-Lehmann, H.; Aínsa, J. A.; Camarasa, M.-J.; Pérez-Pérez, M.-J., Design, synthesis and inhibitory activity against *Mycobacterium tuberculosis* thymidine monophosphate kinase of acyclic nucleoside analogues with a distal imidazoquinolinone. *Eur. J. Med. Chem.* **2010,** *45*, 5910-5918.

291. Kumar, A.; Chaturvedi, V.; Bhatnagar, S.; Sinha, S.; Siddigi, M. I., Knowledge based indentification of potent antitubercular compounds using structure based virtual screening and structure interaction fingerprints. *J. Chem. Inf. Model.* **2009,** *49*, 35-42.

292. Kumar, M.; Sharma, S.; Srinivasan, A.; Singh, T. P.; Kaur, P., Structure-based *in-silico* rational design of a selective peptide inhibitor for thymidine monophosphate kinase of *Mycobacterium tuberculosis*. *J. Mol. Model.* **2011,** *17*, 1173-182.

293. Brown, L. R., Commercial challenges of protein drug delivery. *Expert Opin. Drug Deliv.* **2005,** *2*, 29-42.

294. Robertson, D.; Carroll, P.; Parish, T., Rapid recombination screening to test gene essentiality demonstrates that pyrH is essential in *Mycobacterium tuberculosis*. *Tuberculosis* **2007,** *87*, 450-458.

295. Rostirolla, D. C.; Breda, A.; Rosado, L. A.; Palma, M. S.; Basso, L. A.; Santos, D. S., UMP kinase from *Mycobacterium tuberculosis*: Mode of action and allosteric interactions, and their likely role in pyrimidine metabolism regulation. *Arch. Biochem. Biophys.* **2011,** *505*, 202-212.

296. Labesse, G.; Benkali, K.; Salard-Arnaud, I.; Gilles, A. M.; Munier-Lehmann, H., Structural and functional characterization of the *Mycobacterium tuberculosis* uridine monophosphate kinase: insights into the allosteric regulation. *Nucleic Acids Res.* **2010,** *39*, 3458-3472.

297. Tiwari, S., Amino acid residues involved in autophosphorylation and phosphotransfer activities are distinct in nucleoside diphosphate kinase from *Mycobacterium tuberculosis*. *J. Biol. Chem.* **2004,** *279*, 43595-43603.

298. Parish, T.; Stoker, N. G., The common aromatic amino acid biosynthesis pathway is essential in *Mycobacterium tuberculosis*. *Microbiology* **2002,** *148*, 3069-3077.

299. Pereira, J. H.; Vasconcelos, I. B.; Oliveira, J. S.; Caceres, R. A.; de Azevedo, W. F. J.; Basso, L. A.; Santos, D. S., Shikimate kinase: A potential target for development of novel antitubercular agents. *Curr. Drug Targets* **2007,** *8*, 459-468.

300. Bentley, R., The shikimate pathway - a metabolic tree with many branches. *Biochemistry and Molecular Biology* **1990,** *25*, 307-384.

301. Hartmann, M. D.; Bourenkov, G. P.; Oberschall, A.; Strizhov, N.; Bartunik, H. D., Mechanism of phosphoryl transfer catalyzed by shikimate kinase from *Mycobacterium tuberculosis*. *J. Mol. Biol.* **2006,** *364*, 411-423.

302. Gan, J.; Gu, Y.; Li, Y.; Yan, H.; Ji, X., Crystal structure of *Mycobacterium tuberculosis* shikimate kinase in complex with shikimic acid and an ATP analogue. *Biochemistry (Mosc.)* **2006,** *45*, 8539-8545.

303. Gu, Y.; Reshetnikova, L.; Li, Y.; Wu, Y.; Yan, H.; Singh, S.; Ji, X., Crystal structure of shikimate kinase from *Mycobacterium tuberculosis* reveals the dynamic role of the LID domain in catalysis. *J. Mol. Biol.* **2002,** *319*, 779-789.

304. Dhaliwal, B.; Nichols, C. E.; Ren, J.; Lockyer, M.; Charles, I.; Hawkins, A. R.; Stammers, D. K., Crystallographic studies of shikimate binding and induced conformational changes in *Mycobacterium tuberculosis* shikimate kinase. *FEBS Lett.* **2004,** *574*, 49-54.

305. Pereira, J. H.; de Oliveira, J. S.; Canduri, F.; Dias, M. V. B.; Palma, M. S.; Basso, L. A.; Santos, D. S.; de Azevedo, W. F. J., Structure of shikimate kinase from *Mycobacterium tuberculosis* reveals the binding of shikimic acid. *Acta Crystallogr. D Biol. Crystallogr.* **2004,** *60*, 2310-2319.

306. Dias, M. V. B.; Faím, L. M.; Vasconcelos, I. B.; de Oliveira, J. S.; Basso, L. A.; Santos, D. S.; de Azevedo, W. F., Effects of the magnesium and chloride ions and shikimate on the structure of shikimate kinase from *Mycobacterium tuberculosis*. *Acta Crystallograph. Sect. F Struct. Biol. Cryst. Commun.* **2007,** *63*, 1-6.

307. Saidemberg, D. M.; Passarelli, A. W.; Rodrigues, A. V.; Basso, L. A.; Santos, D. S.; Palma, M. S., Shikimate kinase (EC 2.7.1.71) from *Mycobacterium tuberculosis*: kinetics and structural dynamics of a potential molecular target for drug development. *Curr. Med. Chem.* **2011,** *18*, 1299-1310.

308. Bandodkar, B. S.; Schmitt, S. Pyrazolone derivatives for the treatment of tuberculosis. WO 2007/020426 A1, 2007.

309. Segura-Cabrera, A.; Rodríguez-Pérez, M. A., Structure-based prediction of *Mycobacterium tuberculosis* shikimate kinase inhibitors by high-throughput virtual screening. *Bioorg. Med. Chem. Lett.* **2008,** *18*, 3152-3157.

310. Vianna, C. P.; de Azevedo, W. F., Identification of new potential *Mycobacterium tuberculosis* shikimate kinase inhibitors through molecular docking simulations. *J. Mol. Model.* **2012,** *18*, 755-764.

311. Kumar, M.; Verma, S.; Sharma, S.; Srinivasan, A.; Singh, T. P.; Kaur, P., Structure-based in *silico* design of a high-affinity dipeptide inhibitor for novel protein drug target shikimate kinase of *Mycobacterium tuberculosis*. *Chem. Biol. Drug Des.* **2010,** *76*, 277-284.

312. Kawai, S.; Mori, S.; Mukai, T.; Suzuki, S.; Yamada, T.; Hashimoto, W.; Murata, K., Inorganic polyphosphate/ATP-NAD kinase of *Micrococcus flavus* and *Mycobacterium tuberculosis* H37Rv. *Biochem. Biophys. Res. Commun.* **2000,** *276*, 57-63.

313. Raffaelli, N.; Finaurini, L.; Mazzola, F.; Pucci, L.; Sorci, L.; Amici, A.; Magni, G., Characterization of *Mycobacterium tuberculosis* NAD kinase: Functional analysis of the full-length enzyme by site-directed mutagenesis. *Biochemistry (Mosc.)* **2004,** *43*, 7610-7617.

314. Lerner, F.; Niere, M.; Ludwig, A.; Ziegler, M., Structural and functional characterization of human NAD kinase. *Biochem. Biophys. Res. Commun.* **2001,** *288*, 69-74.

315. Bonnac, L.; Chen, L.; Pathak, R.; Gao, G.; Ming, Q.; Bennett, E.; Felczak, K.; Kullberg, M.; Patterson, S. E.; Mazzola, F.; Magni, G.; Pankiewicz, K. W., Probing binding requirements of NAD kinase with modified substrate (NAD) analogues. *Bioorg. Med. Chem. Lett.* **2007,** *17*, 1512-1515.

316. Garavaglia, S., A novel fold revealed by *Mycobacterium tuberculosis* NAD kinase, a key allosteric enzyme in NADP biosynthesis. *J. Biol. Chem.* **2004,** *279*, 40980-40986.

317. Mori, S.; Yamasaki, M.; Maruyama, Y.; Momma, K.; Kawai, S.; Hashimoto, W.; Mikami, B.; Murata, K., NAD-binding mode and the significance of intersubunit contact revealed by the crystal structure of *Mycobacterium tuberculosis* NAD kinase–NAD complex. *Biochem. Biophys. Res. Commun.* **2005,** *327*, 500-508.

318. Petrelli, R.; Sham, Y. Y.; Chen, L.; Felczak, K.; Bennett, E.; Wilson, D.; Aldrich, C.; Yu, J. S.; Cappellacci, L.; Franchetti, P.; Grifantini, M.; Mazzola, F.; Di Stefano, M.; Magni, G.; Pankiewicz, K. W., Selective inhibition of nicotinamide adenine dinucleotide kinases by dinucleoside disulfide mimics of nicotinamide adenine dinucleotide analogues. *Bioorg. Med. Chem.* **2009,** *17*, 5656-5664.

319. Begley, T. P.; Kinsland, C.; Strauss, E., The biosynthesis of coenzyme A in bacteria. *Vitam. Horm.* **2001,** *61*, 157-171.

320. Cheek, S.; Ginalski, K.; Zhang, H.; Grishin, N. V., A comprehensive update of the sequence and structure classification of kinases. *BMC Struct. Biol.* **2005,** *5*, 6.

321. Awasthy, D.; Ambady, A.; Bhat, J.; Sheikh, G.; Ravishankar, S.; Subbulakshmi, V.; Mukherjee, K.; Sambandamurthy, V.; Sharma, U., Essentiality and functional analysis of type I and type III pantothenate kinases of *Mycobacterium tuberculosis*. *Microbiology* **2010,** *156*, 2691-2701.

322. Das, S.; Kumar, P.; Bhor, V.; Surolia, A.; Vijayan, M., Invariance and variability in bacterial PanK: a study based on the crystal structure of *Mycobacterium tuberculosis* PanK. *Acta Crystallogr. D Biol. Crystallogr.* **2006,** *62*, 628-638.

323. Chetnani, B.; Das, S.; Kumar, P.; Surolia, A.; Vijayan, M., *Mycobacterium tuberculosis* pantothenate kinase: possible changes in location of ligands during enzyme action. *Acta Crystallogr. D Biol. Crystallogr.* **2009,** *65*, 312-325.

324. Chetnani, B.; Kumar, P.; Surolia, A.; Vijayan, M., *M. tuberculosis* pantothenate kinase: dual substrate specificity and unusual changes in ligand locations. *J. Mol. Biol.* **2010,** *400*, 171-185.

325. Chetnani, B.; Kumar, P.; Abhinav, K. V.; Chhibber, M.; Surolia, A.; Vijayan, M., Location and conformation of pantothenate and its derivatives in *Mycobacterium tuberculosis* pantothenate kinase: Insights into enzyme action. *Acta Crystallogr. D Biol. Crystallogr.* **2011,** *67*, 774-783.

326. Zhang, Y. M., Feedback regulation of murine pantothenate kinase 3 by coenzyme A and coenzyme A thioesters. *J. Biol. Chem.* **2005,** *280*, 32594-32601.

327. Saliba, K. J.; Ferru, I.; Kirk, K., Provitamin B5 (Pantothenol) inhibits growth of the intraerythrocytic malaria parasite. *Antimicrob. Agents Chemother.* **2005,** *49*, 632-637.

328. Spry, C.; Chai, C. L. L.; Kirk, K.; Saliba, K. J., A class of pantothenic acid analogs inhibits *Plasmodium falciparum* pantothenate kinase and represses the proliferation of malaria parasites. *Antimicrob. Agents Chemother.* **2005,** *49*, 4649-4657.

329. Kumar, P.; Chhibber, M.; Surolia, A., How pantothenol intervenes in coenzyme-A biosynthesis of *Mycobacterium tuberculosis*. *Biochem. Biophys. Res. Commun.* **2007,** *361*, 903-909.

330. Venkatraman, J.; Bhat, J.; Solapure, S. M.; Sandesh, J.; Sarkar, D.; Aishwarya, S.; Mukherjee, K.; Datta, S.; Malolanarasimhan, K.; Bandodkar, B.; Das, K. S., Screening, identification, and characterization of mechanistically diverse inhibitors of the *Mycobacterium tuberculosis* enzyme, pantothenate kinase (CoaA). *J. Biomol. Screen.* **2011,** *17*, 293-302.

331. Bereswill, S.; Walia, G.; Kumar, P.; Surolia, A., The role of UPF0157 in the folding of *M. tuberculosis* dephosphocoenzyme A kinase and the regulation of the latter by CTP. *PLoS ONE* **2009,** *4*, e7645.

332. Walia, G.; Surolia, A., Insights into the regulatory characteristics of the mycobacterial dephosphocoenzyme A kinase: implications for the universal CoA biosynthesis pathway. *PLoS ONE* **2011,** *6*, e21390.

333. Friedland, N.; Mack, T. R.; Yu, M.; Hung, L.-W.; Terwilliger, T. C.; Waldo, G. S.; Stock, A. M., Domain orientation in the inactive response regulator *Mycobacterium tuberculosis* MtrA provides a barrier to activation. *Biochemistry (Mosc.)* **2007,** *46*, 6733-6743.

334. Schnell, R.; Ågren, D.; Schneider, G., 1.9 Å structure of the signal receiver domain of the putative response regulator NarL from *Mycobacterium tuberculosis*. *Acta Crystallograph. Sect. F Struct. Biol. Cryst. Commun.* **2008,** *64*, 1096-1100.

335. Morth, J. P.; Feng, V.; Perry, L. J.; Svergun, D. I.; Tucker, P. A., The crystal and solution structure of a putative transcriptional antiterminator from *Mycobacterium tuberculosis*. *Structure* **2004,** *12*, 1595-1605.

336. Wang, S.; Engohang-Ndong, J.; Smith, I., Structure of the DNA-binding domain of the response regulator PhoP from *Mycobacterium tuberculosis*. *Biochemistry (Mosc.)* **2007,** *46*, 14751-14761.

337. Matsushita, M.; Janda, K. D., Histidine kinases as targets for new antimicrobial agents. *Bioorg. Med. Chem.* **2002,** *10*, 855-867.

338. Lee, H.-N.; Jung, K.-E.; Ko, I.-J.; Baik, H. S.; Oh, J.-I., Protein-protein interactions between histidine kinases and response regulators of *Mycobacterium tuberculosis* H37Rv. *J. Microbiol.* **2012,** *50*, 270-277.

339. Gotoh, Y.; Eguchi, Y.; Watanabe, T.; Okamoto, S.; Doi, A.; Utsumi, R., Two-component signal transduction as potential drug targets in pathogenic bacteria. *Curr. Opin. Microbiol.* **2010,** *13*, 232-239.

340. Thompson, J. D.; Higgins, D. G.; Gibson, T. J., CLUSTAL W: improving the sensitivity of progressive multiple sequence alignment through sequence weighting, position-specific gap penalties and weight matrix choice. *Nucleic Acids Res.* **1994,** *22*, 4673-4680.

341. Hall, T. A., BioEdit: a user-friendly biological sequence alignment editor and analysis program for Windows 95/98/NT *Nucleic Acids Symp. Ser.* **1999,** *41*.

342. Kang, C. M.; Jahng, W. J.; Husson, R. N.; Lee, S. H., A modified immunoblot method to identify substrates of protein kinases. *J. Microbiol.* **2011,** *49*, 499-501.

343. Russell, R. B.; Mészáros, B.; Tóth, J.; Vértessy, B. G.; Dosztányi, Z.; Simon, I., Proteins with complex architecture as potential targets for drug design: A case study of *Mycobacterium tuberculosis*. *PLoS Comput. Biol.* **2011,** *7*, e1002118.

344. Wessels, M.; Konig, G. M.; Wright, A. D., A new tyrosine kinase inhibitor from the marine brown alga *Stypopodium zonale*. *J. Nat. Prod.* **1999,** *62*, 927-930.

345. Laurent, D.; Jullian, V.; Parenty, A.; Knibiehler, M.; Dorin, D.; Schmitt, S.; Lozach, O.; Lebouvier, N.; Frostin, M.; Alby, F.; Maurel, S.; Doerig, C.; Meijer, L.; Sauvain, M., Antimalarial potential of xestoquinone, a protein kinase inhibitor isolated from a Vanuatu marine sponge *Xestospongia* sp. *Bioorg. Med. Chem.* **2006,** *14*, 4477-4482.

346. Kono, K.; Tanaka, M.; Ogita, T.; Kohama, T., Characterization of B-5354c, a new sphingosine kinase inhibitor, produced by a marine bacterium. *J. Antibiot. (Tokyo)* **2000,** *53*, 759-764.

347. Fujiwara, H.; Matsunaga, K.; Saito, M.; Hagiya, S.; Furukawa, K.; Nakamura, H.; Ohizumi, Y., Halenaquinone, a novel phosphatidylinositol 3-kinase inhibitor from a marine sponge, induces apotosis in PC12 cells. *Eur. J. Pharmacol.* **2001,** *413*, 37-45.

348. Meijer, L.; Thunnissen, A. M.; White, A. W.; Garnier, M.; Nikolic, M.; Tsai, L. H.; Walter, J.; Cleverley, K. E.; Salinas, P. C.; Wu, Y. Z.; Biernat, J.; Mandelkow, E. M.; Kim, S. H.; Pettit, G. R., Inhibition of cyclin-dependent kinases, GSK-3beta and CK1 by hymenialdisine, a marine sponge constituent. *Chem. Biol.* **2000,** *7*, 51-63.

349. Killday, K. B.; Yarwood, D.; Sills, M. A.; Murphy, P. T.; Hooper, J. N.; Wright, A. E., Microxine, a new cdc2 kinase inhibitor from the Austrilian marine sponge *Microxina* species. *J. Nat. Prod.* **2001,** *64*, 525-526.

350. Ina, A.; Hayashi, K.; Nozaki, H.; Kamei, Y., Pheophytin a, a low molecular weight compound found in the marine brown alga *Sargassum fulvellum*, promotes the differentiation of PC12 cell. *Int. J. Dev. Neurosci.* **2007,** *25*, 63-68.

351. Simone, M.; Erba, E.; Damia, G.; Vikhanskaya, F.; Di Francesco, A. M.; Riccardi, R.; Bailly, C.; Cuevas, C.; Fernandez Sousa-Faro, J. M.; D'Incalci, M., Variolin B and its derivate deoxy-variolin B: new marine natural compounds with cyclin-dependent kinase inhibitor activity. *Eur. J. Cancer* **2005,** *41*, 2366-2377.

VITA

BIN WANG

354 Faser Hall • University, MS 38677 • (662) 915-7037 • bwang1@go.olemiss.edu

EDUCATION

M.S., Pharmaceutical Analysis, Second Military Medical University, China, May 2005.
Thesis: Study on Clinical Monitoring Methods for Immunosuppressants used in Organ Transplantation.

B.S., Pharmacy, Second Military Medical University, China, May 2001.
Research paper: Determination of Cyclosporine A in Whole blood.

A.S., Medical Technique, Second Military Medical University, China, May 1993.

EMPLOYMENT

Research Assistant, 2007-2012
Department of Pharmacognosy, The University of Mississippi

Pharmacist, Supervisor of Clinical Pharmacology Laboratory, 2001-2007
Shanghai Eastern Hepatobiliary Hospital, Shanghai, China

Pharmacist, supervisor of Pharmacy Intravenous Admixture Service (PIVAS), 1999-2001
Shanghai Eastern Hepatobiliary Hospital, Shanghai, China

Pharmacist, In-patient Pharmacy, 1996-1999
Shanghai Eastern Hepatobiliary Hospital, Shanghai, China

Assistant Pharmacist, Out-patient Pharmacy, 1993-1996.
Shanghai Eastern Hepatobiliary Hospital, Shanghai, China

HONORS and AWARDS

Triton Biopharma LLC. Graduate student fellowship, 2009

ROCHI Honor Society, 2009

PUBLICATIONS

1. Wang, B.; Patel, R.Y.; Calderon, A.; Prasanna, S.; Doerksen, R.J.; Hamann, M.T., Kinases of *Mycobacterium tuberculosis*: classification, structures, and the development of inhibitors. *Chem. Rev*. **2012**, *abstract accepted*.

2. Wang, B.; Waters, A.L.; Sims, J.W.; Fullmer, A.; Ellison, S.; Hamann, M.T., Epigenetic regulation in *Pseudomonas aeruginosa* to increase antibiotic production. *Microb. Ecol.* **2012**, *submitted*.

3. Peng, J.; Kudrimoti, S.; Prasanna, S.; Odde, S.; Doerksen, R.J.; Pennaka, H.K.; Choo, Y.M.; Rao, K.V.; Tekwani, B.L.; Madgula, V.; Khan, S.I.; Wang, B.; Mayer, A.M.; Jacob, M.R.; Tu, L.C.; Gertsch, J.; Hamann, M.T., Structure-activity relationship and mechanism of action studies of manzamine analogues for the control of neuroinflammation and cerebral infections. *J. Med. Chem*. **2012**, *53*, 61-76.

4. Na, M.; Ding, Y.; Wang, B.; Tekwani, B.L.; Schinazi, R.F.; Franzblau, S.; Kelly, M.; Stone, R.; Li, X-C.; Ferreira, D.; Hamann, M.T., Anti-infective discorhabdins from a deep-water Alaskan sponge of the genus *Latrunculia*. *J. Nat. Prod*. **2010**, *73*, 383-387.

5. Gao, J.; Caballero-George, C.; Wang, B.; Rao, K.V.; Shilabin, A.G.; Hamann, M.T., 5-OHKA and NorKF, depsipeptides from a Hawaiian collection of *Bryopsis pennata*: binding proterties for NorKA to the human neuropeptide Y Y1 receptor. *J. Nat. Prod.* **2009**, *72*, 2172-2176.

6. Donia, M.S.; Wang, B.; Dunbar, D.C.; Desai, P.V.; Patny, A.; Avery, M.; Hamann, M.T., Mollamides B and C, cyclic hexapeptides from an Indonesian tunicate *Didemnum molle*. *J. Nat. Prod.* **2008**, *71*, 941-945.